Functional Mechanisms of Neuronal Mismatch in the Auditory Midbrain and the Medial Prefrontal Cortex

Lorena Casado Román

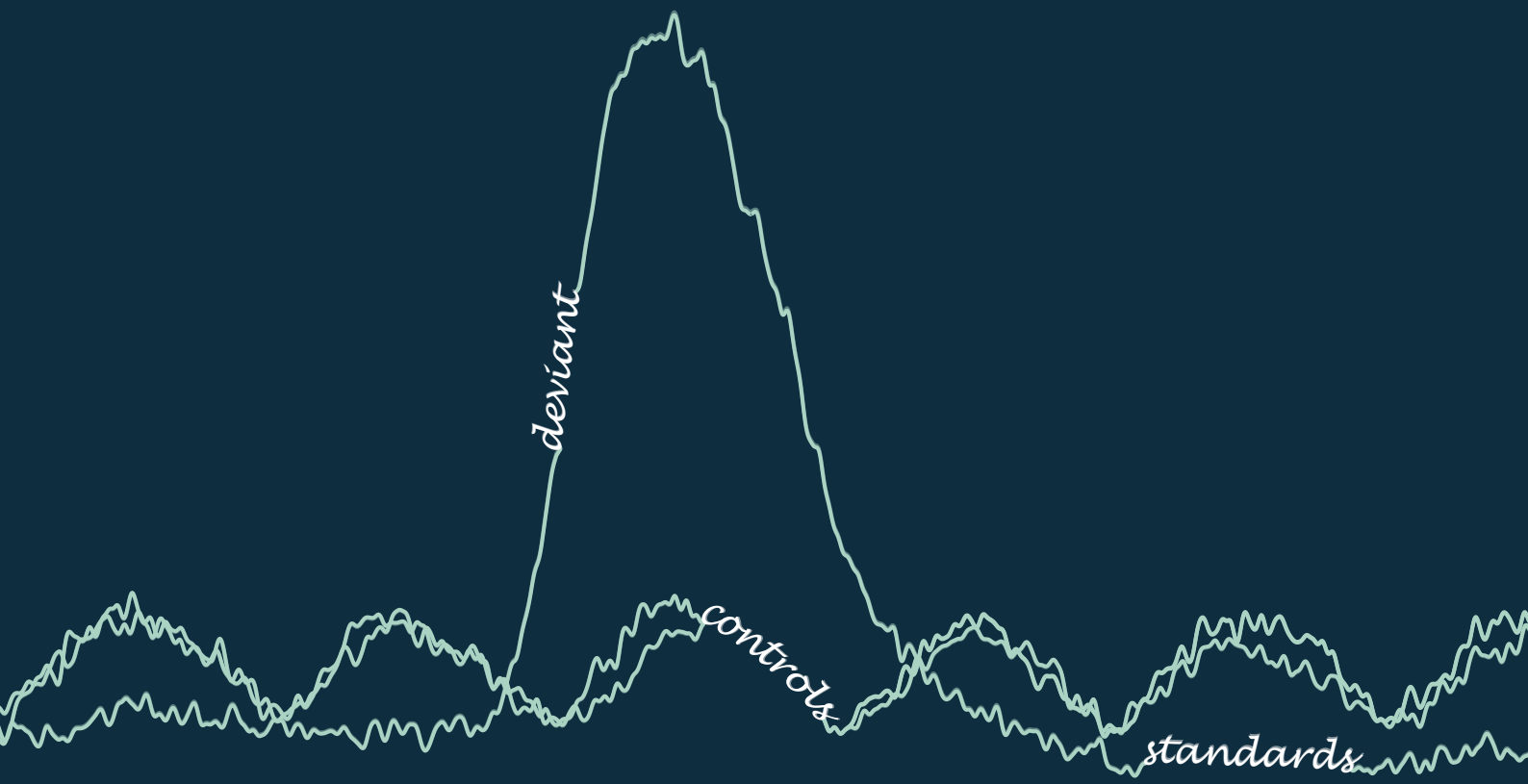

PhD Thesis
2021

Funtional Mechanisms of Neuronal Mismatch in the Auditory Midbrain and the Medial Prefrontal Cortex

Doctoral Thesis

To obtain the degree of

PhD in Neuroscience and the International Doctor Mention

Doctoral Program in Neurosciences

University of Salamanca

Institute of Neuroscience of Castilla y León (INCYL)

Cognitive and Auditory Neuroscience Laboratory (CANELAB)

Supervised by

Prof. Dr. Manuel Sánchez Malmierca and Dr. David Pérez González

Salamanca, May 2021

"Mientras nuestro cerebro sea un arcano, el universo, reflejo de su estructura, será también un misterio."

"As long as our brain is a mystery, the universe, the reflection of the structure of the brain will also be a mystery."

— Santiago Ramón y Cajal

Funding Sources

Financial support for this study was provided by the European Union Framework Programme for Research and Innovation Horizon 2020 (Marie Skłodowska-Curie ITN-LISTEN, Grant No. 722098, http://www.listenscience.eu/), the Spanish Ministry of Science and Innovation (MICINN, Grant No. SAF2016-75803-P) and the Spanish AEI (PID2019-104570RB-I00).

Lorena Casado Román held an early stage researcher fellowship from the Marie Skłodowska-Curie ITN-LISTEN Grant No. 722098.

Este trabajo ha sido financiado por el Programa Marco de Investigación e Innovación de la Unión Europea Horizonte 2020 (Marie Skłodowska-Curie ITN-LISTEN, Subvención No. 722098, http://www.listenscience.eu/), el Ministerio de Ciencia e Innovación Español (MICINN, Subvención No. SAF2016-75803-P) y la Agencia Estatal de Investigación (PID2019-104570RB-I00).

Lorena Casado Román disfrutó de un contrato para jóvenes investigadores de la subvención Marie Skłodowska-Curie ITN-LISTEN No. 722098.

List of Publications

The Doctoral Thesis entitled *'Functional mechanisms of neuronal mismatch in the auditory midbrain and the medial prefrontal cortex'* presented by Lorena Casado Román to obtain the degree of PhD in Neuroscience correspond to a **compendium the following published scientific articles**.

La tesis doctoral titulada *'Mecanismos funcionales de mismatch neuronal en el mesencéfalo auditivo y la corteza prefrontal medial'* que presenta Lorena Casado Román para obtener el título de Doctorado en Neurociencias corresponde a un **compendio de los siguientes trabajos científicos publicados.**

Study I

In vivo whole-cell recordings of stimulus-specific adaptation in the inferior colliculus

Authors: Catalina Valdés-Baizabal [1,2,☯], Lorena Casado-Román [1,2,☯], Edward L. Bartlett [3,4], Manuel S. Malmierca [1,2,5,*]
Journal: Hearing Research | 399:107978 | 2020 April 30
DOI: 10.1016/j.heares.2020.107978

Study II

Prediction error signaling explains neuronal mismatch responses in the medial prefrontal cortex

Authors: Lorena Casado-Román [1,2,☯], Guillermo V. Carbajal [1,2,☯], David Pérez-González [1,2*], Manuel S. Malmierca[1,2,5*]
Journal: PLOS Biology | 18(12):e3001019 | 2020 December 21
DOI: 10.1371/journal.pbio.3001019

Affiliations

☯ These authors contributed equally to this work
[1] Cognitive and Auditory Neuroscience Laboratory, Institute of Neuroscience of Castilla y León, University of Salamanca, 37007, Salamanca, Spain
[2] The Salamanca Institute for Biomedical Research (IBSAL), 37007, Salamanca, Spain
[3] Department of Biological Sciences, Purdue University, West Lafayette, IN, 47907, USA
[4] Weldon School of Biomedical Engineering, Purdue University, West Lafayette, IN, 47907, USA
[5] Department of Cell Biology and Pathology, Faculty of Medicine, Campus Miguel de Unamuno, University of Salamanca, 37007, Salamanca, Spain

Manuel Sánchez Malmierca, catedrático del Departamento de Biología Celular y Patología de la Universidad de Salamanca y director del Instituto de Neurociencias de Castilla y León.

David Pérez González, investigador postdoctoral senior del Instituto de Neurociencias de Castilla y León.

CERTIFICAN

Que la tesis doctoral titulada:

FUNCTIONAL MECHANISMS OF NEURONAL MISMATCH IN THE AUDITORY MIDBRAIN AND THE MEDIAL PREFRONTAL CORTEX

Ha sido redactada en inglés como un compendio de artículos científicos, contiene un resumen en español y describe el trabajo de investigación realizado por Lorena Casado Román bajo nuestra dirección durante los últimos 4 años.

La memoria de este estudio recoge un análisis detallado y exhaustivo de las respuestas de *mismatch* neuronal y de codificación predictiva en el colículo inferior y en la corteza prefrontal medial en un modelo animal. Los datos presentados en esta memoria constituyen una aportación original y podemos afirmar que ponen de manifiesto un gran avance y progreso en el área de la Neurociencia.

Por todo ello, consideramos que esta tesis reúne los requisitos, calidad y rigor científicos necesarios para que sea defendida en la Universidad de Salamanca como trámite para que **Doña Lorena Casado Román opte al grado de 'Doctora en Neurociencias con Mención Internacional' por la Universidad de Salamanca**.

Y para que así conste, firmamos el presente certificado en Salamanca, a 12 de mayo de 2021.

SANCHEZ MALMIERCA MANUEL - 11764607S
Firmado digitalmente por SANCHEZ MALMIERCA MANUEL - 11764607S
Fecha: 2021.05.13 09:48:39 +02'00'

Manuel Sánchez Malmierca

PEREZ GONZALEZ DAVID - 70863212M
Firmado digitalmente por PEREZ GONZALEZ DAVID - 70863212M
Fecha: 2021.05.12 19:19:56 +02'00'

David Pérez González

INSTITUTO DE NEUROCIENCIAS DE CASTILLA Y LEÓN (INCYL)
Doctorado Neurociencias

La Comisión Académica del Programa de Doctorado en Neurociencias de la Universidad de Salamanca, una vez examinada la solicitud enviada por Dª Lorena Casado Román, para presentar la Tesis Doctoral en el formato de compendio de artículos cuando el número de aportaciones es inferior a tres.

Informa favorablemente sobre la calidad de las aportaciones presentadas de por la Doctoranda Dª Lorena Casado Román, consistentes en dos artículos científicos, uno de los cuales está publicado en Plos Biology con un índice de impacto en el año de la publicación de 7.076 (primer decil) y del cual la doctoranda es primera autora con autoría compartida y un segundo trabajo publicado en Hearing Research (índice de impacto de 3.693; Q1) en el que la doctoranda es primera autora con autoría compartida.

En Salamanca a 9 de diciembre de 2020

TABERNERO URBIETA MARIA ARANZAZU - 07863000J

Firmado digitalmente por TABERNERO URBIETA MARIA ARANZAZU - 07863000J
Nombre de reconocimiento (DN): c=ES, serialNumber=IDCES-07863000J, givenName=MARIA ARANZAZU, sn=TABERNERO URBIETA, cn=TABERNERO URBIETA MARIA ARANZAZU - 07863000J
Fecha: 2020.12.09 17:02:20 +01'00'

Profª. Aránzazu Tabernero Urbieta
Coordinadora Programa de Doctorado
en Neurociencias INCYL

Arantxa Tabernero – lab 15. Instituto de Neurociencias de Castilla y León (INCYL). *Universidad de Salamanca* -37007 Salamanca Spain -Teléf.: 923 294500 ext: 5311 -Email: ataber@usal.es

MODELO DE INFORME DE MENCIÓN DOCTOR INTERNACIONAL

STANDARD FORM FOR THE INTERNATIONAL DOCTORATE MENTION

NOMBRE Y APELLIDOS / NAME OF THE EXAMINER

Patricia T. Michie

CATEGORÍA ACADÉMICA O PROFESIONAL/ ACADEMIC OR PROFESIONAL RANK

Emeritus Professor

UNIVERSIDAD U ORGANISMO Y PAÍS / UNIVERSITY OR INSTITUTION AND COUNTRY

Centre for Brain and Mental Health Research, University of Newcastle, Australia

TÍTULO DE LA TESIS OBJETO DE INFORME / TITLE OF THE TESIS

Functional mechanisms of neuronal mismatch in the auditory midbrain and the medial prefrontal cortex

NOMBRE Y APELLIDOS DEL DOCTORANDO / NAME OF THE CANDIDATE

Lorena Casado Román

NOMBRE Y APELLIDOS DEL DIRECTOR/A(S) DE LA TESIS / NAME OF THE THESIS DIRECTOR(S)

Prof. Dr. Manuel Sánchez Malmierca y Dr. David Pérez-González

INFORME RAZONADO/REASONED REPORT

SOBRE LA CALIDAD CIENTÍFICA DE LA TESIS DOCTORAL (puede añadir las hojas que crea necesarias adjuntando a este informe)

ABOUT THE SCIENTIFIC QUALITY OF PhD (you can use all the pages you might need including this form)

The thesis entitled 'Functional mechanisms of neuronal mismatch in the auditory midbrain and the medial prefrontal cortex' prepared by PhD candidate, Lorena Casado Román, is an impressive document. It starts with a brief review of how context shapes our perception and the neural mechanisms that underpin this property of perception focussing on stimulus specific adaptation (SSA) as perhaps a neuronal equivalent of the human mismatch negativity (MMN) response. MMN is an automatic auditory brain potential elicited when an unexpected deviant sound is presented in background of predictable standard sounds. SSA is a distinct type of neuronal adaptation to repeated predictable stimuli while maintaining responsiveness to other different and unpredictable stimuli. The candidate's introduction briefly reviewing the various explanations of the mechanisms responsible for MMN is beautifully written and argued. It is a masterful exposition of the adaptation, deviance detection, and memory trace explanations of the phenomenon and demonstrates beautifully how the predictive coding framework incorporates all of the previous accounts of MMN generation. The candidate then outlines the hierarchical structure of cortical networks with feedforward and feedback connections that underpin predictive coding in general followed by a very nice presentation of the pathways and networks involved in sound processing, SSA and auditory predictive coding.

This review sets the scene for the first published study by the candidate which attempts to understand what distinguishes those cells in the inferior colliculus (IC) that exhibit SSA vs those that don't. The IC integrates inputs from a number of lower level auditory centres and is the first centre of the ascending auditory system that demonstrates SSA. This study published in Hearing Research is based on a detailed investigation of IC neurons in 10 mice and represents the first attempt to examine neuronal electrophysiological properties of adapting and non-adapting neurons and non-spiking neurons. Few differences were found – other than intrinsic properties probably related to potassium conductance. The results point to a need for future research focussing on analysing the properties and distributions of these potassium channels in order to understand how SSA is generated at the cellular level.

The second study published in PLOS Biology in contrast to the first paper that focusses on IC, the earliest auditory centre in the ascending auditory system exhibiting SSA, focusses on what would generally be regarded as the highest centre in the processing hierarchy, namely, the medial prefrontal cortex or mPFC. Strictly speaking the mPFC is not part of the auditory system but it is clear that many PFC cells respond to sound, although not demonstrating typical frequency responses that exemplify the response of cells in auditory cortex (AC). This study is a 'tour de force' – a beautiful piece of work. It builds on the methodology developed by the CANELAB that enables separation of the adaptation effects (more appropriately called in this context, repetition suppression) from deviance detection (or prediction error) and their contributions to the equivalent of MMN. What this study demonstrates is that in contrast to AC and lower levels of the auditory system, cells in most divisions of the rat mPFC exhibit only prediction error. This is true of both spike activity and LFPs. What is most surprising is the long latency of the response in both spike density recordings and LFPs, with responses not evident before 100 ms in most regions of mPFC and increasing slowly over a course or 200 ms before peaking. Comparison of the latencies of mPFC responses with those from AC using identical methodology and stimulus sequences shows that the AC response is completed before the onset of the mPFC responses consistent with a hierarchical relationship between AC and PFC. Furthermore, whereas earlier processing in AC and subcortical areas are mainly induced by stimulus-dependent effects, it is clear that the PFC response is qualitatively different and therefore not simply inherited from prior processing in the auditory system. The PFC response is driven by unpredictability producing delayed and long lasting responses that almost solely comprise prediction error signals and plausibly exerts top-down influences on AC. This is a very important paper and although further research is needed to demonstrate for example the mechanisms by which these top-down effects are implemented, it will have a major impact on the field.

It is my opinion that the thesis is ready for a public defence.

Informo que la calidad científica de esta Tesis es merecedora de obtener la Mención Doctor Internacional (marcar con una cruz una opción)

I inform that the scientific quality of this thesis is worthy of obtaining the International Doctor Mention (mark with across one option)

Favorable [X] No favorable/Not favorable [ ]

FECHA / DATE : 19 May, 2021

FIRMA / SIGNATURA original: Patricia G. Michie

SELLO DE LA INSTITUCIÓN DEL FIRMANTE / THE INSTITUTION'S STAMP OF THE PERSON WHO FIRMS

ESCUELA DE DOCTORADO
EDIFICIO MULTIUSOS I+D+I
C/ ESPEJO Nº 2 – 1ª PLANTA. 37007 SALAMANCA

MODELO DE INFORME DE MENCIÓN DOCTOR INTERNACIONAL

STANDARD FORM FOR THE INTERNATIONAL DOCTORATE MENTION

NOMBRE Y APELLIDOS / NAME OF THE EXAMINER

Yaneri A. Ayala

CATEGORÍA ACADÉMICA O PROFESIONAL/ ACADEMIC OR PROFESIONAL RANK

Investigadora Postdoctoral

UNIVERSIDAD U ORGANISMO Y PAÍS / UNIVERSITY OR INSTITUTION AND COUNTRY

New York University

TÍTULO DE LA TESIS OBJETO DE INFORME / TITLE OF THE TESIS

Functional mechanisms of neuronal mismatch in the auditory midbrain and the medial prefrontal cortex

NOMBRE Y APELLIDOS DEL DOCTORANDO / NAME OF THE CANDIDATE

Lorena Casado Román

NOMBRE Y APELLIDOS DEL DIRECTOR/A(S) DE LA TESIS / NAME OF THE THESIS DIRECTOR(S)

Prof. Dr. Manuel Sánchez Malmierca y Dr. David Pérez-González

INFORME RAZONADO/REASONED REPORT

SOBRE LA CALIDAD CIENTÍFICA DE LA TESIS DOCTORAL (puede añadir las hojas que crea necesarias adjuntando a este informe)
ABOUT THE SCIENTIFIC QUALITY OF PhD (you can use all the pages you might need including this form)

La presente tesis titulada 'Functional mechanisms of neuronal mismatch in the auditory midbrain and the medial prefrontal cortex' reune dos trabajos experimentales originales en el área de neurofisiología sensorial. El primer trabajo determina las propiedades intrínsecas de células nerviosas auditivas las cuales han sido ampliamente estudiadas anteriormente, pero con técnicas electrofisiológicas más sencillas. Estas técnicas sencillas de registro extracelular capturan únicamente la salida final de la activación neuronal. La técnica empleada en el primer estudio, i.e., registro intracelular permiten determinar como las propiedades biofísicas de las células modifican o generan esta activación final ante la presentación de sonidos frecuentes e infrecuentes. El segundo trabajo explora por primera vez la respuesta de neuronas de la corteza prefrontal de roedores a sonidos frecuentes e infrecuentes utilizando la técnica de registro extracelular, pero empleando una serie de protocolos de estimulación complejos que permite segregar diferentes señales cerebrales que contribuyen a la codificación diferencial de sonidos en función de su contexto de presentación. Este ultimo trabajo es exhaustivo no solo por los protocolos de estimulación empleados sino porque además caracteriza las propiedades funcionales de varias regiones corticales. Ambos trabajos cumplen con el rigor científico necesario para haber sido publicados en revistas arbitradas internacionales y a su vez, representan una contribución novedosa en el campo de la neurociencia auditiva tanto por las técnicas experimentales empleadas, así como por los datos neurofisiológicos obtenidos. La tesis no es un trabajo tradicional ya que no aborda una única pregunta general, sino que estudia una propiedad de respuesta neural desde dos extremos metodológicos y experimentales, i.e., a nivel intracelular en un núcleo subcortical de la vía nerviosa auditiva y a nivel extracelular en áreas corticales de alto orden jerárquico. Los resultados son satisfactoriamente interpretados y discutidos con datos e hipótesis de otras áreas del campo de la neurociencia tales como la psicofísica y modelaje matemático representado un esfuerzo por conectar diferentes campos de la neurociencia. Dicho lo anterior, considero que la tesis realizada por Doña Lorena Casado Román es un trabajo científico solido y valioso que no solo refleja un esfuerzo experimental considerable, sino que también contribuye con resultados novedosos y exhaustivos al entendimiento del procesamiento de señales novedosas en el cerebro de mamíferos. La tesis en su presente formato esta lista para una defensa publica.

Informo que la calidad científica de esta Tesis es merecedora de obtener la Mención Doctor Internacional (marcar con una cruz una opción)
I inform that the scientific quality of this thesis is worthy of obtaining the International Doctor Mention (mark with across one option)

Favorable [X] No favorable/Not favorable [ ]

FECHA / DATE : 19 Mayo 2021

FIRMA / SIGNATURA original:

SELLO DE LA INSTITUCIÓN DEL FIRMANTE / THE INSTITUTION'S STAMP OF THE PERSON WHO FIRMS

Contents

Abbreviations ..... **i**

Abstract ..... **iii**

1 General Introduction **1**

1.1. Neuronal adaptation and stimulus-specific adaptation 3

1.2. Auditory deviance detection 5

1.2.1. The memory trace or detection hypothesis 8

1.2.2. The adaptation hypothesis 8

1.2.3. The predictive coding framework 8

1.3. The pathways of sound processing 11

1.4. Hierarchical organization of auditory predictive coding 12

2 Study I: Intracellular SSA in the auditory midbrain **15**

2.1. Introduction 17

2.2. Hypothesis and Objectives 19

2.3. Summary of Results and Discussion 20

3 Study II: Prediction error signaling in the medial prefrontal cortex **23**

3.1. Introduction 25

3.2. Hypotheses and Objectives 27

3.3. Summary of Results and Discussion 28

4 General Discussion **35**

5 Conclusions **39**

6 Summary in Spanish/Resumen en Castellano 43

6.1. Introducción General 45

6.1.1. La adaptación neuronal y la adaptación específica a estímulos 45

6.1.2. Detección de la disparidad auditiva 46

6.1.3. Las vías de procesamiento del sonido 49

6.1.4. Organización jerárquica de la codificación predictiva auditiva 49

6.2. Estudio I: SSA intracelular en el mesencéfalo auditivo 51

6.2.1. Introducción 51

6.2.2. Hipótesis y Objetivos 52

6.2.3. Resumen de Resultados y Discusión 53

6.3. Estudio II: Señalización de errores de predicción en la corteza prefrontal medial 55

6.3.1. Introducción 55

6.3.2. Hipótesis y Objetivos 56

6.3.3. Resumen de Resultados y Discusión 58

6.4. Conclusiones 63

7 List of References 65

8 Publications 83

9 Acknowledgments/Agradecimientos 129

Abbreviations

AC	Auditory cortex
ACC	Anterior cingulate cortex
ERP	Event-related potential
FRA	Frequency response area
IC	Inferior colliculus
IL	Infralimbic cortex
iMM	Index of neuronal mismatch
iPE	Index of prediction error
iRS	Index of repetition suppression
LFP	Local field potential
M2	Secondary motor cortex
MGB	Medial geniculate body
MMN	Mismatch negativity
mPFC	Medial prefrontal cortex
PFC	Prefrontal cortex
PL	Prelimbic cortex
PSP	Postsynaptic potential
SSA	Stimulus-specific adaptation

Abstract

Context in the environment around us highly influences our perceptions and the neural processing of sensory information. This doctoral thesis studies the mechanisms that shape the neural representations of sounds depending on the context in which they occur. Neurons in all sensory systems adapt rapidly, preserving energy while simultaneously enabling stimuli with potential survival or behavioral relevance to use additional processing resources. Stimulus-specific adaptation (SSA) is a special type of neuronal adaptation, specific to repeated and predictable stimuli, while preserving responsiveness to other different, unexpected, and probably more informative input.

SSA has been linked to high-order brain processing such as deviance detection and perceptual inference. The nonlemniscal subdivisions of the inferior colliculus (IC) are the first sites in which these multifaceted coding properties emerge in the auditory hierarchy. Nevertheless, the molecular, cellular, and network mechanisms contributing to the generation of SSA are controversial and a matter of debate. SSA has been classically studied at the somatic spiking output, which results from the interaction of the synaptic inputs, its tuning characteristics, and membrane properties. Hence, in Study I, I report the passive properties, intrinsic properties, and auditory postsynaptic potentials under the oddball paradigm stimulation in 10 whole-cell patch-clamp recordings *in vivo* in the mouse IC (Valdés-Baizabal et al., 2020b). Although passive properties were similar, data suggest that intrinsic properties such as the firing patterns differed between lemniscal nonadapting and nonlemniscal adapting cells. SSA is absent at the synaptic level of the recorded neurons, which further demonstrates that SSA emerges in the nonlemniscal IC.

Ascending along the auditory hierarchy, the encoding of the spectral properties of sound is subsequently substituted by more abstract representations allowing the detection of contextual changes in prefrontal regions. These high-order areas have been classically studied for the generation of automatic deviance detection using the scalp-recorded mismatch negativity (MMN) using similar oddball paradigms that also elicit SSA. However, the mechanisms that generate MMN and its neuronal correlate are neither clearly located nor understood in frontal cortices. Thus, Study II analyses the mechanisms governing deviance detection under the oddball paradigm in the rat medial prefrontal cortex (mPFC) within the predictive processing framework (Casado-Román et al., 2020). My results demonstrate in all mPFC fields and cortical layers that unpredictable auditory stimulation elicited stronger responses than the weak or even absent activity driven by predictable sounds. The time course of prefrontal spiking and LFP activity coincides with

the large-scale MMN-like signals in the rat providing the missing link at the microscopic, mesoscopic, and macroscopic levels of automatic deviance detection. Hence, mPFC cells could model the possible neuronal correlate of the frontal MMN generators. Mismatch responses in mPFC are almost purely made of prediction error signaling activity and different in nature from those at the IC, auditory thalamus, and auditory cortex with an important effect of repetition suppression (comparisons with a previous study in our lab by Parras et al., 2017).

1 General Introduction

How can our brains ignore the continuous honking of car horns in a traffic jam but immediately react to the same sound of a horn when crossing a road? It's all about context: our perceptions and sensorineural processing are notoriously influenced by the surrounding context. This doctoral thesis aims to shed light and deepen our understanding on the mechanisms that shape the neural representations of sounds depending on the context in which they occur. One of these mechanisms refers to the neuronal adaptation that enables efficient information coding by reducing responsiveness to predictable, usual, irrelevant events while responding to unpredictable, uncommon, and more informative changes in the environment. This strategy preserves energy while simultaneously enables stimuli with potential survival or behavioral relevance to "stand out" and obtain additional processing resources. This allocation of the finite neuronal resources to the most improbable sensory input may also underlay an efficient general strategy of brain functioning known as perceptual inference.

1.1. Neuronal adaptation and stimulus-specific adaptation

The nervous system's ubiquitous adaptation capacities constitute a fundamental principle of its organization and function (Whitmire and Stanley, 2016). Adaptation enables flexible, efficient coding depending on the stimulation context while optimizing neuronal resources, energy expenditure, and maximizing the capacity of transmitting information (Barlow, 1961). Under sensory physiological terms, adaptation denotes the reduction of neuronal responses in a short time scale, spanning from milliseconds to a few minutes (Whitmire and Stanley, 2016). Sensory systems undergo receptive field adaptation, which constitutes the decrease in neuronal selectivity to the most common stimulus features, whereas the selectivity to the less common features is retained or even enhanced (Dragoi et al., 2000; Kohn, 2007). This is precisely the case for stimulus-specific adaptation (SSA), a distinct and singular type of neuronal adaptation to specific, repeated, and predictable stimuli while preserving responsiveness to other different or unpredictable stimuli (Movshon and Lennie, 1979; Ulanovsky et al., 2003). Thus, sensory neurons encode apart from the physical stimulus features, its relevance, and the degree of match/mismatch within the ongoing context. Not surprisingly, SSA has been linked to high-order brain processes as deviance detection and perceptual inference (see below *Auditory deviance detection*). Also, SSA has been described at different stages of sensory processing and across sensory modalities (Bibkov, 1977; Dalton, 2000; Ulanovsky et al., 2003, 2004; Kohn and Movshon, 2003; Reches and Gutfreund, 2008; Malmierca et al., 2009a; Antunes et al., 2010; Zhao et al., 2011; Duque et al., 2012; Dhruv and Carandini,

2014; Nieto-Diego and Malmierca, 2016; Musall et al., 2017). Neuronal responses are modulated by past experience and can adapt over multiple spatial and temporal scales, which suggests that a combination of molecular, cellular, and network mechanisms must be operating in parallel (Malmierca et al., 2014).

Intrinsic neuronal mechanisms are rapid changes in the cellular dynamics of passive membrane properties such as ion conductances and active membrane properties, including action potential thresholds. These changes translate into modifications of the neuronal sensibility such as nonspecific decrements of neuronal activity (i.e., fatigue-like effects) and most forms of dynamic range adaptation. Empirical evidence demonstrated that intrinsic membrane properties contribute to adaptive coding in the auditory cortex (AC; Abolafia et al., 2011) and other sensory-modal cortices (Schwindt et al., 1988; Carandini and Ferster, 1997; Sanchez-Vives et al., 2000a; Díaz-Quesada and Maravall, 2008).

Stimulus- or input-specific effects underlying receptive field adaptation cannot be exclusively explained by intrinsic membrane mechanisms (Nelken, 2014; Malmierca et al., 2015). Also, ***synaptic mechanisms*** such as activity-dependent depression of synapses (Chung et al., 2002; Wehr and Zador, 2005), increased inhibition (Zhang et al., 2003), and excitatory/inhibitory imbalance (de Ribaupierre et al., 1972; Volkov and Galazjuk, 1991; Ojima and Murakami, 2002; Oswald et al., 2006) are believed to play a role on SSA generation.

It seems unlikely that a single neuron can recognize and habituate to complex background regularities by itself. Nerve cells are interconnected, creating neuronal assemblies in which simple ***network mechanisms*** can underlie adaptation, such as disynaptic feedforward inhibition (Wehr and Zador, 2003; Isaacson and Scanziani, 2011). Adaptation of excitatory and inhibitory inputs, which interact in a complex manner, can affect feature selectivity and response timing (Whitmire and Stanley, 2016) and even efficient coding (Denève and Machens, 2016). Hence, SSA is probably a functional property of neuronal networks. Neurons with extensive dendritic arbors covering multiple sensory inputs would probably depress the recurrently activated synapses through plastic mechanisms. Therefore, the interaction of all intrinsic neuronal, synaptic, and network mechanisms is likely what enables the complex forms of adaptation encountered in neuronal responses. The degree to which these mechanisms contribute to generate SSA is addressed in Study I of intracellular recordings in the mouse inferior colliculus (IC).

1.2. Auditory deviance detection

Adaptation filters repetitive stimulation inputs and prevents that redundant information arrives at high processing levels. This simple adaptation only depends on the number of repetitions that a specific stimulus feature has been recently encountered, regardless of the complex structure or the input patterns' predictability. Therefore, adaptation alone does not allow separating uninformative sounds from more informative or unexpected events occurring approximately at the same frequency in the auditory scene. Deviance detection is then the brain´s ability to pre-attentively detect specific sensory events that do not match expectations generated by that regularity encountered in recent sensory stimulation. This deviance detection is a relevant aspect of auditory scene analysis, which might be at the basis of fast and efficient formation and segregation of auditory objects (Grimm and Escera, 2012). Brains generate perceptual mismatch signals, which reflect deviance detection mechanisms from predictions to unexpected sensory inputs (Zelano et al., 2011; Escera and Malmierca, 2014; Stefanics et al., 2014; Harms et al., 2016; Musall et al., 2017).

The human scalp-recorded mismatch negativity (MMN) reflects an automatic process of deviance detection. Since its discovery four decades ago (Näätänen et al., 1978; Näätänen and Michie, 1979), this biomarker has become a pivotal tool for cognitive and clinical research of the human brain (Kujala et al., 2007; Näätänen et al., 2007) and diagnostic application (Schall, 2016) in schizophrenia (Todd et al., 2013; Gaebler et al., 2015; Näätänen et al., 2016), Alzheimer's disease (Pekkonen, 2000; Horvath et al., 2018), autism spectrum disorder (Vlaskamp et al., 2017; Schwartz et al., 2018), and psychosis (Näätänen et al., 2016; Ranlund et al., 2016a), among others. The MMN reflects a processing mechanism that is key for survival (Fitzgerald and Todd, 2020). The brain automatically encodes regular patterns in the sensorium, creates internal models to explain away those regularities, whereas it detects deviations from the internal representations in upcoming sensory inputs.

MMN is usually studied using an oddball paradigm in which a deviant sound is embedded in a sequence of repeated standard sounds (Figure 1A). During electrophysiological recordings, neural responses to deviant, unpredictable tones are significantly larger than responses to predictable standard tones. This differential response during the oddball paradigm can be measured at the macroscopic level. For this, the scalp-recorded auditory event-related potential (ERP) elicited by a tone presented in the standard condition is subtracted from the ERP prompted by that same tone presented in the deviant condition. From this subtraction, a "mismatch" response (deviant – standard) is clear at temporal and frontal electrode recordings in the form of a slow negative

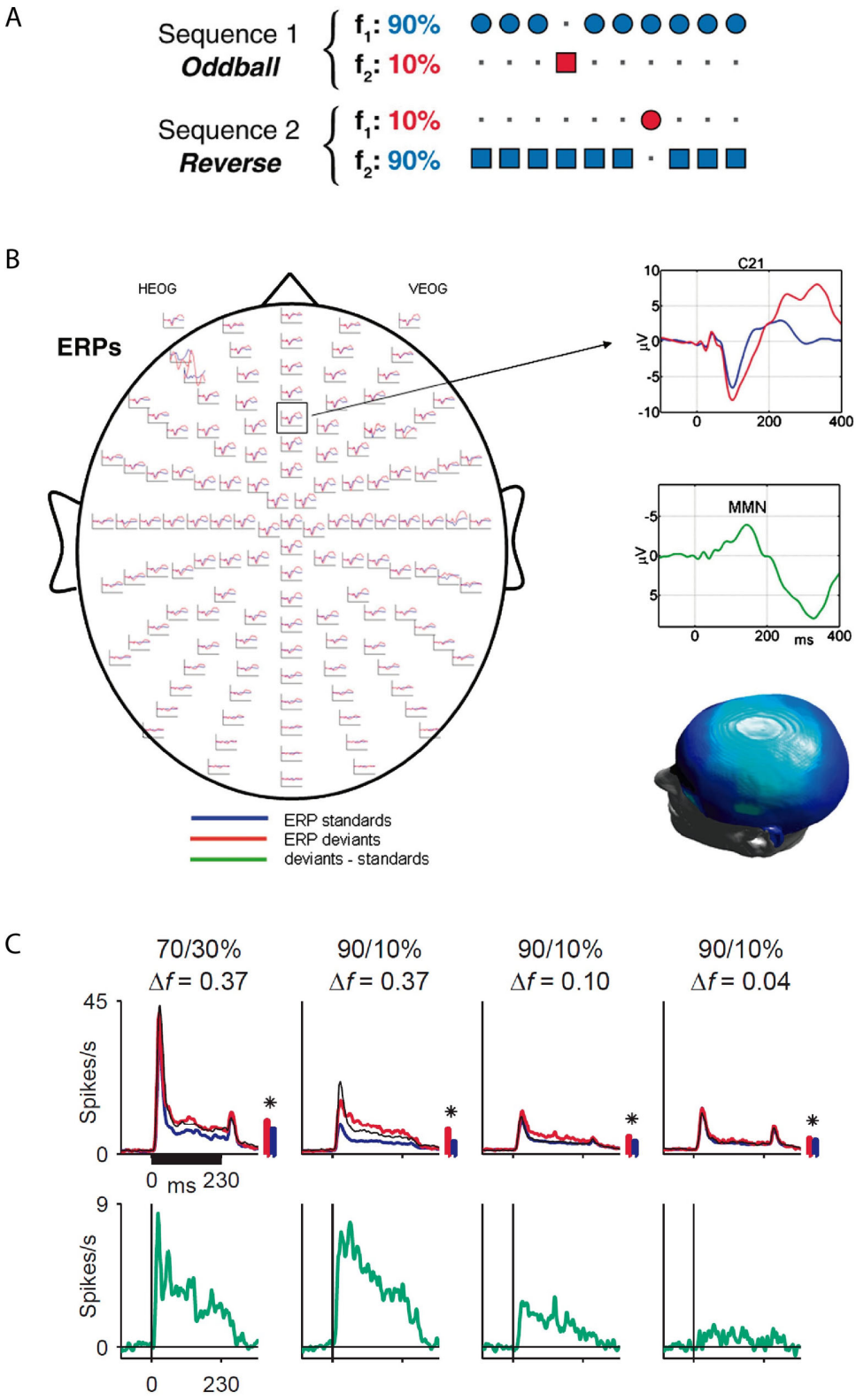

Figure 1. A, Example of the classic oddball paradigm with high probability standard tones (90%, blue) of frequency f_1 and low probability pseudorandom deviant stimuli (10%, red) of frequency f_2. In the reverse condition or the flip-flop design, the probability of the two frequency-tones is swapped to subtract frequency-specific effects from deviance contextual effects. Adapted from Pérez-González and Malmierca, (2014). **B,** Left, mean event-related potentials (ERPs) of standard and deviant tones overlaid on a scalp map of 128 electroencephalography electrodes. Right top, ERPs at a fronto-central channel (C21). Right middle,

mismatch negativity (MMN) response computed as the difference wave between deviants minus standards at the same channel. Right bottom, 3D scalp topography of mean MMN responses in the 100-200 ms time window. Adapted from Garrido et al., (2007). **C,** Population peristimulus time histograms of neurons in the cat primary auditory cortex to deviant (red) and standard (blue) tones at various probabilities and frequency separations between tones. Below, the difference signal between deviant minus standard stimuli. Adapted from Ulanovsky et al., (2003).

deflection giving the name of mismatch negativity (Figure 1B; Fitzgerald and Todd, 2020; Näätänen et al., 1978; Näätänen and Michie, 1979).

At the microscopic scale, the neuronal firing rate also ceases exclusively to stimuli at higher probability of occurrence despite their physical features, in the form of SSA (Figure 1C). The physiological connection of these similar phenomena at two different levels has been a matter of debate for decades. Due to the obvious functional similarities, cortical SSA has been suggested to be the neuronal correlate of the MMN (Ulanovsky et al., 2003; Jääskeläinen et al., 2004), causing an intense debate in the literature (Näätänen et al., 2005). Importantly, the presence of SSA has been demonstrated extensively in the auditory system of birds, insects, amphibians, and specially in multiple mammalian species (reviewed in Carbajal and Malmierca, 2020). Therefore, the physiological mechanisms that generate SSA are probably old and preserved during evolution. It seems reasonable to assume that SSA also takes place in the human brain, and it could consequently be the neural correlate of the MMN. Nevertheless, SSA and MMN still have some obvious dissimilarities, primarily due to the experimental limitations to record human neurons as done in animal research. More precisely, these animal experiments have confirmed their co-occurrence throughout the auditory pathway, in the IC, the medial geniculate body of the thalamus (MGB), and all over the AC (for review, see Carbajal and Malmierca, 2018). Notwithstanding, the link between MMN and SSA in nonauditory areas such as the integrative frontal cortices remains unexplored. Hence, Study II aimed to shed some light on this brain region.

Three main conceptual hypotheses have been put forward to explain the MMN generation; firstly, the memory trace or detection hypothesis is a cognitive approach based on MMN studies; secondly, the adaptation hypothesis is a neurophysiological interpretation based on SSA studies; lastly, the predictive coding framework which integrates and unifies the previous accounts.

1.2.1. The memory trace or detection hypothesis

The topographic distribution of the MMN shows a fronto-temporal network in charge of automatic deviance detection (Figure 1B; Näätänen et al., 1992; Opitz et al., 2002; Paavilainen et al., 2003). The classic cognitive interpretation of the MMN proposes that a sensory-memory of acoustic regularities is primarily encoded in temporal sources from the AC (Näätänen, 1990; Näätänen et al., 2007), allowing to detect specific sensory deviances between that memory trace and subsequent incoming input (Näätänen and Alho, 1995). Then, the behavioral relevance of that sensory deviance is assessed in sources from the prefrontal cortex (PFC) and potentially triggers an attention switch towards the change (Giard et al., 1990; Escera et al., 1998, 2003; Doeller et al., 2003; Costa-Faidella et al., 2017; Sikkens et al., 2019). This detection or memory trace hypothesis assumes that the sum of that neural activity that mobilizes cognitive resources to further process deviant events is reflected in the ERP as the MMN (Winkler et al., 1996; Näätänen and Winkler, 1999).

1.2.2. The adaptation hypothesis

The adaptation hypothesis challenged the detection account, offering a simpler physiological mechanism of synaptic adaptation to explain MMN with a more neurophysiologically grounded and parsimonious interpretation. This theory denies the existence of a genuine deviance detection process, arguing that the standard stimuli induce SSA due to passive mechanisms such as synaptic depression on AC neurons (Ulanovsky et al., 2003; Jääskeläinen et al., 2004). The frequency channels of AC neurons simply remain fresh to keep responding to the deviant tones (May and Tiitinen, 2010; Fishman, 2014). Despite the conceptual differences, the memory trace and the adaptation models agree that early AC processing is highly sensitive to specific stimulus features. Beyond the initial sensory discrimination processes, frontal activity seems more reliant on an overall evaluation of global properties (Alho, 1995; Fitzgerald and Todd, 2020).

1.2.3. The predictive coding framework

Recent proposals under the predictive coding framework have attempted to integrate the previous accounts of the MMN generation, establishing a hierarchical and reciprocal relationship across sensory processing levels (reviewed in Garrido et al., 2009c; Carbajal and Malmierca, 2018, 2020). The predictive processing framework is a renewed conceptual

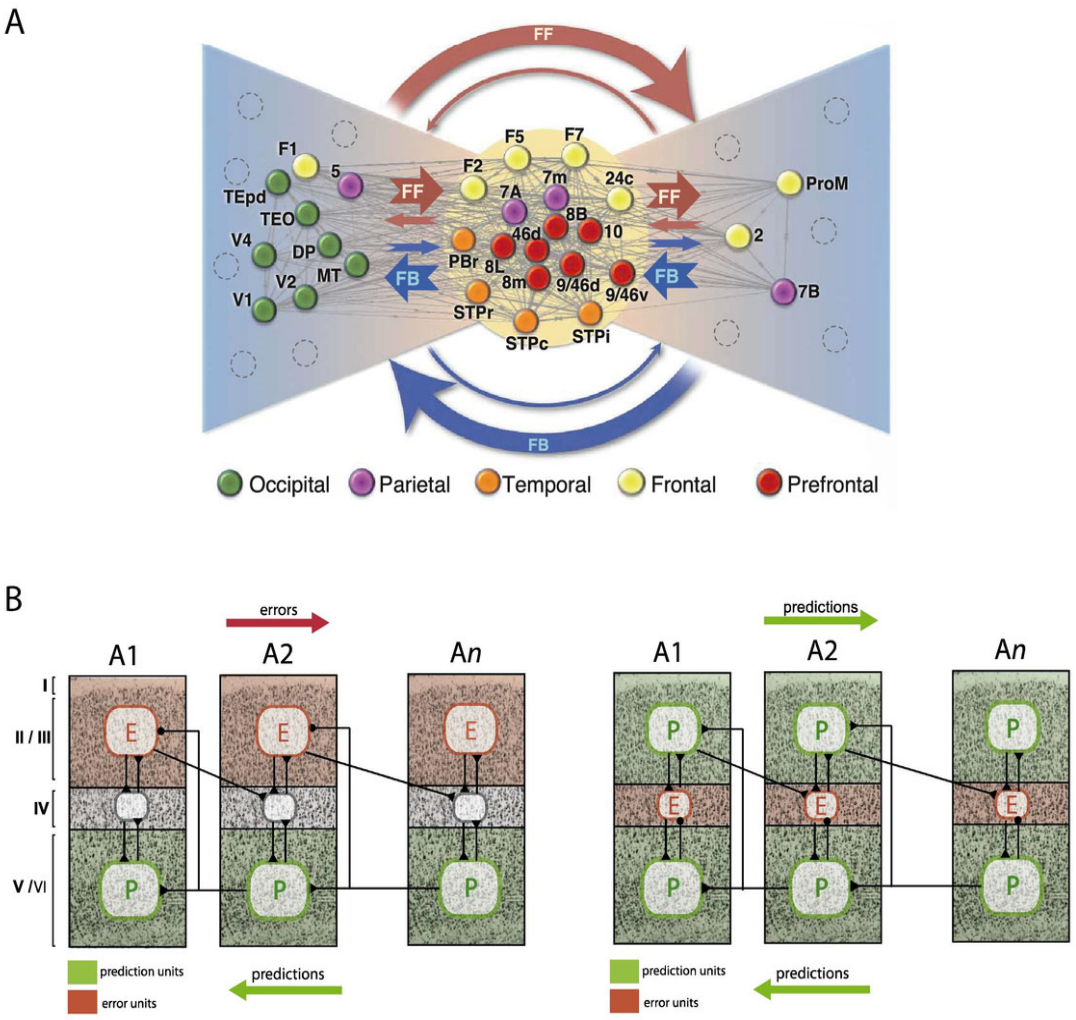

Figure 2. *Functional architecture of cortical connectivity*. **A,** Macaque cortical topology depicted as a bow-tie representation based on connectivity tracer studies. Heavily interconnected fronto-parietal areas form the core. The tie emerges from the core with feedforward (FF) and feedback (FB) connections with the early sensory areas placed at the extremes. Adapted from Markov et al., (2013). Abbreviations: 2, lateral postcentral gyrus; 5, Brodmann Area (BA) 5; 10, frontopolar prefrontal cortex; 24c, lower bank of the anterior cingulate sulcus; 46d, dorsolateral prefrontal cortex; 7A, BA 7A; 7B, BA 7B; 7m, medial posterior parietal cortex; 8B, frontal eye fields; 8L, lateral prefrontal cortex; 8m, medial prefrontal cortex; 9/46d, mid-dorsolateral frontal cortex; DP, dorsomedial portion of the prelunate gyrus; F1, primary motor cortex; F2, premotor dorsal, caudal; F5, premotor ventral, rostral; F7, premotor dorsal, rostral; MT, middle temporal visual area; PBr, rostral parabelt; ProM, proisocortical motor cortex; STP, superior temporal polysensory area; TEO, temporo-occipital area; TEpd, dorsal subregion of posterior visual association area TE; V1, primary visual cortex; V2, secondary visual cortex; V4, visual area V4. **B,** Two simplified examples of different circuits proposed for the neurobiological implementation of predictive coding based on the differential computational roles across cortical layers. They depict hierarchically arranged cortical columns between primary (A1), secondary (A2), and higher-order (An) auditory areas. Left, the canonical microcircuit of predictive coding proposes that errors flow bottom-up whereas predictions top-down (Bastos et al., 2012). Above the input layer (4), error units are located in supragranular layers (2/3), while prediction units are in the infragranular layers (5/6). Prediction units of higher hierarchical levels can suppress error units at lower levels through feedback inhibitory connections (notice black circles compared to excitatory triangles). Right, other predictive coding models posit that prediction errors are computed in the input layers (Spratling, 2008a, 2008b). Predictions flow bottom-up in the supragranular layers and top-down in the infragranular

layers. Prediction units exerted inhibition intracolumnarly, whereas feedback connectivity among areas is excitatory. Adapted from Heilbron and Chait, (2018).

framework and unifying general account to explain how the brain makes sense of the world or a neurobiologically informed theory of perceptual inference (Rao and Ballard, 1999; Friston, 2009; Heilbron and Chait, 2018). This account sits on the classical and general ideas from Helmholtz, back in the 19th century formulated in a renewed conceptual framework with mathematical models based on the Bayes' Theorem (Friston, 2003, 2005, 2010, 2018; Hohwy, 2013; Swanson, 2016; Aitchison and Lengyel, 2017). In his study of vision, Helmholtz (1867) incorporated the traditional Kantian thought affirming that humans cannot directly access the world, and all the information humans have about it comes through our senses. Hence, perception is strongly affected by top-down influences or prior beliefs instead of being conceived as a purely bottom-up process (Kant, 1781; Helmholtz, 1867). Perception is understood as a process of unconscious inference about the causes of the sensory neural activity relying on our prior beliefs.

The predictive coding account considers SSA and MMN as the respective microscopic and macroscopic signs of automatic deviance detection with a unified explanation of their emergence at both scales (Garrido et al., 2009c; Carbajal and Malmierca, 2018, 2020). Mismatch responses are widely regarded as a signature of prediction error signals in predictive coding terms (Friston, 2005, 2010; Garrido et al., 2009c; Bastos et al., 2012; Stefanics et al., 2014). Under the predictive coding framework, brains are considered hierarchically organized systems within distributed neuronal networks (Figure 2A). Each level compares the bottom-up sensory input from the level below with the top-down predictions of the higher level. During perceptual learning, when an incoming input is repeated, statistical regularities of the natural world are learned such that forthcoming inputs are predicted. Prediction error signals are suppressed through a process of repetition suppression. Conversely, if a new stimulus arrives, such as a deviant event, there will be a failure to predict the bottom-up input and suppress the prediction error signal. The prediction error will be forwarded to the level above to update the more abstract predictive model that will be subsequently fed back as a new expectation (Figure 2B). This process continues iteratively until the prediction error is explained away and the expectations fit to the actual sensory input from lower levels. Consequently, perception emerges from the hierarchy of causal inferences in which each level is restricted by the processing of its nested levels (Friston, 2003).

1.3. The pathways of sound processing

The mammalian auditory system is complex and includes several brainstem and forebrain structures. Auditory information is progressively processed and forwarded from the ears to higher auditory areas through multiple relay stations and synaptic interruptions. The mechanical pressure waves of sound are transduced into electrical signals in the cochlea. From the cochlea, the auditory information is sent through the cochlear nuclear complex, the superior olivary complex, and the nuclei of the lateral lemniscus. The sensory information is funneled into the midbrain at the IC and then, it is forwarded to the MGB of the thalamus and the AC. Multiple neuronal populations with different structural and functional characteristics form all these structures. The neuronal populations receive excitatory and inhibitory inputs, which may arise from a few or many sources, including commissural connections between both hemispheres, other sensory-modal areas, and modulatory systems (reviewed in Oliver et al., 2018).

At the IC level in the midbrain, two parallel processing systems emerge; the lemniscal and nonlemniscal pathways (Figure 3). The lemniscal pathway includes the central nucleus of the IC, the ventral division of the MGB, and the primary fields in the AC. These anatomical structures are at the core of their respective auditory centers, with sharply tuned neurons organized tonotopically following a bottom-up flow of sensory input (Malmierca, 2015). Responses in the lemniscal pathway are essentially driven by the physical sound features. By contrast, the nonlemniscal pathway encloses the lemniscal areas within the IC's cortices, the dorsal and medial divisions of the MGB, and the nonprimary ACs. Their neurons are broadly tuned with longer response latencies and more diffuse tonotopic organization with more integrative functions. Nonlemniscal cells receive inputs from lemniscal divisions, other nonlemniscal areas, and the AC. Their output is sent bottom-up to the next nonlemniscal division and from the AC top-down to nonlemniscal areas back again (Saldaña et al., 1996; Malmierca and Ryugo, 2011).

Thus, the central auditory system is functionally organized in a hierarchical manner (Grimm and Escera, 2012; Parras et al., 2017; Oliver et al., 2018). Each structure receives both bottom-up and top-down projections that highly preserve the topographical organization of the cochlear frequency map (Oliver et al., 2018). More multifaceted computations occur successively as one ascends in the auditory processing hierarchy up to the frontal lobes. In the AC, auditory objects are already assembled and recognized (Nelken, 2004) and the PFC plays a chief role in contextual processing essential for deviance detection and perceptual inference (Deouell, 2007; Fogelson et al., 2009; Chao et al., 2018).

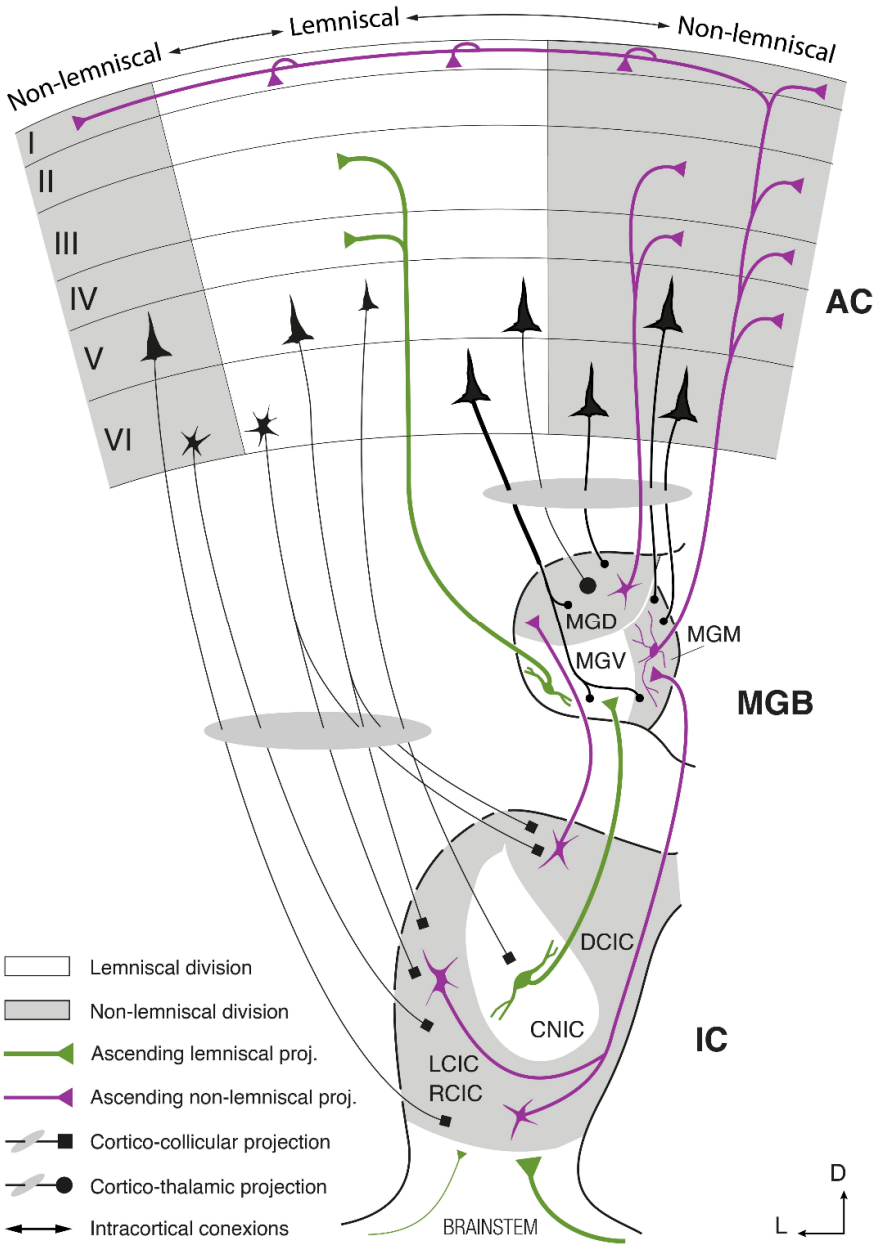

Figure 3. *Schematic representation of the connectivity among the principal subdivisions of the rat IC, the auditory thalamus (MGB), and the AC.* The lemniscal pathway presents tonotopic laminae connecting with the same lamina in the next level and receives limited cortical inputs. Nonlemniscal subdivisions connect mainly with higher nonlemniscal levels while receiving dense cortical projections. Abbreviations: CNIC, central nucleus of the inferior colliculus; DCIC, LCIC and RCIC: dorsal, lateral, and rostral cortex of the inferior colliculus, respectively; MGD, MGM and MGV: dorsal, medial, and ventral division of the medial geniculate body, respectively. Adapted from Malmierca et al., (2015) and Carbajal and Malmierca, (2018).

1.4. Hierarchical organization of auditory predictive coding

The hierarchical organization of the auditory system with dense feedforward and feedback connections makes it a suitable substrate to ascertain the predictive coding theory. Indeed, predictive activity is hierarchically organized along two anatomical axes: from lemniscal towards nonlemniscal regions and from the IC to the MGB, and to the AC as demonstrated in awake and anesthetized rodents (Parras et al., 2017).

To distinguish genuine deviance detection from the effects caused by SSA, the repetition suppression effect of the standard stimuli in the oddball paradigm needs to be controlled. For this, the many-standards control sequence presents the stimulus of interest within a random sequence of different tones, where each tone shares an equal occurrence probability as the deviant condition in the oddball paradigm (Schröger and Wolff, 1996). Nevertheless, it has been argued that this sequence of a disorganized succession of tones precludes from forming the memory trace of a proper *regularity* as the standard condition does. By contrast, the cascade control sequence addresses the alleged caveats of the many-standards sequence by presenting tones in a *regular* increasing or a decreasing frequency succession (Ruhnau et al., 2012). Therefore, the stimulus of interest conforms to *regularity* as opposed to the deviant event, but contrarily to the standard condition, the *regularity* is not established by repetition and prone to undergo SSA. Hence, the cascade sequence is more suited and less conservative control than the many-standards sequence.

With these control sequences, mismatch signals can be quantitatively decomposed into repetition suppression and prediction error signaling (Figure 4). The proportion of prediction error, which explains the neuronal mismatch responses, increases from the IC to the MGB and to the AC, while repetition suppression decreases. Therefore, the adaptation hypothesis or SSA can only account for the mismatch signals of the subcortical lemniscal pathway, whereas predictive activity takes place along the nonlemniscal pathway and the entire AC (Figure 4; Parras et al., 2017, 2020; Valdés-Baizabal et al., 2020a).

The AC is believed to encode sensory stimulation's spectral properties, suppressing responsiveness to redundant auditory input based on the frequency-specific features via short-term plasticity mechanisms (Garrido et al., 2009b, 2009c; Carbajal and Malmierca, 2018). During an oddball paradigm, this would be functionally observable as SSA or repetition suppression (Baldeweg, 2006; Garrido et al., 2009b; Costa-Faidella et al., 2011; Todorovic and de Lange, 2012; Auksztulewicz and Friston, 2016). The sensory information that the predictive model in the AC cannot explain is sent as a bottom-up prediction error signal to higher levels in the processing hierarchy (Friston, 2005, 2009). Eventually, the feedforward flow of prediction errors reaches PFCs. The PFC tries to explain prediction errors away forming higher-order expectations of the sound's emergent properties, such as abstract interstimulus relations and structures (Garrido et al., 2008, 2009a, 2009b). Hence, the AC generates fast purely auditory prediction errors, whereas PFCs would generate prediction errors when more abstract expectations are not met in the current predictive model, requiring its update. Despite the multiple hypotheses of the MMN

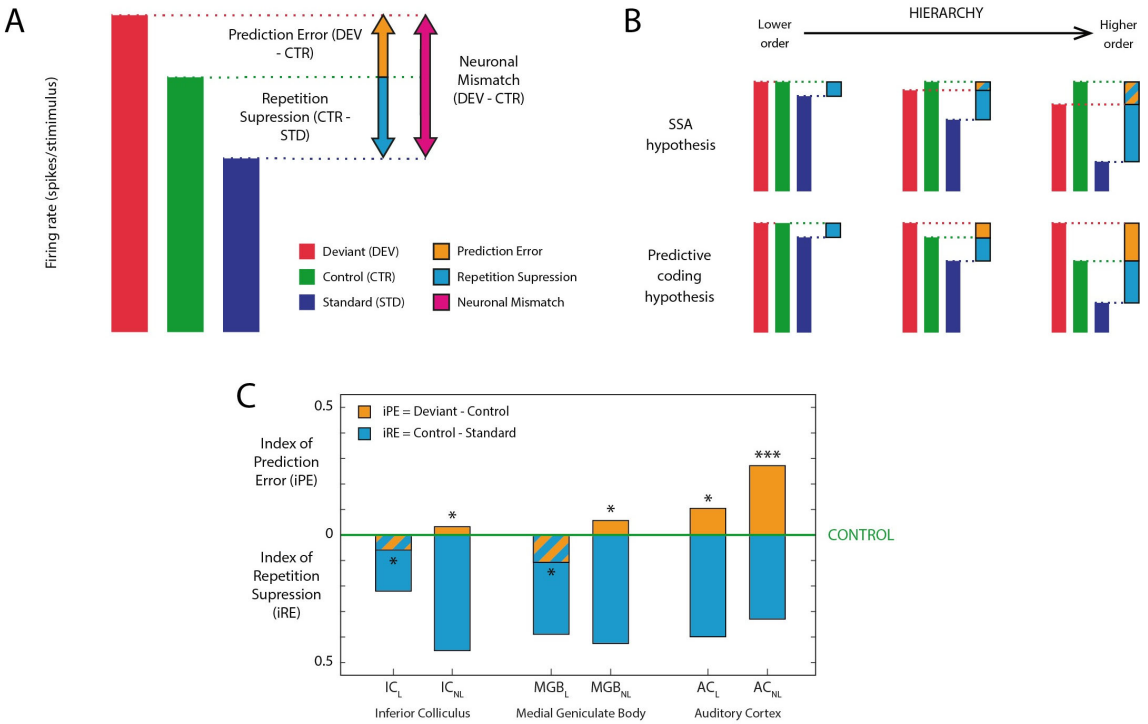

Figure 4. *Experimental design and main results of the study of hierarchical prediction errors from Parras et al., (2017).* **A,** Neuronal mismatch of the oddball paradigm can be computed as the sum of the indices of prediction error and repetition suppression with the cascade or many-standards control sequence. **B,** Two possible mechanisms account for the neuronal mismatch depending on the influence of prediction error and repetition suppression. In the SSA or adaptation hypothesis, deviant responses are mainly explained by stimulus-dependent effects due to a higher response for the control condition. Response suppression to the standard increases from lower to higher processing levels, and due to the relative suppression of the deviant to the control, the index of prediction error becomes increasingly negative. In the predictive coding hypothesis, a positive index of prediction error emerges since context-dependent effects of interstimulus relationships dominate over stimulus-dependent effects in deviant responses. Response suppression to the standard increases from lower to higher processing levels, and deviant responses become larger than the control. **C,** Adaptation effects dominate in the lemniscal IC (IC_L) and auditory thalamus (MGB_L), whereas predictive activity emerged in the nonlemniscal IC (IC_{NL}), auditory thalamus (MGB_{NL}), and the entire AC (AC_L, AC_{NL}). Adapted from Parras et al., (2017).

generation, its neuronal substrate remains elusive and poorly understood in frontal areas. Animal models can serve to define the neuronal substrate of the human MMN and ratify its generation hypotheses as covered in Study II of the rat medial prefrontal cortex (mPFC). The PFC exerts this modulatory role over the sensory hierarchy innervating relatively low levels of the hierarchy as the IC (Fogelson et al., 2009; Olthof et al., 2019).

2 Study I: Intracellular SSA in the auditory midbrain

2.1. Introduction

The IC in the mammalian auditory system is located in the dorsocaudal portion of the midbrain. The IC is the earliest known anatomical source of SSA and predictive coding activity (Ayala and Malmierca, 2013; Parras et al., 2017; Duque et al., 2018; Valdés-Baizabal et al., 2020a). Almost all auditory pathways ascending through the brainstem converge in the IC (Malmierca et al., 2002) and, therefore, cover a pivotal position in the vertebrates' auditory system (Malmierca, 2003, 2015; Kandel et al., 2013; Ito and Malmierca, 2018). Each IC receives bilateral ascending inputs, but the majority is from the contralateral side. Due to its neuroanatomical complexity, the IC has been suggested to play a similar role in the auditory system to that of the primary visual cortex in vision (King and Nelken, 2009).

The IC is made of a central nucleus surrounded by the collicular cortices in humans, other mammals, and even nonmammalian clades (Geniec and Morest, 1971; Morest and Oliver, 1984; Oliver and Morest, 1984; Malmierca, 1991, 2003, 2015; Malmierca and Ryugo, 2011). The rodent IC, a large, oval-shaped structure, is among the most studied ones (Figure 5; Malmierca et al., 2009b; Ito and Malmierca, 2018). The ICs of both hemispheres are interconnected by a large and heavily myelinated commissure (Saldaña and Merchán, 1992; Malmierca et al., 1995, 2009b). The rodent IC is subdivided into the central nucleus within the lemniscal pathway and the surrounding cortices (dorsal, lateral, and rostral) belonging to the nonlemniscal pathway (Faye-Lund and Osen, 1985; Coleman and Clerici, 1987; Zook and Casseday, 1987; Malmierca et al., 1993; Ito and Malmierca, 2018). A key feature of the IC is that it is the origin center of two parallel pathways of sound processing: the lemniscal and the nonlemniscal. Both pathways exhibit multiple connectivity patterns and neuronal-type organizations (Ito and Malmierca, 2018).

The IC is almost a mandatory relay structure for all ascending auditory pathways, which converge there before innervating the thalamus and AC. The central nucleus takes most of the ascending information from the cochlear nuclei, the superior olivary complex, and the nuclei of the lateral lemniscus. The central nucleus of the IC receives massive ascending information from the brainstem in tonotopically organized thin fibrodendritic laminae. Each lamina processes a single frequency band or a narrow frequency channel. By contrast, the cortices have a layered circuitry that resembles the neocortex, suggesting advanced pattern recognition capabilities. These cortical subdivisions receive more mixed inputs with substantial projections from the central nucleus, the contralateral IC, excitatory, inhibitory, and neuromodulatory cortical innervation, and even nonauditory inputs (Saldaña and Merchán, 1992; Malmierca et al., 1995; Winer and Schreiner, 2005; Cant and Oliver, 2018).

Even if multiple approaches tried to classify neuronal types in the IC with molecular profiles, morphological and electrophysiological properties, there is no simple correlation among classes defined with different methods (Ito and Malmierca, 2018). Most IC neurons are considered glutamatergic or GABAergic (gamma-aminobutyric acid), and glycine seems not to be used (Tanaka and Ezure, 2004; Ito et al., 2011). Morphological characterizations of the IC have defined two main classes in the central nucleus: flat or disc-shaped cells with flattened dendritic arbors extending parallel to the laminae and less flat or stellate cells in the interlaminar compartments with dendritic arbors extending across the laminae (Morest and Oliver, 1984; Malmierca et al., 1993). The dendritic morphologies of IC cortices are less known with multiple neuron types, varying across the layers and subdivision (Malmierca et al., 2011; Ito and Malmierca, 2018).

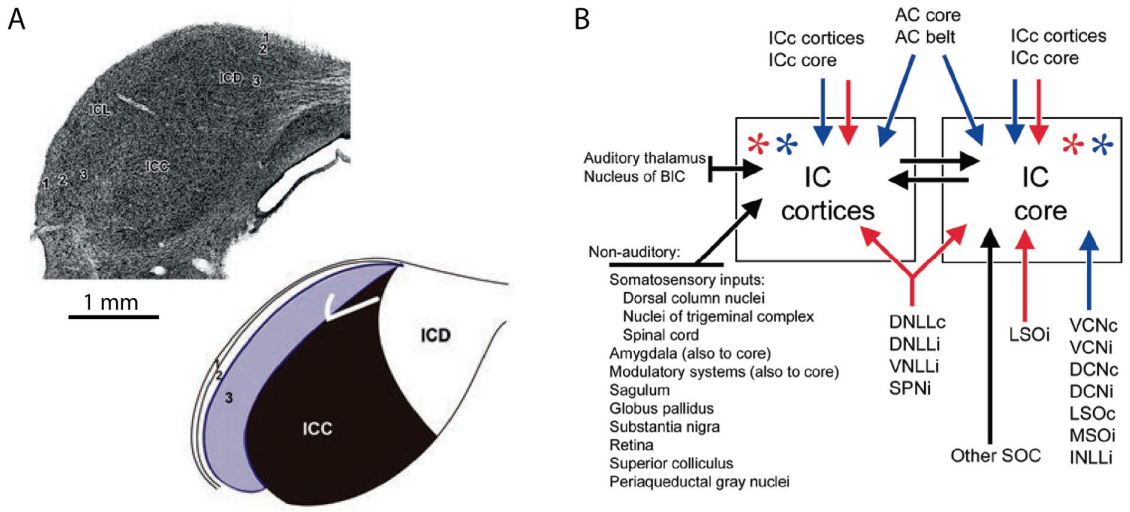

Figure 5. **A,** Cytoarchitecture of the rat IC demonstrating the central nucleus (ICC), dorsal cortex (ICD), lateral cortex (ICL) subdivisions, and its three layers in a coronal histological section (Nissl staining, left) and a schematic diagram (right). Adapted from Loftus et al., (2008); Ito et al., (2011); Ito and Malmierca, (2018). **B,** Summary diagram of the projections received by the IC. Known excitatory (blue) and inhibitory (red) inputs are colored, and uncharacterized synaptic effects are in black. Asterisks denote excitatory and inhibitory synaptic inputs arising from cells intrinsic to the structure. Abbreviations: BIC, brachium of the inferior colliculus; c, contralateral; DCN, dorsal cochlear nucleus; DNLL, dorsal nucleus of the lateral lemniscus; i, ipsilateral; INLL, intermediate nucleus of the lateral lemniscus; LSO, lateral superior olive; MSO, medial superior olive; SOC, superior olivary complex; SPN, superior paraolivary nucleus; VCN, ventral cochlear nucleus; VNLL, ventral nucleus of the lateral lemniscus. Adapted from Cant and Oliver, (2018).

The physiology of the IC neurons demonstrates a large variety of auditory-evoked responses, which can be inherited from lower brainstem nuclei or emerge *de novo* from the integration of diverse inputs from multiple nuclei. The intrinsic membrane properties differ between the central nucleus and the cortices and play a role in encoding sound-evoked discharges (Ito and Malmierca, 2018). Neurons in the central nucleus show onset

and various types of sustained firing patterns in response to depolarizing current injections, which are well suited for temporal and intensity information coding (Peruzzi et al., 2000; Sivaramakrishnan and Oliver, 2001; Tan et al., 2007). Firing patterns of the IC cortex show fewer neuron types with regular firing in the lateral cortex (Ahuja and Wu, 2007) and sustained and buildup responses in the dorsal cortex (Sun and Wu, 2008).

A fundamental physiological characteristic of the nucleus of the IC is its tonotopic organization. Low-frequency sounds are located in the dorsolateral laminae, and higher-frequency sounds are progressively encoded more ventrally (Schreiner and Langner, 1997; Malmierca et al., 2008). Pure tone stimulation induces multiple frequency response areas (FRA), including V-shaped (sharply tuned) and non-V-shaped ones in single units from the central nucleus (Palmer et al., 2013). Moreover, these neurons demonstrate onset, on-sustained, pauser, sustained, and regular responses to pure tones (Duque et al., 2012) and are sensitive to sound duration (Pérez-González et al., 2006), binaural stimulation, and sound location (Zhang and Kelly, 2010). By contrast, the cortices exhibit multisensory integration similarly to higher levels of the nonlemniscal auditory pathway (Malmierca and Ryugo, 2011; Olthof et al., 2019). This unique local circuitry enables the emergence of multifaceted coding properties of auditory information such as SSA, deviance detection (Hernández et al., 2005; Malmierca et al., 2009a; Zhao et al., 2011; Duque et al., 2012; Ayala and Malmierca, 2013), and auditory prediction error signaling (Parras et al., 2017; Valdés-Baizabal et al., 2020a).

2.2. Hypothesis and Objectives

The IC integrates multiple auditory inputs from ascending and descending pathways (Ito and Malmierca, 2018), and it is precisely the site of emergence of SSA (Pérez-González et al., 2005; Malmierca et al., 2009a; Ayala et al., 2013; Duque et al., 2018). However, the mechanisms that mediate SSA generation are elusive and still under debate. SSA has been classically studied at the somatic spiking output, which results from the interaction of the synaptic inputs, the tuning characteristics of those inputs, and the membrane properties such as the spiking threshold. To date, there are no studies that analyze within the same IC neurons their intrinsic properties, subthreshold responses, and the level of acoustic SSA. In consequence, I specifically propose the hypothesis:

In the IC, adapting neurons exhibiting SSA differ in their intrinsic neuronal properties and/or subthreshold responses from those nonadapting neurons lacking SSA.

Therefore, the objectives of Study I were two:

1. Determine whether SSA properties correlate with the intrinsic neuronal properties, passive membrane properties, and subthreshold responses.

2. Correlate within single cells, the degree of adaptation from their synaptic inputs with the SSA levels of the spiking output.

2.3. Summary of Results and Discussion

In this study, I report the passive properties, intrinsic properties, and auditory postsynaptic potentials (PSP) of whole-cell patch-clamp recordings *in vivo* in the anesthetized mouse IC, while stimulating with current injections and the oddball paradigm (Valdés-Baizabal et al., 2020b). The data obtained from these 10 neuronal examples shows that the passive properties such as membrane capacitance, membrane resistance, and resting membrane potential were similar. However, among the analyzed intrinsic properties (firing pattern, action potential threshold, depolarizing *sag* of hyperpolarizing pulses, and rebound action potentials), only the firing patterns differed between adapting and nonadapting neurons (cells with or without SSA, respectively). Nonadapting cells demonstrated a sustained-regular firing pattern and V-shaped FRAs that corresponded to central nucleus neurons, whereas adapting cells at the IC cortices showed variable firing patterns and non-V-shaped FRAs. The current results indicate that SSA is not present at the synaptic level in the IC neurons. I also observed a small trend towards hyperpolarized membrane potentials and increased synaptic inhibition with consecutive stimulus repetitions, suggesting a simpler type of adaptation, potentially related to potassium conductances.

The neuronal firing pattern, which is dependent on the interaction of several voltage-dependent ion conductances (Rutecki, 1992), is a key feature to distinguish between adapting and nonadapting neurons in our sample. All nonadapting neurons showed a sustained-regular firing, abundant in neurons of the central nucleus of the IC (see Figure 6 & Table 6 in Valdés-Baizabal et al., 2020b; Peruzzi et al., 2000; Sivaramakrishnan and Oliver, 2001; Tan et al., 2007), probably due to a high degree of persistent sodium currents (Chatelier et al., 2010; Boeri et al., 2018). By contrast, adapting neurons showed variable firing patterns, including sustained, accommodating, and burst onset cells, which are more

typical of the IC cortices (Geis et al., 2011). Interestingly, I also observed differences in the neuronal receptive fields. FRAs of nonadapting neurons showed typical V-shapes of the central nucleus of the IC, whereas adapting neurons showed non-V-shaped FRAs without a clear characteristic frequency common in the IC cortices (Malmierca et al., 2009a; Duque et al., 2012; Ayala and Malmierca, 2013; Palmer et al., 2013; Duque and Malmierca, 2015).

Adaptation could be primarily due to decreases in PSP probability even if the PSP amplitudes are stable. I observed a similar amplitude of sound-evoked PSPs received for deviant and standard conditions by each neuron, regardless of the degree of spiking SSA. Because both frequencies selected for the oddball paradigms fell within the receptive field, neurons consistently demonstrated PSPs to both tones. Although PSP amplitudes and conductances varied along with auditory adaptation in the MGB (Jia et al., 2021) and the AC (Wehr and Zador, 2005; Abolafia et al., 2011), differences in synaptic inhibition and excitation do not predict the levels of spiking SSA in the IC. The relative timing of inhibition can also influence adaptation. Nevertheless, only inhibition for standards was faster in nonadapting than in adapting neurons. Indeed, synaptic depression is expected to be weak at the 3-4 Hz presentation rate as used in the current study (Bartlett and Smith, 2002; Malmierca et al., 2009a; Pérez-González and Malmierca, 2014).

Along the auditory system, the cochlear nuclei and the superior olivary complex lack SSA (Ayala et al., 2013; Duque et al., 2018), but as early as the cortical regions of the IC, SSA is robust (Pérez-González et al., 2005; Malmierca et al., 2009a; Lumani and Zhang, 2010; Ayala et al., 2013; Duque and Malmierca, 2015; Duque et al., 2018). I studied whether this spiking SSA in the IC results from PSP adaptation. Neurons in the IC cortices receive auditory inputs from other IC neurons and the AC (Malmierca et al., 1995, 2005, 2009b; Loftus et al., 2008; Malmierca and Ryugo, 2012; Malmierca, 2015; Cant and Oliver, 2018; Ito and Malmierca, 2018). Our sample showed variable synaptic adaptation, with weak or no SSA in some cases, clear synaptic SSA in a couple of neurons, and even reduced deviant excitatory PSP amplitudes coupled with spiking SSA. Hence, synaptic adaptation fails to foresee the presence of spiking SSA in this study. Nevertheless, SSA has been previously observed at subthreshold levels in the AC (Hershenhoren et al., 2014; Wang et al., 2014; Chen et al., 2015) due to synaptic depression of thalamocortical projections (Chung et al., 2002; Katz et al., 2006). Therefore, considering the absence of synaptic SSA in the IC and previous evidence where despite AC deactivation, subcortical SSA is maintained (Antunes and Malmierca, 2011; Anderson and Malmierca, 2013; Malmierca et al., 2015), the nonlemniscal IC is postulated as the first site at the auditory pathway where SSA emerges.

I observed a subtle trend towards hyperpolarized membrane potentials in adapting neurons and increased synaptic inhibition with increasing standard repetitions at the population level (see Figure 4 in Valdés-Baizabal et al., 2020b). This denotes a moderate level of adaptation only observed when a stimulus is consecutively repeated. Similarly, adaptation in the cat primary visual cortex was linked with a subtle tonic hyperpolarization (Carandini and Ferster, 1997). These tendencies at the population level suggest a simpler type of adaptation related to potassium conductances, which have been associated with sensory adaptation in the barrel (Díaz-Quesada and Maravall, 2008), sensorimotor (Schwindt et al., 1988), and visual cortices (Sanchez-Vives et al., 2000a, 2000b; Wang et al., 2003). The activation of potassium currents hyperpolarizes the membrane potential, decreasing the neuronal responsiveness to subsequent synaptic inputs from tens of milliseconds to tens of seconds. Such slow time courses are supported by the dynamics of intracellular ions such as the Na^+ and the binding/unbinding to K^+ channels (Abolafia et al., 2011). These potassium currents play a role as activity-dependent mechanisms of adaptation (Malmierca et al., 2014). The depolarization and high-frequency firing during sensory responses cause the activation of voltage-dependent potassium currents and ions such as Ca^{2+}, and Na^+ rise intracellularly, activating ion-dependent K^+ channels (Sah and Faber, 2002; Bhattacharjee and Kaczmarek, 2005; Rabang et al., 2012). This cascade of events occurs equally for deviant and standard conditions and can explain similarities among responses.

Although the present work represents a first important step in understanding intracellular SSA responses *in vivo* in the IC, conclusions should be considered as example case reports and be strengthened by further studies, increasing the sample. The present results show the potential for future studies of this type to understand how SSA is generated at the cellular level. I demonstrated the similarity of excitatory or inhibitory synaptic inputs that each neuron receives regardless of their SSA properties at the spiking activity. Synaptic SSA was variable and could not be used to predict the presence of spiking SSA. These data suggest that intrinsic properties may contribute to classifying adapting and nonadapting neurons since they displayed different firing patterns. Therefore, future studies will need to be expanded with pharmacological manipulations to disentangle specific ionic channel participation.

3 Study II: Prediction error signaling in the medial prefrontal cortex

3.1. Introduction

In the mammalian brain, the PFC comprises the neocortex covering the front portion of the frontal lobe. The PFC is not a sensory processor *per se* but rather an executive center involved in functions such as attention, working memory, rule learning, temporal processing, planning, and decision making (Dalley et al., 2004; Kesner and Churchwell, 2011). In natural conditions, the PFC integrates the information it receives from multiple input structures to generate very complex cross-modality sensorimotor representations and converges updated information to output structures (Hoover and Vertes, 2007; Parr et al., 2019).

The rodent PFC is divided into three subregions based on their cytoarchitecture and connectivity patterns: the lateral PFC or insular cortex, the orbitofrontal cortex, and the mPFC (Figure 6). The mPFC covers most of the middle walls between the anterior hemispheres and the dorsal part above the knee of the corpus callosum (Sarter and Markowitsch, 1983, 1984; Sesack et al., 1989; Condé et al., 1990, 1995; Divac et al., 1993). The rat mPFC can be further subdivided into at least four main cytoarchitectonic areas: medial agranular cortex or secondary motor cortex (M2, area Fr2), anterior cingulate cortex (ACC, area 24), prelimbic cortex (PL, area 32), and infralimbic cortex (IL, area 25 in the primate; Gabbott et al., 1997; Hoover and Vertes, 2007; Uylings et al., 2003; van Eden and Uylings, 1985; Vogt and Paxinos, 2014).

Primates and rodents share a general hierarchical organization principle despite different connectivity patterns of PFCs, which is one of the most relevant aspects to validate investigations into hierarchical predictive coding at the neuronal level inaccessible in human brain research (Uylings et al., 2003; Seamans et al., 2008). The rodent mPFC integrates anatomo-electrophysiological components of the primate dorsolateral PFC and the ACC at a rudimentary level and is studied to understand the general function of PFCs (Brown and Bowman, 2002; Seamans et al., 2008).

As typical in the neocortex, the PFC is formed mainly by excitatory pyramidal neurons projecting to cortical and extra-cortical areas and 10-20% of GABAergic inhibitory interneurons (Dégenètais et al., 2002; DeFelipe et al., 2013). The rat mPFC is characterized by the lack of granular or layer 4 (van Eden and Uylings, 1985; Uylings et al., 2003) and a gradual transition along the dorsoventral axis from the typical neocortex to three layers with unclear laminar boundaries (Figure 6C; van Eden and Uylings, 1985).

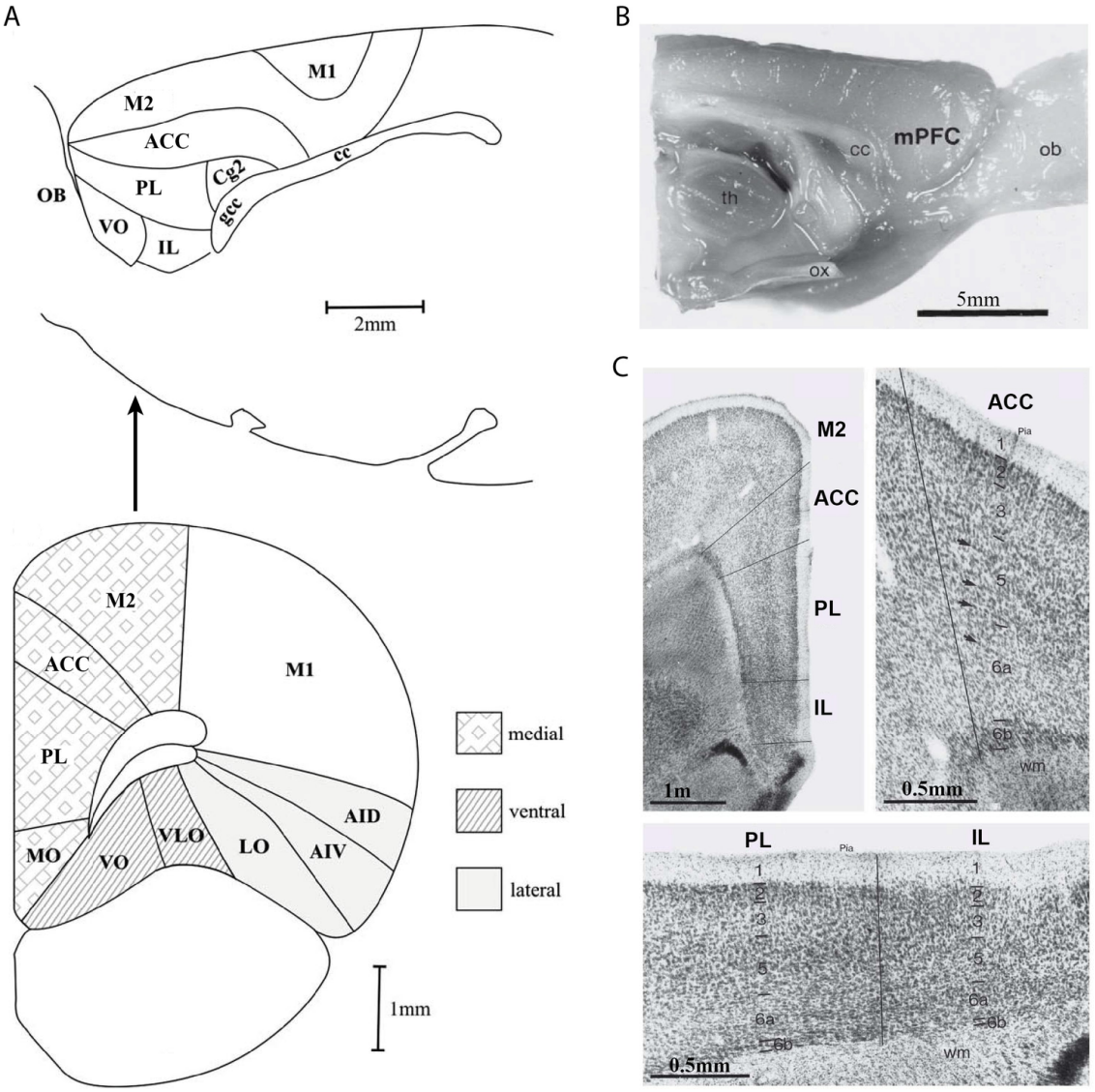

Figure 6. A, Schematic diagram of the medial, ventral and lateral rat PFC. Lateral view at 0.9 mm from the midline and unilateral coronal section at the arrow level (~3.5 mm rostral from bregma). Adapted from Dalley et al., (2004). **B,** Macroscopic structure of the rat mPFC of the left hemisphere. **C,** Cytoarchitecture of the rat mPFC in coronal Nissl staining histological sections. The cortical layer distribution is marked in the different fields at higher magnification. Abbreviations: ACC, anterior cingulate cortex; AID, dorsal agranular insular cortex; AIV, ventral agranular insular cortex; cc, corpus callosum; Cg2, cingulate cortex area 2; gcc, genu of the corpus callosum; IL, infralimbic cortex; LO, lateral orbital cortex; M1, primary motor cortex; M2, secondary motor cortex; MO, medial orbital cortex; OB, ob, olfactory bulb; ox, optic chiasm; PL, prelimbic cortex; th, thalamus; VLO, ventrolateral orbital cortex; VO, ventral orbital cortex; wm, white matter. B, C modified from Gabbott et al., (1997).

Efferent connections from the mPFC to subcortical areas mainly originate in layers 5/6. This efferent connectivity differentiates the dorsal M2 and ACC from the ventral PL and IL (Gabbott et al., 2005; Heidbreder and Groenewegen, 2003). Similarly, the primary sources of afferent connections shift along the dorsoventral axis from sensory, motor, and association cortical inputs to the dorsal M2 and ACC to primarily limbic afferents to the ventral PL and IL (Hoover and Vertes, 2007). Layers 2/3 receive dense cortico-cortical

projections (Douglas and Martin, 2004; Riga et al., 2014), but layer 5 also receives long-range inputs from other prefrontal areas, including the contralateral mPFC, the agranular insula, the motor cortical regions, as well as the dorsal polymodal thalamic nuclei and other subcortical regions (Uylings and Van Eden, 1991; Denardo et al., 2015). Moreover, the dorsal M2 and ACC have feedforward connections from the AC. The ventral PL and IL receive mainly limbic inputs and are strongly connected with the dorsal mPFC; therefore, auditory information may arrive through this projection (Martin-Cortecero and Nuñez, 2016).

The PFC is believed to exert a modulatory role over the sensory hierarchy. This role is critical for contextual processing and, thus, in deviance detection and predictive coding (Fogelson et al., 2009). Even relatively low levels of the hierarchy, such as the IC, receive dense projections from high hierarchical areas as the mPFC (Olthof et al., 2019). Moreover, it is important to highlight that this processing in the PFC is affected in many psychiatric and neurological disorders (Gaebler et al., 2015; Ranlund et al., 2016b).

3.2. Hypotheses and Objectives

Many hypotheses account for the generation of the MMN, but its neuronal correlate in frontal areas is neither clearly located nor understood. This is primarily due to the ethical limitations of human research studies (Rinne et al., 2000; Edwards et al., 2005; Rosburg et al., 2005; Deouell, 2007; Tse and Penney, 2008; Dürschmid et al., 2016; Nourski et al., 2018a). Conveniently, the use of invasive techniques in animal models ensures enough spatial and temporal resolution to determine whether AC mismatch potentials precede or coincide with those of the PFC. Spiking and local field potential (LFP) activity can offer the specific time course and location of mismatch signals at the microscopic and mesoscopic levels, respectively (Hamm and Yuste, 2016; Nieto-Diego and Malmierca, 2016; Parras et al., 2017). Simultaneously, I can correlate the local-scale mismatch signals with the epidural large-scale MMN-like potentials in the corresponding animal model, which are regarded as the specific analog of the human MMN (Harms et al., 2014, 2016). Therefore, animal studies facilitate and serve to define the neuronal correlate of the human MMN and prove its generation hypotheses.

The predictive processing framework has recently attempted to integrate the former adaptation and memory trace hypotheses for the MMN generation, establishing a hierarchical and reciprocal interconnection between the AC and PFC (reviewed in Garrido

et al., 2009c; Carbajal and Malmierca, 2020). The AC would first suppress redundant auditory inputs based on the spectral features of the sensory stimulation through short-term plasticity mechanisms such as lateral inhibition and synaptic depression (Garrido et al., 2009b, 2009c; Carbajal and Malmierca, 2018). Hence, I propose the following hypothesizes:

1. Redundant information is filtered before reaching the mPFC by means of repetition suppression because it is explained away and suppressed in lower levels of the hierarchy, such as the AC.

2. Unpredictable or unexplained auditory information at lower levels of the processing hierarchy is forwarded as a prediction error signal to higher levels such as the mPFC.

3. mPFC encodes more abstract representations such as complex interstimulus relationships and structures by means of higher-order expectations regarding emergent properties of the auditory sequences.

In consequence, in the present work, I studied the following objectives:

1. Determine the influence of prediction error and repetition suppression under an acoustic oddball paradigm using two no-repetition controls, namely, the many-standards, and the cascade sequences, as well as the deviant alone paradigm in the mPFC.

2. Establish a possible neuronal substrate of the large-scale MMN-like potentials of the rat brain by recording simultaneously ERPs and spiking activity in one possible frontal source, the mPFC.

3. Study the predictive coding hierarchy of mismatch signals, with special emphasis on the mPFC as a further step from previous data in the IC, MGB, and AC (Parras et al., 2017).

3.3. Summary of Results and Discussion

In this work, I studied the mechanims that govern deviance dectection in the anesthetised rat mPFC (M2, ACC, PL and IL; Casado-Román et al., 2020). I analyzed multiunit and LFP responses to the auditory oddball paradigm, deviant alone condition (Näätänen et al.,

1989), and suitable no-repetition controls, namely, the many-standards (Schröger and Wolff, 1996) and cascade sequences (Ruhnau et al., 2012; see Figure 1 in Casado-Román et al., 2020). I found that the four mPFC fields and supra- (2/3) and infragranular (5/6) layers were largely equivalent in the evoked responses. Unpredictable auditory stimulation prompted stronger responses than the weak, or even absent, activity elicited by sounds that could be expected. Whereas mismatch responses in the auditory system are mainly evoked by stimulus-dependent effects (Parras et al., 2017), I found that auditory responsiveness in the mPFC was driven by unpredictability, yielding context-dependent, comparatively delayed, more robust, and longer-lasting mismatch signals. The time course of the mismatch responses recorded in the mPFC spiking and LFP activity correlated with that of the frontal sources of the large-scale MMN-like potentials reported in the rat brain (Imada et al., 2013; Harms et al., 2014; Jodo et al., 2019). Most importantly, these data indicated that mismatch responses of the mPFC are almost purely made of prediction error signaling activity, in contrast to the mismatch responses recorded throughout the auditory system in a previous study by Parras et al. (2017) in our lab.

Across the four fields of the mPFC, the cascade, and the many-standards sequences worked as largely equivalent controls, probably generating an expectation of a succession of pitch alternations regular in time (Horváth and Winkler, 2004; Mittag et al., 2016; Parras et al., 2017; Wiens et al., 2019). Therefore, the auditory-evoked responses of the control conditions were suppressed to a certain extent, but without inducing stimulus-specific effects of repetition suppression as those of the standard condition. By contrast, responses to unexpected auditory stimulation of the deviant and deivant alone conditions (statistically comparable as previous evidence; Imada et al., 2013) peaked earlier and doubled or even tripled in magnitude the response elicited by the predictable control and standard conditions. The robust mismatch between responses to unexpected and predictable conditions resulted in similarly high values of the index of neuronal mismatch (iMM = deviant – standard) and the index of prediction error (iPE = deviant – control). Conversely, the low and insignificant values of the index of repetition suppression (iRS = control – standard) suggest a rather irrelevant influence of frequency-specific effects in the mPFC. Hence, the mismatch signals evoked in the mPFC by the auditory oddball paradigm are best explained as pure prediction error signaling (see Figure 3 in Casado-Román et al., 2020).

Previous reports from other frontal sources have found analogous results in spite of using different methodologies, recording techniques, and model species. A great predominance of deviant over standard and/or control responses was reported in the

spiking activity of the orbitofrontal cortex of anesthetized and alert mice (Srivastava and Bandyopadhyay, 2020), PFC of awake macaques (Takaura and Fujii, 2016; Camalier et al., 2019), ERPs above the frontal cortices of awake rats (Harms et al., 2014; Jodo et al., 2019) and frontal electrocorticography in human patients (Rosburg et al., 2005; Dürschmid et al., 2016; Phillips et al., 2016; Nourski et al., 2018a). The different prefrontal locations analyzed in the studies above across species should not be hastily regarded as direct homologs (Seamans et al., 2008). However, despite different connectivity patterns of PFCs, primates, and rodents share a general hierarchical organization principle, which is one of the most relevant conditions validating investigations into hierarchical predictive coding at the neuronal level inaccessible in human research (Uylings et al., 2003; Seamans et al., 2008). Consistently, all these works confirm that unpredictability is the key driver of auditory responsiveness in the frontal cortices.

The results from the present study demonstrated a distinct link between prediction error signaling at microscopic and mesoscopic levels because the time course of prediction error spiking coincides with all the significant prediction error-LFP modulations in every mPFC field. At the macroscopic level, ERPs from awake rats exhibited strong mismatch responses beginning around 40 ms poststimulus onset (Imada et al., 2013; Harms et al., 2014; Jodo et al., 2019). Similarly, both our spiking and LFP activity confirmed that prediction error signaling starts around 40 ms poststimulus onset in the AC until around 150 ms when the PFC takes over and continues prediction error signaling beyond 600 ms poststimulus onset (see Figure 6 in Casado-Román et al., 2020). Furthermore, the strongest MMN-like potentials are reported in the time window between 100–500 ms (Imada et al., 2013; Harms et al., 2014; Jodo et al., 2019), precisely when the most intense prediction error spiking and LFP activity takes place in the mPFC. Hence, our data allow to correlate the microscopic, mesoscopic, and macroscopic levels at which prediction error signaling and automatic deviance detection can be detected in the rat PFC. Since the so-called MMN-like potentials are considered as the rat analog of the human MMN (Harms et al., 2016), our results model the possible neuronal substrate of the frontal MMN generators.

To achieve a more general perspective of auditory deviance detection and mismatch responses in the rat brain, I compared our results with previous work from our lab with a similar methodology (Parras et al., 2017; see Figure 6 in Casado-Román et al., 2020). The adaptation hypothesis could only be validated in the subcortical lemniscal pathway (IC and MGB), whereas predictive activity was identified at the nonlemniscal IC, the nonlemniscal MGB, the entire AC, and the mPFC (Parras et al., 2017; Carbajal and Malmierca, 2018). Auditory sensitivity in mPFC cells seemed solely dependent on contextual or abstract

characteristics, whereas processing in the auditory system was clearly driven by the spectral properties of the sound (Nieto-Diego and Malmierca, 2016; Parras et al., 2017). These findings are consistent with reports in the AC and dorsolateral PFC of the alert macaque (Camalier et al., 2019). Although the iRS in the rat AC can still account for more than half of the mismatch responses (Parras et al., 2017), the mPFC shows negligible or even insignificant values of iRS, thus, dismissing any relevant spectral influences in PFC processing.

Interestingly, while iMM values in the AC and the mPFC of anesthetized rats are analogous, iPE values are significantly different. This means that the nature of mismatch signals at the AC is distinct from those at the PFC, despite been paired in their magnitude. For this reason, generators at both the AC and the PFC are prominent contributors to the MMN. However, their contributions are fundamentally different in nature, something that has been advocated since the classic sensory-memory or memory trace interpretation of the human MMN (Giard et al., 1990; Näätänen, 1990; Näätänen et al., 1992, 2007), and has also been inherited by the more modern predictive processing framework (Carbajal and Malmierca, 2020; Garrido et al., 2009). The iPE can account for 90% of the iMM value, and both indices are significantly similar and analogous in most mPFC fields. Hence, prefrontal mismatch responses can be safely interpreted as genuine deviance detection in classic terminology or pure prediction error signaling in predictive processing terminology.

Following this logic, the mPFC would be generating a high-order abstracted mismatch response *de novo*, signaling deviance or a prediction error without reflecting the low-level spectral properties of the driving acoustic input, which have been already represented at earlier processing regions of the auditory system (Parras et al., 2017; Carbajal and Malmierca, 2020). This interpretation is consistent with the substantial latency disparities observed between the AC and the mPFC in our anesthetized rats and the orbitofrontal cortex of anesthetized and awaked mice (Srivastava and Bandyopadhyay, 2020), and even the dorsolateral PFC of alert macaques (Camalier et al., 2019). Even though AC responses to pure tones take just a few milliseconds to emerge (Nieto-Diego and Malmierca, 2016; Parras et al., 2017), evoked responses in the mPFC take hundreds of milliseconds to appear. Additionally, the mPFC only needed two stimulus repetitions to explain away redundant standard input, being much faster than the lemniscal and nonlemniscal ACs, which took more than twice as long (Nieto-Diego and Malmierca, 2016; Parras et al., 2017; see Figure 6 in Casado-Román et al., 2020). This suggests that AC and PFC processing occurs to a certain extent in a sequential manner, as described by both the classic sensory-memory (Näätänen et al., 2007) and the predictive processing hypotheses (Garrido et al., 2009c) of the MMN generation. Acoustic deviances from spectral

regularities must be detected first, at the AC (temporal sources), and only after that, the PFC (frontal sources) can identify global and behaviorally relevant deviations from more abstract internal representations.

Given that the PFC responds much later to sound but suppresses redundant auditory input more effectively than the AC, the mismatch signals registered at the PFC cannot be simply inherited or amplified subsequently from the auditory system. The inverse hierarchical arrangement, proposed by the predictive coding framework (Garrido et al., 2009c), is thereby more plausible. The PFC is an executive center and not a sensory processor *per se*. In more natural conditions, the PFC most likely integrates various inputs to generate very complex cross-modality sensorimotor representations (Hoover and Vertes, 2007; Parr et al., 2019). The gestalt acquired at the PFC could be fed back to the AC, generating specific expectations in its native format, the spectral domain. However, this feedback signal ultimately regards higher-order properties such as interstimulus relationships, auditory tokens, or sequence structures that could not have been computed otherwise at the local AC circuitry. This top-down predictive activity would exert an inhibitory influence on AC responsiveness whenever a certain auditory input is already explained by the prefrontal gestalt. However, any unpredicted information would be conveyed bottom-up as a prediction error to update the internal PFC representation. Thus, hierarchical predictive coding can explain why the PFC shows longer latencies than the AC while also performing more efficient and general expectation suppression, capable of fully explaining away standard input, and even the control sequences. As soon as auditory information becomes redundant to the global auditory scene, it halts reaching the PFC, preventing cognitive overload, and saving high-order processing resources for more productive endeavors.

More recently, this causal role of top-down signals has been further evidenced with the reduction of contextual selectivity of deviance-detecting cells after suppressing mPFC inputs to the primary visual cortex (Hamm et al., 2021). Our results suggest that the mPFC generates and maintains an internal memory representation of the stimulation sequence by means of perceptual learning. Hence, the prolonged neuronal firing may represent an intracortical recurrent message passing among or within hierarchically disposed processing levels. The unique mPFC microcircuitry made of dense recurrent intrinsic connectivity and extrinsic connections with a range of brain areas is an ideal anatomical substrate to support complex computations such as the prediction error suppression (Wang et al., 2006; Zaborszky et al., 2015; Parr et al., 2019). Four main divisions comprise the mPFC with a shift of afferent projections from a majority of sensorimotor inputs to the M2 and ACC to mostly limbic inputs, including the amygdala, to the PL and IL (Hoover

and Vertes, 2007). It is likely that nonauditory subcortical nuclei such as the amygdala (Kiehl et al., 2005; Czisch et al., 2009; Camalier et al., 2019), or the hippocampus (Barascud et al., 2016; Rummell et al., 2016), could compute prediction errors and then sent the signal to the PFC for further processing and integration. Indeed, it has been recently demonstrated that the emergence of robust and long-lasting mismatch signals in the mouse orbitofrontal cortex is controlled from the nonlemniscal MGB through the basolateral amygdala (Srivastava and Bandyopadhyay, 2020). Therefore, all these auditory and nonauditory subcortical nuclei could be important middle players in the automatic process of deviance detection and prediction error signaling reflected in the MMN. This possibility should be further explored in future studies.

The theoretical implementations of the predictive coding hypothesis assume that expectations and prediction errors are computed by separated neuronal types distributed across different cortical layers, which should result in characteristic laminar profiles (Bastos et al., 2012; Keller and Mrsic-Flogel, 2018). In contrast to what predictive coding models expect, I have been unable to identify any significant response differences between infra- and supragranular layers of the mPFC. This lack of differences across layers could be due to the unspecific nature of the multiunit measurements. Notwithstanding, the concrete role of neuronal types and their laminar distribution is still under intense debate within the predictive coding framework. Multiple possible but conflicting implementations have been proposed, and empirical evidence from human research is mixed (reviewed in Heilbron and Chait, 2018). In fact, previous attempts to find a laminar distribution of mismatch responses fitting the standard implementation of cortical predictive coding (Bastos et al., 2012) agreed in the mouse primary visual cortex (Hamm et al., 2021) but also failed in the rat and mouse ACs (Szymanski et al., 2009; Rummell et al., 2016; Parras et al., 2017). The functional relationship across fields, brain areas, and cortical layers awaits future studies. For instance, a more detailed functional correlation of predictive activity across areas could be tested with dynamic causal modeling, and neurons could be allocated to feedforward and feedback layers with current-source density analyses (Garrido et al., 2009a; Bastos et al., 2015; Phillips et al., 2016; Keller and Mrsic-Flogel, 2018). In addition, the specific contribution of different neuronal types such as somatostatin- and parvalbumin-positive interneurons, which are known to be involved in the generation of mismatch responses in primary sensory cortices, merits further investigation (Chen et al., 2015; Natan et al., 2015; Hamm and Yuste, 2016).

The MMN is a notorious, obligatory element of the human ERP, remaining persistent in situations where consciousness is absent, e.g., during sleep (Nashida et al.,

2000; Strauss et al., 2015), anesthesia (Koelsch et al., 2006; Quaedflieg et al., 2014), or even coma (Morlet and Fischer, 2014; Rodríguez et al., 2014). Hence, the fact that I was able to record very robust mismatch responses in the rat mPFC under anesthesia further strengthens the link between our dataset and human MMN evidence.This indicates that predictive coding takes place in the auditory system even in the absence of consciousness. Moreover, previous studies of mismatch responses in both, the rodent auditory system and PFC did not find significant differences between anesthetized and awake preparations (Duque and Malmierca, 2015; Ayala et al., 2016; Parras et al., 2017; Srivastava and Bandyopadhyay, 2020). Notwithstanding, direct comparisons between awake and anesthetized evidence should be considered with care, especially in higher-order cortical areas with minimized cortical feedback connectivity (Mashour and Hudetz, 2017), or extrapolating possible behavioral implications from the conclusions presented in our study (Nourski et al., 2018b).

Last, the predictive coding theory posits to explain perceptual brain function across sensory modalities and species. Results similar to ours have also been reported in humans and other sensory modalities. Human evidence demonstrated that visual (Stefanics and Czigler, 2012; Cléry et al., 2013) and somatosensory oddball experiments (Zhang et al., 2019) encountered mismatch responses and visual predictive activity with a sequence of randomly rotating stimuli comparable to our many-standards control in PFC (Kimura and Takeda, 2015). Hence, the neurons recorded in the current study may represent a neuronal substrate of mismatch signals classically measured at the frontal network scale in rats across sensory modalities.

In sum, the present findings demonstrate that mPFC neurons signal the detection of unpredictable stimuli in the auditory scene and support a hierarchical predictive model of perceptual processing, where prediction errors propagate bottom-up. The mPFC acts as one of the highest levels in the hierarchy and likely exerts top-down control over the AC. I uncover that neuronal predictive activity in the form of prediction error signaling underlies mismatch signals in the mPFC. The AC and PFC have prominent MMN generators but, with a fundamentally different contributuion in nature ascertaining and unifying both, the classic memory trace and the more recent predictive processing interpretations. These neurons most likely create the neuronal basis of prediction error signaling and automatic deviance detection. These findings provide an incentive for future studies to discover how these neurons interact in microcircuits to generate sensory predictions.

4 General Discussion

The present PhD thesis includes the results of two electrophysiological studies performed with intracellular and extracellular recordings in mice and rats at two very different areas of auditory sensory processing, respectively. This work allowed to follow the emergence of auditory SSA or mismatch responses from the IC to one of the highest areas in the sensory hierarchy, the mPFC, which also exerts a modulatory role back to the auditory hierarchy. I have based my work on the study of both, the neurophysiological mechanisms and the hypotheses for the generation of automatic deviance detection.

I have demonstrated two different mechanisms taking place at two very different levels of the processing hierarchy to encode mismatch responses from the auditory scene. At the IC, responses are governed by low-level stimulus-dependent effects, whereas at the PFC context-abstract features can be already computed to exert an inhibitory influence at lower levels of the hierarchy. The adaptation hypothesis can only be endorsed in the subcortical lemniscal pathway, whereas predictive activity is clear at the subcortical nonlemniscal pathway, the entire AC, and the mPFC. Remarkably, mismatch responses are different in nature with an important effect of repetition suppression along the auditory system, whereas they are almost entirely comprised of prediction error signaling activity at the mPFC. These context-selective computations in hierarchically organized circuits are key for behavior, survival, and deficient in many psychiatric disorders.

5 Conclusions

1. Nonadapting neurons show V-shaped FRAs, and sustained-regular firing patterns distinctive of the lemniscal IC. By contrast, adapting neurons show non-V-shaped FRAs, and diverse firing patterns characteristic of the nonlemniscal IC.

2. SSA is absent at the synaptic level of the recorded IC neurons, which further demonstrates that SSA emerges in the nonlemniscal IC throughout the auditory pathway.

3. In all mPFC fields and cortical layers, unpredictability drives auditory responsiveness with comparatively delayed, more robust, and longer-lasting mismatch responses than the auditory system.

4. Prefrontal mismatch responses are explained as genuine deviance detection or pure prediction errors. These responses are context-dependent abstracted from spectral properties and thus, fundamentally different from those at the AC. This supports the sensory-memory and the predictive coding interpretations of the MMN generation.

5. The mPFC generates a precise repetition expectation that suppresses responsiveness to redundant and predictable inputs more efficiently and faster than the AC supporting a hierarchical predictive processing.

6. The time course of prefrontal spiking and LFP activity coincides with the large-scale MMN-like signals in the rat. This fact provides the missing link at the microscopic, mesoscopic, and macroscopic levels of automatic deviance detection. Hence, mPFC cells could model the possible neuronal correlate of the frontal MMN generators.

6 Summary in Spanish

Resumen en Castellano

6.1. Introducción General

El contexto que nos rodea influye profundamente en nuestra percepción y procesamiento neurosensorial. Esta tesis doctoral tiene como objeto ampliar nuestro conocimiento sobre los mecanismos que modelan las representaciones neuronales de los sonidos en función del contexto en el que ocurren. La adaptación neuronal es uno de estos mecanismos y hace posible una codificación eficiente de la información al reducir la capacidad de respuesta a los eventos predecibles, habituales e irrelevantes mientras se mantienen las respuestas a cambios impredecibles, poco comunes y más informativos del entorno.

6.1.1. La adaptación neuronal y la adaptación específica a estímulos

La capacidad de adaptación es una propiedad ubicua en sistema nervioso y constituye un principio fundamental de su organización y función (Whitmire y Stanley, 2016). Esta adaptación permite una codificación flexible y eficiente en función del contexto de estimulación, al tiempo que optimiza los recursos neuronales, el gasto energético y maximiza la capacidad de transmitir información (Barlow, 1961).

En términos de fisiología sensorial, la adaptación hace referencia a la reducción de las respuestas neuronales en una escala de tiempo corta, que va desde los milisegundos hasta unos pocos minutos (Whitmire y Stanley, 2016). Los sistemas sensoriales sufren adaptación de sus campos receptivos mediante la disminución de la selectividad neuronal a las características más comunes de los estímulos. Al mismo tiempo, la selectividad a las características menos comunes se mantiene o incluso aumenta (Dragoi et al., 2000; Kohn, 2007). Este es precisamente el caso de la adaptación específica a estímulos (SSA, de la terminología anglosajona), un tipo distinto y singular de adaptación neuronal a estímulos repetidos y predecibles, al tiempo que se conserva la capacidad de respuesta a otros estímulos diferentes o impredecibles (Movshon y Lennie, 1979; Ulanovsky et al., 2003). Por tanto, las neuronas sensoriales codifican aparte de las características del estímulo físico, su relevancia y el grado de adecuación/sorpresa dentro del contexto actual. No es sorprendente que la SSA se haya relacionado con procesos cerebrales superiores como la detección de la disparidad y la inferencia perceptiva. Las respuestas neuronales están moduladas por la experiencia previa y pueden sufrir adaptación en varias escalas espaciotemporales, lo que sugiere que una combinación de mecanismos neuronales intrínsecos, sinápticos y de circuitos o redes neuronales deben operar en paralelo

(Malmierca et al., 2014). El Estudio I analiza el grado en el que estos mecanismos contribuyen a generar la SSA con registros intracelulares en el colículo inferior (IC) de ratón.

6.1.2. Detección de la disparidad auditiva

La adaptación filtra las entradas de estimulación repetitivas y evita que la información redundante llegue a niveles de procesamiento superiores. Esta adaptación simple solo depende del número de repeticiones con las que una característica específica de un estímulo se ha encontrado recientemente, independientemente de la estructura compleja o la predictibilidad de los patrones de estimulación. Por lo tanto, la adaptación por sí sola no permite separar los sonidos poco informativos de los eventos más informativos o inesperados que ocurren en la escena auditiva aproximadamente con la misma frecuencia. Así pues, la detección de la disparidad es la capacidad cerebral de identificar pre-atencionalmente eventos sensoriales específicos que no coinciden con las expectativas generadas por la regularidad de la estimulación sensorial reciente. Esta detección de la disparidad es un aspecto relevante en el análisis de la escena auditiva que podría constituir la base de la formación y la segregación rápida y eficiente de los objetos auditivos (Grimm y Escera, 2012).

El potencial de disparidad (*mismatch negativity* o MMN), que se registra en humanos en con electrodos superficiales en el cuero cabelludo, refleja un proceso automático de detección de la disparidad o de un cambio distinguible. Desde su descubrimiento hace cuatro décadas (Näätänen et al., 1978; Näätänen y Michie, 1979), este biomarcador se ha convertido en una herramienta fundamental para la investigación cognitiva y clínica del cerebro humano (Kujala et al., 2007; Näätänen et al., 2007), así como en aplicaciones diagnósticas (Schall, 2016). El MMN refleja un mecanismo de procesamiento clave para la supervivencia (Fitzgerald y Todd, 2020). El cerebro codifica automáticamente patrones regulares en el sensorio, crea modelos internos para explicar esas regularidades, a la vez que detecta las discrepancias de esas representaciones internas con las nuevas entradas sensoriales.

El MMN generalmente se estudia utilizando un paradigma *oddball* en el que un tono discrepante está intercalado pseudoaleatoriamente en una secuencia de tonos estándar repetidos (Figura 1A en pág. 6). En los registros electrofisiológicos, las respuestas neuronales a eventos discrepantes e impredecibles son significativamente mayores que las

de los estímulos estándar predecibles. Esta respuesta diferencial del paradigma *oddball* se puede medir a nivel macroscópico registrando los potenciales auditivos con electrodos superficiales. A la respuesta evocada por el estímulo discrepante se le substrae la generada por el mismo tono presentado en la condición estándar. De esta resta se obtiene una respuesta de "disparidad o *mismatch*" clara (discrepante - estándar) en los electrodos temporales y frontales en forma de una desviación negativa dando lugar al término *mismatch negativity* en inglés (ver Figura 1B en pág. 6; Fitzgerald y Todd, 2020; Näätänen et al., 1978; Näätänen y Michie, 1979).

A escala microscópica en forma de SSA, las neuronas también cesan los potenciales de acción exclusivamente a aquellos estímulos con mayor probabilidad de ocurrencia a pesar de sus características físicas (Figura 1C en pág. 6). La conexión fisiológica de estos dos fenómenos similares a niveles diferentes ha sido un tema de debate durante décadas. Debido a sus similitudes funcionales, se ha sugerido que la SSA cortical es el correlato neuronal del MMN (Ulanovsky et al., 2003; Jääskeläinen et al., 2004), provocando un intenso debate en la literatura (Näätänen et al., 2005). Sin embargo, la SSA y el MMN muestran algunas discrepancias claras, principalmente debidas a las limitaciones experimentales para registrar neuronas en humanos como se hace en la investigación animal. Más concretamente, estos experimentos con animales han confirmado su solapamiento a lo largo de la vía auditiva en el IC, el cuerpo geniculado medial del tálamo (MGB) y en toda la corteza auditiva (AC; revisado en Carbajal y Malmierca, 2018). No obstante, hasta el momento no se había estudiado el vínculo entre el MMN y la SSA en áreas no auditivas como las cortezas frontales integradoras. Por lo tanto, nuestro Estudio II tiene como objetivo discernir el papel de esta región cerebral.

Para explicar cómo se genera el MMN se han propuesto tres hipótesis conceptuales principales. La distribución topográfica del MMN revela una red frontotemporal a cargo de la detección automática de la disparidad (Näätänen et al., 1992; Opitz et al., 2002; Paavilainen et al., 2003). De acuerdo a la interpretación cognitiva clásica del MMN o ***la hipótesis de la memoria sensorial o de la detección*** (Näätänen, 1990; Näätänen et al., 2007), las fuentes temporales de la AC codificarían primero las regularidades acústicas en una memoria sensorial y detectan desviaciones sensoriales específicas entre ese rastro de memoria y la nueva información entrante (Näätänen y Alho, 1995). Posteriormente, fuentes adicionales de la corteza prefrontal (PFC) evalúan la relevancia conductual de esa desviación sensorial, lo que potencialmente desencadena un cambio atencional hacia ese evento (Giard et al., 1990; Doeller et al., 2003; Sikkens et al., 2019). La ***hipótesis de la adaptación*** es una interpretación del MMN fundamentada en la neurofisiología. Esta

hipótesis niega la existencia de un proceso genuino de detección de la disparidad, argumentando que el estímulo estándar induce SSA en las neuronas de la AC (Ulanovsky et al., 2003; Jääskeläinen et al., 2004), en las cuales sus canales de frecuencia simplemente permanecen sin saturarse para responder al estímulo discrepante (May y Tiitinen, 2010; Fishman, 2014). A pesar de las diferencias conceptuales, tanto la hipótesis de la memoria sensorial como la de la adaptación coinciden en que el procesamiento temprano de la AC es muy sensible a las características específicas de los estímulos. Por el contrario, la actividad de la PFC parece depender más de una evaluación general de las propiedades globales, que ocurre tras los procesos iniciales de discriminación sensorial (Alho, 1995; Fitzgerald y Todd, 2020).

Recientemente, han surgido nuevas propuestas que han tratado de integrar las hipótesis anteriores de la generación del MMN, en el ***marco del procesamiento predictivo o la codificación predictiva*** estableciendo una relación jerárquica y recíproca entre los niveles del procesamiento sensorial (revisado en Garrido et al., 2009c; Carbajal y Malmierca, 2018, 2020). El marco del procesamiento predictivo supone un elemento conceptual general, integrador y renovado para explicar cómo el cerebro le encuentra sentido al mundo o una teoría de inferencia perceptual basada en información neurobiológica (Rao y Ballard, 1999; Friston, 2009; Heilbron y Chait, 2018).

La teoría de la codificación predictiva considera la SSA y el MMN como los respectivos signos microscópicos y macroscópicos de la detección automática de la disparidad y propone una explicación unificada de su generación a ambas escalas (Garrido et al., 2009c; Carbajal y Malmierca, 2018, 2020). Las respuestas de disparidad son consideradas ampliamente como la huella de las señales de error de predicción en la terminología de la codificación predictiva (Friston, 2005, 2010; Garrido et al., 2009c; Bastos et al., 2012; Stefanics et al., 2014). En el marco de codificación predictiva, los cerebros se consideran sistemas organizados jerárquicamente en redes neuronales distribuidas (Figura 2A en pág. 9). Cada nivel en la jerarquía de procesamiento compara cada entrada sensorial ascendente desde el nivel inferior con las predicciones descendentes desde nivel superior. Durante el aprendizaje perceptivo, cuando se repite la información sensorial entrante, se aprenden las regularidades estadísticas del mundo natural de tal manera que se predicen las entradas futuras. Las señales de error de predicción se suprimen mediante un proceso de supresión de la repetición. Por el contrario, si llega un nuevo estímulo, como un evento discrepante, habrá un fallo para predecir esa entrada ascendente y suprimir la señal de error de predicción. El error de predicción se enviará al nivel superior para actualizar el modelo predictivo más abstracto que posteriormente descenderá como una nueva expectativa

(Figura 2B en pág. 9). Este proceso continúa iterando hasta que se explica el error de predicción y las expectativas se ajustan a la entrada sensorial real de los niveles inferiores. En consecuencia, la percepción surge de la jerarquía de inferencias causales en la que cada nivel está restringido por el procesamiento de sus niveles contiguos (Friston, 2003).

6.1.3. Las vías de procesamiento del sonido

El sistema auditivo de los mamíferos se compone de varias estructuras del tronco del encéfalo y del prosencéfalo. La información auditiva se envía y procesa progresivamente desde los oídos a las áreas auditivas superiores a través de múltiples estaciones de relevo e interrupciones sinápticas. Las ondas de presión mecánica del sonido se transducen en señales eléctricas en la cóclea. Desde la cóclea, la información auditiva se envía a través de los núcleos cocleares, a partir de los cuales emergen una serie de canales paralelos de procesamiento dirigidos al complejo olivar superior, los núcleos del lemnisco lateral y IC. La información sensorial vuelve a converger en el mesencéfalo en el IC y luego se envía al MGB y desde ahí a la AC (revisado en Oliver et al., 2018).

Desde el nivel del IC en el mesencéfalo hasta la AC, emergen dos sistemas o vías de procesamiento paralelos: lemniscal y no-lemniscal (Figura 3 en pág. 12). Las estructuras lemniscales se encuentran en el núcleo de sus respectivos centros auditivos, con neuronas con que se organizan tonotópicamente siguiendo un flujo ascendente de información sensorial (Malmierca, 2015). Las respuestas en la vía lemniscal son evocadas esencialmente por las características físicas del sonido. Por el contrario, las células no-lemniscales reciben información de las divisiones lemniscales, otras áreas no-lemniscales y la AC. Sus salidas se envían hacia arriba a la siguiente división no-lemniscal y de la AC de hacia abajo a las áreas no-lemniscales de regreso nuevamente. Esta vía tiene neuronas con campos receptivos amplios, latencias de respuesta más largas y una organización tonotópica más difusa con funciones más integradoras (Saldaña et al., 1996; Malmierca y Ryugo, 2011).

6.1.4. Organización jerárquica de la codificación predictiva auditiva

La organización jerárquica del sistema auditivo con conexiones ascendentes y descendentes muy abundantes lo convierte en un sustrato adecuado para verificar la teoría de la codificación predictiva. De hecho, la actividad predictiva está organizada

jerárquicamente a lo largo de dos ejes anatómicos: desde las regiones lemniscales hacia las no-lemniscales y desde el IC, al MGB, y a la AC, como se ha demostrado en roedores despiertos y anestesiados (Parras et al., 2017).

Para distinguir la detección de la disparidad genuina de los efectos causados por la SSA, es necesario controlar el efecto de supresión de la repetición de los estímulos estándar en el paradigma *oddball*. Para esto, la secuencia de control con múltiples estándares (*many-standards control*; Schröger y Wolff, 1996) presenta el estímulo de interés dentro de una secuencia aleatoria de diferentes tonos, donde cada tono comparte una probabilidad de ocurrencia igual que la condición discrepante en el paradigma *oddball*. Sin embargo, se ha argumentado que esta secuencia con una sucesión desorganizada de tonos impide formar el rastro de memoria de una regularidad propiamente dicha como lo hace la condición estándar. Por el contrario, la secuencia de control en cascada (*cascade control*; Ruhnau et al., 2012) aborda las supuestas limitaciones de la secuencia de múltiples estándares al presentar los tonos en una sucesión regular de frecuencia creciente o decreciente. Por lo tanto, el estímulo de interés se ajusta a la regularidad al contrario que el evento discrepante. Además, en la secuencia en cascada al contario que en la condición estándar la regularidad no se establece por repetición y no es propensa a sufrir SSA. Por tanto, la secuencia en cascada es un control más adecuado y menos conservador que la secuencia de múltiples estándares.

Con estas secuencias control, las señales de disparidad o *mismatch* se pueden descomponer cuantitativamente en supresión de la repetición y señalización del error de predicción (Figura 4 en pág. 14). La proporción del error de predicción, que explica las respuestas de disparidad neuronal o *mismatch* neuronal, aumenta desde el IC al MGB y a la AC, mientras que la supresión de la repetición disminuye. Por lo tanto, la hipótesis de la adaptación o la SSA solo se puede considerar como cierta en las señales de disparidad de la vía lemniscal subcortical, mientras que la actividad predictiva se produce a lo largo de la vía no-lemniscal y toda la AC (Figura 4 en pág. 14; Parras et al., 2017, 2020; Valdés-Baizabal et al., 2020a).

Se considera que la AC codifica las propiedades espectrales de la estimulación sensorial, suprimiendo las respuestas a entradas auditiva redundantes basándose en las características específicas de frecuencia a través de mecanismos de plasticidad a corto plazo (Garrido et al., 2009b, 2009c; Carbajal y Malmierca, 2018). Durante un paradigma *oddball*, esto se observaría funcionalmente como SSA o supresión de la repetición (Baldeweg, 2006; Garrido et al., 2009b; Costa-Faidella et al., 2011; Todorovic y de Lange, 2012; Auksztulewicz y Friston, 2016). La información sensorial que no puede explicar el modelo

predictivo de la AC se envía como una señal de error de predicción ascendente a niveles superiores en la jerarquía del procesamiento (Friston, 2005, 2009). Finalmente, el flujo de errores de predicción ascendentes llega a la PFC. La PFC trata de explicar los errores de predicción formando expectativas de orden superior mediante las propiedades emergentes del sonido, tales como relaciones y estructuras abstractas entre los estímulos (Garrido et al., 2008, 2009a, 2009b). Por lo tanto, la AC genera errores de predicción rápidos, puramente auditivos, mientras que la PFC generaría errores de predicción cuando no se cumplen las expectativas más abstractas del modelo predictivo actual que requeriría su actualización. A pesar de las múltiples hipótesis de generación del MMN, su sustrato neuronal sigue sin caracterizarse en las áreas frontales. Los modelos animales pueden servir para definir el sustrato neuronal del MMN humano y ratificar sus hipótesis de generación tal y como se aborda en el Estudio II de la corteza prefrontal medial (mPFC) de rata. La PFC ejerce su papel modulador sobre la jerarquía sensorial inervando niveles relativamente bajos de la jerarquía como el IC (Fogelson et al., 2009; Olthof et al., 2019).

6.2. Estudio I: SSA intracelular en el mesencéfalo auditivo

6.2.1. Introducción

El IC en el sistema auditivo de los mamíferos, se encuentra en la porción dorsocaudal del mesencéfalo. El IC es primer centro auditivo conocido que muestra actividad de codificación predictiva y SSA (Ayala y Malmierca, 2013; Parras et al., 2017; Duque et al., 2018; Valdés-Baizabal et al., 2020a). Casi todas las vías auditivas que ascienden por el tronco del encéfalo convergen en el IC confiriéndole una posición esencial en el sistema auditivo de los vertebrados (Malmierca et al., 2002; Malmierca, 2003, 2015; Kandel et al., 2013; Ito y Malmierca, 2018). Cada IC recibe entradas ascendentes bilaterales, siendo la mayoría contralaterales. Debido a su complejidad neuroanatómica, se ha sugerido que el papel que desempeña el IC en el sistema auditivo es similar al de la corteza visual primaria en la visión (King y Nelken, 2009).

El IC está formado por un núcleo central rodeado por las cortezas coliculares en humanos, otros mamíferos e incluso en los clados no mamíferos (Geniec y Morest, 1971; Morest y Oliver, 1984; Oliver y Morest, 1984; Malmierca, 1991, 2003, 2015; Malmierca y Ryugo, 2011). El IC de roedores es una gran estructura de forma ovalada siendo de los más estudiados (Figura 5 en pág. 18; Malmierca et al., 2009b; Ito y Malmierca, 2018). Los ICs de ambos hemisferios están interconectados por una comisura grande y muy mielinizada

(Saldaña y Merchán, 1992; Malmierca et al., 1995, 2009b). El IC de roedores se subdivide en el núcleo central perteneciente a la vía lemniscal y las cortezas circundantes (dorsal, lateral y rostral) de la vía no-lemniscal (Faye-Lund y Osen, 1985; Coleman y Clerici, 1987; Zook y Casseday, 1987; Malmierca et al., 1993; Ito y Malmierca, 2018). El núcleo central recibe información auditiva ascendente de los núcleos cocleares, del complejo olivar superior y núcleos del lemnisco lateral. Las cortezas coliculares reciben entradas más mixtas con proyecciones sustanciales del núcleo central, el IC contralateral, inervación cortical excitadora, inhibitoria y neuromoduladora, e incluso entradas no auditivas (Saldaña y Merchań, 1992; Malmierca et al., 1995; Winer y Schreiner, 2005; Cant y Oliver, 2018). Existen muchos patrones de conectividad y organización de tipos neuronales en el IC. No obstante, a pesar de que múltiples enfoques han intentado clasificar los tipos neuronales en el IC combinando perfiles moleculares, propiedades morfológicas y electrofisiológicas, no existe una correlación simple entre clases definidas con diferentes métodos (Ito y Malmierca, 2018).

Una característica fisiológica fundamental del núcleo del IC es su organización tonotópica. Los sonidos de baja frecuencia se localizan en las láminas dorsolaterales y los de alta frecuencia se codifican progresivamente más ventralmente (Schreiner y Langner, 1997; Malmierca et al., 2008). Las neuronas del núcleo central son sensibles a la duración del sonido (Pérez-González et al., 2006), la estimulación binaural y la localización del sonido (Zhang y Kelly, 2010). Por el contrario, las cortezas exhiben una integración multisensorial de manera similar a niveles superiores de la vía auditiva no-lemniscal (Malmierca y Ryugo, 2011; Olthof et al., 2019). Esta microcircuitería tan singular permite la aparición de propiedades de codificación multifacéticas de la información auditiva como la SSA, la detección de la disparidad (Hernández et al., 2005; Malmierca et al., 2009a; Zhao et al., 2011; Duque et al., 2012; Ayala y Malmierca, 2013), y la señalización de errores de predicción auditivos en el IC (Parras et al., 2017; Valdés-Baizabal et al., 2020a).

6.2.2. Hipótesis y Objetivos

El IC integra múltiples entradas auditivas de vías ascendentes y descendentes (Ito y Malmierca, 2018) y es precisamente el sitio donde emerge la SSA (Pérez-González et al., 2005; Malmierca et al., 2009a; Ayala et al., 2013; Duque et al., 2018). Sin embargo, no hay un consenso sobre cuáles son los mecanismos encargados de la generación de la SSA. La SSA se ha estudiado clásicamente en los potenciales de acción extracelulares que a su vez son el resultado de la interacción entre las entradas sinápticas, el campo receptivo de esas

entradas y las propiedades de membrana como el umbral de disparo. Actualmente, no existen estudios de registros intracelulares que analicen dentro de las mismas neuronas del IC las propiedades intrínsecas, las respuestas subumbrales y el nivel de la SSA acústica. Por ello, nuestra hipótesis de trabajo es:

> En el IC, las neuronas adaptadas que exhiben SSA difieren en sus propiedades neuronales intrínsecas y/o respuestas subumbrales de aquellas neuronas no adaptadas que carecen de SSA.

Por tanto, los objetivos del Estudio I son dos:

1. Determinar si las propiedades de SSA se correlacionan con las propiedades neuronales intrínsecas, las propiedades pasivas de membrana y las respuestas subumbrales.

2. Correlacionar en células individuales, el grado de adaptación de las entradas sinápticas con los niveles de SSA de los potenciales de acción.

6.2.3. Resumen de Resultados y Discusión

En este estudio, presentamos las propiedades pasivas, las propiedades intrínsecas y los potenciales postsinápticos (PSP) de registros en configuración de "célula completa o *whole-cell*" *in vivo* en el IC del ratón anestesiado durante la estimulación con inyecciones de corriente y el paradigma *oddball* (Valdés-Baizabal et al., 2020b). Los datos obtenidos de 10 ejemplos neuronales muestran similitudes en las propiedades pasivas, la capacitancia, la resistencia y el potencial en reposo de membrana. Sin embargo, los patrones de disparo sirvieron para diferenciar a las neuronas adaptadas de las no adaptadas (células con o sin SSA, respectivamente), entre todas las propiedades intrínsecas analizadas (patrón de disparo, umbral del potencial de acción, *sag* despolarizante durante los pulsos hiperpolarizantes y potenciales de acción de rebote). Las células no adaptadas demostraron un patrón de disparo regular-sostenido (ver Figura 6 y Tabla 6 en Valdés-Baizabal et al., 2020b; Peruzzi et al., 2000; Sivaramakrishnan y Oliver, 2001; Tan et al., 2007), probablemente debido a un alto grado de corrientes persistentes de sodio (Chatelier et al., 2010; Boeri et al., 2018) y además, mostraron campos receptivos con una sintonización estrecha o áreas de respuesta en frecuencia (FRA) en forma de V que corresponden a las neuronas del núcleo central (Malmierca et al., 2009a; Duque et al., 2012; Ayala y Malmierca, 2013; Palmer et al., 2013; Duque y Malmierca, 2015). Por el contrario, las células adaptadas mostraron patrones de disparo más variables tales como sostenido, con

acomodación y células con ráfagas de disparos iniciales (Geis et al., 2011) y FRAs sin forma de V típicos de las cortezas del IC (Malmierca et al., 2009a; Duque et al., 2012; Ayala y Malmierca, 2013; Palmer et al., 2013; Duque y Malmierca, 2015).

Independientemente del nivel de SSA de los potenciales de acción, hemos observado una amplitud similar en los PSPs evocadas tanto para el estímulo estándar como el discrepante en cada neurona. Esto indica que la SSA no se localiza a nivel sináptico en las neuronas del IC. Debido a que ambas frecuencias seleccionadas para los paradigmas *oddball* se encuentran dentro del campo receptivo, las neuronas muestran consistentemente PSPs para ambos tonos. Aunque la amplitud de los PSPs y la conductancia variaron acorde a la adaptación auditiva en el MGB (Jia et al., 2021) y la AC (Wehr y Zador, 2005; Abolafia et al., 2011), las diferencias entre la inhibición y excitación sinápticas no sirven para predecir los niveles de SSA de los potenciales de acción en el IC. El momento relativo en el que ocurre la inhibición también puede influir en la adaptación. Sin embargo, solo la inhibición de los estímulos estándar fue más rápida en las neuronas no adaptadas que en las adaptadas. De hecho, se espera que la depresión sináptica sea débil a la tasa de presentación de 3-4 Hz que se usa en nuestro estudio (Bartlett y Smith, 2002; Malmierca et al., 2009a; Pérez-González y Malmierca, 2014).

A lo largo del sistema auditivo, los núcleos cocleares y el complejo olivar superior carecen de SSA (Ayala et al., 2013; Duque et al., 2018), pero ya en las regiones corticales del IC, la SSA es robusta (Pérez-González et al., 2005; Malmierca et al., 2009a; Lumani y Zhang, 2010; Ayala et al., 2013; Duque y Malmierca, 2015; Duque et al., 2018). Nuestra muestra presenta una adaptación sináptica variable, con una SSA débil o nula en algunos casos, SSA sináptica clara en un par de neuronas e incluso reducción de la amplitud de los PSP excitatorios a los estímulos discrepantes junto con SSA de los potenciales de acción. Esto indica que en nuestro estudio la adaptación sináptica no sirve para predecir la presencia de SSA de los potenciales de acción. En conjunto, considerando la ausencia de SSA sináptica en el IC y evidencia previa donde a pesar de la desactivación de la AC se mantuvo la SSA subcortical (Antunes y Malmierca, 2011; Anderson y Malmierca, 2013; Malmierca et al., 2015), el IC no-lemniscal se postula como la primera estación de la vía auditiva donde emerge la SSA.

Así mismo, también hemos observado una tendencia sutil hacia potenciales de membrana hiperpolarizados en las neuronas adaptadas y una creciente inhibición sináptica acorde al número de repeticiones del estímulo estándar a nivel poblacional (ver Figura 4 en Valdés-Baizabal et al., 2020b). Esto denota un nivel moderado de adaptación que solo se produce cuando un estímulo se repite consecutivamente. Estas tendencias a

nivel poblacional son indicativas de un tipo de adaptación más simple relacionada con las conductancias de potasio. Estudios previos han asociado estas conductancias a la adaptación sensorial en las cortezas de barriles (Díaz-Quesada y Maravall, 2008), sensorial-motora (Schwindt et al., 1988) y visual (Sanchez-Vives et al., 2000a, 2000b; Wang et al., 2003). La activación de las corrientes de potasio hiperpolariza el potencial de membrana, disminuyendo la capacidad de respuesta neuronal a las entradas sinápticas posteriores durante decenas de milisegundos a decenas de segundos (Abolafia et al., 2011). Esta cascada de eventos ocurre de igual modo para las condiciones estándar y discrepante pudiendo explicar las similitudes entre las respuestas.

Aunque nuestro trabajo representa un primer paso importante en la comprensión de las respuestas de la SSA intracelular *in vivo* en el IC, nuestras conclusiones deben considerarse como ejemplos de diferentes casos y reforzarse con estudios adicionales, aumentando la muestra. Nuestros resultados muestran el potencial de futuros estudios con la misma metodología para comprender cómo se genera la SSA a nivel celular.

6.3. Estudio II: Señalización de errores de predicción en la corteza prefrontal medial

6.3.1. Introducción

En el cerebro de los mamíferos, la PFC comprende el neocórtex que cubre el lóbulo frontal. La PFC no es un procesador sensorial *per se*, sino un centro ejecutivo involucrado en funciones como la atención, la memoria de trabajo, el aprendizaje de reglas, el procesamiento temporal, la planificación y la toma de decisiones (Dalley et al., 2004; Kesner y Churchwell, 2011). En condiciones naturales, la PFC integra la información que recibe desde múltiples estructuras para generar representaciones motosensoriales de modalidad cruzada muy complejas y converge la información actualizada a estructuras de salida (Hoover y Vertes, 2007; Parr et al., 2019).

En roedores, la PFC está dividida en tres regiones según su citoarquitectura y patrones de conectividad: la PFC lateral o corteza insular, la corteza orbitofrontal y la mPFC (Figura 6 en pág. 26). La mPFC cubre la mayor parte de los muros mediales de los hemisferios anteriores y la parte dorsal a la rodilla del cuerpo calloso (Sarter y Markowitsch, 1983, 1984; Sesack et al., 1989; Condé et al., 1990, 1995; Divac et al., 1993). La mPFC de rata se puede subdividir al menos en cuatro áreas citoarquitectónicas

principales: corteza agranular medial o corteza motora secundaria (M2, área Fr2), corteza cingular anterior (ACC, área 24), corteza prelímbica (PL, área 32) y corteza infralímbica (IL, área 25 en primates; Gabbott et al., 1997; Hoover y Vertes, 2007; Uylings et al., 2003; van Eden y Uylings, 1985; Vogt y Paxinos, 2014).

La mPFC presenta conexiones eferentes a áreas subcorticales (Gabbott et al., 2005; Heidbreder y Groenewegen, 2003). Las fuentes primarias de conexiones aferentes sufren una gradación a lo largo del eje dorsoventral desde las entradas corticales sensoriales, motoras y de asociación en las M2 y ACC dorsales hasta las aferencias principalmente límbicas en las PL e IL ventrales (Hoover y Vertes, 2007). Además, las M2 y ACC dorsales reciben proyecciones ascendentes desde la AC. Las PL e IL ventrales están densamente conectadas con la mPFC dorsal; por tanto, la información auditiva puede llegar a través de estas proyecciones (Martin-Cortecero y Nuñez, 2016).

A pesar de los diferentes patrones de conectividad entre ambas PFCs, los primates y roedores comparten un principio de organización jerárquica general, que constituye uno de los aspectos más relevantes para validar investigaciones sobre la codificación predictiva jerárquica al nivel neuronal inaccesible en la investigación cerebral humana (Uylings et al., 2003; Seamans et al., 2008). La mPFC de los roedores integra componentes anátomo-electrofisiológicos de la PFC dorsolateral de los primates y la ACC a un nivel rudimentario (Brown y Bowman, 2002; Seamans et al., 2008). Se cree que la PFC ejerce un papel modulador sobre la jerarquía sensorial. Este papel es fundamental para el procesamiento contextual y, por lo tanto, en la detección de la disparidad y la codificación predictiva (Fogelson et al., 2009). Además, cabe destacar que este procesamiento de la PFC se ve afectado en multitud de trastornos psiquiátricos y neurológicos (Gaebler et al., 2015; Ranlund et al., 2016).

6.3.2. Hipótesis y Objetivos

Muchas hipótesis tratan de explicar la generación del MMN, pero no se comprende muy bien su correlato neuronal en las áreas frontales ni está claramente localizado. Esto se debe principalmente a las limitaciones éticas en los estudios de investigación en humanos (Rinne et al., 2000; Edwards et al., 2005; Rosburg et al., 2005; Deouell, 2007; Tse y Penney, 2008; Dürschmid et al., 2016; Nourski et al., 2018). El uso de técnicas invasivas en modelos animales asegura suficiente resolución espacial y temporal para determinar de manera adecuada si los potenciales de disparidad de la AC preceden o coinciden con aquellos de la

PFC. La actividad de los potenciales de acción y los potenciales de campo local (LFP) puede proporcionarnos el curso temporal específico y la localización de las señales de disparidad o *mismatch* a niveles microscópico y mesoscópico, respectivamente (Hamm y Yuste, 2016; Nieto-Diego y Malmierca, 2016; Parras et al., 2017). Al mismo tiempo, podemos correlacionar estas señales de disparidad con potenciales de campo de MMN registrados a gran escala epiduralmente en el correspondiente modelo animal. Estos potenciales de campo obtenidos a gran escala en animales se consideran el análogo específico del MMN humano (Harms et al., 2014, 2016). Por tanto, los estudios animales facilitan y nos sirven para definir el correlato neuronal del MMN humano y probar así las hipótesis de su generación.

Recientemente, el marco del procesamiento predictivo ha tratado de integrar las hipótesis previas de la adaptación y la memoria sensorial de la generación del MMN (revisado en Garrido et al., 2009c; Carbajal y Malmierca, 2020), estableciendo una interconexión jerárquica y recíproca entre la AC y la PFC. La AC en primer lugar suprimiría las entradas auditivas redundantes basándose en las características espectrales de la estimulación sensorial mediante mecanismos de plasticidad a corto plazo como la inhibición lateral y la depresión sináptica (Garrido et al., 2009b, 2009c; Carbajal y Malmierca, 2018). Por tanto, proponemos las siguientes hipótesis:

1. La información redundante se filtra antes de llegar a la mPFC mediante el mecanismo de supresión de la repetición ya que se puede explicar y suprimir en niveles inferiores de la jerarquía como la AC.

2. La información auditiva impredecible o sin explicar en los niveles inferiores de procesamiento jerárquico se envía como una señal de error de predicción a los niveles superiores, como la mPFC.

3. La mPFC codifica representaciones más abstractas, tales como estructuras y relaciones complejas entre estímulos. Para ello, genera expectativas de orden superior sobre las propiedades emergentes de las secuencias auditivas.

En consecuencia, en el presente trabajo, estudiamos los siguientes objetivos:

1. Determinar la influencia del error de predicción y la supresión de la repetición en la mPFC bajo un paradigma auditivo *oddball* junto a dos controles sin repeticiones; las secuencias de múltiples estándares y en cascada y además, el paradigma del estímulo discrepante en solitario.

2. Establecer un posible sustrato neuronal de los potenciales de MMN registrados a gran escala epiduralmente en el cerebro de rata, registrando simultáneamente LFPs y potenciales de acción en una posible fuente de actividad frontal, la mPFC.

3. Estudiar la jerarquía de codificación predictiva de las señales de disparidad, con especial énfasis en la mPFC que constituye un nivel superior a los datos previos del IC, el MGB y la AC (Parras et al., 2017).

6.3.3. Resumen de Resultados y Discusión

En este trabajo, estudiamos los mecanismos que gobiernan la detección de disparidad en la mPFC de la rata anestesiada (M2, ACC, PL e IL; Casado-Román et al., 2020). Analizamos las respuestas de potenciales de acción conjunta en múltiples neuronas y los LFPs en la mPFC de rata al paradigma auditivo *oddball*, el estímulo discrepante en solitario (Näätänen et al., 1989) y los controles adecuados sin repeticiones: las secuencias de múltiples estándares (Schröger y Wolff, 1996) y en cascada (Ruhnau et al., 2012; ver Figure 1 en Casado-Román et al., 2020). Nuestros resultados muestran que las respuestas evocadas eran equivalentes en gran medida en los cuatro campos de la mPFC y las capas supra (2/3)- e infragranulares (5/6). Los estímulos auditivos impredecibles provocaron respuestas más fuertes que la actividad débil, o incluso ausente causada por los sonidos que podrían esperarse. A diferencia de las respuestas de disparidad en el sistema auditivo que se generan principalmente por efectos dependientes del estímulo (Parras et al., 2017), descubrimos que las respuestas a sonido en la mPFC se desencadenan por su impredecibilidad, generando señales de disparidad dependientes del contexto y comparativamente más tardías, robustas y prolongadas. Las respuestas de disparidad registradas en los potenciales de acción y los LFP de la mPFC coinciden temporalmente con los potenciales de MMN obtenidos a gran escala en fuentes frontales del cerebro de rata (Imada et al., 2013; Harms et al., 2014; Jodo et al., 2019). Además, estos datos sugieren que las respuestas de disparidad de la mPFC se componen casi exclusivamente de actividad de señalización de errores de predicción, lo que contrasta con las respuestas de disparidad registradas a lo largo del sistema auditivo en un estudio anterior de nuestro laboratorio (Parras et al., 2017).

En los cuatro campos de la mPFC, las secuencias de múltiples estándares y en cascada fueron controles en gran medida equivalentes, ya que probablemente generan una expectativa de una sucesión regular en el tiempo de alternancia de tonos (Horváth y Winkler, 2004; Mittag et al., 2016; Parras et al., 2017; Wiens et al., 2019). Por lo tanto, las

respuestas auditivas evocadas por las condiciones controles se suprimieron hasta cierto punto, pero sin inducir los efectos específicos de estímulo de supresión de la repetición de la condición estándar. Por el contrario, las respuestas a la estimulación auditiva inesperada de las condiciones discrepante y discrepante en solitario (estadísticamente comparables en consonancia con evidencia anterior; Imada et al., 2013) alcanzaron su punto máximo antes y duplicaron o incluso triplicaron en magnitud la respuesta provocada por las condiciones predecibles; control y estándar. La gran diferencia entre las respuestas a condiciones inesperadas y predecibles se tradujo en valores altos y similares del índice de disparidad o *mismatch* neuronal (iMM = discrepante - estándar) y el índice de error de predicción (iPE = discrepante - control). Por el contrario, los valores bajos e insignificantes del índice de supresión de la repetición (iRS = control - estándar) indican que los efectos específicos de frecuencia tienen una influencia bastante irrelevante en la mPFC. Todo ello sugiere que las señales de disparidad evocadas en la mPFC por el paradigma auditivo *odbball* se explican cómo señalización de error de predicción pura (ver Figura 3 en Casado-Román et al., 2020).

Estudios previos sobre la actividad frontal han encontrado resultados análogos a los nuestros a pesar de utilizar metodologías, técnicas de registro y modelos de especies diferentes. Se ha observado una mayor predominancia de respuestas al estímulo discrepante que al estándar y/o los controles en la actividad de los potenciales de acción de la corteza orbitofrontal de ratones anestesiados y despiertos (Srivastava y Bandyopadhyay, 2020), en la PFC de macacos despiertos (Takaura y Fujii, 2016; Camalier et al., 2019), en los potenciales de campo obtenidos a gran escala sobre cortezas frontales de ratas despiertas (Harms et al., 2014; Jodo et al., 2019) y en electrocorticografía frontal en humanos (Rosburg et al., 2005; Dürschmid et al., 2016; Phillips et al., 2016; Nourski et al., 2018). Las ubicaciones prefrontales diferentes analizadas en estos estudios no deben considerarse directamente como homólogos entre especies (Seamans et al., 2008). No obstante, a pesar de los patrones de conectividad diferente de las PFCs, los primates y los roedores comparten un principio general de organización jerárquica siendo uno de los aspectos más relevantes para validar las investigaciones sobre la codificación predictiva jerárquica a un nivel neuronal inaccesible en la investigación humana (Uylings et al., 2003; Seamans et al., 2008). Todos estos trabajos confirman de manera uniforme que la sorpresa o impredecibilidad de los cambios es el factor clave que genera las respuestas auditivas en las cortezas frontales.

Los resultados de nuestro trabajo muestran una relación directa entre la señalización del error de predicción a niveles microscópicos y mesoscópicos ya que el curso temporal del error de predicción de los potenciales de acción coincide con las fluctuaciones del error

de predicción en los LFPs en cada campo de la mPFC. A nivel macroscópico, los potenciales de campo obtenidos a gran escala en ratas despiertas exhiben respuestas de disparidad muy fuertes que comienzan unos 40 ms tras el inicio del estímulo (Imada et al., 2013; Harms et al., 2014; Jodo et al., 2019). De manera similar, nuestra actividad de potenciales de acción y LFP confirmaron que la señalización del error de predicción comienza ~unos 40 ms postestimulación en la AC hasta los 150 ms, cuando la PFC toma el control y continúa la señalización del error de predicción más allá de los 600 ms postestimulación (ver Figura 6 en Casado-Román et al., 2020). Además, los potenciales de MMN a gran escala más robustos se han descrito en la ventana temporal entre 100 y 500 ms (Imada et al., 2013; Harms et al., 2014; Jodo et al., 2019), precisamente cuando ocurre el error de predicción de los potenciales de acción y los LFPs más intensos en la mPFC. De esta manera, nuestros datos permiten correlacionar los niveles microscópicos, mesoscópicos y macroscópicos en los que se puede detectar la señalización del error de predicción y la detección automática de la disparidad en la PFC de rata. Dado que los potenciales MMN registrados a gran escala se consideran el análogo en la rata del MMN humano (Harms et al., 2016), nuestros resultados confirman el sustrato neuronal más plausible de los generadores frontales del MMN.

Para lograr una perspectiva más general de la detección de la disparidad auditiva y las respuestas de *mismatch* en el cerebro de la rata, comparamos nuestros resultados con trabajos previos de nuestro laboratorio empleando una metodología similar (Parras et al., 2017; ver Figura 6 en Casado-Román et al., 2020). La hipótesis de la adaptación solo se puede verificar en la vía lemniscal subcortical (IC y MGB), en cambio, la codificación predictiva ocurre el IC no-lemniscal, el MGB no-lemniscal, toda la AC y la mPFC (Parras et al., 2017; Carbajal y Malmierca, 2018). La sensibilidad auditiva en las células de la mPFC parece depender únicamente de características contextuales o abstractas, mientras que el procesamiento en el sistema auditivo está claramente impulsado por las propiedades espectrales del sonido (Nieto-Diego y Malmierca, 2016; Parras et al., 2017). Estos hallazgos son consistentes con estudios en la AC y la PFC dorsolateral del macaco despierto (Camalier et al., 2019). Aunque el iRS en la AC de rata representa más de la mitad de las respuestas *mismatch* (Parras et al., 2017), la mPFC muestra valores insignificantes del iRS, descartando así cualquier influencia espectral relevante en el procesamiento de la PFC.

Curiosamente, a pesar de que los valores del iMM en la AC y la mPFC de ratas anestesiadas son análogos, los valores del iPE son significativamente diferentes. Esto quiere decir que a pesar de tener una magnitud comparable, la naturaleza de las señales de disparidad en la AC es distinta de las de la PFC y que ambos generadores contribuyen significativamente al MMN. Sin embargo, sus contribuciones son de naturaleza

fundamentalmente diferente, algo que se ha defendido desde la interpretación clásica de la memoria sensorial del MMN humano (Giard et al., 1990; Näätänen, 1990; Näätänen et al., 1992, 2007), y también ha sido heredado por el marco más moderno del procesamiento predictivo (Carbajal y Malmierca, 2020; Garrido et al., 2009). El iPE puede explicar el 90% del valor del iMM, y ambos índices son significativamente similares y análogos en la mayoría de los campos de la mPFC. Por consiguiente, las respuestas de disparidad prefrontal se pueden interpretar fehacientemente como detección de la disparidad genuina en terminología clásica o señalización del error de predicción pura en terminología del procesamiento predictivo.

Siguiendo esta lógica, la mPFC estaría generando una respuesta *mismatch*, *de novo* señalando una disparidad o un error de predicción sin reflejar las propiedades espectrales de las señales acústicas, que ya se han representado en regiones inferiores de procesamiento del sistema auditivo (Parras et al., 2017; Carbajal y Malmierca, 2020). Esta interpretación esta abalada por la gran diferencia entre las latencias de respuesta de la AC y la PFC en nuestras ratas anestesiadas y en estudios previos (Camalier et al., 2019; Srivastava y Bandyopadhyay, 2020). Además, la mPFC solo necesitó dos repeticiones del estímulo estándar para explicar su entrada redundante, siendo mucho más rápido que las ACs lemniscal y no-lemniscal, que necesitaron más del doble de repeticiones (Nieto-Diego y Malmierca, 2016; Parras et al., 2017; ver Figura 6 en Casado-Román et al., 2020). Esto sugiere que el procesamiento de la AC y la PFC ocurre hasta cierto punto de manera secuencial, como lo describen tanto las hipótesis de memoria sensorial clásica (Näätänen et al., 2007), como la de procesamiento predictivo (Garrido et al., 2009c) para la generación del MMN. Las discrepancias acústicas en las regularidades espectrales deben detectarse primero, en la AC (fuentes temporales), y únicamente después, la PFC (fuentes frontales) puede identificar discrepancias globales de representaciones internas más abstractas.

Dado que la PFC responde mucho más tarde al sonido pero suprime las entradas auditivas redundantes de manera más eficaz que la AC, las señales de *mismatch* registradas en la PFC no pueden simplemente heredarse o amplificarse posteriormente desde el sistema auditivo. El marco conceptual de la codificación predictiva ha propuesto la disposición jerárquica inversa y parece una explicación más plausible (Garrido et al., 2009c). La PFC es un centro ejecutivo y no un procesador sensorial *per se*. En condiciones más naturales, lo más probable es que la PFC integre entradas de múltiples centros y varias modalidades sensoriales para generar representaciones motosensoriales muy complejas (Hoover y Vertes, 2007; Parr et al., 2019). La configuración o *gestalt* adquirido en la PFC podría retroalimentarse a la AC, generando expectativas específicas en su formato nativo,

el dominio espectral. No obstante, esta señal de retroalimentación contempla en última instancia propiedades de orden superior, como las relaciones entre estímulos o estructuras de las secuencias que no podrían haberse calculado de otra manera en la circuitería local de la AC. Esta actividad predictiva descendente ejercería una influencia inhibitoria sobre la capacidad de respuesta de la AC siempre que una determinada entrada auditiva se explique por el *gestalt* prefrontal. Sin embargo, cualquier información imprevista se transmitiría hacia arriba como un error de predicción para actualizar la representación interna de la PFC. Por todo ello, la codificación predictiva jerárquica puede explicar por qué la PFC muestra latencias más largas que la AC al mismo tiempo que realiza una supresión de expectativas más general y eficiente, capaz de explicar completamente la entrada de estímulos estándar e incluso las secuencias controles. Tan pronto como la información auditiva se vuelve redundante para la escena auditiva global, deja de llegar a la PFC, lo que evita una sobrecarga cognitiva y ahorra recursos de procesamiento de orden superior para esfuerzos más productivos.

6.4. Conclusiones

1. Las neuronas no adaptadas muestran FRAs en forma de V y un patrón de disparo regular-sostenido distintivos del IC lemniscal. Por el contrario, las neuronas adaptadas muestran FRAs sin forma de V y patrones de disparo más variables característicos del IC no-lemniscal.

2. En las neuronas del IC registradas no se encontró SSA a nivel sináptico, aportando más evidencia de que la SSA emerge en el IC no-lemniscal a lo largo de la vía auditiva.

3. En todos los campos y capas corticales de la mPFC, los cambios impredecibles promueven la capacidad de respuesta auditiva, generando respuestas de *mismatch* neuronal comparativamente más tarde, robustas y duraderas que en el sistema auditivo.

4. Las respuestas de disparidad o *mismatch* prefrontales se explican cómo detección de la disparidad genuina o errores de predicción puros. Estas respuestas reflejan propiedades contextuales, pero no espectrales, y por ello, son fundamentalmente diferentes de las de la AC. Todo ello apoya las hipótesis de la memoria sensorial y codificación predictiva para la generación de MMN.

5. La mPFC genera una expectativa de repetición precisa capaz de suprimir las respuestas a estímulos redundantes y predecibles de manera más eficiente y rápida que la AC. Esto concuerda con un procesamiento predictivo jerárquico.

6. El curso temporal de la actividad prefrontal de potenciales de acción y potenciales de campo local coinciden con las señales de MMN registradas a gran escala en la rata. Este hecho proporciona una relación directa en la detección de disparidad automática a niveles microscópico, mesoscópico y macroscópico. Por lo tanto, las células de la mPFC podrían representar el correlato neuronal de los generadores frontales de MMN.

7 List of References

Abolafia JM, Vergara R, Arnold MM, Reig R, Sanchez-Vives M V. (2011) Cortical Auditory Adaptation in the Awake Rat and the Role of Potassium Currents. Cereb Cortex 21:977–990.

Ahuja TK, Wu SH (2007) Intrinsic membrane properties and synaptic response characteristics of neurons in the rat's external cortex of the inferior colliculus. Neuroscience 145:851–865.

Aitchison L, Lengyel M (2017) With or without you: predictive coding and Bayesian inference in the brain. Curr Opin Neurobiol 46:219–227.

Alho K (1995) Cerebral generators of mismatch negativity (MMN) and its magnetic counterpart (MMNm) elicited by sound changes. Ear Hear 16:38–51.

Anderson LA, Malmierca MS (2013) The effect of auditory cortex deactivation on stimulus-specific adaptation in the inferior colliculus of the rat. Eur J Neurosci 37:52–62.

Antunes FM, Malmierca MS (2011) Effect of Auditory Cortex Deactivation on Stimulus-Specific Adaptation in the Medial Geniculate Body. J Neurosci 31:17306–17316.

Antunes FM, Nelken I, Covey E, Malmierca MS (2010) Stimulus-Specific Adaptation in the Auditory Thalamus of the Anesthetized Rat Yan J, ed. PLoS One 5:e14071.

Auksztulewicz R, Friston K (2016) Repetition suppression and its contextual determinants in predictive coding. Cortex 80:125–140.

Ayala YA, Malmierca MS (2013) Stimulus-specific adaptation and deviance detection in the inferior colliculus. Front Neural Circuits 6:1–16.

Ayala YA, Pérez-González D, Duque D, Nelken I, Malmierca MS (2013) Frequency discrimination and stimulus deviance in the inferior colliculus and cochlear nucleus. Front Neural Circuits 6:1–19.

Ayala YA, Pérez-González D, Duque D, Palmer AR, Malmierca MS (2016) Extracellular Recording of Neuronal Activity Combined with Microiontophoretic Application of Neuroactive Substances in Awake Mice. J Vis Exp e53914.

Baldeweg T (2006) Repetition effects to sounds: evidence for predictive coding in the auditory system. Trends Cogn Sci 10:93–94.

Barascud N, Pearce MT, Griffiths TD, Friston KJ, Chait M (2016) Brain responses in humans reveal ideal observer-like sensitivity to complex acoustic patterns. Proc Natl Acad Sci 113:E616–E625.

Barlow HB (1961) Possible Principles Underlying the Transformations of Sensory Messages. Sens Commun:217–234.

Bartlett EL, Smith PH (2002) Effects of paired-pulse and repetitive stimulation on neurons in the rat medial geniculate body. Neuroscience 113:957–974.

Bastos AM, Litvak V, Moran R, Bosman CA, Fries P, Friston KJ (2015) A DCM study of

spectral asymmetries in feedforward and feedback connections between visual areas V1 and V4 in the monkey. Neuroimage 108:460–475.

Bastos AM, Usrey WM, Adams RA, Mangun GR, Fries P, Friston KJ (2012) Canonical Microcircuits for Predictive Coding. Neuron 76:695–711.

Bhattacharjee A, Kaczmarek LK (2005) For K+ channels, Na+ is the new Ca2+. Trends Neurosci 28:422–428.

Bibkov NG (1977) Novelty" neurons in the frog auditory system. Zhurnal Vyss Nervn Deyatelnosti Im IP Pavlov 27:1075–1082.

Boeri J, Le Corronc H, Lejeune FX, Le Bras B, Mouffle C, Angelim MKSC, Mangin JM, Branchereau P, Legendre P, Czarnecki A (2018) Persistent sodium current drives excitability of immature renshaw cells in early embryonic spinal networks. J Neurosci 38:7667–7682.

Brown VJ, Bowman EM (2002) Rodent models of prefrontal cortical function. Trends Neurosci 25:340–343.

Camalier CR, Scarim K, Mishkin M, Averbeck BB (2019) A Comparison of Auditory Oddball Responses in Dorsolateral Prefrontal Cortex, Basolateral Amygdala, and Auditory Cortex of Macaque. J Cogn Neurosci 31:1054–1064.

Cant NB, Oliver DL (2018) Overview of Auditory Projection Pathways and Intrinsic Microcircuits. In: The Mammalian Auditory Pathways. Springer Handbook of Auditory Research, vol 65, pp 7–39. Springer, Cham.

Carandini M, Ferster D (1997) A tonic hyperpolarization underlying contrast adaptation in cat visual cortex. Science (80-) 276:949–952.

Carbajal GV, Malmierca MS (2018) The Neuronal Basis of Predictive Coding Along the Auditory Pathway: From the Subcortical Roots to Cortical Deviance Detection. Trends Hear 22:233121651878482.

Carbajal G V., Malmierca MS (2020) Novelty Processing in the Auditory System: Detection, Adaptation or Expectation? In: Reference Module in Neuroscience and Biobehavioral Psychology. Elsevier.

Casado-Román L, Carbajal G V., Pérez-González D, Malmierca MS (2020) Prediction error signaling explains neuronal mismatch responses in the medial prefrontal cortex Deouell L, ed. PLoS Biol 18:e3001019.

Chao ZC, Takaura K, Wang L, Fujii N, Dehaene S (2018) Large-Scale Cortical Networks for Hierarchical Prediction and Prediction Error in the Primate Brain. Neuron 100:1252-1266.e3.

Chatelier A, Zhao J, Bois P, Chahine M (2010) Biophysical characterisation of the persistent sodium current of the Nav1.6 neuronal sodium channel: A single-channel analysis. Pflugers Arch Eur J Physiol 460:77–86.

Chen I-W, Helmchen F, Lutcke H (2015) Specific Early and Late Oddball-Evoked Responses in Excitatory and Inhibitory Neurons of Mouse Auditory Cortex. J Neurosci 35:12560–12573.

Chung S, Li X, Nelson SB (2002) Short-term depression at thalamocortical synapses contributes to rapid adaptation of cortical sensory responses in vivo. Neuron 34:437–446.

Cléry H, Andersson F, Fonlupt P, Gomot M (2013) Brain correlates of automatic visual change detection. Neuroimage 75:117–122.

Coleman JR, Clerici WJ (1987) Sources of projections to subdivisions of the inferior colliculus in the rat. J Comp Neurol 262:215–226.

Condé F, Audinat E, Maire-Lepoivre E, Crépel F (1990) Afferent connections of the medial frontal cortex of the rat. A study using retrograde transport of fluorescent dyes. I. Thalamic afferents. Brain Res Bull 24:341–354.

Condé F, Maire-lepoivre E, Audinat E, Crépel F (1995) Afferent connections of the medial frontal cortex of the rat. II. Cortical and subcortical afferents. J Comp Neurol 352:567–593.

Costa-Faidella J, Baldeweg T, Grimm S, Escera C (2011) Interactions between "what" and "when" in the auditory system: Temporal predictability enhances repetition suppression. J Neurosci 31:18590–18597.

Costa-Faidella J, Sussman ES, Escera C (2017) Selective entrainment of brain oscillations drives auditory perceptual organization. Neuroimage 159:195–206.

Czisch M, Wehrle R, Stiegler A, Peters H, Andrade K, Holsboer F, Sämann PG (2009) Acoustic oddball during NREM sleep: A combined EEG/fMRI study Grothe B, ed. PLoS One 4:e6749.

Dalley JW, Cardinal RN, Robbins TW (2004) Prefrontal executive and cognitive functions in rodents: Neural and neurochemical substrates. In: Neuroscience and Biobehavioral Reviews, pp 771–784. Neurosci Biobehav Rev.

Dalton P (2000) Psychophysical and Behavioral Characteristics of Olfactory Adaptation.

de Ribaupierre F, Goldstein MH, Yeni-Komshian G (1972) Intracellular study of the cat's primary auditory cortex. Brain Res 48:185–204.

DeFelipe J et al. (2013) New insights into the classification and nomenclature of cortical GABAergic interneurons. Nat Rev Neurosci 14:202–216.

Dégenètais E, Thierry AM, Glowinski J, Gioanni Y (2002) Electrophysiological properties of pyramidal neurons in the rat prefrontal cortex: An in vivo intracellular recording study. Cereb Cortex 12:1–16.

Denardo LA, Berns DS, Deloach K, Luo L (2015) Connectivity of mouse somatosensory and prefrontal cortex examined with trans-synaptic tracing. Nat Neurosci 18:1687–

1697.

Denève S, Machens CK (2016) Efficient codes and balanced networks. Nat Neurosci 19:375–382.

Deouell LY (2007) The frontal generator of the mismatch negativity revisited. J Psychophysiol 21:188–203.

Dhruv NT, Carandini M (2014) Cascaded Effects of Spatial Adaptation in the Early Visual System. Neuron 81:529–535.

Díaz-Quesada M, Maravall M (2008) Intrinsic mechanisms for adaptive gain rescaling in barrel cortex. J Neurosci 28:696–710.

Divac I, Mogensen J, Petrovic-Minic B, Zilles K, Regidor J (1993) Cortical projections of the thalamic mediodorsal nucleus in the rat. Definition of the prefrontal cortex. Acta Neurobiol Exp (Wars) 53:425–429.

Doeller CF, Opitz B, Mecklinger A, Krick C, Reith W, Schröger E (2003) Prefrontal cortex involvement in preattentive auditory deviance detection: Neuroimaging and electrophysiological evidence. Neuroimage 20:1270–1282.

Douglas RJ, Martin KAC (2004) Neuronal circuits of the neocortex. Annu Rev Neurosci 27:419–451.

Dragoi V, Sharma J, Sur M (2000) Adaptation-induced plasticity of orientation tuning in adult visual cortex. Neuron 28:287–298.

Duque D, Malmierca MS (2015) Stimulus-specific adaptation in the inferior colliculus of the mouse: anesthesia and spontaneous activity effects. Brain Struct Funct 220:3385–3398.

Duque D, Pais R, Malmierca MS (2018) Stimulus-specific adaptation in the anesthetized mouse revealed by brainstem auditory evoked potentials. Hear Res 370:294–301.

Duque D, Pérez-González D, Ayala YA, Palmer AR, Malmierca MS (2012) Topographic distribution, frequency, and intensity dependence of stimulus-specific adaptation in the inferior colliculus of the rat. J Neurosci 32:17762–17774.

Dürschmid S, Edwards E, Reichert C, Dewar C, Hinrichs H, Heinze H-J, Kirsch HE, Dalal SS, Deouell LY, Knight RT (2016) Hierarchy of prediction errors for auditory events in human temporal and frontal cortex. Proc Natl Acad Sci 113:6755–6760.

Edwards E, Soltani M, Deouell LY, Berger MS, Knight RT (2005) High gamma activity in response to deviant auditory stimuli recorded directly from human cortex. J Neurophysiol 94:4269–4280.

Escera C, Alho K, Winkler I, Näätänen R (1998) Neural mechanisms of involuntary attention to acoustic novelty and change. J Cogn Neurosci 10:590–604.

Escera C, Malmierca MS (2014) The auditory novelty system: an attempt to integrate human and animal research. Psychophysiology 51:111–123.

Escera C, Yago E, Corral M-J, Corbera S, Nunez MI (2003) Attention capture by auditory significant stimuli: semantic analysis follows attention switching. Eur J Neurosci 18:2408–2412.

Faye-Lund H, Osen KK (1985) Anatomy of the inferior colliculus in rat. Anat Embryol (Berl) 171:1–20.

Fishman YI (2014) The mechanisms and meaning of the mismatch negativity. Brain Topogr 27:500–526.

Fitzgerald K, Todd J (2020) Making Sense of Mismatch Negativity. Front Psychiatry 11:468.

Fogelson N, Shah M, Scabini D, Knight RT (2009) Prefrontal cortex is critical for contextual processing: evidence from brain lesions. Brain 132:3002–3010.

Friston K (2003) Learning and inference in the brain. Neural Networks 16:1325–1352.

Friston K (2005) A theory of cortical responses. Philos Trans R Soc B Biol Sci 360:815–836.

Friston K (2009) The free-energy principle: a rough guide to the brain? Trends Cogn Sci 13:293–301.

Friston K (2010) The free-energy principle: a unified brain theory? Nat Rev Neurosci 11:127–138.

Friston K (2018) Does predictive coding have a future? Nat Neurosci 21:1019–1021.

Gabbott PLA, Dickie BGM, Vaid RR, Headlam AJN, Bacon SJ (1997) Local-circuit neurones in the medial prefrontal cortex (areas 25, 32 and 24b) in the rat: Morphology and quantitative distribution. J Comp Neurol 377:465–499.

Gabbott PLA, Warner TA, Jays PRL, Salway P, Busby SJ (2005) Prefrontal cortex in the rat: Projections to subcortical autonomic, motor, and limbic centers. J Comp Neurol 492:145–177.

Gaebler AJ, Mathiak K, Koten JW, König AA, Koush Y, Weyer D, Depner C, Matentzoglu S, Edgar JC, Willmes K, Zvyagintsev M (2015) Auditory mismatch impairments are characterized by core neural dysfunctions in schizophrenia. Brain 138:1410–1423.

Garrido MI, Friston KJ, Kiebel SJ, Stephan KE, Baldeweg T, Kilner JM (2008) The functional anatomy of the MMN: a DCM study of the roving paradigm. Neuroimage 42:936–944.

Garrido MI, Kilner JM, Kiebel SJ, Friston KJ (2009a) Dynamic causal modeling of the response to frequency Deviants. J Neurophysiol 101:2620–2631.

Garrido MI, Kilner JM, Kiebel SJ, Stephan KE, Baldeweg T, Friston KJ (2009b) Repetition suppression and plasticity in the human brain. Neuroimage 48:269–279.

Garrido MI, Kilner JM, Kiebel SJ, Stephan KE, Friston KJ (2007) Dynamic causal modelling of evoked potentials: A reproducibility study. Neuroimage 36:571–580.

Garrido MI, Kilner JM, Stephan KE, Friston KJ (2009c) The mismatch negativity: A review

of underlying mechanisms. Clin Neurophysiol 120:453–463.

Geis HR, van der Heijden M, Borst JGG (2011) Subcortical input heterogeneity in the mouse inferior colliculus. J Physiol 589:3955–3967.

Geniec P, Morest DK (1971) The neuronal architecture of the human posterior colliculus. A study with the Golgi method. Acta Oto-Laryngologica, Suppl 295:1–33.

Giard MH, Perrin F, Pernier J, Bouchet P (1990) Brain generators implicated in the processing of auditory stimulus deviance: a topographic event-related potential study. Psychophysiology 27:627–640.

Grimm S, Escera C (2012) Auditory deviance detection revisited: Evidence for a hierarchical novelty system. Int J Psychophysiol 85:88–92.

Hamm JP, Shymkiv Y, Han S, Yang W, Yuste R (2021) Cortical ensembles selective for context. Proc Natl Acad Sci U S A 118:In press.

Hamm JP, Yuste R (2016) Somatostatin Interneurons Control a Key Component of Mismatch Negativity in Mouse Visual Cortex. CellReports 16:597–604.

Harms L, Fulham WR, Todd J, Budd TW, Hunter M, Meehan C, Penttonen M, Schall U, Zavitsanou K, Hodgson DM, Michie PT (2014) Mismatch negativity (MMN) in freely-moving rats with several experimental controls. PLoS One 9:e110892.

Harms L, Michie PT, Näätänen R (2016) Criteria for determining whether mismatch responses exist in animal models: Focus on rodents. Biol Psychol 116:28–35.

Heidbreder CA, Groenewegen HJ (2003) The medial prefrontal cortex in the rat: Evidence for a dorso-ventral distinction based upon functional and anatomical characteristics. Neurosci Biobehav Rev 27:555–579.

Heilbron M, Chait M (2018) Great Expectations: Is there Evidence for Predictive Coding in Auditory Cortex? Neuroscience 389:54–73.

Helmholtz H (1867) Handbuch der physiologischen Optik,. Leipzig: Voss.

Hernández O, Espinosa N, Pérez-González D, Malmierca MS (2005) The inferior colliculus of the rat: A quantitative analysis of monaural frequency response areas. Neuroscience 132:203–217.

Hershenhoren I, Taaseh N, Antunes FM, Nelken I (2014) Intracellular correlates of stimulus-specific adaptation. J Neurosci 34:3303–3319.

Hohwy J (2013) The predictive mind. England: Oxford University Press.

Hoover WB, Vertes RP (2007) Anatomical analysis of afferent projections to the medial prefrontal cortex in the rat. Brain Struct Funct 212:149–179.

Horvath A, Szucs A, Csukly G, Sakovics A, Stefanics G, Kamondi A (2018) EEG and ERP biomarkers of Alzheimer's disease: A critical review. Front Biosci - Landmark 23:183–220.

Horváth J, Winkler I (2004) How the human auditory system treats repetition amongst

change. Neurosci Lett 368:157–161.

Imada A, Morris A, Wiest MC (2013) Deviance detection by a P3-like response in rat posterior parietal cortex. Front Integr Neurosci 6:127.

Isaacson JS, Scanziani M (2011) How inhibition shapes cortical activity. Neuron 72:231–243.

Ito T, Bishop DC, Oliver DL (2011) Expression of glutamate and inhibitory amino acid vesicular transporters in the rodent auditory brainstem. J Comp Neurol 519:316–340.

Ito T, Malmierca MS (2018) Neurons, Connections, and Microcircuits of the Inferior Colliculus. In: The Mammalian Auditory Pathways. Springer Handbook of Auditory Research, vol 65, pp 127–167. Springer, Cham.

Jääskeläinen IP, Ahveninen J, Bonmassar G, Dale AM, Ilmoniemi RJ, Levänen S, Lin F-H, May PJC, Melcher J, Stufflebeam S, Tiitinen H, Belliveau JW (2004) Human posterior auditory cortex gates novel sounds to consciousness. Proc Natl Acad Sci 101:6809–6814.

Jia G, Li X, Liu C, He J, Gao L (2021) Stimulus-Specific Adaptation in Auditory Thalamus Is Modulated by the Thalamic Reticular Nucleus. ACS Chem Neurosci:acschemneuro.1c00137.

Jodo E, Inaba H, Narihara I, Sotoyama H, Kitayama E, Yabe H, Namba H, Eifuku S, Nawa H (2019) Neonatal exposure to an inflammatory cytokine, epidermal growth factor, results in the deficits of mismatch negativity in rats. Sci Rep 9:7503.

Kandel ER, James H. Schwartz TMJ, Siegelbaum SA, A. J. Hudspeth (2013) The Auditory Central Nervous System. In: Principles of Neural Science, Fifth. McGraw-Hill Companies.

Kant I (1781) Critik der reinen Vernunft. Hamburg.

Katz Y, Heiss JE, Lampl I (2006) Cross-whisker adaptation of neurons in the rat barrel cortex. J Neurosci 26:13363–13372.

Keller GB, Mrsic-Flogel TD (2018) Predictive Processing: A Canonical Cortical Computation. Neuron 100:424–435.

Kesner RP, Churchwell JC (2011) An analysis of rat prefrontal cortex in mediating executive function. Neurobiol Learn Mem 96:417–431.

Kiehl KA, Stevens MC, Laurens KR, Pearlson G, Calhoun VD, Liddle PF (2005) An adaptive reflexive processing model of neurocognitive function: Supporting evidence from a large scale (n = 100) fMRI study of an auditory oddball task. Neuroimage 25:899–915.

Kimura M, Takeda Y (2015) Automatic prediction regarding the next state of a visual object: Electrophysiological indicators of prediction match and mismatch. Brain Res 1626:31–44.

King AJ, Nelken I (2009) Unraveling the principles of auditory cortical processing: Can we learn from the visual system? Nat Neurosci 12:698–701.

Koelsch S, Heinke W, Sammler D, Olthoff D (2006) Auditory processing during deep propofol sedation and recovery from unconsciousness. Clin Neurophysiol 117:1746–1759.

Kohn A (2007) Visual Adaptation: Physiology, Mechanisms, and Functional Benefits. J Neurophysiol 97:3155–3164.

Kohn A, Movshon JA (2003) Neuronal adaptation to visual motion in area MT of the macaque. Neuron 39:681–691.

Kujala T, Tervaniemi M, Schröger E (2007) The mismatch negativity in cognitive and clinical neuroscience: Theoretical and methodological considerations. Biol Psychol 74:1–19.

Loftus WC, Malmierca MS, Bishop DC, Oliver DL (2008) The cytoarchitecture of the inferior colliculus revisited: a common organization of the lateral cortex in rat and cat. Neuroscience 154:196–205.

Lumani A, Zhang H (2010) Responses of neurons in the rat's dorsal cortex of the inferior colliculus to monaural tone bursts. Brain Res 1351:115–129.

Malmierca M s. (1991) Reconstrucción tridimensional por ordenador de neuronas impregnadas con el método de Golgi en el coliculo inferior de la rata.

Malmierca MS (2003) The structure and physiology of the rat auditory system: An overview. Int Rev Neurobiol 56:147–211.

Malmierca MS (2015) Auditory system. In: The Rat Nervous System, 4th Editio. (Paxinos G, ed), pp 865–946. Amsterdam: Academic Press.

Malmierca MS, Anderson LA, Antunes FM (2015) The cortical modulation of stimulus-specific adaptation in the auditory midbrain and thalamus: a potential neuronal correlate for predictive coding. Front Syst Neurosci 9:19.

Malmierca MS, Blackstad TW, Osen KK (2011) Computer-assisted 3-D reconstructions of Golgi-impregnated neurons in the cortical regions of the inferior colliculus of rat. Hear Res 274:13–26.

Malmierca MS, Blackstad TW, Osen KK, Karagülle T, Molowny RL (1993) The central nucleus of the inferior colliculus in rat: A Golgi and computer reconstruction study of neuronal and laminar structure. J Comp Neurol 333:1–27.

Malmierca MS, Cristaudo S, Pérez-González D, Covey E (2009a) Stimulus-specific adaptation in the inferior colliculus of the anesthetized rat. J Neurosci 29:5483–5493.

Malmierca MS, Hernández O, Antunes FM, Rees A (2009b) Divergent and point-to-point connections in the commissural pathway between the inferior colliculi. J Comp Neurol 514:226–239.

Malmierca MS, Izquierdo MA, Cristaudo S, Hernández O, Pérez-González D, Covey E, Oliver DL (2008) A discontinuous tonotopic organization in the inferior colliculus of the rat. J Neurosci 28:4767–4776.

Malmierca MS, Merchán MA, Henkel CK, Oliver DL (2002) Direct projections from cochlear nuclear complex to auditory thalamus in the rat. J Neurosci 22:10891–10897.

Malmierca MS, Rees A, Le Beau FEN, Bjaalie JG (1995) Laminar organization of frequency-defined local axons within and between the inferior colliculi of the guinea pig. J Comp Neurol 357:124–144.

Malmierca MS, Ryugo DK (2011) Descending connections of auditory cortex to the midbrain and brain stem. In: The Auditory Cortex, pp 189–208. Springer US.

Malmierca MS, Ryugo DK (2012) Cortical descending projections to auditory midbrain and brainstem. The auditory cortex. San Diego: Springer-Verlag.

Malmierca MS, Saint Marie RL, Merchan MA, Oliver DL (2005) Laminar inputs from dorsal cochlear nucleus and ventral cochlear nucleus to the central nucleus of the inferior colliculus: two patterns of convergence. Neuroscience 136:883–894.

Malmierca MS, Sanchez-Vives M V, Escera C, Bendixen A (2014) Neuronal adaptation, novelty detection and regularity encoding in audition. Front Syst Neurosci 8:111.

Markov NT, Ercsey-Ravasz M, Van Essen DC, Knoblauch K, Toroczkai Z, Kennedy H (2013) Cortical high-density counterstream architectures. Science (80-) 342.

Martin-Cortecero J, Nuñez A (2016) Sensory responses in the medial prefrontal cortex of anesthetized rats. Implications for sensory processing. Neuroscience 339:109–123.

Mashour GA, Hudetz AG (2017) Bottom-Up and Top-Down Mechanisms of General Anesthetics Modulate Different Dimensions of Consciousness. Front Neural Circuits 11:44.

May PJC, Tiitinen H (2010) Mismatch negativity (MMN), the deviance-elicited auditory deflection, explained. Psychophysiology 47:66–122.

Mittag M, Takegata R, Winkler I (2016) Transitional Probabilities Are Prioritized over Stimulus/Pattern Probabilities in Auditory Deviance Detection: Memory Basis for Predictive Sound Processing. J Neurosci 36:9572–9579.

Morest DK, Oliver DL (1984) The neuronal architecture of the inferior colliculus in the cat: Defining the functional anatomy of the auditory midbrain. J Comp Neurol 222:209–236.

Morlet D, Fischer C (2014) MMN and novelty P3 in coma and other altered states of consciousness: A review. Brain Topogr 27:467–479.

Movshon JA, Lennie P (1979) Pattern-selective adaptation in visual cortical neurones. Nature 278:850–852.

Musall S, Haiss F, Weber B, von der Behrens W (2017) Deviant Processing in the Primary

Somatosensory Cortex. Cereb Cortex 27:863–876.

Näätänen R (1990) The role of attention in auditory information processing as revealed by event-related potentials and other brain measures of cognitive function. Behav Brain Sci 13:201–233.

Näätänen R, Alho K (1995) Mismatch negativity-a unique measure of sensory processing in audition. Int J Neurosci 80:317–337.

Näätänen R, Gaillard AWK, Mäntysalo S (1978) Early selective-attention effect on evoked potential reinterpreted. Acta Psychol (Amst) 42:313–329.

Näätänen R, Jacobsen T, Winkler I (2005) Memory-based or afferent processes in mismatch negativity (MMN): A review of the evidence. Psychophysiology 42:25–32.

Näätänen R, Michie PT (1979) Early selective-attention effects on the evoked potential: A critical review and reinterpretation. Biol Psychol 8:81–136.

Näätänen R, Paavilainen P, Alho K, Reinikainen K, Sams M (1989) Do event-related potentials reveal the mechanism of the auditory sensory memory in the human brain? Neurosci Lett 98:217–221.

Näätänen R, Paavilainen P, Rinne T, Alho K (2007) The mismatch negativity (MMN) in basic research of central auditory processing: A review. Clin Neurophysiol 118:2544–2590.

Näätänen R, Teder W, Alho K, Lavikainen J (1992) Auditory attention and selective input modulation: A topographical ERP study. Neuroreport 3:493–496.

Näätänen R, Todd J, Schall U (2016) Mismatch negativity (MMN) as biomarker predicting psychosis in clinically at-risk individuals. Biol Psychol 116:36–40.

Näätänen R, Winkler I (1999) The concept of auditory stimulus representation in cognitive neuroscience. Psychol Bull 125:826–859.

Nashida T, Yabe H, Sato Y, Hiruma T, Sutoh T, Shinozaki N, Kaneko S (2000) Automatic auditory information processing in sleep. Sleep 23:821–828.

Natan RG, Briguglio JJ, Mwilambwe-Tshilobo L, Jones SI, Aizenberg M, Goldberg EM, Geffen MN (2015) Complementary control of sensory adaptation by two types of cortical interneurons. Elife 4.

Nelken I (2004) Processing of complex stimuli and natural scenes in the auditory cortex. Curr Opin Neurobiol 14:474–480.

Nelken I (2014) Stimulus-specific adaptation and deviance detection in the auditory system: experiments and models. Biol Cybern 108:655–663.

Nieto-Diego J, Malmierca MS (2016) Topographic Distribution of Stimulus-Specific Adaptation across Auditory Cortical Fields in the Anesthetized Rat Zatorre R, ed. PLoS Biol 14:e1002397.

Nourski K V, Steinschneider M, Rhone AE, Kawasaki H, Howard MA, Banks MI (2018a)

Processing of auditory novelty across the cortical hierarchy: An intracranial electrophysiology study. Neuroimage 183:412–424.

Nourski K V, Steinschneider M, Rhone AE, Kawasaki H, Howard MA, Banks MI (2018b) Auditory Predictive Coding across Awareness States under Anesthesia: An Intracranial Electrophysiology Study. J Neurosci 38:8441–8452.

Ojima H, Murakami K (2002) Intracellular characterization of suppressive responses in supragranular pyramidal neurons of cat primary auditory cortex in vivo. Cereb Cortex 12:1079–1091.

Oliver DL, Cant NB, Fay RR, Popper AN (2018) The mammalian auditory pathways : synaptic organization and microcircuits. Springer.

Oliver DL, Morest DK (1984) The central nucleus of the inferior colliculus in the cat. J Comp Neurol 222:237–264.

Olthof BMJ, Rees A, Gartside SE (2019) Multiple Nonauditory Cortical Regions Innervate the Auditory Midbrain. J Neurosci 39:8916–8928.

Opitz B, Rinne T, Mecklinger A, Von Cramon DY, Schröger E (2002) Differential contribution of frontal and temporal cortices to auditory change detection: FMRI and ERP results. Neuroimage 15:167–174.

Oswald A-MM, Schiff ML, Reyes AD (2006) Synaptic mechanisms underlying auditory processing. Curr Opin Neurobiol 16:371–376.

Paavilainen P, Mikkonen M, Kilpeläinen M, Lehtinen R, Saarela M, Tapola L (2003) Evidence for the different additivity of the temporal and frontal generators of mismatch negativity: A human auditory event-related potential study. Neurosci Lett 349:79–82.

Palmer AR, Shackleton TM, Sumner CJ, Zobay O, Rees A (2013) Classification of frequency response areas in the inferior colliculus reveals continua not discrete classes. J Physiol 591:4003–4025.

Parr T, Rikhye RV, Halassa MM, Friston KJ (2019) Prefrontal Computation as Active Inference. Cereb Cortex:1–14.

Parras GG, Nieto-Diego J, Carbajal G V., Valdés-Baizabal C, Escera C, Malmierca MS (2017) Neurons along the auditory pathway exhibit a hierarchical organization of prediction error. Nat Commun 8:2148.

Parras GG, Valdés-Baizabal C, Harms L, Michie PT, Malmierca MS (2020) The effect of NMDA-R antagonist, MK-801, on neuronal mismatch along the rat auditory thalamocortical pathway. Sci Rep 10:12391.

Pekkonen E (2000) Mismatch Negativity in Aging and in Alzheimer's and Parkinson's Diseases. Audiol Neurotol 5:216–224.

Pérez-González D, Malmierca MS (2014) Adaptation in the auditory system: an overview.

Front Integr Neurosci 8:19.

Pérez-González D, Malmierca MS, Covey E (2005) Novelty detector neurons in the mammalian auditory midbrain. Eur J Neurosci 22:2879–2885.

Pérez-González D, Malmierca MS, Moore JM, Hernández O, Covey E (2006) Duration selective neurons in the inferior colliculus of the rat: Topographic distribution and relation of duration sensitivity to other response properties. J Neurophysiol 95:823–836.

Peruzzi D, Sivaramakrishnan S, Oliver DL (2000) Identification of cell types in brain slices of the inferior colliculus. Neuroscience 101:403–416.

Phillips HN, Blenkmann A, Hughes LE, Kochen S, Bekinschtein TA, Cam-Can, Rowe JB (2016) Convergent evidence for hierarchical prediction networks from human electrocorticography and magnetoencephalography. Cortex 82:192–205.

Quaedflieg CW, Münte S, Kalso E, Sambeth A (2014) Effects of remifentanil on processing of auditory stimuli: A combined MEG/EEG study. J Psychopharmacol 28:39–48.

Rabang CF, Parthasarathy A, Venkataraman Y, Fisher ZL, Gardner SM, Bartlett EL (2012) A computational model of inferior colliculus responses to amplitude modulated sounds in young and aged rats. Front Neural Circuits 6:77.

Ranlund S, Adams RA, Díez Á, Constante M, Dutt A, Hall MH, Maestro Carbayo A, Mcdonald C, Petrella S, Schulze K, Shaikh M, Walshe M, Friston K, Pinotsis D, Bramon E (2016a) Impaired prefrontal synaptic gain in people with psychosis and their relatives during the mismatch negativity. Hum Brain Mapp 37:351–365.

Ranlund S, Adams RA, Díez Á, Constante M, Dutt A, Hall MH, Maestro Carbayo A, Mcdonald C, Petrella S, Schulze K, Shaikh M, Walshe M, Friston K, Pinotsis D, Bramon E (2016b) Impaired prefrontal synaptic gain in people with psychosis and their relatives during the mismatch negativity. Hum Brain Mapp 37:351–365.

Rao RPN, Ballard DH (1999) Predictive coding in the visual cortex: A functional interpretation of some extra-classical receptive-field effects. Nat Neurosci 2:79–87.

Reches A, Gutfreund Y (2008) Stimulus-specific adaptations in the gaze control system of the barn owl. J Neurosci 28:1523–1533.

Riga D, Matos MR, Glas A, Smit AB, Spijker S, Van den Oever MC (2014) Optogenetic dissection of medial prefrontal cortex circuitry. Front Syst Neurosci 8:230

Rinne T, Alho K, Ilmoniemi RJ, Virtanen J, Näätänen R (2000) Separate Time Behaviors of the Temporal and Frontal Mismatch Negativity Sources. Neuroimage 12:14–19.

Rodríguez RA, Bussière M, Froeschl M, Nathan HJ (2014) Auditory-evoked potentials during coma: Do they improve our prediction of awakening in comatose patients? J Crit Care 29:93–100.

Rosburg T, Trautner P, Dietl T, Korzyukov OA, Boutros NN, Schaller C, Elger CE, Kurthen

M (2005) Subdural recordings of the mismatch negativity (MMN) in patients with focal epilepsy. Brain 128:819–828.

Ruhnau P, Herrmann B, Schröger E (2012) Finding the right control: the mismatch negativity under investigation. Clin Neurophysiol 123:507–412.

Rummell BP, Klee JL, Sigurdsson T (2016) Attenuation of responses to self-generated sounds in auditory cortical neurons. J Neurosci 36:12010–12026.

Rutecki PA (1992) Neuronal excitability: voltage-dependent currents and synaptic transmission. J Clin Neurophysiol 9:195–211.

Sah P, Faber ESL (2002) Channels underlying neuronal calcium-activated potassium currents. Prog Neurobiol 66:345–353.

Saldaña E, Feliciano M, Mugnaini E (1996) Distribution of descending projections from primary auditory neocortex to inferior colliculus mimics the topography of intracollicular projections. J Comp Neurol 371:15–40.

Saldaña E, Merchán MA (1992) Intrinsic and commissural connections of the rat inferior colliculus. J Comp Neurol 319:417–437.

Sanchez-Vives M V., Nowak LG, McCormick DA (2000a) Cellular mechanisms of long-lasting adaptation in visual cortical neurons in vitro. J Neurosci 20:4286–4299.

Sanchez-Vives M V., Nowak LG, McCormick DA (2000b) Membrane mechanisms underlying contrast adaptation in cat area 17 in vivo. J Neurosci 20:4267–4285.

Sarter M, Markowitsch HJ (1983) Convergence of basolateral amygdaloid and mediodorsal thalamic projections in different areas of the frontal cortex in the rat. Brain Res Bull 10:607–622.

Sarter M, Markowitsch HJ (1984) Collateral innervation of the medial and lateral prefrontal cortex by amygdaloid, thalamic, and brain-stem neurons. J Comp Neurol 224:445–460.

Schall U (2016) Is it time to move mismatch negativity into the clinic? Biol Psychol 116:41–46.

Schreiner CE, Langner G (1997) Laminar fine structure of frequency organization in auditory midbrain. Nature 388:383–386.

Schröger E, Wolff C (1996) Mismatch response of the human brain to changes in sound location. Neuroreport 7:3005–3008.

Schwartz S, Shinn-Cunningham B, Tager-Flusberg H (2018) Meta-analysis and systematic review of the literature characterizing auditory mismatch negativity in individuals with autism. Neurosci Biobehav Rev 87:106–117.

Schwindt PC, Spain WJ, Foehring RC, Stafstrom CE, Chubb MC, Crill WE (1988) Multiple potassium conductances and their functions in neurons from cat sensorimotor cortex in vitro. J Neurophysiol 59:424–449.

Seamans JK, Lapish CC, Durstewitz D (2008) Comparing the prefrontal cortex of rats and primates: Insights from electrophysiology. Neurotox Res 14:249–262.

Sesack SR, Deutch AY, Roth RH, Bunney BS (1989) Topographical organization of the efferent projections of the medial prefrontal cortex in the rat: An anterograde tract-tracing study with Phaseolus vulgaris leucoagglutinin. J Comp Neurol 290:213–242.

Sikkens T, Bosman CA, Olcese U (2019) The Role of Top-Down Modulation in Shaping Sensory Processing Across Brain States: Implications for Consciousness. Front Syst Neurosci 13:31.

Sivaramakrishnan S, Oliver DL (2001) Distinct K currents result in physiologically distinct cell types in the inferior colliculus of the rat. J Neurosci 21:2861–2877.

Spratling MW (2008a) Predictive coding as a model of biased competition in visual attention. Vision Res 48:1391–1408.

Spratling MW (2008b) Reconciling predictive coding and biased competition models of cortical function. Front Comput Neurosci 2:4.

Srivastava HK, Bandyopadhyay S (2020) Parallel lemniscal and non-lemniscal sources control auditory responses in the orbitofrontal cortex (OFC). eneuro:ENEURO.0121-20.2020.

Stefanics G, Czigler I (2012) Automatic prediction error responses to hands with unexpected laterality: an electrophysiological study. Neuroimage 63:253–261.

Stefanics G, Kremlácek J, Czigler I (2014) Visual mismatch negativity: a predictive coding view. Front Hum Neurosci 8:19.

Strauss M, Sitt JD, King J-R, Elbaz M, Azizi L, Buiatti M, Naccache L, van Wassenhove V, Dehaene S (2015) Disruption of hierarchical predictive coding during sleep. Proc Natl Acad Sci U S A 112:E1353-62.

Sun H, Wu SH (2008) Modification of membrane excitability of neurons in the rat's dorsal cortex of the inferior colliculus by preceding hyperpolarization. Neuroscience 154:257–272.

Swanson LR (2016) The Predictive Processing Paradigm Has Roots in Kant. Front Syst Neurosci 10:79.

Szymanski FD, García-Lázaro JA, Schnupp JWH (2009) Current source density profiles of stimulus-specific adaptation in rat auditory cortex. J Neurophysiol 102:1483–1490.

Takaura K, Fujii N (2016) Facilitative effect of repetitive presentation of one stimulus on cortical responses to other stimuli in macaque monkeys - a possible neural mechanism for mismatch negativity Foxe J, ed. Eur J Neurosci 43:516–528.

Tan ML, Theeuwes HP, Feenstra L, Borst JGG (2007) Membrane Properties and Firing Patterns of Inferior Colliculus Neurons: An In Vivo Patch-Clamp Study in Rodents. J Neurophysiol 98:443–453.

Tanaka I, Ezure K (2004) Overall distribution of GLYT2 mRNA-containing versus GAD67 mRNA-containing neurons and colocalization of both mRNAs in midbrain, pons, and cerebellum in rats. Neurosci Res 49:165–178.

Todd J, Harms L, Schal l U, Michie PT (2013) Mismatch negativity: Translating the potential. Front Psychiatry 4:171.

Todorovic A, de Lange FP (2012) Repetition suppression and expectation suppression are dissociable in time in early auditory evoked fields. J Neurosci 32:13389–13395.

Tse CY, Penney TB (2008) On the functional role of temporal and frontal cortex activation in passive detection of auditory deviance. Neuroimage 41:1462–1470.

Ulanovsky N, Las L, Farkas D, Nelken I (2004) Multiple time scales of adaptation in auditory cortex neurons. J Neurosci 24:10440–10453.

Ulanovsky N, Las L, Nelken I (2003) Processing of low-probability sounds by cortical neurons. Nat Neurosci 6:391–398.

Uylings HBM, Groenewegen HJ, Kolb B (2003) Do rats have a prefrontal cortex? Behav Brain Res 146:3–17.

Uylings HBM, Van Eden CG (1991) Qualitative and quantitative comparison of the prefrontal cortex in rat and in primates, including humans. In: Progress in Brain Research. The Prefrontal Its Structure, Function and Cortex Pathology. (H.B.M. Uylings, C.G. Van Eden, J.P.C. De Bruin, M.A. Corner MGPF, ed), pp 31–62. Elsevier.

Valdés-Baizabal C, Carbajal G V., Pérez-González D, Malmierca MS (2020a) Dopamine modulates subcortical responses to surprising sounds. PLoS Biol 18.

Valdés-Baizabal C, Casado-Román L, Bartlett EL, Malmierca MS (2020b) In vivo whole-cell recordings of stimulus-specific adaptation in the inferior colliculus. Hear Res.

van Eden CG, Uylings HBM (1985) Cytoarchitectonic development of the prefrontal cortex in the rat. J Comp Neurol 241:253–267.

Vlaskamp C, Oranje B, Madsen GF, Møllegaard Jepsen JR, Durston S, Cantio C, Glenthøj B, Bilenberg N (2017) Auditory processing in autism spectrum disorder: Mismatch negativity deficits. Autism Res 10:1857–1865.

Vogt BA, Paxinos G (2014) Cytoarchitecture of mouse and rat cingulate cortex with human homologies. Brain Struct Funct 219:185–192.

Volkov IO, Galazjuk A V. (1991) Formation of spike response to sound tones in cat auditory cortex neurons: Interaction of excitatory and inhibitory effects. Neuroscience 43:307–321.

Wang H, Han Y-F, Chan Y-S, He J (2014) Stimulus-specific adaptation at the synapse level in vitro. Maravall M, ed. PLoS One 9:e114537.

Wang X-J, Liu Y, Sanchez-Vives M V, McCormick DA (2003) Adaptation and temporal decorrelation by single neurons in the primary visual cortex. J Neurophysiol 89:3279–

3293.

Wang Y, Markram H, Goodman PH, Berger TK, Ma J, Goldman-Rakic PS (2006) Heterogeneity in the pyramidal network of the medial prefrontal cortex. Nat Neurosci 9:534–542.

Wehr M, Zador AM (2003) Balanced inhibition underlies tuning and sharpens spike timing in auditory cortex. Nature 426:442–446.

Wehr M, Zador AM (2005) Synaptic mechanisms of forward suppression in rat auditory cortex. Neuron 47:437–445.

Whitmire CJ, Stanley GB (2016) Rapid Sensory Adaptation Redux: A Circuit Perspective. Neuron 92:298–315.

Wiens S, Szychowska M, Eklund R, van Berlekom E (2019) Cascade and no-repetition rules are comparable controls for the auditory frequency mismatch negativity in oddball tasks. Psychophysiology 56:e13280.

Winer JA, Schreiner CE (2005) The Inferior Colliculus. Springer New York.

Winkler I, Karmos G, Näätänen R (1996) Adaptive modeling of the unattended acoustic environment reflected in the mismatch negativity event-related potential. Brain Res 742:239–252.

Zaborszky L, Csordas A, Mosca K, Kim J, Gielow MR, Vadasz C, Nadasdy Z (2015) Neurons in the basal forebrain project to the cortex in a complex topographic organization that reflects corticocortical connectivity patterns: an experimental study based on retrograde tracing and 3D reconstruction. Cereb Cortex 25:118–137.

Zelano C, Mohanty A, Gottfried JA (2011) Olfactory Predictive Codes and Stimulus Templates in Piriform Cortex. Neuron 72:178–187.

Zhang H, Kelly JB (2010) Time dependence of binaural responses in the rat's central nucleus of the inferior colliculus. Hear Res 268:271–280.

Zhang LI, Tan AYY, Schreiner CE, Merzenich MM (2003) Topography and synaptic shaping of direction selectivity in primary auditory cortex. Nature 424:201–205.

Zhang Z, Guo G, Zhang J, Li C, Huang Q, Go R, Fukuyama H, Funahashi S, Yan T, Wu J (2019) Do theta oscillations explain the somatosensory change detection mechanism? Biol Psychol 143:103–112.

Zhao L, Liu Y, Shen L, Feng L, Hong B (2011) Stimulus-specific adaptation and its dynamics in the inferior colliculus of rat. Neuroscience 181:163–174.

Zook JM, Casseday JH (1987) Convergence of ascending pathways at the inferior colliculus of the mustache bat,pteronotus parnellii. J Comp Neurol 261:347–361.

8 Publications

Hearing Research 399 (2021) 107978

Contents lists available at ScienceDirect

Hearing Research

journal homepage: www.elsevier.com/locate/heares

Research Paper

In vivo whole-cell recordings of stimulus-specific adaptation in the inferior colliculus

Catalina Valdés-Baizabal [a, b, 1, 2], Lorena Casado-Román [a, b, 2], Edward L. Bartlett [c, d], Manuel S. Malmierca [a, b, e, *]

[a] Cognitive and Auditory Neuroscience Laboratory, Institute of Neuroscience of Castilla y León, University of Salamanca, 37007, Salamanca, Spain
[b] The Salamanca Institute for Biomedical Research (IBSAL), 37007, Salamanca, Spain
[c] Department of Biological Sciences, Purdue University, West Lafayette, IN, 47907, USA
[d] Weldon School of Biomedical Engineering, Purdue University, West Lafayette, IN, 47907, USA
[e] Department of Cell Biology and Pathology, Faculty of Medicine, Campus Miguel de Unamuno, University of Salamanca, 37007, Salamanca, Spain

ARTICLE INFO

Article history:
Received 10 January 2020
Received in revised form
17 April 2020
Accepted 18 April 2020
Available online 30 April 2020

Keywords:
Stimulus-specific adaptation
Inferior colliculus
In vivo whole-cell
Current-clamp
Intrinsic properties
Subthreshold responses

ABSTRACT

The inferior colliculus is an auditory structure where inputs from multiple lower centers converge, allowing the emergence of complex coding properties of auditory information such as stimulus-specific adaptation. Stimulus-specific adaptation is the adaptation of neuronal responses to a specific repeated stimulus, which does not entirely generalize to other new stimuli. This phenomenon provides a mechanism to emphasize saliency and potentially informative sensory inputs. Stimulus-specific adaptation has been traditionally studied analyzing the somatic spiking output. However, studies that correlate within the same inferior colliculus neurons their intrinsic properties, subthreshold responses and the level of acoustic stimulus-specific adaptation are still pending. For this, we recorded *in vivo* whole-cell patch-clamp neurons in the mouse inferior colliculus while stimulating with current injections or the classic auditory oddball paradigm.

Our data based on cases of ten neuron, suggest that although passive properties were similar, intrinsic properties differed between adapting and non-adapting neurons. Non-adapting neurons showed a sustained-regular firing pattern that corresponded to central nucleus neurons and adapting neurons at the inferior colliculus cortices showed variable firing patterns. Our current results suggest that synaptic stimulus-specific adaptation was variable and could not be used to predict the presence of spiking stimulus-specific adaptation. We also observed a small trend towards hyperpolarized membrane potentials in adapting neurons and increased synaptic inhibition with consecutive stimulus repetitions in all neurons. This finding indicates a more simple type of adaptation, potentially related to potassium conductances. Hence, these data represent a modest first step in the intracellular study of stimulus-specific adaptation in inferior colliculus neurons *in vivo* that will need to be expanded with pharmacological manipulations to disentangle specific ionic channels participation.

1. Introduction

The inferior colliculus (IC) is a midbrain structure that integrates auditory inputs from ascending and descending pathways in the auditory system. The IC is the first auditory structure where inputs from lower auditory centers, including the cochlear nucleus, superior olivary complex and lateral lemniscus, converge and send information to the thalamus (Ito and Malmierca, 2018; Malmierca, 2015). The IC is divided into the central nucleus (CNIC) within the lemniscal pathway and the surrounding cortices (dorsal, lateral and rostral) belonging to the nonlemniscal pathway (Ito and Malmierca, 2018; Loftus et al., 2008; Malmierca et al., 2011, 1993). Both pathways present different connection patterns and neuronal type organization (Ito and Malmierca, 2018; Malmierca, 2015). The multiple patterns of afferent convergence allow the emergence of complex coding properties of auditory information such as

* Corresponding author. Cognitive and Auditory Neuroscience Laboratory, Institute of Neuroscience of Castilla y León, University of Salamanca, 37007, Salamanca, Spain.
E-mail address: msm@usal.es (M.S. Malmierca).
[1] Present address: Laboratory of Cellular Neurobiology, Department of Basic Medical Sciences, Section of Medicine, Faculty of Health Sciences, University of La Laguna, 38200 Sta. Cruz de Tenerife, Spain.
[2] These authors contributed equally.

https://doi.org/10.1016/j.heares.2020.107978

List of abbreviations

AP	action potential
CNIC	central nucleus of the inferior colliculus
CSI	common stimulus-specific adaptation index
DCIC	dorsal cortex of the inferior colliculus
DEV	deviant tones
EPSP	excitatory postsynaptic potentials
EPSP-CSI	excitatory postsynaptic potential common stimulus-specific adaptation index
FRA	frequency response area
IC	inferior colliculus
IPSP	inhibitory postsynaptic potentials
IPSP-CSI	inhibitory postsynaptic potential common stimulus-specific adaptation index
last-STD	last-standard tones before a deviant events
LCIC	lateral cortex of the inferior colliculus
next-STD	next-standard tones after a deviant events
n.s.	non-statistically significant difference
PSPs	postsynaptic potentials
PSTH	peristimulus time histogram
SEM	standard error of the mean
SSA	stimulus-specific adaptation
STD	all standard tones
Vm	membrane potential

stimulus-specific adaptation (SSA; Ayala and Malmierca, 2013; Duque et al., 2012; Lumani and Zhang, 2010; Malmierca et al., 2009a,b; Pérez-González et al., 2005; Zhao et al., 2011). SSA is the adaptation of neuronal responses to a specific repeated stimulus, which does not entirely generalize to other different stimuli (Movshon and Lennie, 1979; Ulanovsky et al., 2003). Comparing the responses to a highly repeated standard sound and a rare deviant sound in an oddball paradigm, strong SSA occurs when the responses to the deviant sound are much larger than those for the standard events. This phenomenon provides a mechanism to emphasize salient and potentially informative sensory inputs, which may serve multiple functions such as deviance detection, auditory memory and recognition of acoustic objects (Ayala and Malmierca, 2013).

The IC is also the first region where SSA is evident in the mammalian auditory pathway (Ayala et al., 2013; Duque et al., 2018; Pérez-González et al., 2005), but the cellular mechanisms that govern and contribute to SSA generation are elusive. SSA is typically measured for the somatic spiking output, which results from the interaction between membrane properties, especially the spiking threshold, synaptic inputs, and the tuning characteristics of the inputs. SSA is not evenly distributed within the IC. Neurons in the cortices exhibit strong SSA, while neurons in the CNIC typically have much weaker or lack SSA (Ayala and Malmierca, 2013; Duque et al., 2012; Malmierca et al., 2009a). The inputs associated with the neurons of both the cortices and the CNIC of the IC have been characterized (Ayala et al., 2016). There is a diversity of IC membrane properties, but they broadly fit into onset, accommodating and sustained classes (Geis and Borst, 2013; Kuwada et al., 1997; Ma et al., 2002; Peruzzi et al., 2000; Rabang et al., 2012; Sun et al., 2006; Tan et al., 2007; Wu et al., 2004). Post-synaptic responses to randomly presented pure tones have also been characterized in the IC and are similar to suprathreshold activity. The dorsal cortex of the IC (Geis and Borst, 2013; Geis et al., 2011) shows broad and complex frequency response areas, whereas the CNIC displays sharp tuning, clear tonotopic organization and shorter-latency responses (Geis and Borst, 2009). However, to fully understand SSA, the intrinsic biophysical excitability of a neuron should be integrated with its synaptic physiology, which shapes dynamic information processing (Malinowski et al., 2019). To date, studies that determine within the same neurons their intrinsic neuronal properties, subthreshold responses and their level of acoustic SSA are still pending in the IC *in vivo*. It is important to study these interactions because they might help to understand why non-lemniscal or cortical IC regions exhibit stronger SSA. We propose the hypothesis that adapting (SSA) neurons and non-adapting (no SSA) neurons in the IC differ in their intrinsic neuronal properties and/or subthreshold responses. Thus, the present study aims at determining the possible correlation between the intrinsic neuronal properties (i.e., firing patterns in response to current injections), passive membrane properties, subthreshold responses with their adaptation properties of the IC neurons. These correlations can only be addressed with intracellular recordings, which allow measuring subthreshold postsynaptic responses and responses to current injection. Likewise, we can correlate the level of adaptation from the synaptic input with that of the spiking output response.

2. Methods

2.1. Surgical procedure

Experiments were performed in 10 adult mice (CBA/J; body weights: 22–36 g; ~2–3 months old). All experimental procedures were carried out at the University of Salamanca using methods conforming to the standards of the European Union Directive 2010/63/EU and the Spanish Royal Decree 53/2013 for the use of animals in research and approved by the Bioethics Committee of the University of Salamanca.

Surgical anesthesia was induced with an intraperitoneal injection of ketamine-acepromazine-dexmedetomidine (75, 1 and 1 mg/kg, respectively), which is an optimum cocktail recommended for long surgical or experimental procedures (Flecknell, 2009). A stable anesthetic level was maintained with supplementary doses of ¼ of the induction dose when pedal withdrawal reflexes were present. Body temperature was maintained at 37 °C with a homeothermic blanket system (Cibertec). Glucosaline solution was administered subcutaneously to prevent dehydration (~0.25 ml). The animal was placed in a stereotaxic frame and the skull was surgically exposed. A head-post was cemented with dental acrylic to immobilize the head during recordings. To expose the IC, a craniotomy of ~2 mm in diameter was performed and the dura was removed.

2.2. Whole-cell patch-clamp electrophysiological recordings

We obtained *in vivo* whole-cell recordings with a non-visually guided or blind approach (Margrie et al., 2002). We pulled borosilicate glass pipettes with filament (1.5 mm outer diameter, 0.315 mm wall thickness; World Precision Instruments) to have a resistance of 8 ± 1 MΩ (1–2 μm tip, P-1000 puller from Sutter Instruments). Pipettes were filled with intracellular solution containing (in mM): K-gluconate 125, KCl 20, EGTA 0.5, HEPES 10, Na_2-phosphocreatine 10, Mg-ATP 4 and Na_2-GTP 0.3 (pH 7.2 with KOH and osmolarity between 290 and 300 mOsm).

To keep the brain surface moist and reduce the cerebral pulsations during recordings, the craniotomy was covered with a thin

layer of 2% agarose in ringer solution ([in mM]: NaCl 135, KCl 5.4, $MgCl_2$ 1, $CaCl_2$ 1.8 and HEPES 5 [pH 7.2 with NaOH]). The pipette was introduced into the mouse IC with penetration angles from 10° to 30° and advanced with a micromanipulator (Scientifica). The initial pipette pressure was ~200 mmHg and the pressure was reduced to ~30 mmHg when approaching a cell. The recorded neurons were located at penetration depths ranging from 81 to 600 μm.

2.3. Current injection protocol

We recorded membrane potential (Vm) variations in current-clamp mode during sound stimulation (see section 2.4. below) and during the injection of square current pulse series from −400 pA to 200 pA above the firing threshold, with 100 pA steps and 300 ms pulse lengths. Signals were sampled at 10 kHz, low-pass filtered at 10 kHz and amplified with a MultiClamp 700B Amplifier (Molecular Devices). Command pulse generation and data acquisition were performed with the Axon™ Digidata® 1550A Low-Noise Data Acquisition System *plus* HumSilencer™ Adaptive Noise Cancellation (Molecular devices) controlled by pCLAMP 10.5.0.9 software (Molecular Devices). Thereby, we determined the action potential (AP) threshold and the discharge pattern, the interspike interval, the depolarizing sag generated by hyperpolarizing current pulses (Almanza et al., 2012) and the number of rebound APs of each neuron. We estimated the AP threshold as the value of the current injection at which each neuron discharged AP(s). The amplitude of the depolarizing sag was calculated as the ratio between the voltage at the maximum peak of the most hyperpolarizing pulse (−400 pA) and the voltage of the stable state at the end of the most hyperpolarizing pulse. We assessed the time constant tau adjusting the most hyperpolarizing pulse to a single-exponential function (correlation coefficient > 0.99).

Based on the discharge pattern, we classified neurons as sustained, accommodating, accelerating or burst onset cells. We used the term "accommodating" instead of adapting used by others (Sivaramakrishnan and Oliver, 2001) to avoid confusion with the SSA property treated in the context of this paper. Firing patterns were determined following the work of Sivaramakrishnan and Oliver (2001) and Tan et al. (2007). Briefly, firing patterns were classified at 100 pA above the smallest suprathreshold current injection. Burst-onset cells fire a cluster of two or more APs at the depolarization onset. Accelerating neurons increase their firing rate along with the depolarizing current injection. Accommodating cells present precisely the opposite profile with decreasing firing rates. Sustained neurons fire with a nearly constant interspike interval during the depolarizing pulse. Cells with rebound spikes present them after hyperpolarization pulses. The interspike interval was measured as the time between spikes, while the instantaneous frequency was calculated (automatically by clampfit) by converting each interspike interval into a frequency, and then, averaging these frequencies together.

Membrane potentials were corrected offline for an estimated −11 mV junction potential (Neher, 1992). Data of passive properties (capacitance and membrane resistance) were acquired online and verified offline. We performed analyses offline using Clampfit in the pClamp 10.5.0.9 bundle (Molecular Devices) and SigmaPlot® 11.0 software. To ensure reliable data quality, neurons were discarded from the study when membrane voltage depolarized beyond −44 mV and did not recover the initial membrane potential; auditory or current injection protocols were incomplete; cells did not show APs nor PSPs after sound stimulation with pure tones, following previous work (Tan et al., 2007).

2.4. Sound stimulation and data analyses

We performed experiments in a sound-attenuating chamber. Stimuli were delivered through an electrostatic open-field speaker (TDT-EC1, Tucker-Davis Technologies [TDT]) placed close to the contralateral ear. Stimulus generation and online data visualization were controlled with the RZ6 Multi I/O Processor (TDT), pCLAMP 10.5 (Molecular Devices) and custom software programmed with OpenEx Suite (TDT) and MATLAB (Mathworks). We calibrated the sound system *in situ* using a ¼ inch condenser microphone (model 4136, Brüel & Kjær) and a dynamic signal analyzer (Photon+, Brüel & Kjær). The maximum sound system output was flat between 0.5 and 4.5 kHz (77.11 ± 0.38 dB SPL) and between 5 and 40 kHz (~85 ± 5 dB SPL). The second and third signal harmonics were at least 40 dB lower than the fundamental frequency at the highest output level (Malmierca et al., 2009a).

The monaural frequency response area (FRA; i.e., the combination of frequencies and intensities capable of evoking a response), was then obtained using a randomized presentation of pure tones. Pure tones lasted 75 ms (5 ms rise/fall ramps) and were separated by an onset-to-onset interval of 250 ms. Frequency and intensity of the stimulus varied randomly (0–70 dB SPL in 10 dB steps and 0.1–40 kHz in 25 frequency steps to cover approximately 2–3 octaves above and below the best frequency (i.e., the frequency with the lowest intensity threshold; Hernández et al., 2005).

To study the level of SSA per neuron, we used the classic oddball paradigm following previous studies in our laboratory (Ayala et al., 2013; Ayala and Malmierca, 2018, 2015; Duque et al., 2016, 2012; Malmierca et al., 2019, 2009a; Pérez-González et al., 2012, 2005; Valdés-Baizabal et al., 2017). We selected two frequencies from the FRA of each cell to generate the oddball paradigm. The two frequencies elicited comparable firing rates in the FRA. They were around the characteristic frequency, which is the tone frequency that produces a response at the lowest stimulus level. We presented trains of 400 stimuli at a specific repetition rate (4 Hz) and a level of 10–40 dB above the response threshold. For each neuron, sequences consisted of pure tones of two different frequencies with a ~0.28-octave frequency separation, which were selected within its excitatory FRA. One frequency (f_1) was presented as standard (i.e., a higher probability of occurrence within the sequence, $p = 0.9$); interspersed pseudo-randomly with the second frequency (f_2) presented as deviant (i.e., low probability within the sequence, $p = 0.1$). Sequences began with a minimum of 10 repetitions of standard stimuli, and a minimum of 3 standard tones separated deviant events. After obtaining one data set, the relative probabilities of the two stimuli were reversed, with f_2 as the standard and f_1 as the deviant. Pure tones lasted 75 or 30 ms (5 ms rise/fall ramps) and were separated by an onset-to-onset interval of 250 or 300 ms, respectively.

We analyzed and illustrated data with Clampfit 10.5 (Molecular Devices), SigmaPlot® 11.0 software and custom-written MATLAB scripts. We computed spike counts and peristimulus time histograms (PSTH) with the AP times in response to every stimulus and tested condition, both in the FRA and oddball paradigm. To visualize responses to oddball paradigms, PSTHs were computed with the mean firing rate of the 40 trials of deviant events, 360 trials of standard events and the 40 trials of the standard events preceding the deviant tones (i.e., the tones with the strongest adaptation; named from now onwards as last-standard stimuli). To calculate the adaptation properties of each neuron, we computed the Common SSA Index (CSI); we measured the total firing rate for each condition as the average spike count within the 40 trials of deviant tones and the 40 trials of the last-standard events. The CSI determines the level of SSA for both frequencies of the oddball paradigm at each condition and classifies neurons as adapting

(CSI > 0.25) and non-adapting (CSI ≤ 0.25) as previous studies (Antunes et al., 2010; Ayala et al., 2015, 2013; Duque et al., 2012; Malmierca et al., 2009a). The CSI was calculated with the spike counts for each neuron and the two frequencies of the oddball paradigm (f_1 and f_2):

$$CSI = \frac{\sum Deviant(f_i) - \sum Standard(f_i)}{\sum Deviant(f_i) + \sum Standard(f_i)}; i = 1, 2$$

where Deviant (f_i), Standard (f_i) are spike counts in response to frequency f_i presented as a deviant and standard event, respectively. CSI reflects to what extent the response of standard stimuli was suppressed or adapted. The index ranges between −1 and 1, being positive if the response to the deviant stimulus was greater than the response to the standard stimulus. Thereby, we classified neurons as classically done with CSI values derived from APs measurements. Similarly, we also computed CSIs with postsynaptic potentials (PSPs) to determine whether SSA is reflected in membrane potentials at the subthreshold level. Hence, we can correlate the adaptation-level of the final firing output response with the synaptic input of each cell. Accordingly, we tested the changes in the membrane voltage around stimulus presentation. For this purpose, we removed spiking activity from the voltage trace by replacing the spike with a linear interpolation between the start to the end of the spike and measured the mean membrane potential and areas of excitatory PSPs (EPSPs) and inhibitory PSPs (IPSPs) in analysis windows. We defined the baseline window 75 ms before each stimulus onset and the analysis window of 0–150 ms after stimulus onset for both onset-to-onset intervals and tone durations. Excitatory areas were measured above the mean membrane potential of the baseline plus 1 standard deviation, whereas inhibitory areas were measured below the mean membrane potential of the baseline minus 1 standard deviation. We then computed the CSI values for the excitatory (EPSP-CSI) and the inhibitory (IPSP–CSI) areas in separate with the same CSI equation. This time instead of using the number of APs, we computed the response to standard events as the sum of the area measurements of the 40 stimulus repetitions of the last-standard stimuli and the response to deviant events the sum of the 40 deviant events similarly to previous work in the auditory cortex (Chen et al., 2015). With the measurement of excitatory and inhibitory PSPs areas, we could calculate the CSI with the previous equation. Additionally, to explore the time course of EPSPs and IPSPs, we analyzed the onset latencies of the largest excitatory and inhibitory areas as the first time point of each stimulus repetition. Mean latencies were calculated separately for excitation and inhibition per neuron and stimulus condition.

In the same analysis window from 0 to 150 ms after stimulus onset, we also analyzed mean evoked responses of the excitatory areas, inhibitory areas and the membrane potential according to each stimulus condition: deviant tones, all standard tones, last-standard tones, next-standard tones after deviant events and the standard tones separated according to the number of consecutive standard tones previously presented. To be considered for the analysis, at least a minimum of 20 repetitions of each condition within a stimulation sequence needed to occur. We normalized each response variable within each neuron with the greatest response of all stimuli presented as part of the two oddball sequences. We then determined the correlation between the number of consecutive standard repetitions and the mean values of the normalized mean membrane potential responses, excitatory or inhibitory areas in the entire population with *Pearson correlation analyses.*

2.5. Statistical testing

Data are denoted as means ± standard error of the mean (SEM). To statistically compare the analyzed parameters between neurons grouped according to their CSI levels (adapting neurons, non-adapting neurons and non-spiking neurons with sound-evoked PSPs [i.e., neurons without tone-evoked APs but with tone-evoked PSPs]), we calculated One-Way ANOVA as denoted in Results. When comparisons were statistically different, samples were tested with a Holm-Sidak method. The significance level was set at $\alpha = 0.05$.

2.6. Histology

One cell was biocytin-labeled for histological identification. We used an intracellular solution containing 1% biocytin, which was ejected during the current injection protocol. Five min after injection, the patch pipette was retracted slowly. The animal was transcardially perfused with 4% paraformaldehyde in phosphate-buffered saline and cryoprotected in 30% sucrose. 40 μm sections were cut in the coronal plane with a freezing microtome. The location of biocytin-filled neurons was visualized with an avidin-biotinylated horseradish peroxidase complex with minor modifications to that described by Brandt and Apkarian (1992); Veenman et al. (1992).

3. Results

We recorded *in vivo* whole-cell patch-clamp neurons in the mouse IC while using two types of stimulation: current injection and auditory stimulation. We successfully recorded 10 neurons with an adequate average resting membrane potential of −57.8 ± 3.06 mV, average membrane capacitance of 9 ± 2 pF and average membrane resistance of 510 ± 63.5 MΩ. The access resistance was 14.1 ± 3.7 MΩ. Fig. 1 shows one of these neurons that was histologically labeled in the dorsal cortex of the IC with a pipette solution containing 1% biocytin as control of whole-cell patch-clamp. For all neurons, we recorded their FRA and selected the tones comprising the oddball paradigms (tones of a range of frequencies [2.9–31 kHz; mean 14.95 ± 1.10 kHz] and intensities [20.2–57.2 dB SPL; mean 36.19 ± 2.56 dB SPL].

3.1. Classification of the inferior colliculus neurons by their adaptation levels

To quantify the degree of SSA using the oddball paradigm, we computed the CSI with the spiking activity. This analysis allowed us to classify 4 neurons as adapting neurons (CSI > 0.25; mean CSI = 0.79 ± 0.09), 3 as non-adapting neurons (CSI ≤ 0.25; mean CSI = −0.05 ± 0.04) and 3 additional neurons as non-spiking with sound-evoked PSPs (see CSI values in Table 1; Fig. 2 for examples of membrane potential traces). These 3 non-spiking neurons did not fire APs but responded with PSPs to pure tones. Also, the non-spiking neurons with sound-evoked PSPs discharged APs during the injection of current pulses. The adapting neurons exhibited non-V-shaped FRAs without a clear best frequency characteristic of the cortices of the IC (Neuron 3 on Fig. 3A), whereas the non-adapting neurons showed V-shaped FRAs with characteristic frequencies typical of the CNIC (Neuron 5 on Fig. 3A). CSI values accurately represented the adaptation properties of a neuron. CSI levels within the same neurons classified equally across the various stimulation conditions (frequencies, tone duration, intensity and onset-to-onset interval; see Table 1 for specificities) and thus, data were merged for subsequent comparisons according to their CSI. All neuronal groups had two stimulus durations and onset-to-onset

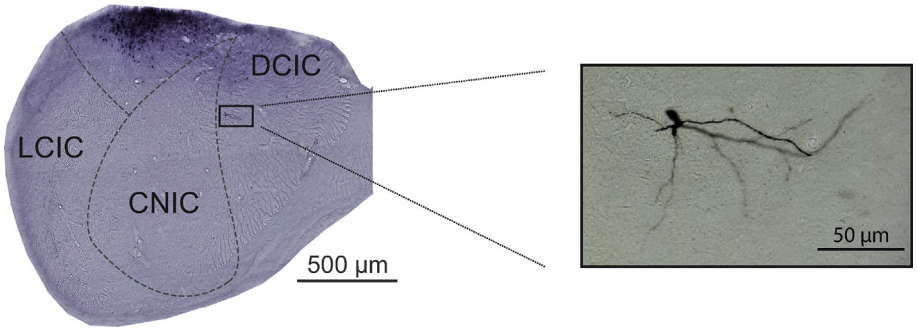

Fig. 1. Anatomical location of neurophysiological recordings. Histological coronal section (40 µm thickness) of one of the non-spiking neurons with sound-evoked PSPs (neuron 10) that was biotinylated (1% of the intracellular solution and a reduced K-gluconate concentration to 115 mM) together with the location of fields of the IC on a mouse brain atlas (bregma −5.3 mm). At higher magnification, this neuron shows a partially labeled dendritic tree extending parallel to the cortical surface. This neuron was localized in the dorsal cortex of the IC. The dark region above the cell is due to the pipette's positive pressure that leaks out biocytin while approaching the cell. The location of biocytin-filled neurons was visualized with an avidin-biotinylated horseradish peroxidase complex with minor modifications to that described by Brandt and Apkarian (1992); Veenman et al. (1992). LCIC: lateral cortex of the inferior colliculus, DCIC: dorsal cortex of the inferior colliculus, CNIC: central nucleus of the inferior colliculus.

Table 1
Common stimulus-specific adaptation indices computed with the absolute number of evoked action potentials (CSI), the sum of excitatory response areas of the membrane voltage (EPSP-CSI) and the sum of inhibitory response areas of the membrane voltage (IPSP−CSI) for all the recorded stimulus conditions.

	Neuron #	Onset-to-onset interval (ms)	Tone duration (ms)	Frequencies (KHz)	Intensity (dB SPL)	CSI	EPSP-CSI	IPSP-CSI
Adapting neurons	1	300	30	11.6 & 14.2	32.5	0.76	0.03	−0.03
		300	30	10.6 & 15.3	32.5	0.95	0.06	−0.19
		300	30	16.2 & 19.8	39.5	0.69	0.14	−0.25
		300	30	14.4 & 20.8	39.5	1	0.45	−0.42
	2	250	75	8.3 & 10.1	43.2	0.86	0.00	0.02
	3	250	75	16.2 & 19.8	30.2	0.96	0.07	−0.09
	4	250	75	13.0 & 16.0	47.2	0.28	−0.06	0.07
Non-adapting neurons	5	250	75	9.0 & 11.0	39.5	−0.05	0.01	−0.01
		250	75	9.5 & 10.5	39.5	−0.09	0.00	−0.01
		300	30	9.6 & 11.7	25.5	−0.14	0.00	−0.10
		300	30	10.0 & 11.2	25.5	−0.11	0.00	0.02
		300	30	9.5 & 10.5	39.5	−0.05	0.00	0.02
	6	300	30	12.7 & 15.5	49.5	−0.1	−0.00	0.05
	7	250	75	18 & 22	20.4	0.17	0.03	0.07
Non-spiking neurons with sound-evoked PSPs	8	250	75	25 & 31	48.5	–	−0.00	−1
		300	30	21.0 & 26.0	21.5	–	0.06	−0.25
	9	250	75	2.9 & 3.5	57.2	–	0.15	−0.17
	10	250	75	23.3 & 28.4	20.2	–	0.04	−0.08

intervals and frequencies and intensities were comparable across groups (One-Way ANOVA, frequencies [$p = 0.170$], intensities [$p = 0.589$]).

Adaptation is a property that has been traditionally studied analyzing APs. However, it is currently unknown whether the neuronal subthreshold responses differ between IC neurons adapting their spiking response to those non-adapting neurons. Given that cochlear nucleus neurons do not exhibit adaptation (Ayala et al., 2013; Duque et al., 2018), then the question arises as to whether or not spiking adaptation results from PSP adaptation in the IC. To correlate the PSPs with the classic CSIs of spiking activity, we computed the CSI for inhibitory and excitatory areas separately to explore what influence excitation and inhibition have under the deviant and standard conditions (Fig. 3C, EPSP-CSI and IPSP-CSI in Table 1). EPSP-CSI and IPSP-CSI were around 0, meaning that deviant and standard tones evoked a comparable amount of excitation and inhibition. Interestingly, a non-spiking neuron with sound-evoked PSPs showed higher inhibitory responses to the last-standard tones than deviant events (IPSP−CSI = −1). Overall, this data demonstrated no general differences in the excitatory or inhibitory synaptic inputs that each neuron receives regardless of its oddball adaptation profile. This finding supports the notion that there is a synaptic signal arrival in the form of PSPs after auditory stimulation regardless of the SSA properties of the APs.

To explore the time course of EPSPs and IPSPs, we further analyzed the mean onset latencies of the largest excitatory and inhibitory areas in deviant and last-standard events. Latencies of EPSPs for deviant and standard tones separately and all stimuli together across groups were comparable (Table 2; One-Way ANOVA, deviant tones [$p = 0.558$], standard tones [$p = 0.327$] and all stimuli [$p = 0.221$]). By contrast, inhibition was significantly faster in the non-adapting neurons than the adapting neurons after standard tones but not after deviant stimuli (One-Way ANOVA, standard events [$p = 0.035$] and deviant tones [$p = 0.05$]).

3.2. Comparisons of membrane potential responses between stimulus conditions

We grouped normalized responses within neurons of evoked responses measured according to stimulus condition. Evoked responses were computed as mean membrane potentials, as well as excitatory and inhibitory areas after stimulus presentation. The stimulus conditions were analyzed as deviant tones, all standard tones, last-standard tones, next-standard tones and the standard tones separated according to the number of consecutive standard tones previously presented (i.e., including up to 9 standard

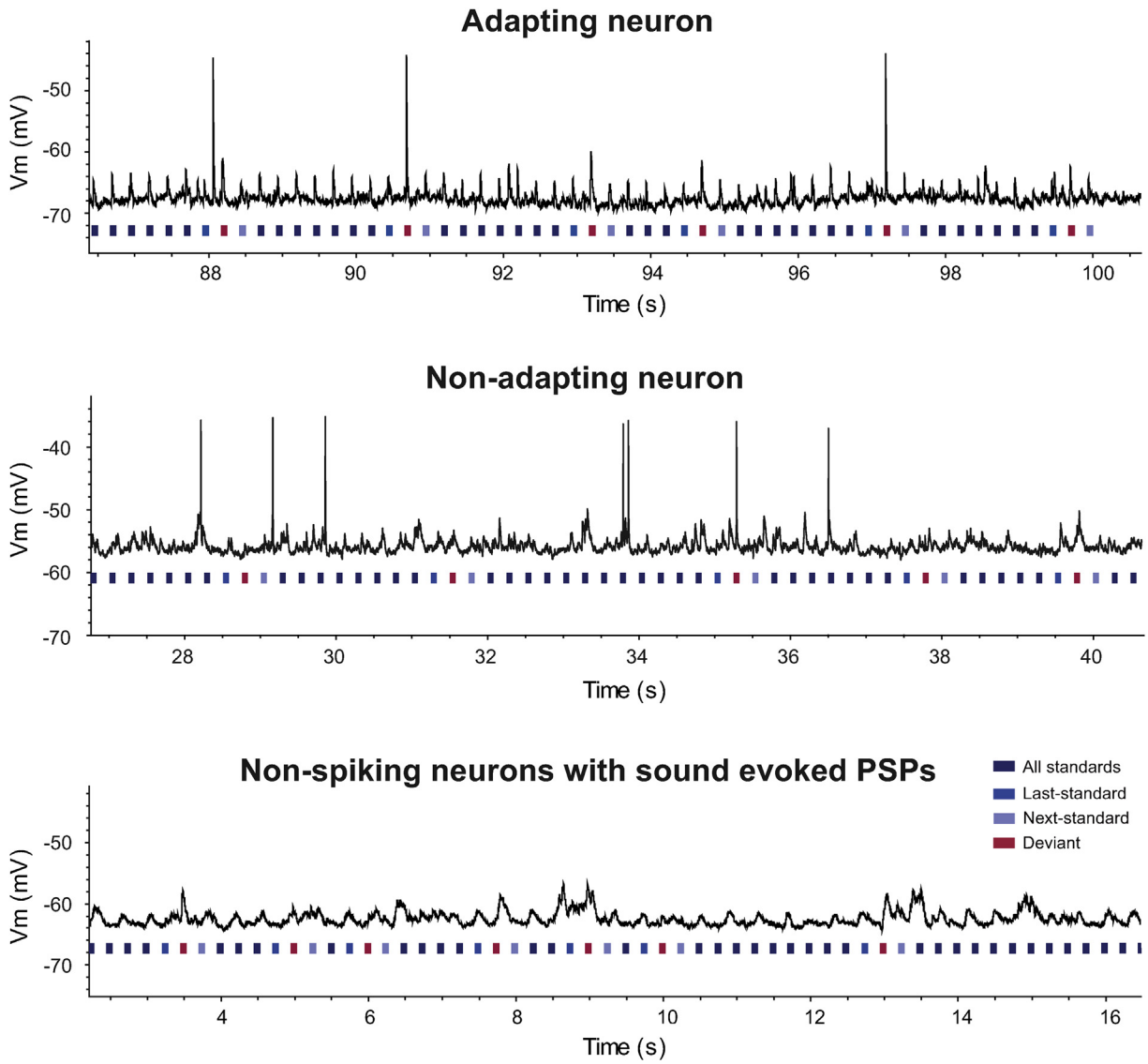

Fig. 2. Examples of membrane voltage traces of an adapting neuron (neuron 2), non-adapting neuron (neuron 7) and a non-spiking neuron with sound-evoked PSPs (neuron 9) classified based on their CSI levels of spiking activity. Horizontal red (deviant tones) and blue (standard tones denoting in separate the last- and next-standard events respect to deviant tones) bars indicate the epoch of sound stimulation. Action potentials and postsynaptic potentials were classified as deviant or standard stimuli accordingly from stimulus onset. Seconds denote time elapsed from the beginning of the stimulation sequence. Pure tones lasted 75 ms with an onset-to-onset interval of 250 ms.

stimulus repetitions). Comparisons among all these conditions of the mean membrane voltage and excitatory areas did not show any significant differences across groups of neurons (One-Way ANOVA with Repeated-Measures; $p > 0.05$ for all). However, inhibitory areas of deviant and next-standard tones were different between non-adapting and non-spiking neurons with sound-evoked PSPs (One-Way ANOVA with Repeated-Measures; $p < 0.05$). Interestingly, the 7th standard repetition demonstrated larger normalized IPSPs for the non-adapting neurons than the adapting cells (0.84 and 0.63, respectively $p = 0.019$). Next, we explored whether differences were within groups of neurons separately. Mean membrane potentials, excitatory and inhibitory areas for all stimulus conditions were similar within adapting neurons, non-adapting neurons and non-spiking neurons with sound-evoked PSPs (One-Way ANOVA; $p > 0.05$). Only adapting neurons showed a significantly more depolarized mean Vm of deviant events than all the other types of standard events ($p < 0.001$).

3.2.1. Data trends in the sequence of consecutive standard stimuli

We explored the membrane potential across the consecutive presentation of standard tones to find a possible link between the number of sound repetitions and the neuron's membrane potential. We performed *Pearson correlation analyses* between the number of consecutive standard repetitions and the mean values of the normalized mean Vm, excitatory or inhibitory areas in the entire population to determine a possible correlation. Results showed a significant relationship between the membrane potential from the 1st to the 6th consecutive standard presentation; mean membrane voltage tended to hyperpolarize in the group of the adapting neurons and slightly depolarized in the non-adapting neurons (adapting neurons, Pearson correlation coefficient $= -0.84$, $p = 0.04$; non-adapting neurons, Pearson correlation coefficient $= 0.57$, $p = 0.24$; non-spiking neurons with sound-evoked PSPs, Pearson correlation coefficient $= 0.03$, $p = 0.95$; population, Pearson correlation coefficient $= -0.24$, $p = 0.64$; see

Fig. 4), whereas inhibition rose with an increasing number of consecutively presented standard tones at the population level (Pearson correlation coefficient = 0.69, p = 0.13) with only small trends within individual groups (adapting neurons, Pearson correlation coefficient = 0.16, p = 0.76; non-adapting neurons, Pearson correlation coefficient = 0.10, p = 0.85; non-spiking neurons with sound-evoked PSPs, Pearson correlation coefficient = 0.34, p = 0.51; see Fig. 4). By contrast, no strong correlation between excitatory areas and the number of consecutive standard tones was found (adapting neurons, Pearson correlation coefficient = 0.61, p = 0.20; non-adapting neurons, Pearson correlation coefficient −0.10, p = 0.85; non-spiking neurons with sound-evoked PSPs, Pearson correlation coefficient = 0.49, p = 0.32; population, Pearson correlation coefficient = 0.15, p = 0.77; Fig. 4).

We also analyzed the response mean membrane potential, inhibitory and excitatory areas to standard tones depending on the number of consecutive presentations for each neuron in separate (One-Way ANOVA and post hoc pairwise multiple comparisons with Holm-Sidak method; Table 3). Most significant differences were found in the groups of adapting neurons and non-spiking neurons with sound-evoked PSPs. These findings highlight a lack of adaptation for the membrane voltage in those non-adapting neurons that showed low SSA levels in their spiking output.

3.3. Morphological characterization of postsynaptic potentials

We next analyzed the morphological properties of the PSPs evoked in response to standard tones versus deviant tones to study whether those PSPs differed in some features even if the absolute area count was comparable to both conditions. Then, we compared all deviant tones with the last-standard stimuli just before deviant events and next-standard stimuli (i.e., the subsequent tone to deviant events). The adapting neurons with the highest SSA levels had significant differences, such as amplitude, half-width, max rise/decay slope when comparing PSPs evoked by deviant stimuli versus standard stimuli (all standard events together and standard stimuli in specific positions before or after a deviant event, Table 4, Fig. 5). One example is neuron 3 that showed a moderate adapting in the PSPs and very high CSI levels even close to the index maximum for some recording conditions. Interestingly, its analyzed parameters were higher for the PSPs evoked by standard tones (Fig. 5). By contrast, the non-adapting group only showed few differences between deviant and standard events for the same properties and the non-spiking neurons with sound-evoked PSPs presented a small number of differences in some of the parameters.

3.4. Membrane passive properties of neurons of the inferior colliculus

To correlate adaptation properties with passive neuronal properties, we compared these passive membrane properties across groups of cells. Although we did not find significant differences across neuronal groups, there was a tendency for higher capacitance values and smaller membrane resistance in the group of adapting neurons. By contrast, the smallest capacitance values and highest membrane resistances were found in the non-adapting neurons (Table 5).

3.5. Intrinsic properties of neurons of the inferior colliculus

To analyze the intrinsic properties of the IC neurons, we studied the presence of depolarizing sags after the application of hyperpolarizing current pulses. We also analyzed the firing pattern, the interspike interval, the AP threshold and the rebound potential in response to current injection pulses. Two neurons displayed a depolarizing sag; neuron 2 showed a 5 mV sag with a 35 ms tau while neuron 8 showed an 11 mV sag with a 23 ms tau (Fig. 6). These two neurons corresponded to different groups, namely, the adapting and non-spiking neurons with sound-evoked PSPs. Therefore, it was not possible to relate the presence of the sag to any particular neuronal class. Interestingly, it should be mentioned that all the remaining neurons that lacked sags ($n = 8$) had an AP response threshold at a current injection of 100 pA, while the two neurons with sag had a higher AP threshold at 200 pA.

Next, we analyzed the AP firing patterns to investigate whether physiological parameters beyond basic biophysics could serve to characterize the three classes of neurons. Therefore, we calculated the interspike interval and the instantaneous frequency or firing rate at the AP threshold. Only the non-adapted neurons lacked rebound APs. In accord with the firing pattern and interspike interval, neurons were classified as sustained, accommodating, accelerating and burst onset cells (Sivaramakrishnan and Oliver, 2001; Tan et al., 2007). All classes of neurons showed an exponential decrease in their instantaneous frequencies with different behaviors depending on the neuronal type. Sustained neurons showed a gradual/constant decrease in the instantaneous frequency according to its interspike intervals, while the accommodating, accelerating, and burst onset did so in an irregular/non-constant manner (Fig. 6B). The groups of adapting neurons and non-spiking neurons with sound-evoked PSPs showed variability in the types of firing patterns, while the group of non-adapting neurons showed a sustained firing pattern (Fig. 6 & Table 6). Thus, one important difference between adapting and non-adapting neurons is their firing patterns.

4. Discussion

In this study, we have recorded 10 neurons in whole-cell mode in the mouse IC while we applied current injection and sound stimulation under the oddball paradigm. These recordings allowed us to report their passive properties (membrane capacitance, membrane resistance and resting membrane potential), intrinsic properties (firing pattern, AP-threshold, depolarizing sag of hyperpolarizing pulse and rebound AP) and postsynaptic potentials in response to sound stimulation.

The firing pattern of neurons is dependent on the interaction of several voltage-dependent ion conductances (Rutecki, 1992). Within our recording sample, we found that the firing pattern is a key feature to distinguish between adapted and non-adapted neurons. All non-adapted neurons showed a sustained-regular firing, probably due to a high degree of sodium persistent current (Boeri et al., 2018; Chatelier et al., 2010). This type of firing pattern is abundant in CNIC neurons both, *in vitro* (Peruzzi et al., 2000; Sivaramakrishnan and Oliver, 2001) and *in vivo* studies (Tan et al., 2007). CNIC neurons are predominantly non-adapted neurons with the lowest, if any, SSA levels (Malmierca et al., 2009a). By contrast, adapting neurons showed variable firing patterns, including sustained, accommodating and burst onset cells. These types of responses have been shown to be more typical of the cortices of the IC (Geis et al., 2011). These findings conform with our previous works of neurons with higher SSA levels found mainly in the cortices of the IC (Ayala and Malmierca, 2013; Duque et al., 2012; Duque and Malmierca, 2015). Interestingly, we also observed differences between the neuronal receptive fields in their FRAs measurements. FRAs of non-adapting neurons showed typical V-shapes, which is exemplary of the CNIC (Ayala and Malmierca, 2013; Duque et al., 2012; Duque and Malmierca, 2015). By contrast, adapting neurons showed non-V-shaped FRAs without a clear characteristic frequency, which typically belong to the cortices of the IC (Ayala and Malmierca, 2013; Duque et al., 2012; Duque and

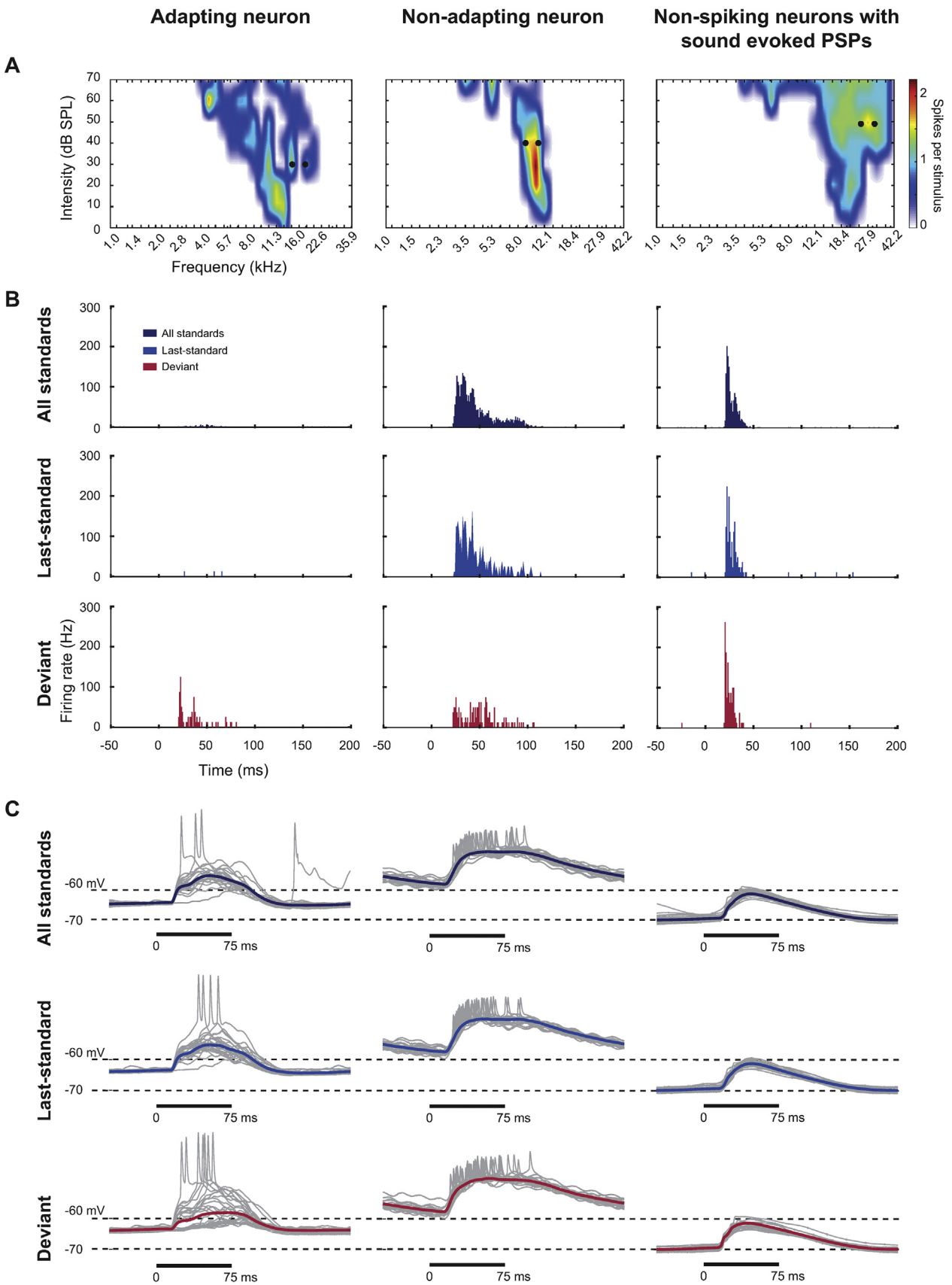

Fig. 3. Examples of an adapting neuron (neuron 3), a non-adapting neuron (neuron 5) and a non-spiking neuron with sound-evoked PSPs (neuron 8). A) Frequency response area for pure tones of a combination of frequencies and intensities. The black dots denote the selected frequencies presented as oddball paradigms. Pure tones lasted 75 ms with an onset-to-onset interval of 250 ms. B) Peristimulus-time histograms of the combined response to the two frequencies presented as each condition: all standard tones (n = 720

Table 2
Onset latencies of evoked excitatory areas (EPSPs) and inhibitory areas (IPSPs) for all the recorded stimulus conditions.the

	Neuron #	Onset-to-onset interval (ms)	Tone duration (ms)	Frequencies (KHz)	Intensity (dB SPL)	Deviant	Last-standard	Mean	SEM	Deviant	Last-standard	Mean	SEM
Adapting neurons	1	300	30	11.6 & 14.2	32.5	48.02	45.89	34.15	5.34	40.08	46.58	62.88	7.77
		300	30	10.6 & 15.3	32.5	28.36	30.33			50.49	58.50		
		300	30	16.2 & 19.8	39.5	42.88	36.08			67.71	79.98		
		300	30	14.4 & 20.8	39.5	38.16	88.24			47.32	25.95		
	2	250	75	8.3 & 10.1	43.2	18.30	12.05			78.49	83.11		
	3	250	75	16.2 & 19.8	30.2	14.82	8.48			108.69	124.10		
	4	250	75	13.0 & 16.0	47.2	30.25	36.20			36.96	32.34		
Non-adapting neurons	5	250	75	9.0 & 11.0	39.5	20.12	21.55	29.36	5.28	0.54	0.59	13.96	6.18
		250	75	9.5 & 10.5	39.5	20.30	21.32			0.43	0.22		
		300	30	9.6 & 11.7	25.5	12.90	14.09			1.30	1.13		
		300	30	10.0 & 11.2	25.5	16.68	18.29			2.07	2.45		
		300	30	9.5 & 10.5	39.5	15.40	15.89			1.37	2.30		
	6	300	30	12.7 & 15.5	49.5	59.40	65.24			31.14	24.92		
	7	250	75	18 & 22	20.4	47.22	62.72			61.83	65.16		
Non-spiking neurons with sound-evoked PSPs	8	250	75	25 & 31	48.5	2.53	2.71	19.57	5.77	–	0.1	50.87	12.20
		300	30	21.0 & 26.0	21.5	25.48	7.96			75.19	103.98		
	9	250	75	2.9 & 3.5	57.2	36.78	47.78			43.67	42.48		
	10	250	75	23.3 & 28.4	20.2	19.12	14.18			51.38	39.26		

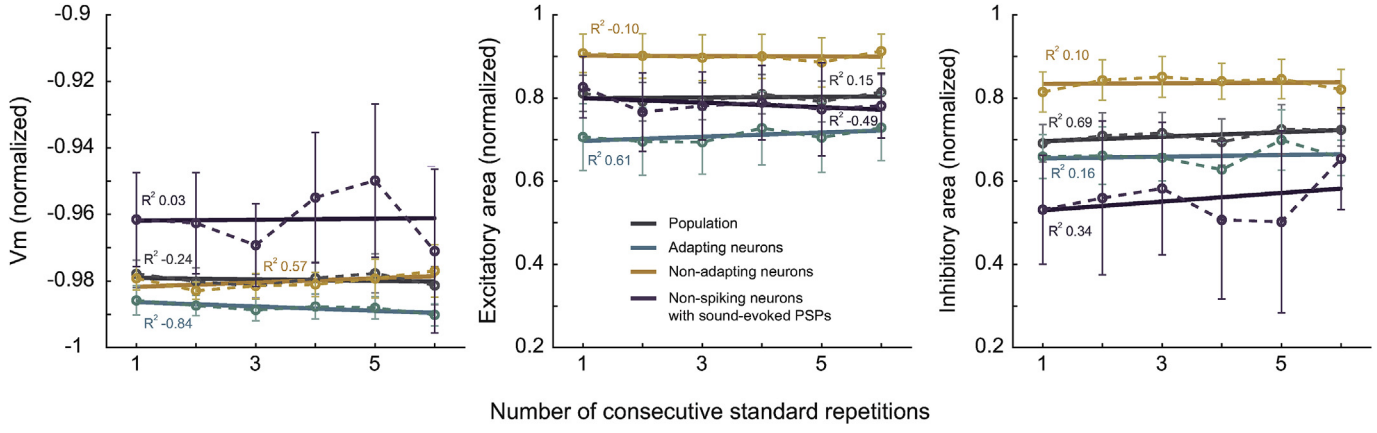

Fig. 4. Correlation between the number of consecutive standard tone presentations and the evoked mean membrane potential, excitatory and inhibitory areas. Data shown as normalized means ± SEM. Linear trends denote the group and population tendency along with adjusted R^2 values, which indicates the goodness of the fit.

Malmierca, 2015).

One possibility for adaptation would be that PSP amplitudes are stable, but the probability of PSPs changes with adaptation, such that adaptation occurs primarily due to decreases in PSP probability. However, the present data demonstrate similarity in the amplitude of sound-evoked PSPs received for each stimulus condition by each neuron, regardless of the degree of spiking adaptation. Because both frequencies selected for the oddball paradigms fell within their receptive field, neurons consistently demonstrated PSPs to both tones. Another possibility, similar to studies in the auditory cortex (Abolafia et al., 2011; Wehr and Zador, 2005), would be that PSP amplitudes and conductances change with adaptation. The analyses of EPSPs and IPSPs separately in this set of neurons do not support this idea and suggest that differences in SSA of synaptic inhibition and excitation are not predictive of spiking SSA levels. Yet another possibility would be changes in the relative timing of inhibition. We observed that inhibition for last-standard stimuli but not for deviant tones was faster for non-adapting neurons than adapting neurons but did not observe changes in IPSP timing related to adaptation. At the 3–4 Hz rate in the present study, although there may be some synaptic depression, it is likely to be weak, on the order of 10–20% (Bartlett and Smith, 2002; Malmierca et al., 2009a; Pérez-González and Malmierca, 2014). However, studies in the IC (Kitagawa and Sakaba, 2019; Malmierca et al., 2009a; Wu et al., 2004) and auditory thalamus (Antunes et al., 2010; Bartlett and Smith, 2002; Venkataraman and Bartlett, 2013) have shown significant synaptic depression that could lead to more prominent SSA and spiking adaptation for faster rates (≥10 Hz).

Previously, it was shown that neurons of the cochlear nucleus and the superior olivary complex lack SSA (Ayala et al., 2013; Duque et al., 2018), while the cortical regions of the IC show strong and robust SSA (Ayala et al., 2013; Lumani and Zhang, 2010; Malmierca

stimulus repetitions), last-standard tones before deviant events (n = 80) and deviant tones (n = 80). Pure tones lasted 75 ms. Bin size: 1 ms. A-B) Frequency response areas and peristimulus-time histograms were computed with the spiking activity for adapting and non-adapting neurons. Responses of the non-spiking neurons with sound-evoked PSPs were computed with the total count of individual PSPs instead of APs since these cells did not fire to the sound stimulation with pure tones. C) Examples of randomly selected traces (gray; n = 25 stimulus repetitions) and average membrane potential responses of all stimulus repetitions after removing action potentials (colored) in the same neurons. This shows how the frequency tones were selected and the time-locked activity to deviant and standard tones.

Table 3
Comparison between number of standard repetitions and evoked responses in the mean membrane potential (Vm), excitatory areas (EPSPs) and inhibitory areas (IPSPs).

	Neuron #	Mean Vm	EPSP	IPSP
Adapting neurons	1	1^{st}, 2^{nd} & 3^{rd} standards different than 4^{th} to 9^{th} 4^{th} standard different than 5^{th} to 9^{th} 5^{th}standard different than 6^{th} to 8^{th} $_{6th}$ standard different than 7th & 8_{th} 7^{th} standard different than 8^{th} & 9^{th} 8^{th} standard different than 9^{th} ($p < 0.001$)	1^{st}, 2^{nd} & 3^{rd} standards different than 5^{th} to 7^{th} 4^{th} standard different than 6^{th} & 7^{th} 6^{th} standard different than 8^{th}($p < 0.001$)	1^{st} standard different than the 7^{th} ($p = 0.001$)
	2	1^{st}standard different than the 6^{th} ($p < 0.001$)	$p = 0.779$	1^{st} standard different than the 7^{th} ($p < 0.001$)
	3	1^{st} standard different than the rest 6^{th} standard different than 1st to 4^{th} 7^{th} standard different than 1^{st} to 5^{th} ($p < 0.001$)	7^{th} & 8^{th} standards different than 1st to 4th ($p < 0.001$) 4^{th} standard different than 6th $p = 0.002$	9^{th} standard different than the 5th to 7th ($p < 0.001$)
	4	$p = 0.484$	$p = 0.788$	$p = 0.783$
Non-adapting neurons	5	$p = 0.824$	$p = 0.161$	$p = 0.072$
	6	$p = 0.662$	$p = 0.984$	$p = 0.688$
	7	7^{th} standard different than 2^{nd} & 3^{rd} 8^{th} standard different than the rest ($p < 0.001$)	8^{th} standard different than the rest ($p < 0.001$)	8^{th} standard different than the rest ($p < 0.001$)
Non-spiking neurons with sound-evoked PSPs	8	6^{th} and 7^{th} standards different than 1st to 3rd ($p < 0.001$)	$p = 0.039$; No significant post hoc comparison.	$p = 0.066$
	9	$p = 0.038$; Non-significant post hoc comparisons	$p = 0.848$	$p = 0.997$
	10	1^{st} standard different than the 2nd ($p = 0.003$) & 3^{rd} ($p = 0.021$)	$p = 0.607$	$p = 0.676$

One-Way ANOVA and post hoc pairwise multiple comparisons procedures with the Holm-Sidak method.

Table 4
Summary of the analyzed parameters of post-synaptic potentials compared between deviant and standard stimuli.

		Adapting neurons		Non-adapting neurons	Non-spiking neurons with sound-evoked PSPs	
Parameter	Comparison	Neuron #				
		2	3	5	8	10
Amplitude	STD vs. DEV	$p < 0.001$	$p < 0.001$	n.s.	$p < 0.001$	n.s.
	last-STD vs. DEV	$p < 0.001$	$p < 0.001$	n.s.	$p < 0.001$	n.s.
	next-STD vs. DEV	$p < 0.001$	$p < 0.001$	n.s.	$p < 0.001$	n.s.
	last-STD vs. next-STD	n.s.	n.s.	n.s.	$p < 0.001$	n.s.
Half-width	STD vs. DEV	n.s.	$p < 0.001$	$p < 0.05$	n.s.	$p < 0.05$
	last-STD vs. DEV	n.s.	$p < 0.001$	n.s.	n.s.	n.s.
	next-STD vs. DEV	n.s.	$p < 0.001$	$p < 0.001$	$p < 0.001$	$p < 0.05$
	last-STD vs. next-STD	n.s.	n.s.	n.s.	n.s.	n.s.
Max Rise Slope	STD vs. DEV	n.s.	$p < 0.001$	$p < 0.05$	$p < 0.001$	$p < 0.05$
	last-STD vs. DEV	$p < 0.001$	$p < 0.001$	n.s.	$p < 0.001$	n.s.
	next-STD vs. DEV	$p = 0.004$	$p < 0.001$	n.s.	$p < 0.001$	n.s.
	last-STD vs. next-STD	n.s.	n.s.	n.s.	n.s.	n.s.
Max Decay Slope	STD vs. DEV	n.s.	$p < 0.001$	n.s.	n.s.	$p < 0.05$
	last-STD vs. DEV	n.s.	$p < 0.001$	n.s.	n.s.	n.s.
	next-STD vs. DEV	n.s.	$p < 0.001$	$p < 0.05$	n.s.	n.s.
	last-STD vs. next-STD	n.s.	n.s.	n.s.	n.s.	n.s.
Rise Slope 10%–90%	STD vs. DEV	$p < 0.005$	$p < 0.005$	n.s.	$p < 0.001$	n.s.
	last-STD vs. DEV	$p < 0.05$	$p < 0.05$	n.s.	$p < 0.001$	n.s.
	next-STD vs. DEV	$p < 0.05$	$p < 0.05$	n.s.	$p < 0.001$	n.s.
	last-STD vs. next-STD	n.s.	n.s.	n.s.	n.s.	n.s.
Rise Time 10%–90%	STD vs. DEV	n.s.	$p < 0.005$	$p < 0.05$	$p < 0.05$	n.s.
	last-STD vs. DEV	n.s.	$p < 0.05$	n.s.	n.s.	n.s.
	next-STD vs. DEV	n.s.	$p < 0.05$	n.s.	n.s.	n.s.
	last-STD vs. next-STD	n.s.	n.s.	n.s.	n.s.	n.s.
Decay Slope 90%–10%	STD vs. DEV	n.s.	$p < 0.005$	n.s.	$p < 0.001$	n.s.
	last-STD vs. DEV	n.s.	$p < 0.05$	n.s.	$p < 0.001$	n.s.
	next-STD vs. DEV	n.s.	$p < 0.05$	n.s.	$p < 0.001$	n.s.
	last-STD vs. next-STD	n.s.	n.s.	n.s.	n.s.	n.s.
Decay Time 90%–10%	STD vs. DEV	n.s.	n.s.	n.s.	$p < 0.05$	n.s.
	last-STD vs. DEV	n.s.	n.s.	n.s.	$p < 0.05$	n.s.
	next-STD vs. DEV	n.s.	n.s.	n.s.	$p < 0.05$	n.s.
	last-STD vs. Next-STD	n.s.	n.s.	n.s.	n.s.	n.s.

Comparisons were performed between standard events (all standard tones [STD], last-standard tones before deviant events [last-STD] and next-standard tones after a deviant event [next-STD]) and deviant tones (DEV). n.s. means a non-statistically significant difference. One-Way Repeated-Measures ANOVA. Neurons that did not show significant changes in any comparison are not included in the table to facilitate visualization.

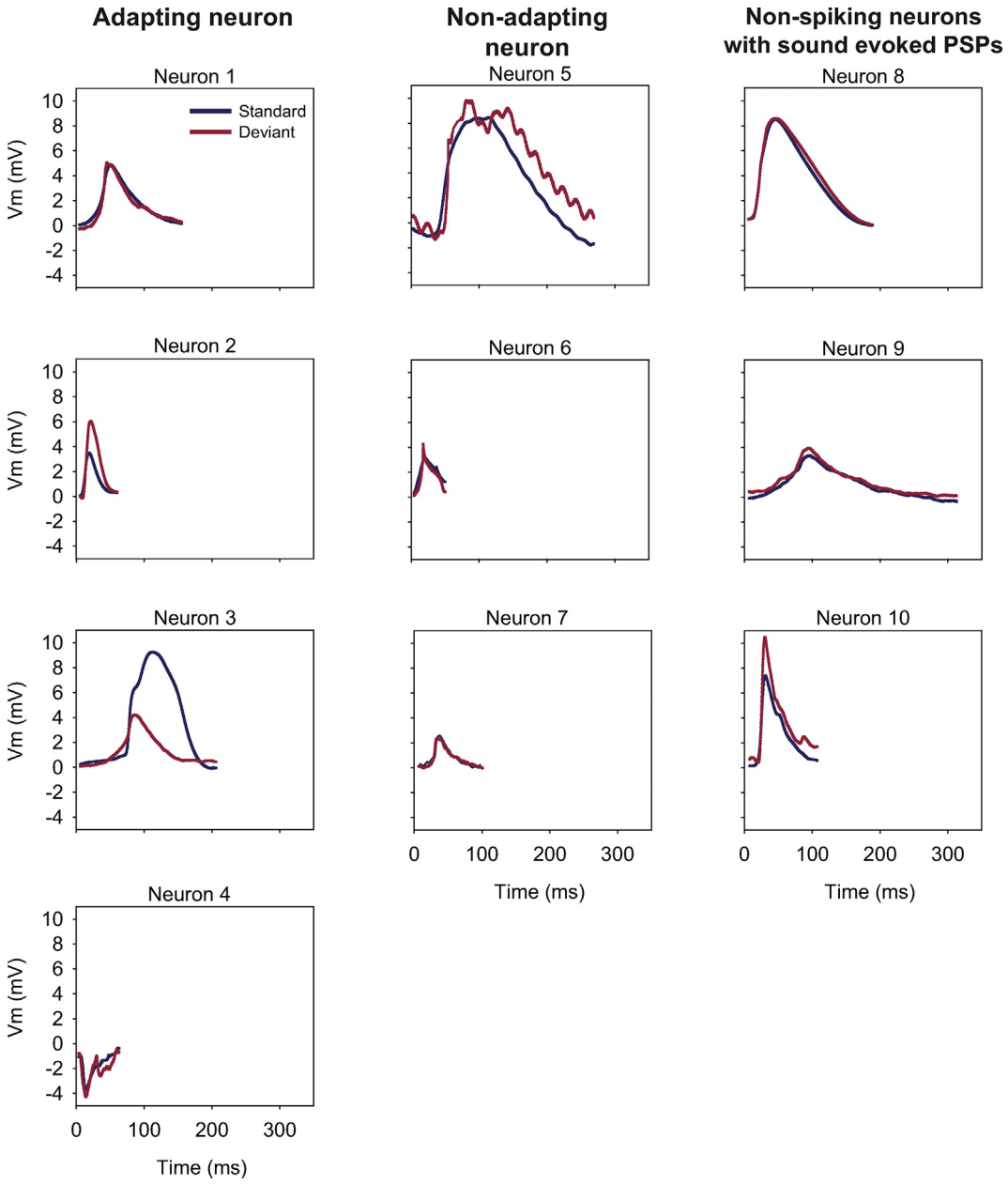

Fig. 5. Mean post-synaptic potentials from each adapting, non-adapting and non-spiking neurons with sound-evoked PSPs. For morphological analyses, postsynaptic potentials were aligned to its maximum peak for excitatory postsynaptic potentials or minimum peak for inhibitory postsynaptic potentials.

Table 5
Membrane passive properties of IC neurons.

	Neuron #	Capacitance (pF)		Membrane resistance (MΩ)		Resting membrane potential (mV)	
		Individual	Mean	Individual	Mean	Individual	Mean
Adapting neurons	1	13	12.75 ± 2.95	660	434 ± 91.89	−45	−56 ± 6.67
	2	21		212		−69	
	3	9		410		−66	
	4	8		454		−44	
Non-adapting neurons	5	3	9.33 ± 4.48	707	769 ± 40.45	−55	−52.67 ± 2.85
	6	7		755		−47	
	7	18		845		−56	
Non-spiking neurons with sound-evoked PSPs	8	2	7.67 ± 4.26	486	463.67 ± 124.34	−66	−65.33 ± 0.33
	9	16		667		−65	
	10	5		238		−65	
p-values		0.433		0.222		0.481	

Average ± SEM; n = 4 adapting neurons, 3 non-adapting neurons & 3 non-spiking neurons with sound-evoked PSPs; One-Way Repeated-Measures ANOVA.

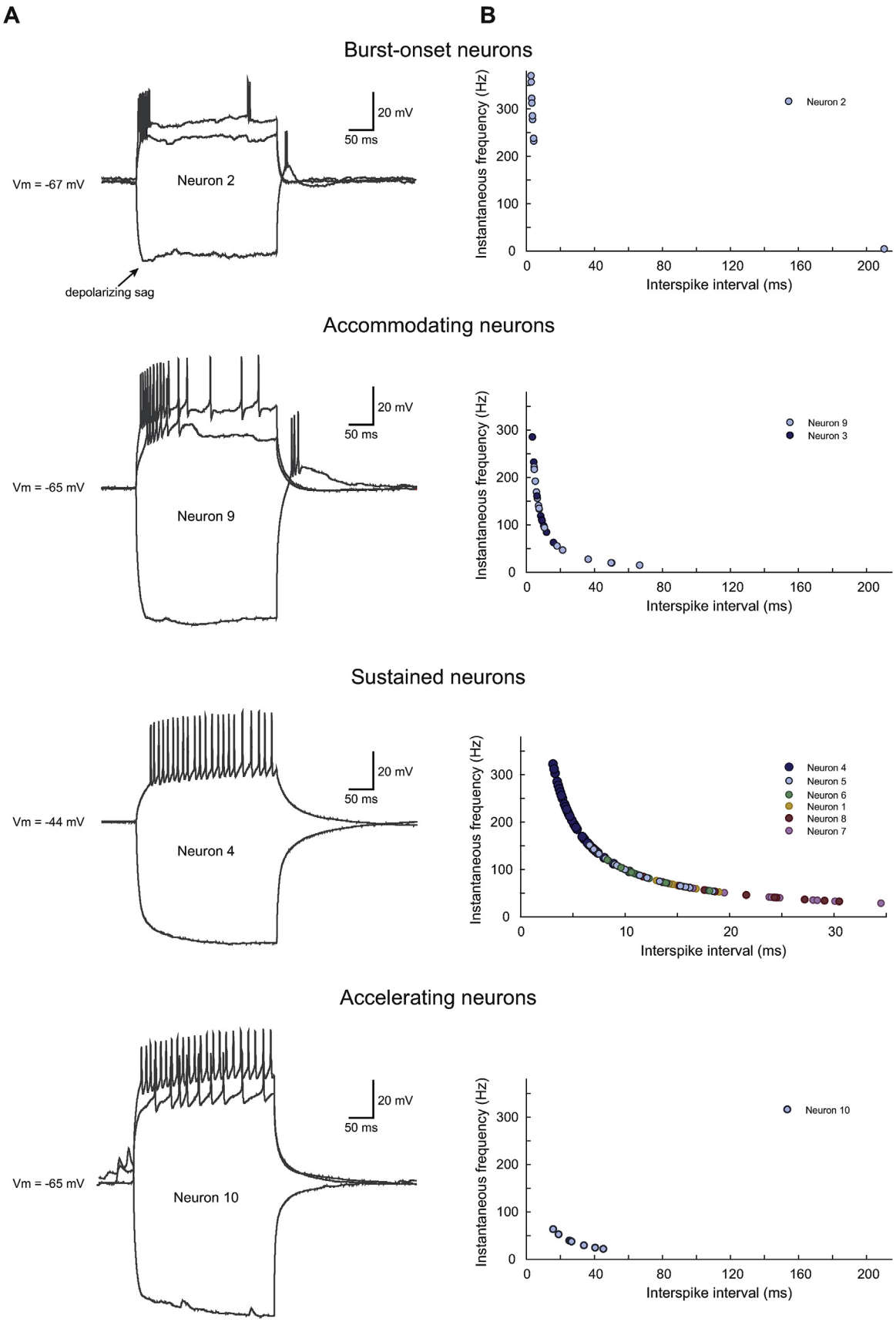

Fig. 6. Example of each type of firing pattern found in the IC neurons. A) Membrane voltage traces under injection of square current pulse series. The most hyperpolarizing current pulse, the depolarizing pulse at the AP threshold and the pulse 100 pA above it are shown. Neurons 2 and 4 are adapting neurons and neurons 8 and 9 are non-spiking neurons with sound-evoked PSPs. B) Interspike interval versus instantaneous frequency of all neurons calculated 100 pA above AP threshold.

Table 6
Classification of types of firing patterns in number of IC neurons within each group .

	Adapting neurons	Non-adapting neurons	Non-spiking neurons with sound-evoked PSPs
Sustained	2	3	1
Accommodating	1		1
Accelerating			1
Burst onset	1		

Adapting neurons, non-adapting neurons and non-spiking neurons with sound-evoked PSPs were classified according to their AP discharge to depolarizing and hyperpolarizing current injections.

et al., 2009a; Pérez-González et al., 2005; Zhao et al., 2011) with extracellular recordings of single units in anesthetized and awake rodents (Duque and Malmierca, 2015) and with brainstem auditory evoked potentials (Duque et al., 2018). These results suggest that SSA emerges at the level of the IC and is prevalent in IC cortex. Thus, the question arises whether spiking adaptation results from PSP adaptation in the IC. Neurons in IC cortex receive ascending auditory inputs, inputs from other IC neurons and auditory cortex (Cant and Oliver, 2018; Ito and Malmierca, 2018; Loftus et al., 2008; Malmierca, 2015; Malmierca et al., 2009b, 2005, 1995; Malmierca and Ryugo, 2012). Our set of IC neurons suggests that synaptic adaptation was variable, with weak or no SSA in some neurons, clear synaptic SSA in a couple of neurons, and even reduced deviant EPSP amplitude coupled with spiking SSA (Fig. 5). This finding extended to both adapting and non-adapting neurons and suggests that synaptic adaptation could not be used to predict the presence of spiking SSA. This finding differs from auditory cortical evidence, where SSA was observed at subthreshold level, both *in vivo* (Chen et al., 2015; Hershenhoren et al., 2014) and *in vitro* (Wang et al., 2014) due to synaptic depression of thalamocortical projections (Chung et al., 2002; Katz et al., 2006). Indeed, the lack of synaptic SSA in the IC further supports previous work where the auditory cortex was deactivated, which did not eliminate subcortical SSA (Anderson and Malmierca, 2013; Antunes and Malmierca, 2011). Thus, the present study further supports the notion that the non-lemniscal IC is the first site at the auditory pathway where SSA emerges.

We observed a small trend towards hyperpolarized membrane potentials in adapting neurons and increased synaptic inhibition with an increasing number of standard repetitions at the population level. This finding denotes a moderate level of adaptation only observed when one stimulus is consecutively repeated. Since we detected these trends of a small increase at the population level, it does not seem to explain the SSA levels observed at the AP activity. This result suggests a more simple type of adaptation related to potassium conductances. Potassium conductances have been associated with adaptation on a scale of seconds to minutes. It is known that potassium conductances contribute to sensory adaptation in sensorimotor, barrel and visual cortices (Díaz-Quesada and Maravall, 2008; Sanchez-Vives et al., 2000a, 2000b; Schwindt et al., 1988; Wang et al., 2003). The activation of potassium currents hyperpolarizes the membrane potential, decreasing the neuronal responsiveness to subsequent synaptic inputs with time courses ranging from tens of milliseconds to tens of seconds. Such slow time courses are supported by the dynamics of the relevant intracellular ions, in particular, Na^+, in the vicinity of K^+ channels and their binding/unbinding to them (Abolafia et al., 2011). The depolarization and high-frequency firing during sensory responses induce not only the activation of voltage-dependent potassium currents but also an intracellular increase of ions like Ca^{2+} and Na^+ that activate ion-dependent K^+ channels (for reviews see Bhattacharjee and Kaczmarek, 2005; Sah and Faber, 2002). This cascade of events occurs equally for all stimulus conditions and can explain similarities among responses.

Adapted/non-spiking and non-adapted neurons differ by the appearance of a rebound depolarization after cessation of hyperpolarization, leading to rebound firing. Specifically, only the non-adapted neurons lacked rebound depolarization and rebound APs. *In vivo*, rebound depolarizations can be evoked by inhibitory synaptic stimuli. The ion channels usually believed to underlie rebound depolarizations are the low voltage activated T-type (Ca_{V3}) calcium channels and hyperpolarization-activated HCN channels (Jahnsen and Llinás, 1984; Molineux et al., 2008). For example, in the medial geniculate body of the rat, it is carried by T-type Ca^{2+} channels, and regulated by HCN channels and likely GIRK channels by changing the resting potential (Wang et al., 2016). These findings could indicate differences in the intrinsic properties of adapted and non-adapted neurons but some experimental strategies such as pharmacological and voltage-clamp mode recordings are needed to disentangle specific ionic channels' contributions. Two cells demonstrated a slight depolarizing sag followed by a rebound action potential suggesting the presence of hyperpolarization-activated current (I_h; Nagtegaal and Borst, 2010). However, given the membrane potential, it could be due to inward rectifier K^+ channels. We could not conclude the role of the depolarizing sag into SSA. Only one neuron classified as adapting and the other lacked sound-evoked spikes and therefore, its SSA level could not be determined.

Although our work represents a first and important step in the study of intracellular responses of SSA neurons *in vivo* in the IC, our conclusions should be considered as example case reports and be strengthened by further studies, increasing the number of intracellularly recorded neurons. It is widely accepted that blind whole-cell patch-clamp is a laborious technique with a low yield, especially *in vivo* using adult animals; success rates are ~25% of the attempts even with automated methods (Kodandaramaiah et al., 2012; Margrie et al., 2002). In our study design, we required a considerable stable time of recording of about 10 min combining the current stimulation and sound stimulation with FRAs, and the selection of two frequencies for at least two oddball sequences. Another limiting factor is that the group of non-spiking neurons with sound-evoked PSPs is difficult to integrate within this study due to the lack of tone-evoked spikes and, therefore, it precludes comparison with classical extracellular spike counts used to compute CSI levels. As a result, these neurons have not been studied classically with extracellular recordings and their auditory adaptation levels are unknown. Here, we can only establish the adaptation properties at their PSPs. In line with previous research, cells without tone-evoked APs have been found in the mouse CNIC *in vivo* (Tan et al., 2007), in the mouse dorsal cortex where the ratio of these neurons was higher with around half of the recorded cells (Geis et al., 2011), in the rat dorsal cortex (Lumani and Zhang, 2010) and even in the primary auditory cortex (Hershenhoren et al., 2014). Hence, this preliminary piece of work will need to be expanded in future studies with a higher population number and more in-depth types of manipulations such as injections of depolarizing currents forcing AP firing in non-spiking neurons to pure tones or more complex forms of auditory stimuli.

5. Conclusion

In this study, we have made the first attempt to correlate some neuronal electrophysiological properties of adapting, non-adapting neurons and non-spiking neurons with sound-evoked PSPs. We demonstrated the similarity of excitatory or inhibitory synaptic inputs that each neuron receives regardless of their SSA properties at the spiking activity. Although a couple of the adapting neurons had synaptics that differed between deviant and standard stimuli, that was not necessary to produce spiking SSA. Thus, synaptic SSA was variable and could not be used to predict the presence of spiking SSA. Our data suggest that intrinsic properties differ between adapting and non-adapting neurons since they displayed different firing patterns (Fig. 6 and Table 6). Our results suggest that intrinsic properties (probably potassium conductances) may contribute to classifying neurons as adapting or non-adapting ones. Therefore, in future studies, it would be worth analyzing in more detail the properties and distributions of these potassium channels. Finally, we should emphasize that the conclusions drawn from this study are modest as our sample is very small, but they show the potential for future studies of this type to understand how SSA is generated at the cellular level.

Declaration of competing interest

The authors declare no competing interests.

CRediT authorship contribution statement

Catalina Valdés-Baizabal: Conceptualization, Methodology, Investigation, Formal analysis, Visualization, Writing - original draft, Writing - review & editing. **Lorena Casado-Román:** Conceptualization, Methodology, Software, Formal analysis, Visualization, Writing - original draft, Writing - review & editing. **Edward L. Bartlett:** Conceptualization, Writing - review & editing. **Manuel S. Malmierca:** Conceptualization, Writing - review & editing, Supervision, Project administration, Funding acquisition.

Acknowledgments

We thank Drs. Doug Oliver, H. Rüdiger A.P. Geis, J. Gerard G. Borst and Aaron B. Wong for the experimental assistance and/or advice. We also thank Mr. Ignacio Plaza for helping with the histological staining. Funding: this project received funding from the Spanish MINECO [grant number SAF2016-75803-P] and the European Union's Horizon 2020 research and innovation programme under the Marie Skłodowska-Curie LISTEN [grant number 722098] to MSM. CVB held a fellowship from the Mexican National Council of Science and Technology [grant number 216652].

References

Abolafia, J.M., Vergara, R., Arnold, M.M., Reig, R., Sanchez-Vives, M.V., 2011. Cortical auditory adaptation in the awake rat and the role of potassium currents. Cerebr. Cortex 21, 977–990. https://doi.org/10.1093/cercor/bhq163.

Almanza, A., Luis, E., Mercado, F., Vega, R., Soto, E., 2012. Molecular identity, ontogeny, and cAMP modulation of the hyperpolarization-activated current in vestibular ganglion neurons. J. Neurophysiol. 108, 2264–2275. https://doi.org/10.1152/jn.00337.2012.

Anderson, L.A., Malmierca, M.S., 2013. The effect of auditory cortex deactivation on stimulus-specific adaptation in the inferior colliculus of the rat. Eur. J. Neurosci. 37, 52–62. https://doi.org/10.1111/ejn.12018.

Antunes, F.M., Malmierca, M.S., 2011. Effect of auditory cortex deactivation on stimulus-specific adaptation in the medial geniculate body. J. Neurosci. 31, 17306–17316. https://doi.org/10.1523/JNEUROSCI.1915-11.2011.

Antunes, F.M., Nelken, I., Covey, E., Malmierca, M.S., 2010. Stimulus-specific adaptation in the auditory thalamus of the anesthetized rat. PloS One 5, e14071. https://doi.org/10.1371/journal.pone.0014071.

Ayala, Y.A., Malmierca, M.S., 2018. The effect of inhibition on stimulus-specific adaptation in the inferior colliculus. Brain Struct. Funct. 223, 1391–1407. https://doi.org/10.1007/s00429-017-1546-4.

Ayala, Y.A., Malmierca, M.S., 2015. Cholinergic modulation of stimulus-specific adaptation in the inferior colliculus. J. Neurosci. 35, 12261–12272. https://doi.org/10.1523/JNEUROSCI.0909-15.2015.

Ayala, Y.A., Malmierca, M.S., 2013. Stimulus-specific adaptation and deviance detection in the inferior colliculus. Front. Neural Circ. 6, 1–16. https://doi.org/10.3389/fncir.2012.00089.

Ayala, Y.A., Pérez-González, D., Duque, D., Nelken, I., Malmierca, M.S., 2013. Frequency discrimination and stimulus deviance in the inferior colliculus and cochlear nucleus. Front. Neural Circ. 6, 1–19. https://doi.org/10.3389/fncir.2012.00119.

Ayala, Y.A., Pérez-González, D., Malmierca, M.S., 2016. Stimulus-specific adaptation in the inferior colliculus: the role of excitatory, inhibitory and modulatory inputs. Biol. Psychol. 116, 10–22. https://doi.org/10.1016/j.biopsycho.2015.06.016.

Ayala, Y.A., Udeh, A., Dutta, K., Bishop, D., Malmierca, M.S., Oliver, D.L., 2015. Differences in the strength of cortical and brainstem inputs to SSA and non-SSA neurons in the inferior colliculus. Sci. Rep. 5, 1–17. https://doi.org/10.1038/srep10383.

Bartlett, E.L., Smith, P.H., 2002. Effects of paired-pulse and repetitive stimulation on neurons in the rat medial geniculate body. Neuroscience 113, 957–974. https://doi.org/10.1016/s0306-4522(02)00240-3.

Bhattacharjee, A., Kaczmarek, L.K., 2005. For K+ channels, Na+ is the new Ca2+. Trends Neurosci. https://doi.org/10.1016/j.tins.2005.06.003.

Boeri, J., Le Corronc, H., Lejeune, F.X., Le Bras, B., Mouffle, C., Angelim, M.K.S.C., Mangin, J.M., Branchereau, P., Legendre, P., Czarnecki, A., 2018. Persistent sodium current drives excitability of immature renshaw cells in early embryonic spinal networks. J. Neurosci. 38, 7667–7682. https://doi.org/10.1523/JNEUROSCI.3203-17.2018.

Brandt, H.M., Apkarian, A.V., 1992. Biotin-dextran: a sensitive anterograde tracer for neuroanatomic studies in rat and monkey. J. Neurosci. Methods 45, 35–40. https://doi.org/10.1016/0165-0270(92)90041-b.

Cant, N.B., Oliver, D.L., 2018. Overview of auditory projection pathways and intrinsic microcircuits. In: The Mammalian Auditory Pathways, vol. 65. Springer, Cham, pp. 7–39. https://doi.org/10.1007/978-3-319-71798-2_6. Springer Handbook of Auditory Research.

Chatelier, A., Zhao, J., Bois, P., Chahine, M., 2010. Biophysical characterisation of the persistent sodium current of the Nav1.6 neuronal sodium channel: a single-channel analysis. Pflugers Arch. Eur. J. Physiol. 460, 77–86. https://doi.org/10.1007/s00424-010-0801-9.

Chen, I.-W., Helmchen, F., Lutcke, H., 2015. Specific early and late oddball-evoked responses in excitatory and inhibitory neurons of mouse auditory cortex. J. Neurosci. 35, 12560–12573. https://doi.org/10.1523/JNEUROSCI.2240-15.2015.

Chung, S., Li, X., Nelson, S.B., 2002. Short-term depression at thalamocortical synapses contributes to rapid adaptation of cortical sensory responses in vivo. Neuron 34, 437–446. https://doi.org/10.1016/S0896-6273(02)00659-1.

Díaz-Quesada, M., Maravall, M., 2008. Intrinsic mechanisms for adaptive gain rescaling in barrel cortex. J. Neurosci. 28, 696–710. https://doi.org/10.1523/JNEUROSCI.4931-07.2008.

Duque, D., Malmierca, M.S., 2015. Stimulus-specific adaptation in the inferior colliculus of the mouse: anesthesia and spontaneous activity effects. Brain Struct. Funct. 220, 3385–3398. https://doi.org/10.1007/s00429-014-0862-1.

Duque, D., Pais, R., Malmierca, M.S., 2018. Stimulus-specific adaptation in the anesthetized mouse revealed by brainstem auditory evoked potentials. Hear. Res. 370, 294–301. https://doi.org/10.1016/j.heares.2018.08.011.

Duque, D., Pérez-González, D., Ayala, Y.A., Palmer, A.R., Malmierca, M.S., 2012. Topographic distribution, frequency, and intensity dependence of stimulus-specific adaptation in the inferior colliculus of the rat. J. Neurosci. 32, 17762–17774. https://doi.org/10.1523/JNEUROSCI.3190-12.2012.

Duque, D., Wang, X., Nieto-Diego, J., Krumbholz, K., Malmierca, M.S., 2016. Neurons in the inferior colliculus of the rat show stimulus-specific adaptation for frequency, but not for intensity. Sci. Rep. 6, 1–15. https://doi.org/10.1038/srep24114.

Flecknell, P., 2009. In: Laboratory Animal Anaesthesia (Ed.), Laboratory Animal Anaesthesia, third ed. Elsevier. https://doi.org/10.1016/B978-0-12-369376-1.X0001-9.

Geis, H.R., Borst, J.G.G., 2013. Large GABAergic neurons form a distinct subclass within the mouse dorsal cortex of the inferior colliculus with respect to intrinsic properties, synaptic inputs, sound responses, and projections. J. Comp. Neurol. 521, 189–202. https://doi.org/10.1002/cne.23170.

Geis, H.R., Borst, J.G.G., 2009. Intracellular responses of neurons in the mouse inferior colliculus to sinusoidal amplitude-modulated tones. J. Neurophysiol. 101, 2002–2016. https://doi.org/10.1152/jn.90966.2008.

Geis, H.R., van der Heijden, M., Borst, J.G.G., 2011. Subcortical input heterogeneity in the mouse inferior colliculus. J. Physiol. 589, 3955–3967. https://doi.org/10.1113/jphysiol.2011.210278.

Hernández, O., Espinosa, N., Pérez-González, D., Malmierca, M.S., 2005. The inferior colliculus of the rat: a quantitative analysis of monaural frequency response areas. Neuroscience 132, 203–217. https://doi.org/10.1016/j.neuroscience.2005.01.001.

Hershenhoren, I., Taaseh, N., Antunes, F.M., Nelken, I., 2014. Intracellular correlates of stimulus-specific adaptation. J. Neurosci. 34, 3303–3319. https://doi.org/10.1523/JNEUROSCI.2166-13.2014.

Ito, T., Malmierca, M.S., 2018. Neurons, connections, and microcircuits of the inferior colliculus. In: The Mammalian Auditory Pathways, vol. 65. Springer, Cham,

pp. 127–167. https://doi.org/10.1007/978-3-319-71798-2_6. Springer Handbook of Auditory Research.
Jahnsen, H., Llinás, R., 1984. Ionic basis for the electro-responsiveness and oscillatory properties of Guinea-pig thalamic neurones in vitro. J. Physiol. 349, 227–247. https://doi.org/10.1113/jphysiol.1984.sp015154.
Katz, Y., Heiss, J.E., Lampl, I., 2006. Cross-whisker adaptation of neurons in the rat barrel cortex. J. Neurosci. 26, 13363–13372. https://doi.org/10.1523/JNEUROSCI.4056-06.2006.
Kitagawa, M., Sakaba, T., 2019. Developmental changes in the excitatory short-term plasticity at input synapses in the rat inferior colliculus. Eur. J. Neurosci. 50, 2830–2846. https://doi.org/10.1111/ejn.14422.
Kodandaramaiah, S.B., Franzesi, G.T., Chow, B.Y., Boyden, E.S., Forest, C.R., 2012. Automated whole-cell patch-clamp electrophysiology of neurons in vivo. Nat. Methods 9, 585–587. https://doi.org/10.1038/nmeth.1993.
Kuwada, S., Batra, R., Yin, T.C., Oliver, D.L., Haberly, L.B., Stanford, T.R., 1997. Intracellular recordings in response to monaural and binaural stimulation of neurons in the inferior colliculus of the cat. J. Neurosci. 17, 7565–7581. https://doi.org/10.1523/JNEUROSCI.17-19-07565.1997.
Loftus, W.C., Malmierca, M.S., Bishop, D.C., Oliver, D.L., 2008. The cytoarchitecture of the inferior colliculus revisited: a common organization of the lateral cortex in rat and cat. Neuroscience 154, 196–205. https://doi.org/10.1016/j.neuroscience.2008.01.019.
Lumani, A., Zhang, H., 2010. Responses of neurons in the rat's dorsal cortex of the inferior colliculus to monaural tone bursts. Brain Res. 1351, 115–129. https://doi.org/10.1016/j.brainres.2010.06.066.
Ma, C.L., Kelly, J.B., Wu, S.H., 2002. AMPA and NMDA receptors mediate synaptic excitation in the rat's inferior colliculus. Hear. Res. 168, 25–34. https://doi.org/10.1016/s0378-5955(02)00370-2.
Malinowski, S.T., Wolf, J., Kuenzel, T., 2019. Intrinsic and synaptic dynamics contribute to adaptation in the core of the avian central nucleus of the inferior colliculus. Front. Neural Circ. 13, 46. https://doi.org/10.3389/fncir.2019.00046.
Malmierca, M.S., 2015. Auditory system. In: Paxinos, G. (Ed.), The Rat Nervous System. Academic Press, Amsterdam, pp. 865–946.
Malmierca, M.S., Blackstad, T.W., Osen, K.K., 2011. Computer-assisted 3-D reconstructions of Golgi-impregnated neurons in the cortical regions of the inferior colliculus of rat. Hear. Res. 274, 13–26. https://doi.org/10.1016/j.heares.2010.06.011.
Malmierca, M.S., Blackstad, T.W., Osen, K.K., Karagülle, T., Molowny, R.L., 1993. The central nucleus of the inferior colliculus in rat: a Golgi and computer reconstruction study of neuronal and laminar structure. J. Comp. Neurol. 333, 1–27. https://doi.org/10.1002/cne.903330102.
Malmierca, M.S., Cristaudo, S., Pérez-González, D., Covey, E., 2009a. Stimulus-specific adaptation in the inferior colliculus of the anesthetized rat. J. Neurosci. 29, 5483–5493. https://doi.org/10.1523/JNEUROSCI.4153-08.2009.
Malmierca, M.S., Hernández, O., Antunes, F.M., Rees, A., 2009b. Divergent and point-to-point connections in the commissural pathway between the inferior colliculi. J. Comp. Neurol. 514, 226–239. https://doi.org/10.1002/cne.21997.
Malmierca, M.S., Niño-Aguillón, B.E., Nieto-Diego, J., Porteros, Á., Pérez-González, D., Escera, C., 2019. Pattern-sensitive neurons reveal encoding of complex auditory regularities in the rat inferior colliculus. Neuroimage 184, 889–900. https://doi.org/10.1016/j.neuroimage.2018.10.012.
Malmierca, M.S., Rees, A., Le Beau, F.E.N., Bjaalie, J.G., 1995. Laminar organization of frequency-defined local axons within and between the inferior colliculi of the Guinea pig. J. Comp. Neurol. 357, 124–144. https://doi.org/10.1002/cne.903570112.
Malmierca, M.S., Ryugo, D.K., 2012. Cortical Descending Projections to Auditory Midbrain and Brainstem. The Auditory Cortex. Springer-Verlag, San Diego.
Malmierca, M.S., Saint Marie, R.L., Merchan, M.A., Oliver, D.L., 2005. Laminar inputs from dorsal cochlear nucleus and ventral cochlear nucleus to the central nucleus of the inferior colliculus: two patterns of convergence. Neuroscience 136, 883–894. https://doi.org/10.1016/j.neuroscience.2005.04.040.
Margrie, T.W., Brecht, M., Sakmann, B., 2002. In vivo, low-resistance, whole-cell recordings from neurons in the anaesthetized and awake mammalian brain. Pflugers Arch. Eur. J. Physiol. 444, 491–498. https://doi.org/10.1007/s00424-002-0831-z.
Molineux, M.L., Mehaffey, W.H., Tadayonnejad, R., Anderson, D., Tennent, A.F., Turner, R.W., 2008. Ionic factors governing rebound burst phenotype in rat deep cerebellar neurons. J. Neurophysiol. 100, 2684–2701. https://doi.org/10.1152/jn.90427.2008.
Movshon, J.A., Lennie, P., 1979. Pattern-selective adaptation in visual cortical neurones. Nature 278, 850–852. https://doi.org/10.1038/278850a0.
Nagtegaal, A.P., Borst, J.G.G., 2010. In vivo dynamic clamp study of Ih in the mouse inferior colliculus. J. Neurophysiol. 104, 940–948. https://doi.org/10.1152/jn.00264.2010.
Neher, E., 1992. Correction for liquid junction potentials in patch clamp experiments. Methods Enzymol. 207, 123–131. https://doi.org/10.1016/0076-6879(92)07008-c.
Pérez-González, D., Hernández, O., Covey, E., Malmierca, M.S., 2012. GABA A-mediated inhibition modulates stimulus-specific adaptation in the inferior colliculus. PloS One 7. https://doi.org/10.1371/journal.pone.0034297.
Pérez-González, D., Malmierca, M.S., 2014. Adaptation in the auditory system: an overview. Front. Integr. Neurosci. https://doi.org/10.3389/fnint.2014.00019.
Pérez-González, D., Malmierca, M.S., Covey, E., 2005. Novelty detector neurons in the mammalian auditory midbrain. Eur. J. Neurosci. 22, 2879–2885. https://doi.org/10.1111/j.1460-9568.2005.04472.x.
Peruzzi, D., Sivaramakrishnan, S., Oliver, D.L., 2000. Identification of cell types in brain slices of the inferior colliculus. Neuroscience 101, 403–416. https://doi.org/10.1016/s0306-4522(00)00382-1.
Rabang, C.F., Parthasarathy, A., Venkataraman, Y., Fisher, Z.L., Gardner, S.M., Bartlett, E.L., 2012. A computational model of inferior colliculus responses to amplitude modulated sounds in young and aged rats. Front. Neural Circ. 6, 77. https://doi.org/10.3389/fncir.2012.00077.
Rutecki, P.A., 1992. Neuronal excitability: voltage-dependent currents and synaptic transmission. J. Clin. Neurophysiol. 9, 195–211.
Sah, P., Faber, E.S.L., 2002. Channels underlying neuronal calcium-activated potassium currents. Prog. Neurobiol. 66, 345–353. https://doi.org/10.1016/s0301-0082(02)00004-7.
Sanchez-Vives, M.V., Nowak, L.G., McCormick, D.A., 2000a. Cellular mechanisms of long-lasting adaptation in visual cortical neurons in vitro. J. Neurosci. 20, 4286–4299. https://doi.org/10.1523/jneurosci.20-11-04286.2000.
Sanchez-Vives, M.V., Nowak, L.G., McCormick, D.A., 2000b. Membrane mechanisms underlying contrast adaptation in cat area 17 in vivo. J. Neurosci. 20, 4267–4285. https://doi.org/10.1523/jneurosci.20-11-04267.2000.
Schwindt, P.C., Spain, W.J., Foehring, R.C., Stafstrom, C.E., Chubb, M.C., Crill, W.E., 1988. Multiple potassium conductances and their functions in neurons from cat sensorimotor cortex in vitro. J. Neurophysiol. 59, 424–449. https://doi.org/10.1152/jn.1988.59.2.424.
Sivaramakrishnan, S., Oliver, D.L., 2001. Distinct K currents result in physiologically distinct cell types in the inferior colliculus of the rat. J. Neurosci. 21, 2861–2877. https://doi.org/10.1523/JNEUROSCI.21-08-02861.2001.
Sun, H., Ma, C.L., Kelly, J.B., Wu, S.H., 2006. GABAB receptor-mediated presynaptic inhibition of glutamatergic transmission in the inferior colliculus. Neurosci. Lett. 399, 151–156. https://doi.org/10.1016/j.neulet.2006.01.049.
Tan, M.L., Theeuwes, H.P., Feenstra, L., Borst, J.G.G., 2007. Membrane properties and firing patterns of inferior colliculus neurons: an in vivo patch-clamp study in rodents. J. Neurophysiol. 98, 443–453. https://doi.org/10.1152/jn.01273.2006.
Ulanovsky, N., Las, L., Nelken, I., 2003. Processing of low-probability sounds by cortical neurons. Nat. Neurosci. 6, 391–398. https://doi.org/10.1038/nn1032.
Valdés-Baizabal, C., Parras, G.G., Ayala, Y.A., Malmierca, M.S., 2017. Endocannabinoid modulation of stimulus-specific adaptation in inferior colliculus neurons of the rat. Sci. Rep. 7, 1–14. https://doi.org/10.1038/s41598-017-07460-w.
Veenman, C.L., Reiner, A., Honig, M.G., 1992. Biotinylated dextran amine as an anterograde tracer for single- and double-labeling studies. J. Neurosci. Methods 41, 239–254.
Venkataraman, Y., Bartlett, E.L., 2013. Postnatal development of synaptic properties of the GABAergic projection from the inferior colliculus to the auditory thalamus. J. Neurophysiol. 109, 2866–2882. https://doi.org/10.1152/jn.00021.2013.
Wang, H., Han, Y.-F., Chan, Y.-S., He, J., 2014. Stimulus-specific adaptation at the synapse level in vitro. PloS One 9, e114537. https://doi.org/10.1371/journal.pone.0114537.
Wang, X.-J., Liu, Y., Sanchez-Vives, M.V., McCormick, D.A., 2003. Adaptation and temporal decorrelation by single neurons in the primary visual cortex. J. Neurophysiol. 89, 3279–3293. https://doi.org/10.1152/jn.00242.2003.
Wang, X.X., Jin, Y., Sun, H., Ma, C., Zhang, J., Wang, M., Chen, L., 2016. Characterization of rebound depolarization in neurons of the rat medial geniculate body in vitro. Neurosci. Bull. 32, 16–26. https://doi.org/10.1007/s12264-015-0006-5.
Wehr, M., Zador, A.M., 2005. Synaptic mechanisms of forward suppression in rat auditory cortex. Neuron 47, 437–445. https://doi.org/10.1016/j.neuron.2005.06.009.
Wu, S.H., Ma, C.L., Kelly, J.B., 2004. Contribution of AMPA, NMDA, and GABAA receptors to temporal pattern of postsynaptic responses in the inferior colliculus of the rat. J. Neurosci. 24, 4625–4634. https://doi.org/10.1523/JNEUROSCI.0318-04.2004.
Zhao, L., Liu, Y., Shen, L., Feng, L., Hong, B., 2011. Stimulus-specific adaptation and its dynamics in the inferior colliculus of rat. Neuroscience 181, 163–174. https://doi.org/10.1016/j.neuroscience.2011.01.060.

PLOS BIOLOGY

RESEARCH ARTICLE

Prediction error signaling explains neuronal mismatch responses in the medial prefrontal cortex

Lorena Casado-Román[1,2☯], **Guillermo V. Carbajal**[1,2☯], **David Pérez-González**[1,2*], **Manuel S. Malmierca**[1,2,3*]

1 Cognitive and Auditory Neuroscience Laboratory (CANELAB), Institute of Neuroscience of Castilla y León (INCYL), Salamanca, Spain, **2** Institute for Biomedical Research of Salamanca (IBSAL), Salamanca, Spain, **3** Department of Biology and Pathology, Faculty of Medicine, University of Salamanca, Salamanca, Spain

☯ These authors contributed equally to this work.
* davidpg@usal.es (DPG); msm@usal.es (MSM)

Citation: Casado-Román L, Carbajal GV, Pérez-González D, Malmierca MS (2020) Prediction error signaling explains neuronal mismatch responses in the medial prefrontal cortex. PLoS Biol 18(12): e3001019. https://doi.org/10.1371/journal.pbio.3001019

Academic Editor: Leon Deouell, Hebrew University of Jerusalem, ISRAEL

Received: March 31, 2020

Accepted: December 3, 2020

Published: December 21, 2020

Peer Review History: PLOS recognizes the benefits of transparency in the peer review process; therefore, we enable the publication of all of the content of peer review and author responses alongside final, published articles. The editorial history of this article is available here: https://doi.org/10.1371/journal.pbio.3001019

Data Availability Statement: All relevant data are within the paper and its Supporting Information files.

Abstract

The mismatch negativity (MMN) is a key biomarker of automatic deviance detection thought to emerge from 2 cortical sources. First, the auditory cortex (AC) encodes spectral regularities and reports frequency-specific deviances. Then, more abstract representations in the prefrontal cortex (PFC) allow to detect contextual changes of potential behavioral relevance. However, the precise location and time asynchronies between neuronal correlates underlying this frontotemporal network remain unclear and elusive. Our study presented auditory oddball paradigms along with "no-repetition" controls to record mismatch responses in neuronal spiking activity and local field potentials at the rat medial PFC. Whereas mismatch responses in the auditory system are mainly induced by stimulus-dependent effects, we found that auditory responsiveness in the PFC was driven by unpredictability, yielding context-dependent, comparatively delayed, more robust and longer-lasting mismatch responses mostly comprised of prediction error signaling activity. This characteristically different composition discarded that mismatch responses in the PFC could be simply inherited or amplified downstream from the auditory system. Conversely, it is more plausible for the PFC to exert top-down influences on the AC, since the PFC exhibited flexible and potent predictive processing, capable of suppressing redundant input more efficiently than the AC. Remarkably, the time course of the mismatch responses we observed in the spiking activity and local field potentials of the AC and the PFC combined coincided with the time course of the large-scale MMN-like signals reported in the rat brain, thereby linking the microscopic, mesoscopic, and macroscopic levels of automatic deviance detection.

Introduction

Since the discovery of the mismatch negativity (MMN) 4 decades ago [1,2], this biomarker has become a pivotal tool for cognitive and clinical research in the human brain [3,4], even showing potential diagnostic capabilities [5]. The MMN reflects how the nervous system

Funding: This project has received funding from the European Union's Horizon 2020 research and innovation programme [Marie Skłodowska-Curie Grant agreement No. 722098 (LISTEN)] to MSM; Spanish AEI (PID2019-104570RB-I00) to MSM. DPG held a Postdoctoral salary from the Spanish Ministry of Science and Innovation (MICINN, Grant No. SAF2016-75803-P). Fellowship from the European Union's Horizon 2020 research and innovation programme [Marie Skłodowska-Curie Grant agreement No. 722098 (LISTEN)] to LCR. Fellowship from the Spanish MICINN (BES-2017-080030) to GVC. The funders had no role in study design, data collection and analysis, decision to publish, or preparation of the manuscript.

Competing interests: I have read the journal's policy and the authors of this manuscript have the following competing interests. Manuel S. Malmierca is an Academic Editor for PLOS Biology. The other authors have declared that no competing interests exist.

Abbreviations: AC, auditory cortex; ACC, anterior cingulate cortex; CTR, control condition; dB SPL, decibels of sound pressure level; DEV, deviant condition; ECoG, electrocorticography; ERP, event-related potential; FDR, false discovery rate; FRA, frequency response area; IC, inferior colliculus; IL, infralimbic cortex; iMM, index of neuronal mismatch; iPE, index of prediction error; iRS, index of repetition suppression; LFP, local field potential; MGB, medial geniculate body; mPFC, medial prefrontal cortex; MMN, mismatch negativity; M2, secondary motor cortex; PE, prediction error; PE-LFP, prediction error potential; PFC, prefrontal cortex; PL, prelimbic cortex; SEM, standard error of the mean; SSA, stimulus-specific adaptation; STD, standard condition.

automatically encodes regular patterns in the sensorium, generates internal models to explain away those regularities, and detects deviations from those internal representations in upcoming sensory input, a processing mechanism that is key for survival [6]. This automatic process of deviance detection is commonly studied using an oddball paradigm, where a sequence of repetitive "standard" tones is randomly interrupted by another rare "deviant" tone. When the scalp-recorded auditory event-related potential (ERP) elicited by a tone presented in the standard condition (STD) is subtracted from the ERP prompted by that same tone presented in the deviant condition (DEV), a "mismatch" response (*DEV–STD*) becomes visible at temporal and frontal electrodes in the form of a slow negative deflection; hence the name mismatch negativity [1,2,6].

The topographic distribution of the MMN reveals a frontotemporal network in charge of automatic deviance detection [7–9]. According to the classic cognitive interpretation of the MMN [4,10], temporal sources from the auditory cortex (AC) would first encode acoustic regularities in a sensory memory, detecting specific sensory deviances between that memory trace and incoming input [11]. Then, additional sources from the prefrontal cortex (PFC) assess the behavioral relevance of that sensory deviance, potentially triggering an attention switch toward the change [12–14]. A more neurophysiologically grounded interpretation of the MMN, known as the adaptation hypothesis, denies the existence of a genuine process of deviance detection, arguing that the STD induces stimulus-specific adaptation (SSA) on AC neurons [15,16], whose frequency channels simply remain fresh to keep responding to the DEV [17,18]. Despite their conceptual disparities, both the sensory-memory and the adaptation hypotheses agree that early AC processing is highly sensitive to specific stimulus features. Conversely, PFC activity seems more reliant on an overall evaluation of global properties, which occurs upstream of initial sensory discrimination processes [6,19].

Recent proposals under the predictive processing framework have attempted to integrate previous accounts of the generation of the MMN (for a recent in-depth discussion, see [20]), establishing a hierarchical and reciprocal relationship between the AC and the PFC. The AC would first represent the spectral properties of sensory stimuli, suppressing redundant auditory inputs based on their frequency-specific features, by means of short-term plasticity mechanisms such as synaptic depression and lateral inhibition [21–23]. During an oddball paradigm, this would be functionally observable as SSA, or more appropriately, as repetition suppression [22,24–26]. The information that could not be explained away in the AC is forwarded as a prediction error signal (PE) to higher levels in the processing hierarchy [27,28]. Eventually, the bottom-up flow of PEs reaches the PFC, which tries to explain PEs away by means of higher-order expectations regarding emergent properties of the auditory stimulation, such as complex interstimulus relationships and structures [22,29,30]. Thus, whereas fast PEs forwarded from the AC are purely auditory in nature, the PFC would generate PEs when more abstract expectations are not met, requiring an update.

Despite the several hypotheses accounting for MMN generation, its neuronal substrate remains elusive and poorly understood, mostly due to the ethical constraints on human brain research. Noninvasive techniques, such as ERP analysis or functional magnetic resonance imaging, cannot pinpoint response measurements with enough temporal and spatial resolution as to deem with absolute certainty whether AC potentials precede those from the PFC [31–33]. When invasive approaches are available, electrocorticography (ECoG) electrode placement in human patients is strictly restrained by clinical criteria, causing intra- and inter-individual variability that hampers systematic and detailed comparisons [34–37]. In contrast, invasive techniques of electrophysiological recording in animal models offer both the spatial and temporal resolution necessary to compare mismatch signals across areas more precisely. Auditory-evoked spiking activity and local field potentials (LFPs) can provide the accurate

locations and time courses of mismatch responses at microscopic and mesoscopic levels, respectively [38,39]. In turn, those local-scale mismatch responses can be correlated with the large-scale MMN-like potentials which are thought to be the specific analog of the human MMN in the corresponding animal model [40,41]. Hence, animal models can help to define the neuronal substrate of the human MMN, as well as to ratify or discard certain hypotheses about its generation.

In the present study, we recorded spiking activity and LFPs from 1 possible frontal source contributing to the emergence of MMN-like potentials in the rat brain: the medial prefrontal cortex (mPFC). Following the standards of the most thorough human MMN studies, we included 2 "no-repetition" controls, namely, the many-standards [42] and the cascade sequences [43], in order to account for the possible stimulus-specific effects that could be induced by the oddball paradigm. We found delayed, context-dependent, more robust, and longer-lasting mismatch responses in the rat mPFC than in our previous studies in the rat AC [38,39]. The mismatch responses recorded from both the AC and the mPFC as spiking activity and LFPs correlated in time with the large-scale MMN-like potentials from the rat brain reported in other studies [40,44,45]. Furthermore, the mismatch responses from the mPFC could be mainly identified with PE signaling activity (or genuine deviance detection, in classic MMN terminology), thus confirming their fundamentally different nature from the mismatch responses recorded in the AC.

Results

In order to find auditory mismatch responses and PEs in the mPFC, we recorded sound-evoked neuronal activity in the secondary motor cortex (M2), the anterior cingulate cortex (ACC), the prelimbic cortex (PL), and the infralimbic cortex (IL) of 33 urethane-anesthetized rats (Fig 1A). For this purpose, we used sets of 10 pure tones arranged in different sequences to create distinctive contextual conditions: the deviant conditions (DEV ascending, DEV descending, and DEV alone) and the standard condition (STD) of the oddball paradigm (Fig 1C), along with their corresponding no-repetition control conditions (CTR), provided by the many-standards (CTR random) and cascade sequences (CTR ascending and CTR descending; Fig 1D).

In the vein of human MMN research [43], we used CTRs to dissociate the higher-order processes of genuine deviance detection or abstract PE signaling from the possible contribution of other lower-order mechanisms related to spectral processing and SSA [21]. On the one hand, CTRs cannot induce SSA or repetition suppression on the auditory-evoked response, in contrast to the STD. On the other hand, CTR patterns remain predictable and should not trigger deviance detection or PE signaling, or at least not as intensely as the DEV [20] (see Oddball paradigm controls for more detailed rationale). By comparing auditory-evoked responses in each condition, we could quantify the estimated contribution of each process to the total mismatch response in the form of 3 indices (Fig 1B): index of neuronal mismatch ($iMM = DEV–STD$), index of repetition suppression ($iRS = CTR–STD$), and index of prediction error ($iPE = DEV–CTR$). Therefore, the iMM quantifies the total mismatch response; the iRS estimates the portion of the mismatch response that can be accounted for by the adaptation hypothesis; and the iPE reveals the component of the mismatch response that can only correspond to genuine deviance detection (according to the sensory-memory hypothesis) or to PE signaling (under a predictive processing interpretation).

In the following sections, we present the results of recording from 83 sound-driven multiunits across all mPFC fields (M2: 25; ACC: 20; PL: 20; IL: 18; Fig 2A), where we were able to test a total of 384 tones at every aforementioned condition (M2: 132; ACC: 90; PL: 81; IL: 81),

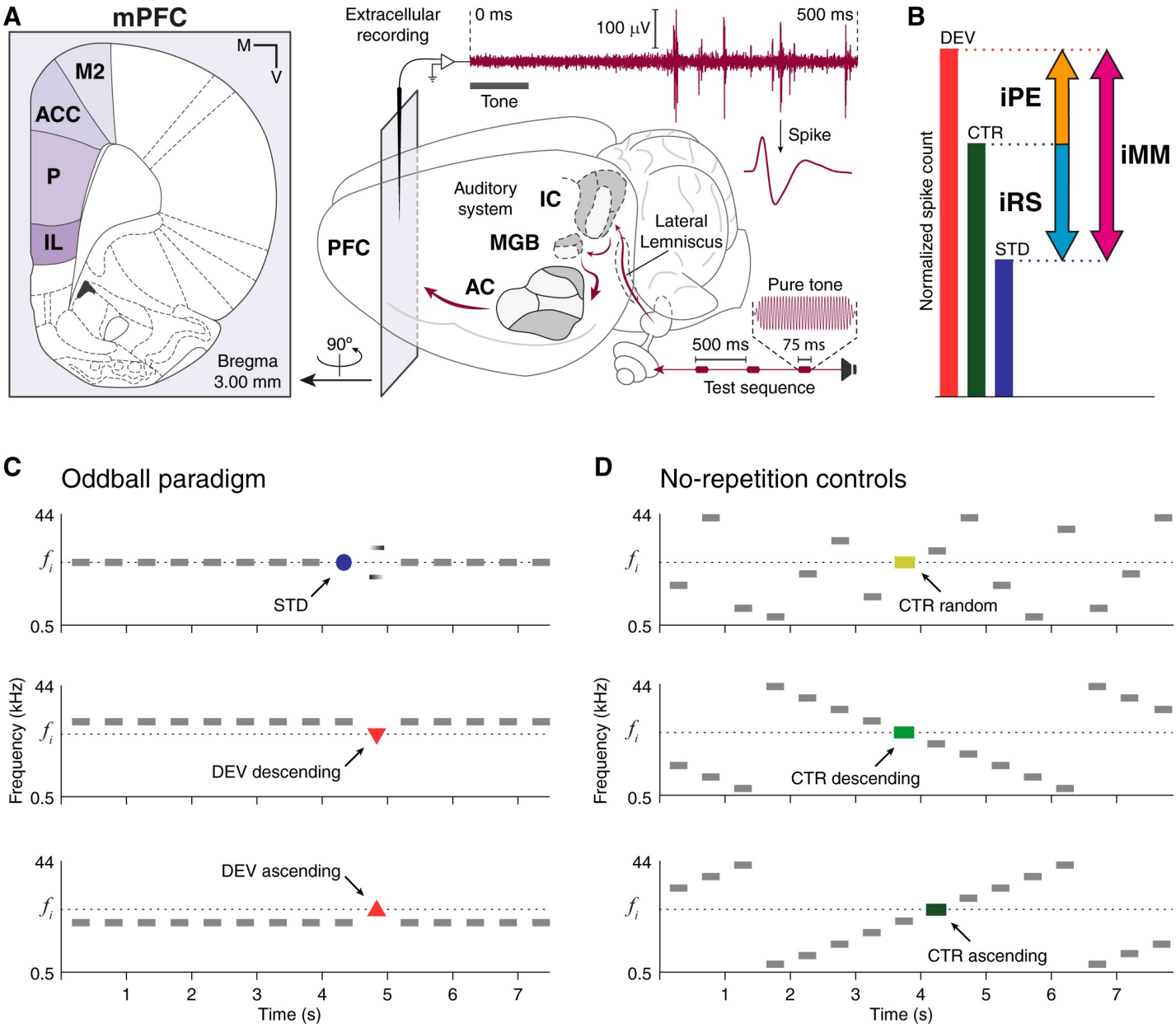

Fig 1. Experimental design. (A) Schematic representation of an experimental setup for extracellular recording of auditory-evoked responses in a rat brain. In the left sublet, a schematic coronal section where mPFC fields are highlighted in violet tones. At the right, maroon elements represent the flow of auditory information during the experimental session, from the speaker through the rat brain and into a raw recording trace. **(B)** Decomposition of mismatch responses using the CTR and quantification in 3 indices. **(C)** Three possible experimental conditions within an oddball paradigm for a given tone of interest f_i (colored). **(D)** Three possible control conditions for a given tone of interest f_i (colored). At the top, the many-standards sequence; at the middle and bottom, 2 versions of the cascade sequence. AC, auditory cortex; ACC, anterior cingulate cortex; CTR, control condition; DEV, deviant condition; IC, inferior colliculus; IL, infralimbic cortex; iMM, index of neuronal mismatch; iPE, index of prediction error; iRS, index of repetition suppression; M, medial; MGB, medial geniculate body; mPFC, medial prefrontal cortex; M2, secondary motor cortex; PFC, prefrontal cortex; PL, prelimbic cortex; SEM, standard error of the mean; STD, standard condition; V, ventral.

https://doi.org/10.1371/journal.pbio.3001019.g001

between 1 and 8 per multiunit (Fig 2C). Although the frequency-response areas (FRAs) appeared unstructured (Fig 2B), these multiunits exhibited robust responses to many combinations of frequency (0.6 to 42.5 kHz) and intensity (25 to 70 dB SPL) during experimental testing (Fig 2C and 2D). This indicates that the auditory sensitivity of mPFC neurons is

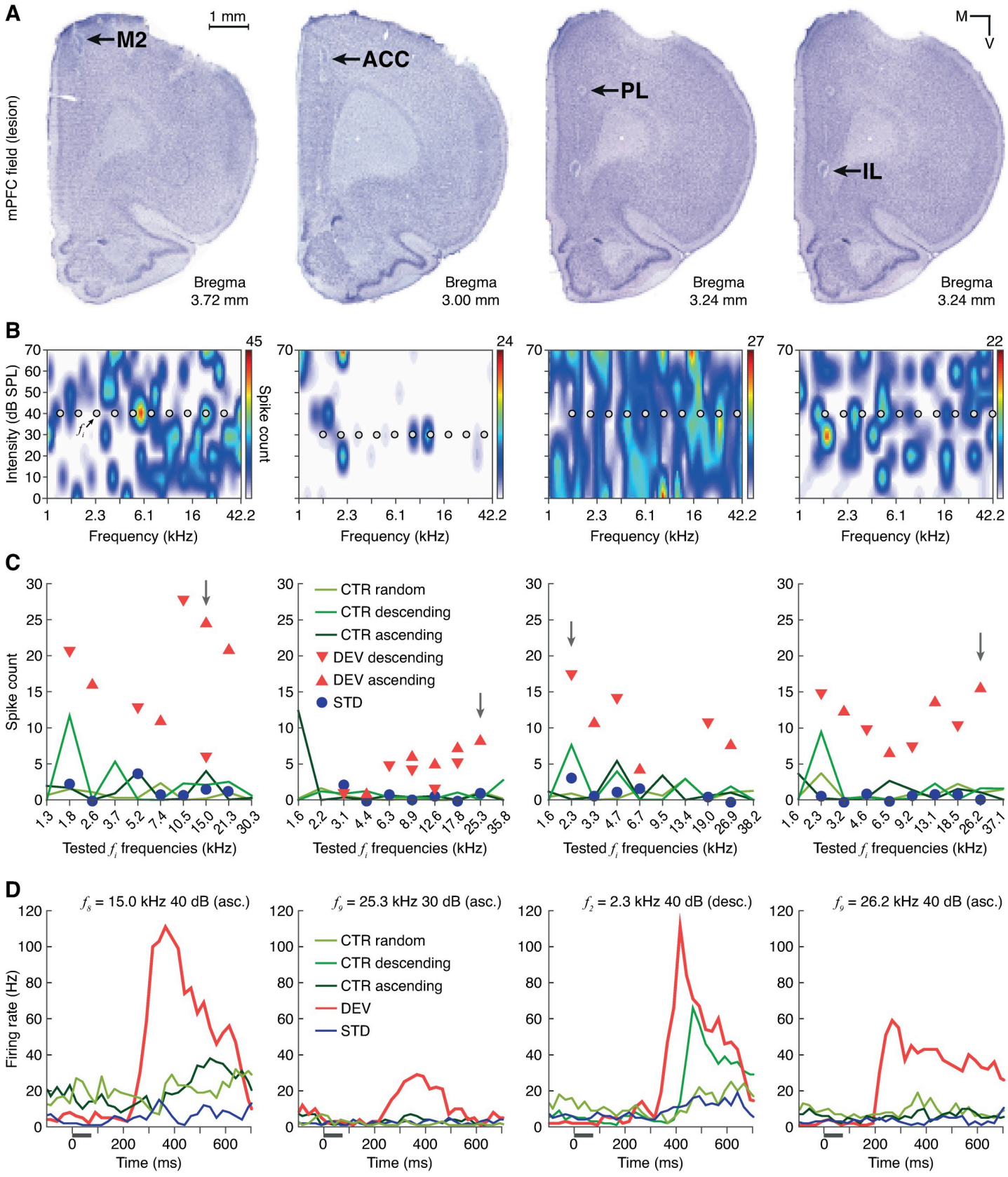
A
1 mm
M2
ACC
PL
IL
M
V
mPFC field (lesion)
Bregma 3.72 mm
Bregma 3.00 mm
Bregma 3.24 mm
Bregma 3.24 mm
B
Intensity (dB SPL)
Spike count
Frequency (kHz)
C
Spike count
CTR random
CTR descending
CTR ascending
DEV descending
DEV ascending
STD
Tested f_i frequencies (kHz)
D
f_8 = 15.0 kHz 40 dB (asc.)
f_9 = 25.3 kHz 30 dB (asc.)
f_2 = 2.3 kHz 40 dB (desc.)
f_9 = 26.2 kHz 40 dB (asc.)
Firing rate (Hz)
CTR random
CTR descending
CTR ascending
DEV
STD
Time (ms)

Fig 2. Multiunit recording examples from each mPFC field. (A) Coronal mPFC sections where electrolytic lesions (black arrows) mark the recording sites of the multiunits whose auditory-evoked responses are plotted in the sublets below. Hence, column-wise sublets correspond to the same multiunit. **(B)** FRA of 1 multiunit from each mPFC station. Within each FRA, 10 gray dots mark the set of 10 pure f_i tones selected to generate the testing sequences (Fig 1C and 1D), whose evoked response is plotted in the sublet below. **(C)** Multiunit spike counts for every experimental condition of the 10 f_i tested. A vertical gray arrow points at the f_i tone whose peristimulus time histogram is plotted in the sublet below. **(D)** Peristimulus time histogram showing the firing rate elicited by each experimental condition tested for 1 f_i tone, illustrated as a gray horizontal line. The underlying data for this Figure can be found in S1 Data. ACC, anterior cingulate cortex; CTR, control condition; DEV, deviant condition; FRA, frequency response area; IL, infralimbic cortex; mPFC, medial prefrontal cortex; M2, secondary motor cortex; PL, prelimbic cortex; STD, standard condition.

https://doi.org/10.1371/journal.pbio.3001019.g002

fundamentally driven by the contextual characteristics of auditory stimulation, rather than its spectral properties.

Context-dependent responses and large PE signals across all mPFC fields

First, we compared the responses elicited by the many-standards and the cascade sequences. Similarly to previous works studying the rat AC [39] and the human MMN [46], we found no significant differences between CTR random, CTR ascending, and CTR descending (Fig 1D), neither within each mPFC field nor for our whole sample (Wilcoxon signed-rank test). Therefore, we used the cascade-evoked responses as CTR for the rest of analyses, based on the theoretical advantages that the cascade sequence offers over the many-standards sequence to control for effects of spectral processing (see Oddball paradigm controls for a detailed rationale) [43].

DEV evoked the most robust discharges across all mPFC fields, usually more than doubling the responses elicited by any other condition (Fig 2C and 2D). Median normalized response to DEV was significantly larger than that to STD or CTR (within-field multiple comparisons Friedman test; Table 1; Fig 3B). Only in M2 the difference in the responses to CTR and STD reached statistical significance ($p = 0.0490$), whereas the distribution of CTR and STD responses proved to be too overlapped in the rest of mPFC fields (within-field multiple comparisons Friedman test; Table 1; Fig 3B). The iMM revealed very large and significant mismatch responses coming from all the mPFC fields (within-field multiple comparisons Friedman test; Table 1; Fig 3C, in magenta). Most of these robust mismatch responses could be accounted for by strong PE signaling, as high iPE values were very significant and very close to those of the iMM (within-field multiple comparisons Friedman test; Table 1; Fig 3C, in orange). Conversely, iRS values were very low in general, and only M2 showed a median iRS significantly different from zero (within-field multiple comparisons Friedman test; Table 1; Fig 3C, in cyan). Remarkably, the values of each index did not differ significantly between mPFC fields (Kruskal–Wallis test with Dunn–Sidak correction; $p > 0.05$ for all comparisons with the 3 indices), so a hierarchical relationship between mPFC fields during the processing of auditory contexts cannot be established in our sample.

According to "standard" implementations of cortical predictive processing [47], error units forwarding PEs are located in superficial layers (II/III), while expectations are encoded by prediction units found in the deep layers (V/VI). Index variations could be expected between superficial and deep mPFC layers, so we attempted to pinpoint the laminar location of our multiunits by means of electrolytic lesions (Fig 2A). Given that such lesions can cover diameters of about 300 μm, half of our multiunit sample had to be excluded from this analysis, as our conservative histological assessment deemed their location inconclusive. Nevertheless, this restrictive histological analysis allowed us to comfortably locate the rest of our multiunit recordings within layers II/III (19 multiunits, 92 tones) or layers V/VI (22 multiunits, 113 tones). Unfortunately, we could not find any significant index changes between II/III and V/VI groups, neither within each mPFC field nor for the whole sample (Wilcoxon signed-rank test).

Table 1. Median spike counts and indices in each mPFC field. Significant *p*-values are highlighted.

	M2	ACC	PL	IL
Number of multiunits	25	20	20	18
Tested frequencies	132	90	81	81
Median raw spike counts				
DEV	8.6875	4.8125	6.4750	6.0750
STD	2.7000	1.5500	1.7750	1.1750
CTR	2.9875	1.7000	2.5750	2.4250
Median normalized spike counts				
DEV	0.8693	0.8653	0.8951	0.8511
STD	0.2751	0.2280	0.2583	0.2202
CTR	0.3389	0.3189	0.3225	0.3926
Raw spike count differences, Friedman test				
DEV − STD	5.9875	3.2625	4.7000	4.9000
p-value	**3.4655×10^{-26}**	**2.6737×10^{-14}**	**4.5502×10^{-20}**	**3.8146×10^{-16}**
DEV − CTR	5.7000	3.1125	3.9000	3.6500
p-value	**6.9089×10^{-18}**	**6.3210×10^{-14}**	**6.0892×10^{-14}**	**3.8465×10^{-11}**
CTR − STD	0.2875	0.1500	0.8000	1.250
p-value	**0.0490**	0.9109	0.0953	0.1249
Normalized spike count differences, Friedman test				
iMM = DEV − STD	0.5941	0.6373	0.6368	0.6310
p-value	**3.4655×10^{-26}**	**2.6737×10^{-14}**	**4.5502×10^{-20}**	**3.8146×10^{-16}**
iPE = DEV − CTR	0.5304	0.5464	0.5726	0.4586
p-value	**6.9089×10^{-18}**	**6.3210×10^{-14}**	**6.0892×10^{-14}**	**3.8465×10^{-11}**
iRS = CTR − STD	0.0638	0.0910	0.0642	0.1724
p-value	**0.0490**	0.9109	0.0953	0.1249

ACC, anterior cingulate cortex; CTR, control condition; DEV, deviant condition; IL, infralimbic cortex; iMM, index of neuronal mismatch; iPE, index of prediction error; iRS, index of repetition suppression; mPFC, medial prefrontal cortex; M2, secondary motor cortex; PL, prelimbic cortex; STD, standard condition.

https://doi.org/10.1371/journal.pbio.3001019.t001

Fast repetition suppression of the response to predictable auditory input

To explore the dynamics of the mismatch responses over time for each mPFC field, we averaged the firing rate to DEV, CTR, and STD in each trial of the sequence across all multiunit recordings. The effect of the position of a stimulus within its sequence is shown in Fig 3D, where each dot indicates the mean response to a given condition, when the position of the trial within the sequence corresponds to the one indicated in the x-axis. We searched for statistical differences between the spike counts of STD and CTR across the trial number. We computed the mean spike counts in groups of 10 trails to obtain 40 measurements (to have the same number of data points for each condition). Then, we calculated the difference of these 40 spike counts to STD minus the 40 spike counts to CTR and tested for statistical significance against zero with a Wilcoxon signed-rank test. Across trial presentation, mean spike counts for STD and CTR events were significantly different only in M2 and IL (Fig 3D; M2: $p = 8.68 \times 10^{-07}$, ACC: $p = 0.87$, PL: $p = 0.14$, IL: $p = 4.87 \times 10^{-06}$).

A power-law model of 3 parameters provided the best fit of the STD responses per mPFC field: $y(t) = at^b + c$ (adjusted R^2, M2: 0.358; ACC: 0.259; PL: 0.076; IL: 0.380). Across trials, DEV events maintained a high firing rate (adjusted R^2, M2: −0.054; ACC: 0.489; PL: 0.213; IL: −0.054). On the other hand, CTR responses showed repetition suppression, although not as strong and prompt as the STD (adjusted R^2, M2: 0.1864; ACC: 0.324; PL: 0.187; IL: 0.245).

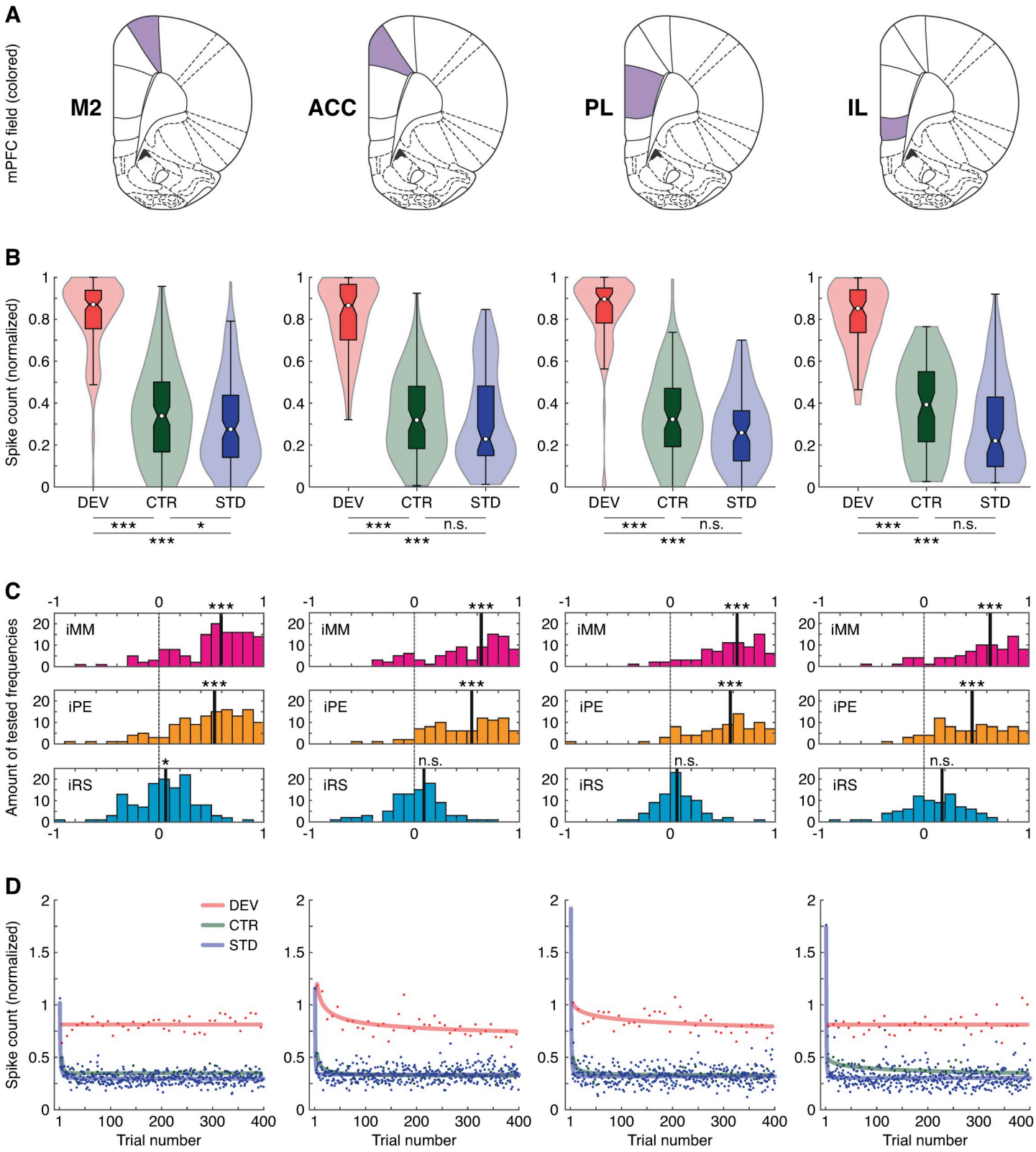

Fig 3. Spiking activity analysis. (A) Schematic representation of coronal planes highlighting each mPFC field for column-wise reference. **(B)** Violin plots representing the distribution of normalized spike counts for each experimental condition. The boxplots inside each distribution indicates the median as a white dot, the interquartile range as the box, and the confidence interval for the median as the notches. Asterisks denote statistically significant difference between conditions (n.s., nonsignificant,

$^{*}p < 0.05$, $^{**}p < 0.01$, $^{***}p < 0.001$). **(C)** Distribution of indices in each mPFC field. **(D)** Average spike count per trial number for each condition along the test sequence. Asterisks denote statistical significance against zero (n.s., nonsignificant, $^{*}p < 0.05$, $^{**}p < 0.01$, $^{***}p < 0.001$). The underlying data for this Figure can be found in S2 Data. AC, auditory cortex; ACC, anterior cingulate cortex; CTR, control condition; DEV, deviant condition; IC, inferior colliculus; IL, infralimbic cortex; iMM, index of neuronal mismatch; iPE, index of prediction error; iRS, index of repetition suppression; MGB, medial geniculate body; M2, secondary motor cortex; PL, prelimbic cortex; STD, standard condition.

https://doi.org/10.1371/journal.pbio.3001019.g003

Only the repetition suppression to STD manifested very fast and robustly across trials in all mPFC fields (*b* parameter [with 95% confidence intervals]: M2, −1.373 [−1.656 to −1.089]; ACC, −2.247 [−3.138 to −1.357]; PL, −1.951 [−3.064 to −0.839]; IL, −2.210 [−2.862 to −1.557]). Only 1 repetition sufficed to yield >50% decay of the initial response. Another repetition attenuated the STD response to levels comparable to the steady-state, where the firing rate remained constant until the end of the sequence (c parameter [with 95% confidence intervals]: M2, 0.296 [0.290 to 0.302]; ACC, 0.337 [0.330 to 0.344]; PL, 0.318 [0.309 to 0.326]; IL, 0.302 [0.293 to 0.312]). These findings mean that only 2 repetitions are needed to generate a precise repetition expectation that suppresses this kind of redundancy in the mPFC.

Microscopic and mesoscopic measurements of PE signals coincide in time

To identify the overall response patterns of each mPFC field, we computed the population temporal dynamics of the average firing rate as normalized spike-density functions. Consistently across all fields, mPFC multiunits exhibited extremely robust and long-lasting firing to DEV (Fig 4B, in red). DEV responses showed very long latencies, needing more than 100 ms poststimulus onset to become discernible from spontaneous activity. Then, DEV firing increased slowly over a course of more than 200 ms before peaking (DEV spike-density function peak latency, M2: 377 ms; ACC: 396 ms; PL: 464 ms; IL: 352 ms). The peak latency in response to DEV stimuli was longer in the PL than in the other mPFC fields (Wilcoxon rank-sum test, PL versus M2: $p = 4.43 \times 10^{-04}$, PL versus ACC: $p = 4.48 \times 10^{-04}$, PL versus IL: $p = 1.50 \times 10^{-04}$; whereas M2 versus ACC: $p = 0.729$, M2 versus IL $p = 0.490$, ACC versus IL $p = 0.756$). This DEV-evoked activity continued in decay, well into the following STD trial of the oddball paradigm. CTR responses tended to follow these same patterns, although with less robust responses and longer latencies (CTR spike-density function peak latency, M2: 516 ms; ACC: 428 ms; PL: 523 ms; IL: 446 ms), such that the response evoked by the previous tone in the cascade sequence is still visible in the current trial (Fig 4B, in green). Finally, the STD did not evoke any robust responses or clear peaks (Fig 4B, in blue).

To analyze PE signaling within each field, we computed the average iPE for each tested tone recorded in 35 time windows of 20 ms width in the range of −50 to 650 ms around tone onset. We tested the indices for significance against zero (Wilcoxon signed-rank test, FDR-corrected for 35 comparisons, $p < 0.05$). iPE started to be significant at 120 ms in the PL, followed by the IL at 140 ms, and later by the M2 and ACC at 180 ms poststimulus onset. In all mPFC fields, iPE signals exceeded half of the index maximum for a sustained length, from about 250 ms poststimulus onset to the end of the analysis window, beyond 600 ms (Fig 4D, in orange).

The extended period of DEV-evoked spiking activity could be the neuronal trace of an updating process of the internal representation by means of PE signals [24,48], as it has been suggested for the human MMN. However, spike responses reflect local activity at the neuron level, whereas the MMN is a large-scale brain potential. One reasonable way of bridging this gap is to probe the correlation between PEs present in the microscopic level with those present within the LFPs [38,39], which constitute the average synaptic activity in local cortical circuits [49]. Hence, we averaged LFP responses for each condition and station (Fig 4C), as well as the difference between DEV and CTR conditions (Fig 4D, in black). We termed this difference as

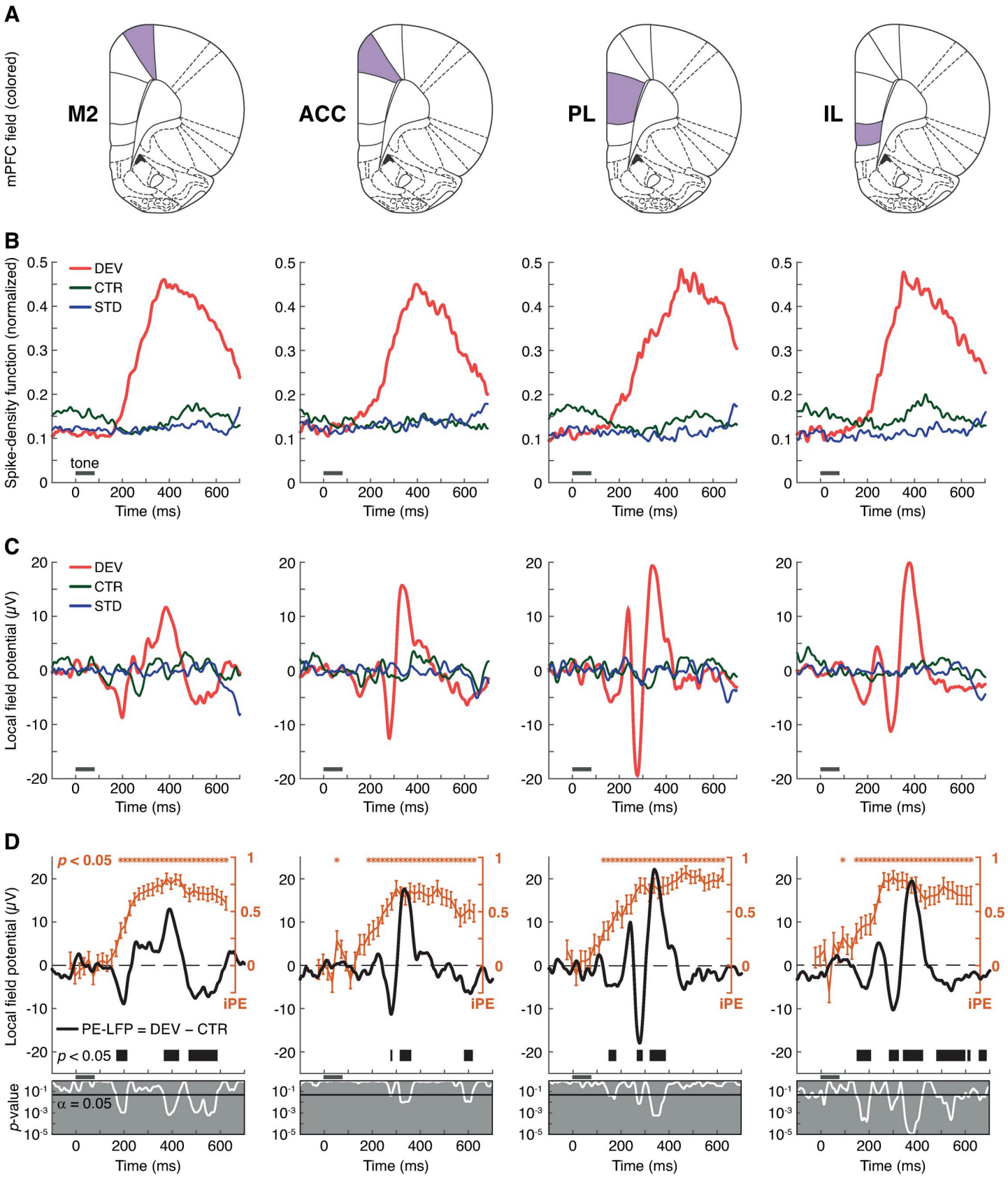
A
mPFC field (colored)
M2
ACC
PL
IL
B
Spike-density function (normalized)
DEV
CTR
STD
tone
Time (ms)
C
Local field potential (μV)
DEV
CTR
STD
Time (ms)
D
Local field potential (μV)
p < 0.05
iPE
PE-LFP = DEV – CTR
p < 0.05
p-value
α = 0.05
Time (ms)

Fig 4. LFP analysis. (A) Schematic representation of coronal planes highlighting each mPFC field for column-wise reference. **(B)** Average firing rate profiles of each mPFC field as the normalized spike-density function for every condition. Gray horizontal lines illustrate tone presentation. **(C)** Average LFP across all tested tones and multiunit recordings from each mPFC field for every condition. **(D)** In orange, the time course of the average iPE of the spiking activity (mean ± SEM) where the asterisks above mark a significant iPE value ($p < 0.05$) for the corresponding time window. In black, PE-LFP is the difference wave between the LFPs of DEV and CTR. The thick black horizontal bar below marks the time intervals were the PE-LFP turns significant ($p < 0.05$). The gray sublets below display with a white trace the instantaneous *p*-values corresponding to the PE-LFP of each mPFC field. The underlying data for this Figure can be found in S3 Data. ACC, anterior cingulate cortex; CTR, control condition; DEV, deviant condition; IL, infralimbic cortex; iPE, index of prediction error; LFP, local field potential; mPFC, medial prefrontal cortex; M2, secondary motor cortex; PE-LFP, prediction error potential; PL, prelimbic cortex; STD, standard condition.

https://doi.org/10.1371/journal.pbio.3001019.g004

"prediction error potential": $PE\text{-}LFP = LFP_{DEV} - LFP_{CTR}$. Indeed, LFP analysis confirmed that the robustness of DEV responses was also clearly observable at the mesoscopic level, in stark contrast to the feeble or nonexistent modulations yielded by CTR and STD (Fig 4C). Significant PE-LFP modulations were also detectable in all mPFC fields, beginning at 147 ms after change onset in IL and PL, followed by M2 at 167 ms and considerably later by ACC at 275 ms (paired *t* test, FDR-corrected for 428 comparisons, $p < 0.05$; Fig 4D, thick black line). Most remarkably, these PE-LFP modulations occur within the time window where iPE values become significant (Fig 4D, compare the distribution of orange asterisks and thick black lines over time), unveiling a correlation between the PE signals recorded at microscopic and mesoscopic levels.

Strong responses to unpredictable sounds over a background of silence

In a subset of 9 multiunits (6 rats) from the previously reported data, we tested 39 frequency tones while muting the STD tones of the oddball paradigm, hence obtaining a condition where DEV was presented "alone" (Fig 5A). DEV alone tones were separated by silent periods of a minimum of 1.925 s, equivalent to 3 silenced STD. DEV and DEV alone median spike counts and response patterns did not differ significantly (multiple comparisons Friedman test; Fig 5B and 5C). Although some differences could be observed in the modulations of their LFPs (Fig 5D), these divergencies are negligible as they failed to reach statistical significance (paired *t* test, FDR-corrected for 428 comparisons; Fig 5E). Thus, the responses of mPFC to unexpected tones are similar, regardless of whether they are presented over a background of silence or interrupting a regular train of other repetitive tones.

Comparisons between the mPFC and the AC in the rat brain

In order to achieve a more general picture of auditory deviance detection in the rat brain, we also used the data set of a previous work from our lab with similar methodology [39] to study the differences between the mismatch responses in the mPFC and the auditory system. In our previous study, the adaptation hypothesis could only be endorsed in the subcortical lemniscal pathway, whereas predictive activity was identified all along the nonlemniscal pathway and the AC [21,39]. Interestingly, the relative magnitude of mismatch responses along all these auditory centers was comparable, as reflected by their respective median iMM values: 0.49 in the nonlemniscal inferior colliculus (IC), 0.52 in the nonlemniscal medial geniculate body (MGB), 0.50 in the lemniscal (or primary) AC, and 0.60 in the nonlemniscal (or nonprimary) AC. This is also the case in the mPFC, with a median iMM value of 0.59 (Wilcoxon signed-rank test, $p = 6.81 \times 10^{-57}$).

However, the composition of these mismatch responses was fundamentally distinct in the PFC as compared to the auditory system. Repetition suppression was the dominant effect contributing to the mismatch responses of all auditory neurons: 0.46 in both the nonlemniscal IC and MGB, 0.39 in the lemniscal AC, and 0.33 in the nonlemniscal AC. Conversely, the influence of frequency-specific effects in mPFC neurons was almost irrelevant, with a median iRS

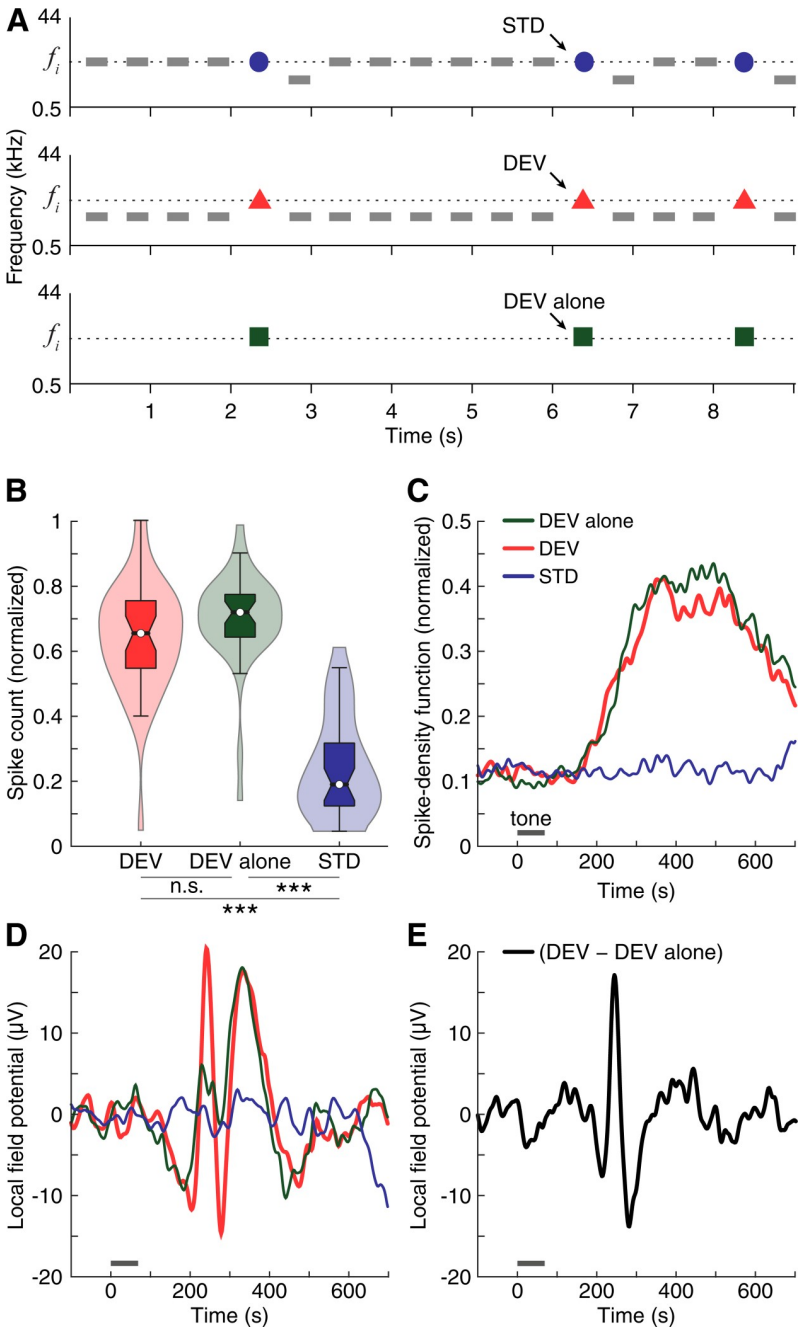

Fig 5. DEV alone analysis. (A) Illustration of the DEV alone condition as an oddball paradigm where the STD train is muted. **(B)** Violin plots representing the distribution of normalized spike counts for each experimental condition. The boxplots inside each distribution indicates the median as a white dot, the interquartile range as the box, and the confidence interval for the median as the notches. **(C)** Average firing rate profiles as the normalized spike-density function for every condition. Gray horizontal lines illustrate tone presentation. **(D)** Average LFP across all tested tones and multiunit recording for different conditions. **(E)** Difference wave between the LFP to the DEV and to the DEV alone. The underlying data for this Figure can be found in S4 Data. DEV, deviant condition; LFP, local field potential; STD, standard condition.

https://doi.org/10.1371/journal.pbio.3001019.g005

value of 0.06 (Wilcoxon signed-rank test, $p = 9.75 \times 10^{-06}$). On the other hand, median iPE values are rather low along the auditory system: 0.03 in the nonlemniscal IC, 0.06 in the nonlemniscal MGB, 0.11 in the lemniscal AC, and 0.27 in the nonlemniscal AC. AC neurons exhibit the most prominent PE signaling, accounting for 22% of the mismatch response in the lemniscal AC and 45% in the nonlemniscal AC. In contrast, PE signaling in mPFC neurons is dominant, with a median iPE value of 0.53 (Wilcoxon signed-rank test, $p = 5.73 \times 10^{-55}$) that accounts for 90% of the total mismatch response (Fig 6A). Thus, spectral properties were the main subject of mismatch responses in the auditory system, while mPFC processing seemed to be abstracted from them.

Statistical comparisons between AC regions and mPFC fields confirmed the general trends described above. The magnitude of the iMM exhibited no significant differences (Kruskal–Wallis test with Dunn–Sidak correction; $p > 0.05$ for all comparisons), but the iPE component grew significantly from the AC to the mPFC (Kruskal–Wallis test with Dunn–Sidak correction; lemniscal AC versus M2: $p = 4.50 \times 10^{-14}$, versus ACC: $p = 1.07 \times 10^{-11}$, versus PL: $p = 4.10 \times 10^{-12}$, versus IL: $p = 1.09 \times 10^{-08}$; nonlemniscal AC versus M2: $p = 3.93 \times 10^{-05}$, versus ACC: $p = 2.12 \times 10^{-04}$, versus PL: $p = 6.74 \times 10^{-05}$, versus IL: $p = 0.011$) to the detriment of iRS, whose proportion drastically shrank to a rather insubstantial contribution to the mismatch response (Kruskal–Wallis test with Dunn–Sidak correction; lemniscal AC versus M2: $p = 1.69 \times 10^{-12}$, versus ACC: $p = 1.11 \times 10^{-12}$, versus PL: $p = 2.61 \times 10^{-10}$, versus IL: $p = 3.12 \times 10^{-06}$; nonlemniscal AC versus M2: $p = 7.46 \times 10^{-08}$, versus ACC: $p = 1.76 \times 10^{-08}$, versus PL: $p = 1.29 \times 10^{-06}$, versus IL: $p = 0.003$). This demonstrates that the nature of mismatch responses in the AC and the PFC is fundamentally different, as predicted by the sensory-memory and the predictive processing hypotheses (Fig 6A).

Temporal dynamics also agree with the abovementioned hypotheses, with the extremely dissimilar latencies observed in the AC and the mPFC point at a sequential processing. Both DEV- and CTR-evoked spiking activity in the AC peaks and stars decaying well before the 75-ms tone has even ended [39]. In stark contrast to the fast AC response, the spiking activity of our whole mPFC multiunit sample began to slowly rise after 150 ms poststimulus onset and took an impressive 462 ms to peak to the DEV and 517 ms to peak to the CTR (Fig 6B). In fact, the entire peristimulus time histogram of a nonlemniscal AC neuron can be represented within the latency of the auditory-evoked responses measured in mPFC neurons (Fig 6C). Regarding the LFPs, an early PE-LFP becomes significant in the AC at about 40 ms and vanishes by 160 ms poststimulus onset, whereas the PE-LFP in our mPFC sample started at 140 ms and lingered with significant magnitudes up to 623 ms poststimulus onset. Both AC and mPFC PE-LFPs coincided precisely with the time course of their respective significant iPE values in spiking activity, thus confirming the PE signaling asynchrony at both microscopic and mesoscopic levels (Fig 6D).

According to data from previous studies in anesthetized rats [38,39], the contrast between AC and mPFC processing is also very apparent in the time needed to explain away STD input. To suppress their initial response to the STD by half, lemniscal AC neurons need 7 repetitions, and nonlemniscal AC neurons 2 repetitions, whereas mPFC neurons only need 1 repetition (Fig 6E, cyan arrow). To reach a steady-state level of maximum attenuation of the auditory-evoked response takes more than the initial 9 STD repetitions in the lemniscal AC, 5 repetitions in the nonlemniscal AC, but only 2 in the mPFC (Fig 6E, dashed lines). This finding rules out the possibility that suppressive effects on the STD could be simply inherited or amplified downstream from the auditory system. On the contrary, the capacity of the mPFC to explain away redundant input more efficiently than the AC supports the predictive processing hypothesis: mPFC expectations are imposed top-down on the AC, thereby influencing earlier stages of auditory processing.

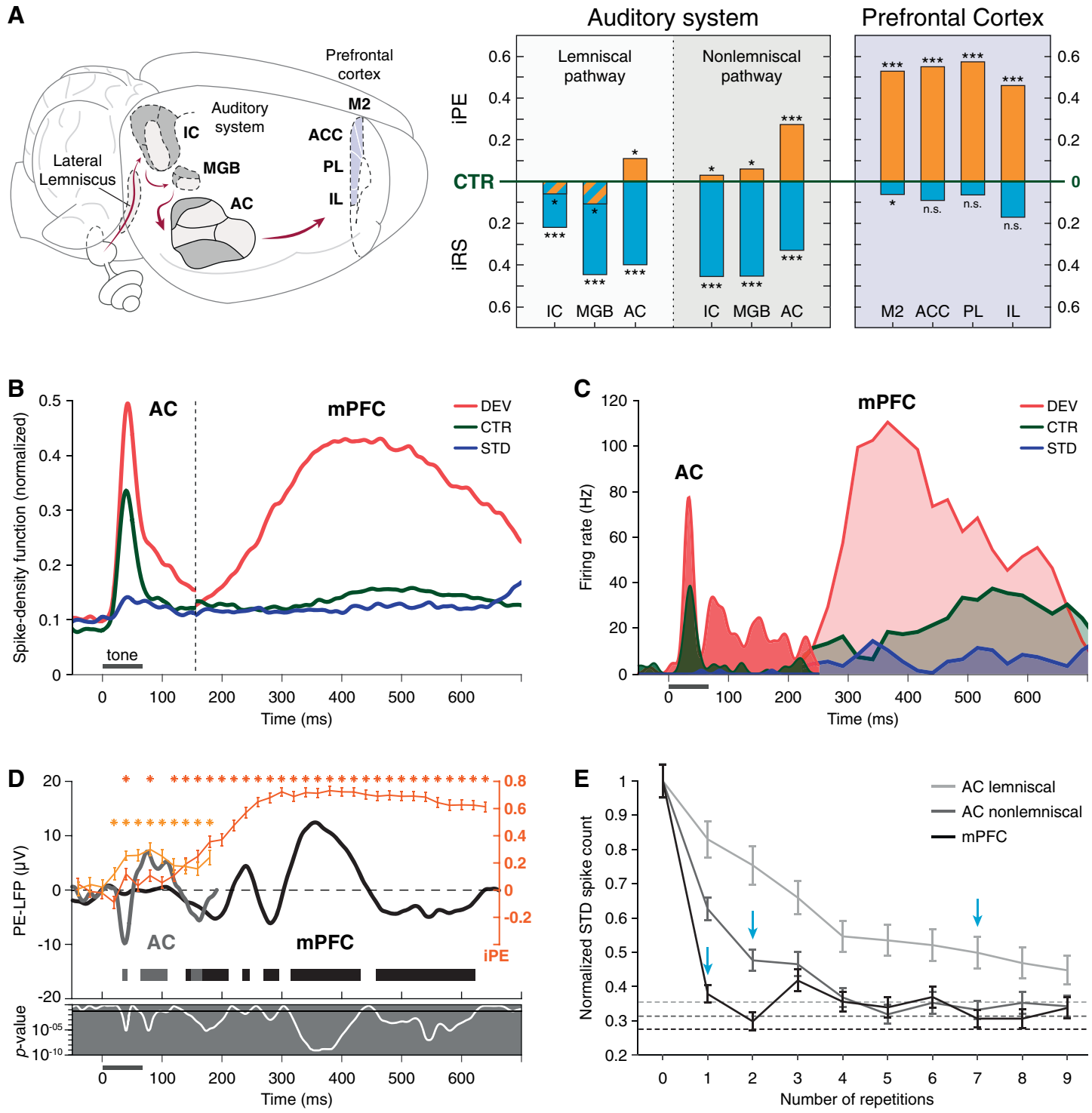

Fig 6. Comparisons between AC and mPFC responses. (A) Median iPE (orange) and iRS (cyan) of each auditory or prefrontal subdivision, represented with respect to the baseline set by the CTR. Thereby, iPE is upwards-positive while iRS is downwards-positive (see Fig 1B). Asterisks denote statistical significance of the indices against zero median (n.s., nonsignificant, $^{*}p < 0.05$, $^{**}p < 0.01$, $^{***}p < 0.001$). **(B)** Within the interval of 0–150 ms poststimulus onset, average firing rate profile of the nonlemniscal AC as the normalized spike-density function for every condition. Similarly, the mPFC firing rate profile is displayed within the interval of 150–700 ms. Gray horizontal line illustrates tone presentation. **(C)** Peristimulus time histogram examples of 1 nonlemniscal AC single unit (in solid colors) and 1 mPFC multiunit (in transparent colors), plotted together. Spontaneous activity in the mPFC before 200 ms poststimulus onset has not been represented for clarity. **(D)** In orange tones, time course of the average iPE of the spiking activity (mean ± SEM) in the nonlemniscal AC (in light orange) and in the mPFC (in dark orange), where the asterisks above mark a significant iPE value ($p < 0.05$) for the corresponding time window. In dark tones, the PE-LFP is the difference wave between the LFP to the DEV and to the CTR

recorded from the nonlemniscal AC (in gray) and from the mPFC (in black). The thick horizontal bar below marks the time intervals were the PE-LFP of the nonlemniscal AC (in gray) and the mPFC (in black) turns significant ($p < 0.05$). The gray sublet below displays the instantaneous *p*-values corresponding to the PE-LFP (in white). **(E)** Average responses for the first 10 STD trials (mean ± SEM) in the lemniscal AC (in light gray), the nonlemniscal AC (in dark gray), and the mPFC (in black). Vertical cyan arrows mark the trial where the initial STD response has undergone more than 50% of attenuation. Dashed lines mark the maximum level of attenuation of the STD response during the sequence (the steady-state parameter of a power-law fit of 3 parameters). The underlying data for this Figure can be found in S5 Data. AC, auditory cortex; ACC, anterior cingulate cortex; CTR, control condition; DEV, deviant condition; IC, inferior colliculus; IL, infralimbic cortex; iPE, index of prediction error; iRS, index of repetition suppression; LFP, local field potential; MGB, medial geniculate body; mPFC, medial prefrontal cortex; M2, secondary motor cortex; PE-LFP, prediction error potential; PL, prelimbic cortex; SEM, standard error of the mean; STD, standard condition.

https://doi.org/10.1371/journal.pbio.3001019.g006

Discussion

In this study, we recorded multiunit responses in the rat mPFC to the auditory oddball paradigm and its no-repetition controls, i.e., the many-standards and cascade sequences (Fig 1). We did not observe meaningful differences in the strength of the evoked responses across the 4 mPFC fields or between superficial and deep cortical layers. Unpredictable auditory stimulation prompted robust responses, as compared to the weak (or even absent) activity elicited by sounds that could be expected (Figs 2–5). The time course of the mismatch responses found in the spiking activity and LPFs of the mPFC (Fig 4C and 4D) correlated with that of the frontal sources of the large-scale MMN-like potentials from the rat brain [40,44,45]. Most importantly, our data indicated that mismatch responses of the mPFC are almost purely comprised of PE signaling activity (Figs 3C and 4D), in contrast to the mismatch responses recorded along the auditory system (Fig 6A) [39].

Unpredictability drives auditory responsiveness in the PFC

Despite the alleged advantages of the cascade over the many-standards sequence for controlling repetition effects during the oddball paradigm [21,43], we did not find any statistically significant differences between the 2 no-repetition controls in the mPFC for the tested parameters. This goes in line with evidence from the auditory system, where the responses evoked by both no-repetition controls were also comparable in AC, MGB, and IC of anaesthetized rats [39]. Such similarity between no-repetition controls tends to be the usual observation in human MMN studies as well [46,50,51]. This suggests that both no-repetition controls are probably processed as a regular succession of pitch alternations, without distinguishing whether those alternations of pitch are random, ascending or descending. Both controls seemingly generate an "alternation expectation" capable of suppressing to a certain extent the auditory-evoked responses in the mPFC, but without inducing stimulus-specific effects of repetition suppression (like STD does). Therefore, the many-standards and the cascade sequences work as largely equivalent CTRs for the oddball paradigm.

Spiking activity in the rat mPFC peaked earlier and higher when evoked by unexpected auditory stimulation, i.e., DEV and DEV alone (which did not differ significantly from each other), more than doubling or even tripling in magnitude the spike response elicited by predictable conditions, i.e., CTR and STD (which only differed significantly from each other in M2; Table 1; Figs 3B, 3D, 4B, 5B and 5C). DEV response dominance was even more pronounced in the LFP analysis, where unexpected DEV and DEV alone conditions prompted robust local field fluctuations whereas the impact of predictable CTR and STD stimulation was negligible (Figs 4C and 5D). We found the same response unbalance between unpredictable and predictable stimulation conditions in all mPFC fields, regardless of whether recordings were performed in superficial or deep cortical layers. The robust mismatch between mPFC responses to unexpected and predictable conditions resulted in similarly high values of iMM (*DEV–STD*) and iPE (*DEV–CTR*). Conversely, the meager or insignificant values of iRS (*CTR–STD*) indicate that the influence of frequency-specific effects is rather irrelevant in the mPFC

(Table 1; Figs 1B, 3C and 6A). Hence, the mismatch responses evoked in the mPFC by the auditory oddball paradigm are better explained as pure PE signaling (for more detailed rationale, see Oddball paradigm controls).

Reports from other frontal sources have found comparable results despite using different methods, recording techniques and model species. Spiking responses in the lateral and ventral orbitofrontal cortex of anesthetized and awake mice also found a great predominance of DEV responses over STD responses [52]. Epidural electrodes placed over the frontal cortices of awake and freely moving rats [40,45] recorded stronger ERPs to DEV than to CTR or STD. In awake macaques, 1 study using multichannel electrodes placed in the dorsolateral PFC found larger responses to DEV than to STD [53], while another using ECoG found strong mismatch responses in the PFC to deviant changes within a roving-standard paradigm, but not to repetitions or the many-standards control [54]. Regarding invasive research in human patients, ECoG studies have consistently proven that, in contrast with the AC, the PFC ceases responding to DEV when its occurrence can be expected [34,37,55]. Although the different prefrontal locations analyzed in the aforementioned studies across rodents, macaques and humans should not be hastily regarded as direct homologs [56], all these works agree in that the key driver of auditory responsiveness in the PFC is unpredictability.

The neuronal substrate of MMN-like potentials in the rat brain

According to our results, PE spiking activity starts appearing at 120 ms poststimulus onset. About 100 ms later, PE signaling becomes very prominent (iPE >0.5), where it remains more or less sustained beyond 600 ms poststimulus onset, even after the next tone in the sequence has been presented (Figs 4D and 6D, in orange). Most remarkably, such time distribution of the iPE spans enough to include all significant PE-LFP modulations in every mPFC field (Figs 4D and 6D, in black). Therefore, the time course of PE signaling observed in the mPFC at microscopic level coincides in time with that observed at mesoscopic level.

At macroscopic level, ERPs from awake rats exhibited strong mismatch responses beginning about 40 ms poststimulus onset [40,44,45]. Similarly, both our spiking activity and LFP analyses confirmed that early PE signaling starts about 40 ms poststimulus onset in the AC until about 150 ms, when the PFC takes over and continues PE signaling beyond 600 ms poststimulus onset (Fig 6B and 6D). Moreover, the strongest MMN-like potentials are reported in the time window of 100 to 500 ms [40,44,45], precisely coinciding with the period where we registered the most intense PE spiking activity (iPE >0.5), as well as the highest peaks in the PE-LFP (Figs 4D and 6D). Thus, our data allow to correlate the microscopic, mesoscopic, and macroscopic levels at which PE signaling can be detected in the rat PFC. Since the so-called MMN-like potentials are regarded as the rat analog of the human MMN [41], our results could model the possible neuronal substrate of the frontal MMN generators.

Different nature of PE signaling in the AC and the PFC

Compared to our previous work in the AC [38,39], evoked responses to pure tones in the mPFC were relatively rare and difficult to find. Multiunits that responded to stochastic bursts of white noise during search then exhibited unstructured FRAs, where a concrete receptive field could not possibly be determined (Fig 2B). However, these same multiunits fired consistently in response to many combinations of frequencies and intensities when the tested pure tones were embedded within an experimental sequence (Fig 2C and 2D). Thus, whereas AC processing was clearly driven by the spectral properties of auditory stimulation, auditory sensitivity in mPFC neurons seemed solely dependent on contextual or abstract characteristics. In the same vein, a previous study of spiking activity and LFPs in alert macaques also found

stimulus specificity in the auditory-evoked responses of the AC, but not the dorsolateral PFC [53]. In addition, frequency-specific effects present in the AC within the train of STD or after a DEV were not apparent in the dorsolateral PFC of those alert macaques [53]. Similarly, whereas the iRS in the rat AC can still account for more than half of the mismatch responses [39], at the rat mPFC we found scant or even not significant values of iRS (Fig 6A), thus dismissing any relevant spectral influences in PFC processing.

Our data show that while iMM values in the AC and the mPFC of anesthetized rats are analogous, iPE values are significantly different (Fig 6A). This means that the nature of mismatch responses at the AC is distinct from those at the PFC, despite been paired in their relative magnitude. For this reason, generators at both the AC and the PFC are important contributors to the MMN, but their contributions are fundamentally different in nature, something that has been advocated since the classic sensory-memory interpretation of the human MMN [4,9,10,12] and has also been inherited by the more modern predictive processing framework [20,23]. Given that the iPE can account for 90% of the iMM value, and that in most mPFC fields both indices are not even significantly different, prefrontal mismatch responses can be safely interpreted as genuine deviance detection (in classic terminology) or as pure PE signaling (in predictive processing terminology).

Following this logic, the mPFC would be generating an abstracted mismatch response de novo, signaling "deviance" or a "PE" without reflecting the low-level spectral properties of the driving acoustic stimuli, which have been already represented at earlier processing stages within the auditory system [20,39]. This interpretation is consistent with the huge latency disparities observed between the AC and the mPFC in our anesthetized rats. Whereas AC responses to pure tones take just a few milliseconds to emerge [38,39], evoked responses in the mPFC take hundreds of milliseconds to appear, both at spike activity (Figs 2D, 4B, 5C and 6B) and LFP recordings (Figs 4C, 4D, 5D, 5E and 6D). Prefrontal response delays over 100 ms with respect to the AC have also been reported in the lateral and ventral orbitofrontal cortex of anesthetized and awaked mice [52], as well as in the dorsolateral PFC of alert macaques [53]. Entire AC responses could fit within the latency of the auditory-evoked responses found in the PFC (Fig 6B and 6C). This suggests that AC and PFC processing occur to a certain extent in sequential manner, as described by both the classic sensory-memory [4] and the predictive processing hypotheses [30] of the generation of the MMN. First, acoustic deviances from spectral regularities must be detected at the AC (temporal sources), and only after that, the PFC (frontal sources) can identify global and behaviorally relevant deviations from more abstract internal representations.

Further evidence of the hierarchical relationship between the AC and the PFC could be found in the notable differences between the time each cortical region needs to explain redundant STD input away. According to our previous studies [38,39], neurons in primary or lemniscal AC need 7 repetitions to suppress their initial auditory-evoked response by half, and 2 repetitions in the nonprimary or nonlemniscal AC (Fig 6E, in gray). By contrast, only 1 repetition was enough for the initial auditory-evoked response in the mPFC to drop between >50% and >70%, and a second repetition to reach maximum suppression levels (Fig 6E, in black). Similar suppressive dynamics were reported in the orbitofrontal cortex of anesthetized and awake mice [52], in the dorsolateral PFC of alert macaques [53], as well as in human frontal sources [22].

Given that the PFC responds much later to sound but suppresses redundant auditory input more efficiently than the AC, the mismatch responses observed at the PFC cannot be simply inherited or amplified downstream from the auditory system. The inverse hierarchical arrangement, proposed by the predictive processing hypothesis [30], is thereby more plausible. The PFC is not part of the auditory system; in fact, it is not a sensory processor per se, but

rather an executive center. In more natural conditions, the PFC most likely integrates manifold inputs to generate very complex cross-modality sensorimotor representations [57,58]. These abstract internal representations at the PFC could in turn guide in top-down manner the processing at lower-level systems, hyperparameterizing the more concrete operations carried in their respective (sensory) modalities, and thus increasing overall processing efficiency. In other words, the gestalt acquired at the PFC could be feedbacked to the AC, generating specific expectations in the spectral domain (the native format of AC), but ultimately regarding higher-order properties (such as interstimulus relationships, auditory tokens, or sequence structures) that could have not been computed otherwise in the local AC circuitry. This top-down predictive activity would exert an inhibitory influence on AC responses whenever certain auditory input is already accounted for by the prefrontal gestalt, but any unpredicted information would be conveyed bottom-up in a PE to update the internal representation at the PFC. Thus, hierarchical predictive processing can explain why the PFC exhibits longer latencies than the AC, while also performing more effective and overarching expectation suppression, capable of fully explaining away STD input, and even CTR input. As soon as auditory information becomes redundant to the big picture, it stops reaching the PFC, avoiding cognitive overload, and saving high-order processing resources for more fruitful endeavors.

Subcortical middle players could relay PE signals to the PFC

Finally, it is worth mentioning that most accounts of deviance detection and PE signaling tend to overrepresent cortical sources, downplaying the role of subcortical contributions. Since the MMN is recorded from the human scalp, the frontotemporal cortical network is more readily accessible for study. The predictive processing framework is also eminently focused on cortical processing [27,47,59]. However, the important contribution of subcortical nuclei is becoming ever clearer in recent literature. Regarding the auditory system, no-repetition controls revealed that SSA could not fully account for the mismatch responses found in the nonlemniscal divisions of the IC and the MGB of anesthetized rats and awake mice. Hence, subcortical auditory nuclei seem to constitute the first levels of the predictive processing hierarchy, which is ultimately responsible for auditory deviance detection [39,60,61].

Human brain research has also identified auditory mismatch signals from subcortical nuclei outside the auditory system, such as the nucleus accumbens [62], the hippocampus [63], or the amygdala [64,65]. Evidence from animal models has been able to confirm these subcortical signals and describe locations and time courses more precisely. Auditory mismatch responses took about 20 ms to appear in the CA1 region of the hippocampus of freely moving mice [66], and 30 to 60 ms to show in the basolateral amygdala of alert macaques [53]. Furthermore, like in the PFC, mismatch responses in the basolateral amygdala did not exhibit stimulus-dependent effects [53]. Minding the different model species, these time delays would place the hippocampus and the amygdala right between the response windows observed in the auditory pathway and those in the PFC.

This could provide a potential explanation for the lack of significant differences between mismatch responses across mPFC fields, despite been quite distinct from each other. The mismatch responses we recorded at the rat mPFC resembled to those recorded at the mouse orbitofrontal cortex [52] and the macaque dorsolateral PFC [53]. It is possible that nonauditory subcortical nuclei such as the hippocampus or the amygdala could compute PEs and then broadcast that signal all over the PFC for further processing and integration. Indeed, a very recent study has demonstrated that the emergence of robust and long-lasting mismatch responses in the mouse orbitofrontal cortex is directly controlled from the nonlemniscal MGB through the basolateral amygdala [52]. Therefore, all these auditory and nonauditory

subcortical nuclei could be fundamental middle players in the automatic process of deviance detection and PE signaling reflected in the MMN. This is a possibility that should be further explored in future studies.

Limitations

All theoretical implementations of the predictive processing hypothesis assume that expectations and PEs are computed by separated neuronal types distributed across distinct cortical layers, which should result in characteristic laminar profiles [47,59]. Unfortunately, we have not been able to identify any significant response differences between superficial and deep layers of the mPFC, in contrast to what predictive processing models expect. This lack of differences between layers could be due to the unspecific nature of our multiunit measurements. Extracellular recordings can capture the evoked responses of several neurons within a considerable volume of up to hundreds of μm^3 around the tip of the electrode. The recorded activity does not always allow for spike sorting and waveform analyses to isolate and assign putative neuronal types to the single units contained within one multiunit recording [67], as it was the case in the present study.

Nevertheless, it is worth mentioning that the concrete role of neuronal types and their laminar distribution is still a subject of intense debate within the predictive processing framework. Several possible but conflicting implementations have been proposed [47,68–71], and empirical evidence from human research is mixed (for an in-depth discussion, see [48]). In fact, previous attempts from our lab and others to find a laminar distribution of mismatch responses which fitted the standard implementation of cortical predictive processing [47] also failed in the AC of rats and mice [38,39,66,72]. Therefore, focused research efforts will be needed to disambiguate this issue in the future.

Lastly, the MMN is a notorious obligatory component of the human ERP, remaining persistent in situations where consciousness is absent, such as during sleep [73,74], anesthesia [75,76], or even coma [77,78]. Hence, the fact that we have been able to record very robust mismatch responses in the rat mPFC during anesthesia further strengthens the link between our data and MMN evidence from human research. Moreover, previous studies of mismatch responses in both the auditory system and the PFC of rodents did not find dramatic differences between anesthetized and awake preparations [39,52,79,80]. Notwithstanding, the use of anesthesia is always a limiting factor that must be minded when comparing these data with those obtained from awake preparations, or when trying to extrapolate possible behavioral implications from the conclusions presented in our study.

Materials and methods

Ethics statement

All methodological procedures were approved by the Bioethics Committee for Animal Care of the University of Salamanca (USAL-ID-195) and performed in compliance with the standards of the European Convention ETS 123, the European Union Directive 2010/63/EU, and the Spanish Royal Decree 53/2013 for the use of animals in scientific research.

Surgical procedures

We conducted experiments on 33 female Long-Evans rats aged 9 to 17 weeks with body weights between 200 and 330 g. Rats were anesthetized with urethane (1.9 g/kg, intraperitoneal). To ensure a stable deep anesthetic level, we administered supplementary doses of urethane (approximately 0.5 g/kg, intraperitoneal) when the corneal or pedal withdrawal reflexes

were present. Urethane preserves balanced neural activity better than other anesthetic agents having a modest balanced effect on inhibitory and excitatory synapses [81]. Normal hearing was verified with auditory brainstem responses recorded with subcutaneous needle electrodes, using a RZ6 Multi I/O Processor (Tucker-Davis Technologies, TDT, Alachua, FL, USA) and processed with BioSig software (TDT), using 0.1 ms clicks presented at a rate of 21/s, delivered monaurally to the right ear in 10 dB steps, from 10 to 90 decibels of sound pressure level (dB SPL), using a close-field speaker. Every 10 hours, we administered 0.1 mg/kg of atropine sulfate (subcutaneous), 0.25 mg/kg of dexamethasone (intramuscular), and 5 to 10 ml of glucosaline solution (subcutaneous) to ameliorate the presence of bronchial secretions, brain edema, and prevent dehydration, respectively. Animals were artificially ventilated through a tracheal cannula with monitored expiratory [CO_2] and accommodated in a stereotaxic frame with hollow specula to facilitate direct sound delivery to the ears. Rectal temperature was maintained at approximately 37˚C with a homeothermic blanket system (Cibertec, Madrid, Spain). We surgically exposed bregma by making an incision in the scalp at the midline and retracting the periosteum. A craniotomy of approximately 3 mm in diameter was performed above the left mPFC and the dura was removed.

Data acquisition

We recorded multiunit activity to look for evidence of predictive coding signals under acoustic oddball stimulation across fields of the mPFC of the urethane-anesthetized rat: M2, ACC, PL, and IL. The rodent mPFC combines anatomo-electrophysiological elements of the primate dorsolateral PFC and ACC at a rudimentary level [56]. Experiments were conducted in an electrically shielded and sound-attenuating chamber. Recording tracts were orthogonal to the brain surface of the left mPFC: approximately 2.5 to 4.68 mm rostral to bregma, approximately 0.2 to 1.8 mm lateral to the midline, and approximately 0.2 to 4.5 mm dorsoventrally. Therefore, we covered the 4 fields of the mPFC and various cortical layers (II–VI). We performed extracellular neurophysiological recordings with glass-coated tungsten microelectrodes (1.4 to 3.5 MΩ impedance at 1 kHz). We used a piezoelectric micromanipulator (Sensapex, Oulu, Finland) to advance a single electrode and measure the penetration depth. We visualized electrophysiological recordings online with custom software programmed with OpenEx suite (TDT, https://www.tdt.com/component/openex-software-suite/) and MATLAB (MathWorks, https://www.mathworks.com/products/matlab.html). Multiunit activity was extracted automatically by manually setting a unilateral action potential threshold above the background noise as an accurate estimation of neuronal population dynamics [82]. Analog signals were digitized with a RZ6 Multi I/O Processor, a RA16PA Medusa Preamplifier and a ZC16 headstage (TDT) at 97 kHz sampling rate and amplified 251×. Neurophysiological signals for multiunit activity were bandpass filtered between 0.5 and 4.5 kHz using a second order Butterworth filter.

The sound stimuli were generated using the RZ6 Multi I/O Processor (TDT) and custom software programmed with OpenEx Suite (TDT) and MATLAB. Sounds were presented monaurally in a close-field condition to the ear contralateral to the left mPFC, through a custom-made speaker. We calibrated the speaker using a ¼-inch condenser microphone (model 4136, Brüel & Kjær) and a dynamic signal analyzer (Photon+, Brüel & Kjær) to ensure a flat response up to 73 ± 1 dB SPL between 0.5 and 44 kHz, and the second and third signal harmonics were at least 40 dB lower than the fundamental at the loudest output level.

Oddball paradigm controls

One limitation of the mismatch measurements obtained using the oddball paradigm is that the effects of high-order processes like genuine deviance detection or PE signaling cannot be

distinguished from lower-order spectral-processing effects such as SSA [21,25]. The so-called "no-repetition" controls allow to assess the relative contribution of both higher- and lower-order processes to the overall mismatch response [43]. These CTRs of the auditory oddball paradigm are tone sequences that must meet 3 criteria: (1) to feature the same tone of interest with the same presentation probability as that of the DEV; (2) to induce an equivalent state of refractoriness by presenting the same rate of stimulus per second (which excludes the DEV alone from being considered a proper CTR); and (3) present no recurrent repetition of any individual stimulus, specially the tone of interest, thus ensuring that no SSA is induced during the CTR [20].

Whether the CTR-evoked response exhibited signs of expectation suppression, that could be only explained by high-order regularity encoding or predictive processing, capable of explaining away interstimulus relationships more complex than sheer repetition [21,25]. Hence, we can assess the portion of the mismatch response (*DEV–STD*) that can be attributed to the effects of spectral repetition yielded during the STD train, such as SSA [15,16], by comparing the auditory-evoked responses to DEV and to CTR. When the auditory-evoked response is similar or higher during CTR than in DEV, then the mismatch response can be fully accounted for by repetition suppression, and no higher-order process of deviance detection or PE signaling can be deduced (i.e., DEV $\leq$ CTR; Fig 1B). In other words, this result would provide support for the adaptation hypothesis [17,18] while severely undermining the sensory-memory account [4,10]. Otherwise, a stronger response to DEV than to CTR unveils a component of the mismatch response that can only be explained by a genuine process of deviance detection or PE signaling (i.e., DEV $>$ CTR; Fig 1B).

In order to dissociate the relative contribution of frequency-specific effects from processes of genuine deviance detection or predictive processing, we generated 2 different no-repetition CTRs for our oddball paradigms: the many-standards and cascaded sequences (Fig 1D). The many-standards sequence presents the tone of interest embedded in a random sequence of assorted tones, where each tone shares the same presentation probability as the DEV in the oddball paradigm [42]. However, some authors have argued that this CTR-random is not fully comparable with the oddball paradigm, inasmuch as the disorganized succession of tones never allows to form the memory trace of a proper regularity, nor can it generate high-precision expectations, whereas the STD does. Moreover, the random succession of stimuli might generate small mismatch responses, which would underestimate the contributions of deviance detection or predictive processing in the comparison of DEV against CTR [21,43].

The cascade sequence [43] tries to overcome the alleged caveats of the many-standards sequence by presenting tones in a regular fashion, e.g., in an increasing or a decreasing frequency succession. Thus, the stimulus of interest conforms to a regularity—as opposed to the DEV—, but not a regularity established by repetition and susceptible to undergo SSA—contrary to the STD—, making the cascade sequence a more fitted and less conservative CTR than the many-standards sequence. As an additional advantage, the tone immediately preceding our tone of interest is the same in both oddball and cascaded sequences, since only versions following the same direction are compared (i.e., DEV-ascending versus CTR-ascending, DEV-descending versus CTR-descending). This allows to control for another possible spectral sensitivity, which are responses to a rise or fall in frequency between 2 successive tones. For these reasons, the cascade sequence is regarded as a better CTR for the oddball paradigm [21,43].

Recording protocol

In search of evoked auditory multiunit responses from the mPFC, we presented stochastic trains of white noise bursts and sinusoidal pure tones of 75 ms duration with 5-ms rise-fall

ramps, varying presentation rate and intensity to avoid possible stimulus-specific effects that could suppress evoked responses.

Once auditory activity was detected, we only used pure tones (also 75 ms duration and 5-ms rise-fall ramps) to record the experimental stimulation protocols. All stimulation sequences ran at 2 stimuli per second. First, a multiunit FRA was computed by randomly presenting pure tones of various frequency and intensity combinations that ranged from 1 to 44 kHz (in 4 to 6 frequency steps/octave) and from 0 to 70 dBs (10 dB steps) with 1 to 3 repetitions per tone. In our previous studies in the auditory system [39,60,61], we selected 10 tones at frequency steps of 0.5 octaves to generate our stimulation paradigms within the receptive field determined by the FRA. However, we could not determine clear receptive fields in the multiunit FRAs of the mPFC, so we had to choose the frequencies and intensity of our test sequences based on our observations during manual search, trying to maximize the auditory-evoked response when possible. Our 400-stimuli test sequences were presented in randomized order leaving periods of >10 min of silence in between to minimize potential long-term habituation effects [83]. All test sequences presented while recording from the same multiunit were delivered at the same intensity, but we varied intensity among the different multiunits of our sample to maximize the auditory-evoked response in each case.

For each multiunit, we used all the 10 preselected tones to generate 3 no-repetition sequences (i.e., the many-standards, cascade ascending, and cascade descending) and pairs of consecutive frequencies (within those 10 tones) to generate oddball sequences. An oddball sequence consisted of a repetitive tone (STD, 90% probability), occasionally replaced by a different tone (DEV, 10% probability) in a pseudorandom manner. The first 10 stimuli of the sequence set the STD, and a minimum of 3 STD tones always preceded each DEV. Oddball sequences were either ascending or descending, depending on whether the DEV tone had a higher or lower frequency than the STD tone, respectively (Fig 1C). Additionally, in a subset of experiments, we muted the STD train to measure the response of the tone of interest over a background of silence, as a DEV alone. The number of test sequences presented to each multiunit depended on the stability of the recording.

Histological verification

At the end of each experiment, we inflicted electrolytic lesions (10 μA, 10 seconds) through the recording electrode. Animals were afterwards euthanized with a lethal dose of pentobarbital, decapitated, and the brains immediately immersed in a mixture of 4% formaldehyde in 0.1 M PB. After fixation, tissue was cryoprotected in 30% sucrose and sectioned in the coronal plane at 40-μm thickness on a freezing microtome. We stained slices with 0.1% cresyl violet to facilitate identification of cytoarchitectural boundaries (Fig 2A). Histological assessment of the electrolytic lesions to any of the fields of the mPFC was processed blindly to each animal history. Multiunit locations were assigned to M2, ACC, PL, or IL within a rat brain atlas, accordingly with the histological verification and the stereotaxic coordinates in the three axes of recording tracts [84].

Data analysis

Offline data analyses were performed with MATLAB functions, the Statistics, and Machine Learning toolbox and custom-made MATLAB scripts. We measured multiunit responses to each tested tone by computing a PSTH with 40 trials of every condition (DEV, STD, and CTR). In the case of the STD, we analyzed the last evoked-response before a DEV to have the same number of trials per condition as in DEV and CTR. PSTHs were smoothed with a 6 ms

Gaussian kernel in 1 ms steps to calculate the spike-density function over time (*ksdensity* function). Thereby, we obtained the mean and standard error of the mean (SEM) of spiking rates from −100 to 700 ms around tone onset. The spike-density function of the DEV responses of the mPFC population showed a response latency of approximately 150 ms with a sustained firing spanning up to the next tone (Fig 4B). To avoid overlap of consecutive tone responses, the response analysis window preserved the interstimulus interval of 500 ms and was delayed 100 ms from stimulus onset. For this reason, we did not perform a baseline correction. We only used a baseline window of 50 ms after stimulus onset to assess significantly increased responses to sound to be included in the analyses. We performed a Monte Carlo simulation, which is a probability simulation that withdraws numerical values from several random samplings. We simulated 10,000 PSTHs with a Poisson model of a constant firing rate equivalent to the baseline spontaneous spiking activity and thus, a null distribution of baseline-corrected spike count was generated from the PSTHs. We computed a p-value for the original baseline-corrected spike count as $p = (g+1)/(N+1)$, where g is the count of null measures $\geq$ baseline-corrected spike count and $N = 10{,}000$ is the size of the null sample. The significance level was set at $\alpha = 0.05$.

To compare across different multiunits, we normalized the auditory-evoked responses to each tone of interest in 3 testing conditions as follows:

$$Normalized\ DEV = DEV/N$$

$$Normalized\ STD = STD/N$$

$$Normalized\ CTR = CTR/N$$

where

$$N = \sqrt{DEV^2 + STD^2 + CTR^2}$$

is the Euclidean norm of the vector defined by the DEV, STD, and CTR responses. Thereby, normalized responses are the coordinates of a 3D unit vector defined by the normalized DEV, normalized STD, and normalized CTR responses that ranged between 0 and 1. This normalized vector has an identical direction to the original vector defined by the non-normalized data and equal proportions among the 3 response measurements.

To quantify and facilitate the interpretation of the oddball paradigm controls, we calculated the indices of neuronal mismatch (iMM, computing the overall mismatch response), repetition suppression (iRS, accounting for lower-order frequency-specific effects), and prediction error (iPE, unveiling higher-order deviance detection or PE signaling activity) with the normalized spike counts as:

$$iMM = Normalized\ DEV - Normalized\ STD$$

$$iRS = Normalized\ CTR - Normalized\ STD$$

$$iPE = Normalized\ DEV - Normalized\ CTR$$

Index values ranged between −1 and 1, where

$$iMM = iRS + iPE$$

Lastly, to analyze the emergence of predictive signals around stimulus presentation, we also calculated the average iPE in 35 time windows of 20 ms width from −50 to 650 ms relative to stimulus onset.

For the LFP signal analysis, we filtered the raw recording between 2.2 and 50 Hz (second order Butterworth filter), and then we aligned the recorded wave to the onset of the stimulus for every trial, and computed the mean LFP for every recording site and stimulus condition (DEV, STD, CTR), as well as the "prediction error potential" (PE-LFP = LFP_{DEV}–LFP_{CTR}). Then, grand-averages were computed for all conditions, for each auditory station separately. The *p*-value of the grand-averaged PE-LFP was determined for every time point with a 2-tailed *t* test (Bonferroni-corrected for 428 comparisons, with family-wise error rate < 0.05), and we computed the time intervals, where PE-LFP was significantly different from zero.

Our data set was not normally distributed so we used distribution-free (nonparametric) tests. These included the Wilcoxon signed-rank test, Wilcoxon rank-sum test, and Friedman test (for spike counts, normalized responses, indices, and response latencies), as well as the Kruskal–Wallis test with Dunn–Sidak correction for multiple index comparisons between each field from the mPFC and AC. Only the difference wave for the LFPs (PE-LFP) was tested using a *t* test, since each LFP trace is itself an average of 40 waves, and thus approximately normal (according to the Central Limit Theorem). For multiple comparison tests, *p*-values were corrected for false discovery rate (FDR = 0.1) using the Benjamini–Hockberg method [85].

To analyze the time course of suppression over the auditory-evoked response, we measured the DEV, STD, and CTR responses of each tone of interest as average spike counts (each unit normalized to the Euclidean norm, as previously explained) for every trial number within the sequence, for each field separately [38]. Given that the Euclidean Norm vector was calculated for each unit based on the mean DEV, CTR, and STD responses, some individual trials have values above 1. We included all the standard tones, not just the last standard before a deviant event as previously. Thereby, we ordered average normalized spike counts at their absolute trial position within the sequence and generated the time course of responses from the beginning of the sequence. Then, we fitted these time series to various models, namely, linear, exponential, double exponential, inverse polynomial, and power-law with 2 or 3 coefficients. We used the *fit* function in MATLAB that computes the confidence intervals of the fitted parameters and the adjusted R^2, the coefficient of determination of the function fit.

For the additional data set including the DEV alone, tests of sound-driven enhanced responses, spike-density functions, spike counts, and normalized responses followed the same previously described analyses. This time, the 3 compared conditions were the DEV alone, DEV, and STD. Since this was an additional experiment to compare the influence of different stimulation contexts on DEV responses, the whole sample was merged along the mPFC.

Supporting information

S1 Data. Multiunit recording examples from each mPFC field. ACC, anterior cingulate cortex; CTR, control condition; DEV, deviant condition; IL, infralimbic cortex; M2, secondary motor cortex; PL, prelimbic cortex; STD, standard condition.
(XLSX)

S2 Data. Spiking activity analysis. ACC, anterior cingulate cortex; CTR, control condition; DEV, deviant condition; IL, infralimbic cortex; iMM, index of neuronal mismatch; iPE, index of prediction error; iRS, index of repetition suppression; M2, secondary motor cortex; PL, prelimbic cortex; STD, standard condition.
(XLSX)

S3 Data. LFP analysis. ACC, anterior cingulate cortex; CTR, control condition; DEV, deviant condition; IL, infralimbic cortex; iPE, index of prediction error; M2, secondary motor cortex; PE-LFP, prediction error potential; PL, prelimbic cortex; SEM, standard error of the mean;

STD, standard condition.
(XLSX)

S4 Data. DEV alone analysis. DEV, deviant condition; LFP, local field potential; SEM, standard error of the mean; STD, standard condition.
(XLSX)

S5 Data. Comparisons between AC and mPFC responses. AC, auditory cortex; ACC, anterior cingulate cortex; CTR, control condition; DEV, deviant condition; IC, inferior colliculus; IL, infralimbic cortex; iMM, index of neuronal mismatch; iPE, index of prediction error; iRS, index of repetition suppression; MGB, medial geniculate body; M2, secondary motor cortex; PE-LFP, prediction error potential; PL, prelimbic cortex; SEM, standard error of the mean; STD, standard condition.
(XLSX)

Acknowledgments

We thank Drs Ryszard Auksztulewicz, Edward L. Bartlett, Conrado A. Bosman, Yves Boubenec, Nell B. Cant, Lucia Melloni, and Kirill V. Nourski for their constructive criticisms and fruitful discussions on previous versions of the manuscript. We also thank Drs Gloria G. Parras and Javier Nieto-Diego for their assistance with neurophysiological recordings and data analyses, as well as Mr. Antonio Rivas Cornejo for the histological processing.

Author Contributions

Conceptualization: Lorena Casado-Román, Guillermo V. Carbajal, David Pérez-González, Manuel S. Malmierca.

Data curation: Lorena Casado-Román, Guillermo V. Carbajal.

Formal analysis: Lorena Casado-Román, Guillermo V. Carbajal, David Pérez-González.

Funding acquisition: Manuel S. Malmierca.

Investigation: Lorena Casado-Román.

Methodology: David Pérez-González, Manuel S. Malmierca.

Project administration: Manuel S. Malmierca.

Software: David Pérez-González.

Supervision: Manuel S. Malmierca.

Visualization: Lorena Casado-Román, Guillermo V. Carbajal.

Writing – original draft: Lorena Casado-Román.

Writing – review & editing: Lorena Casado-Román, Guillermo V. Carbajal, David Pérez-González, Manuel S. Malmierca.

References

1. Näätänen R, Gaillard AWK, Mäntysalo S. Early selective-attention effect on evoked potential reinterpreted. Acta Psychol (Amst). 1978; 42:313–29. https://doi.org/10.1016/0001-6918(78)90006-9 PMID: 685709
2. Näätänen R, Michie PT. Early selective-attention effects on the evoked potential: A critical review and reinterpretation. Biol Psychol. 1979; 8:81–136. https://doi.org/10.1016/0301-0511(79)90053-x PMID: 465623

3. Kujala T, Tervaniemi M, Schröger E. The mismatch negativity in cognitive and clinical neuroscience: Theoretical and methodological considerations. Biol Psychol. 2007; 74:1–19. https://doi.org/10.1016/j.biopsycho.2006.06.001 PMID: 16844278

4. Näätänen R, Paavilainen P, Rinne T, Alho K. The mismatch negativity (MMN) in basic research of central auditory processing: A review. Clin Neurophysiol. 2007; 118:2544–90. https://doi.org/10.1016/j.clinph.2007.04.026 PMID: 17931964

5. Schall U. Is it time to move mismatch negativity into the clinic? Biol Psychol. 2016; 116:41–6. https://doi.org/10.1016/j.biopsycho.2015.09.001 PMID: 26342995

6. Fitzgerald K, Todd J. Making Sense of Mismatch Negativity. Front Psych. 2020; 11:468. https://doi.org/10.3389/fpsyt.2020.00468 PMID: 32595529

7. Opitz B, Rinne T, Mecklinger A, Von Cramon DY, Schröger E. Differential contribution of frontal and temporal cortices to auditory change detection: FMRI and ERP results. Neuroimage. 2002; 15:167–74. https://doi.org/10.1006/nimg.2001.0970 PMID: 11771985

8. Paavilainen P, Mikkonen M, Kilpeläinen M, Lehtinen R, Saarela M, Tapola L. Evidence for the different additivity of the temporal and frontal generators of mismatch negativity: A human auditory event-related potential study. Neurosci Lett. 2003; 349:79–82. https://doi.org/10.1016/s0304-3940(03)00787-0 PMID: 12946557

9. Näätänen R, Teder W, Alho K, Lavikainen J. Auditory attention and selective input modulation: A topographical ERP study. Neuroreport. 1992; 3:493–6. https://doi.org/10.1097/00001756-199206000-00009 PMID: 1391755

10. Näätänen R. The role of attention in auditory information processing as revealed by event-related potentials and other brain measures of cognitive function. Behav Brain Sci. 1990; 13:201–33. https://doi.org/10.1017/S0140525X00078407

11. Näätänen R, Alho K. Mismatch negativity-a unique measure of sensory processing in audition. Int J Neurosci. 1995; 80:317–37. https://doi.org/10.3109/00207459508986107 PMID: 7775056

12. Giard M-H, Perrin F, Pernier J, Bouchet P. Brain Generators Implicated in the Processing of Auditory Stimulus Deviance: A Topographic Event-Related Potential Study. Psychophysiology. 1990; 27:627–40. https://doi.org/10.1111/j.1469-8986.1990.tb03184.x PMID: 2100348

13. Doeller CF, Opitz B, Mecklinger A, Krick C, Reith W, Schröger E. Prefrontal cortex involvement in preattentive auditory deviance detection: Neuroimaging and electrophysiological evidence. Neuroimage. 2003; 20:1270–82. https://doi.org/10.1016/S1053-8119(03)00389-6 PMID: 14568496

14. Sikkens T, Bosman CA, Olcese U. The Role of Top-Down Modulation in Shaping Sensory Processing Across Brain States: Implications for Consciousness. Front Syst Neurosci. 2019; 13:31. https://doi.org/10.3389/fnsys.2019.00031 PMID: 31680883

15. Ulanovsky N, Las L, Nelken I. Processing of low-probability sounds by cortical neurons. Nat Neurosci. 2003; 6:391–8. https://doi.org/10.1038/nn1032 PMID: 12652303

16. Jääskeläinen IP, Ahveninen J, Bonmassar G, Dale AM, Ilmoniemi RJ, Levänen S, et al. Human posterior auditory cortex gates novel sounds to consciousness. Proc Natl Acad Sci. 2004; 101:6809–14. https://doi.org/10.1073/pnas.0303760101 PMID: 15096618

17. May PJC, Tiitinen H. Mismatch negativity (MMN), the deviance-elicited auditory deflection, explained. Psychophysiology. 2010; 47:66–122. https://doi.org/10.1111/j.1469-8986.2009.00856.x PMID: 19686538

18. Fishman YI. The mechanisms and meaning of the mismatch negativity. Brain Topogr. 2014; 27:500–26. https://doi.org/10.1007/s10548-013-0337-3 PMID: 24276221

19. Alho K. Cerebral generators of mismatch negativity (MMN) and its magnetic counterpart (MMNm) elicited by sound changes. Ear Hear. 1995; 16:38–51. https://doi.org/10.1097/00003446-199502000-00004 PMID: 7774768

20. Carbajal G V, Malmierca MS. Novelty Processing in the Auditory System: Detection, Adaptation or Expectation? 2nd ed. In: Fritzsch B, editor. The Senses: A Comprehensive Reference. 2nd ed. Elsevier; 2020. https://doi.org/10.1016/B978-0-12-809324-5.24154–0

21. Carbajal GV, Malmierca MS. The Neuronal Basis of Predictive Coding Along the Auditory Pathway: From the Subcortical Roots to Cortical Deviance Detection. Trends Hear. 2018; 22:233121651878482. https://doi.org/10.1177/2331216518784822 PMID: 30022729

22. Garrido MI, Kilner JM, Kiebel SJ, Stephan KE, Baldeweg T, Friston KJ. Repetition suppression and plasticity in the human brain. Neuroimage. 2009; 48:269–79. https://doi.org/10.1016/j.neuroimage.2009.06.034 PMID: 19540921

23. Garrido MI, Kilner JM, Stephan KE, Friston KJ. The mismatch negativity: A review of underlying mechanisms. Clin Neurophysiol. 2009; 120:453–63. https://doi.org/10.1016/j.clinph.2008.11.029 PMID: 19181570

24. Auksztulewicz R, Friston K. Repetition suppression and its contextual determinants in predictive coding. Cortex. 2016; 80:125–40. https://doi.org/10.1016/j.cortex.2015.11.024 PMID: 26861557

25. Todorovic A, de Lange FP. Repetition suppression and expectation suppression are dissociable in time in early auditory evoked fields. J Neurosci. 2012; 32:13389–95. https://doi.org/10.1523/JNEUROSCI.2227-12.2012 PMID: 23015429

26. Baldeweg T. Repetition effects to sounds: evidence for predictive coding in the auditory system. Trends Cogn Sci. 2006; 10:93–4. https://doi.org/10.1016/j.tics.2006.01.010 PMID: 16460994

27. Friston K. A theory of cortical responses. Philos Trans R Soc B Biol Sci. 2005; 360:815–36. https://doi.org/10.1098/rstb.2005.1622 PMID: 15937014

28. Friston K. The free-energy principle: a rough guide to the brain? Trends Cogn Sci. 2009; 13:293–301. https://doi.org/10.1016/j.tics.2009.04.005 PMID: 19559644

29. Garrido MI, Friston KJ, Kiebel SJ, Stephan KE, Baldeweg T, Kilner JM. The functional anatomy of the MMN: a DCM study of the roving paradigm. Neuroimage. 2008; 42:936–44. https://doi.org/10.1016/j.neuroimage.2008.05.018 PMID: 18602841

30. Garrido MI, Kilner JM, Kiebel SJ, Friston KJ. Dynamic causal modeling of the response to frequency Deviants. J Neurophysiol. 2009; 101:2620–31. https://doi.org/10.1152/jn.90291.2008 PMID: 19261714

31. Deouell LY. The frontal generator of the mismatch negativity revisited. J Psychophysiol. 2007; 21:188–203. https://doi.org/10.1027/0269-8803.21.34.188

32. Rinne T, Alho K, Ilmoniemi RJ, Virtanen J, Näätänen R. Separate Time Behaviors of the Temporal and Frontal Mismatch Negativity Sources. Neuroimage. 2000; 12:14–9. https://doi.org/10.1006/nimg.2000.0591 PMID: 10875898

33. Tse CY, Penney TB. On the functional role of temporal and frontal cortex activation in passive detection of auditory deviance. Neuroimage. 2008; 41:1462–70. https://doi.org/10.1016/j.neuroimage.2008.03.043 PMID: 18474433

34. Dürschmid S, Edwards E, Reichert C, Dewar C, Hinrichs H, Heinze H-J, et al. Hierarchy of prediction errors for auditory events in human temporal and frontal cortex. Proc Natl Acad Sci. 2016; 113:6755–60. https://doi.org/10.1073/pnas.1525030113 PMID: 27247381

35. Edwards E, Soltani M, Deouell LY, Berger MS, Knight RT. High gamma activity in response to deviant auditory stimuli recorded directly from human cortex. J Neurophysiol. 2005; 94:4269–80. https://doi.org/10.1152/jn.00324.2005 PMID: 16093343

36. Rosburg T, Trautner P, Dietl T, Korzyukov OA, Boutros NN, Schaller C, et al. Subdural recordings of the mismatch negativity (MMN) in patients with focal epilepsy. Brain. 2005; 128:819–28. https://doi.org/10.1093/brain/awh442 PMID: 15728656

37. Nourski KV, Steinschneider M, Rhone AE, Kawasaki H, Howard MA, Banks MI. Processing of auditory novelty across the cortical hierarchy: An intracranial electrophysiology study. Neuroimage. 2018; 183:412–24. https://doi.org/10.1016/j.neuroimage.2018.08.027 PMID: 30114466

38. Nieto-Diego J, Malmierca MS. Topographic Distribution of Stimulus-Specific Adaptation across Auditory Cortical Fields in the Anesthetized Rat. Zatorre R, editor. PLoS Biol. 2016; 14: e1002397. https://doi.org/10.1371/journal.pbio.1002397 PMID: 26950883

39. Parras GG, Nieto-Diego J, Carbajal GV, Valdés-Baizabal C, Escera C, Malmierca MS. Neurons along the auditory pathway exhibit a hierarchical organization of prediction error. Nat Commun. 2017; 8:2148. https://doi.org/10.1038/s41467-017-02038-6 PMID: 29247159

40. Harms L, Fulham WR, Todd J, Budd TW, Hunter M, Meehan C, et al. Mismatch negativity (MMN) in freely-moving rats with several experimental controls. PLoS ONE. 2014; 9:e110892. https://doi.org/10.1371/journal.pone.0110892 PMID: 25333698

41. Harms L, Michie PT, Näätänen R. Criteria for determining whether mismatch responses exist in animal models: Focus on rodents. Biol Psychol. 2016; 116:28–35. https://doi.org/10.1016/j.biopsycho.2015.07.006 PMID: 26196895

42. Jacobsen T, Horenkamp T, Schröger E. Preattentive memory-based comparison of sound intensity. Audiol Neuro-Otology. 2003; 8:338–46. https://doi.org/10.1159/000073518 PMID: 14566104

43. Ruhnau P, Herrmann B, Schröger E. Finding the right control: the mismatch negativity under investigation. Clin Neurophysiol. 2012; 123:507–412. https://doi.org/10.1016/j.clinph.2011.07.035 PMID: 21839676

44. Imada A, Morris A, Wiest MC. Deviance detection by a P3-like response in rat posterior parietal cortex. Front Integr Neurosci. 2013; 6:127. https://doi.org/10.3389/fnint.2012.00127 PMID: 23316147

45. Jodo E, Inaba H, Narihara I, Sotoyama H, Kitayama E, Yabe H, et al. Neonatal exposure to an inflammatory cytokine, epidermal growth factor, results in the deficits of mismatch negativity in rats. Sci Rep. 2019; 9:7503. https://doi.org/10.1038/s41598-019-43923-y PMID: 31097747

46. Wiens S, Szychowska M, Eklund R, van Berlekom E. Cascade and no-repetition rules are comparable controls for the auditory frequency mismatch negativity in oddball tasks. Psychophysiology. 2019; 56: e13280. https://doi.org/10.1111/psyp.13280 PMID: 30246255

47. Bastos AM, Usrey WM, Adams RA, Mangun GR, Fries P, Friston KJ. Canonical Microcircuits for Predictive Coding. Neuron. 2012; 76:695–711. https://doi.org/10.1016/j.neuron.2012.10.038 PMID: 23177956

48. Heilbron M, Chait M. Great Expectations: Is there Evidence for Predictive Coding in Auditory Cortex? Neuroscience. 2018:54–73. https://doi.org/10.1016/j.neuroscience.2017.07.061 PMID: 28782642

49. Buzsáki G, Anastassiou CA, Koch C. The origin of extracellular fields and currents-EEG, ECoG. LFP and spikes Nat Rev Neurosci. 2012; 13:407–20. https://doi.org/10.1038/nrn3241 PMID: 22595786

50. Horváth J, Winkler I. How the human auditory system treats repetition amongst change. Neurosci Lett. 2004; 368:157–61. https://doi.org/10.1016/j.neulet.2004.07.004 PMID: 15351440

51. Mittag M, Takegata R, Winkler I. Transitional Probabilities Are Prioritized over Stimulus/Pattern Probabilities in Auditory Deviance Detection: Memory Basis for Predictive Sound Processing. J Neurosci. 2016; 36:9572–9. https://doi.org/10.1523/JNEUROSCI.1041-16.2016 PMID: 27629709

52. Srivastava HK, Bandyopadhyay S. Parallel lemniscal and non-lemniscal sources control auditory responses in the orbitofrontal cortex (OFC). eneuro. 2020; ENEURO.0121-20.2020. https://doi.org/10.1523/eneuro.0121-20.2020 PMID: 32753369

53. Camalier CR, Scarim K, Mishkin M, Averbeck BB. A Comparison of Auditory Oddball Responses in Dorsolateral Prefrontal Cortex, Basolateral Amygdala, and Auditory Cortex of Macaque. J Cogn Neurosci. 2019; 31:1054–64. https://doi.org/10.1162/jocn_a_01387 PMID: 30883292

54. Takaura K, Fujii N. Facilitative effect of repetitive presentation of one stimulus on cortical responses to other stimuli in macaque monkeys—a possible neural mechanism for mismatch negativity. Foxe J, editor. Eur J Neurosci. 2016; 43:516–28. https://doi.org/10.1111/ejn.13136 PMID: 26613160

55. Phillips HN. Blenkmann A, Hughes LE, Kochen S, Bekinschtein TA, Cam-Can, et al. Convergent evidence for hierarchical prediction networks from human electrocorticography and magnetoencephalography. Cortex. 2016; 82:192–205. https://doi.org/10.1016/j.cortex.2016.05.001 PMID: 27389803

56. Seamans JK, Lapish CC, Durstewitz D. Comparing the prefrontal cortex of rats and primates: Insights from electrophysiology. Neurotox Res. 2008; 14:249–62. https://doi.org/10.1007/BF03033814 PMID: 19073430

57. Parr T, Rikhye RV, Halassa MM, Friston KJ. Prefrontal Computation as Active Inference. Cereb Cortex. 2020; 30:682–95. https://doi.org/10.1093/cercor/bhz118 PMID: 31298270

58. Hoover WB, Vertes RP. Anatomical analysis of afferent projections to the medial prefrontal cortex in the rat. Brain Struct Funct. 2007; 212:149–79. https://doi.org/10.1007/s00429-007-0150-4 PMID: 17717690

59. Keller GB, Mrsic-Flogel TD. Predictive processing: a canonical cortical computation. Neuron. 2018; 100:424–35. https://doi.org/10.1016/j.neuron.2018.10.003 PMID: 30359606

60. Parras GG, Valdés-Baizabal C, Harms L, Michie PT, Malmierca MS. The effect of NMDA-R antagonist, MK-801, on neuronal mismatch along the rat auditory thalamocortical pathway. Sci Rep. 2020; 10:12391. https://doi.org/10.1038/s41598-020-68837-y PMID: 32709861

61. Valdés-Baizabal C, Carbajal GV, Pérez-González D, Malmierca MS. Dopamine modulates subcortical responses to surprising sounds. PLoS Biol. 2020; 18. https://doi.org/10.1371/journal.pbio.3000744 PMID: 32559190

62. Dürschmid S, Zaehle T, Hinrichs H, Heinze HJ, Voges J, Garrido MI, et al. Sensory Deviancy Detection Measured Directly Within the Human Nucleus Accumbens. Cereb Cortex. 2016; 26:1168–75. https://doi.org/10.1093/cercor/bhu304 PMID: 25576536

63. Barascud N, Pearce MT, Griffiths TD, Friston KJ, Chait M. Brain responses in humans reveal ideal observer-like sensitivity to complex acoustic patterns. Proc Natl Acad Sci. 2016; 113:E616–25. https://doi.org/10.1073/pnas.1508523113 PMID: 26787854

64. Kiehl KA, Stevens MC, Laurens KR, Pearlson G, Calhoun VD, Liddle PF. An adaptive reflexive processing model of neurocognitive function: Supporting evidence from a large scale (n = 100) fMRI study of an auditory oddball task. Neuroimage. 2005; 25:899–915. https://doi.org/10.1016/j.neuroimage.2004.12.035 PMID: 15808990

65. Czisch M, Wehrle R, Stiegler A, Peters H, Andrade K, Holsboer F, et al. Acoustic oddball during NREM sleep: A combined EEG/fMRI study. Grothe B, editor. PLoS ONE. 2009; 4: e6749. https://doi.org/10.1371/journal.pone.0006749 PMID: 19707599

66. Rummell BP, Klee JL, Sigurdsson T. Attenuation of responses to self-generated sounds in auditory cortical neurons. J Neurosci. 2016; 36:12010–26. https://doi.org/10.1523/JNEUROSCI.1564-16.2016 PMID: 27881785

67. Pérez-González D, Parras GG, Morado-Díaz CJ, Aedo-Sánchez C, Carbajal G V., Malmierca MS. Deviance detection in physiologically identified cell types in the rat auditory cortex. Hear Res. 2020 [cited 24 Sep 2020]. https://doi.org/10.1016/j.heares.2020.107997 PMID: 32482383

68. Spratling MW. Reconciling predictive coding and biased competition models of cortical function. Front Comput Neurosci. 2008; 2:4. https://doi.org/10.3389/neuro.10.004.2008 PMID: 18978957

69. Spratling MW. Predictive coding as a model of biased competition in visual attention. Vision Res. 2008; 48:1391–408. https://doi.org/10.1016/j.visres.2008.03.009 PMID: 18442841

70. Shipp S. Neural elements for predictive coding. Front Psychol. 2016; 7:1792. https://doi.org/10.3389/fpsyg.2016.01792 PMID: 27917138

71. Spratling MW. A review of predictive coding algorithms. Brain Cogn. 2017; 112:92–7. https://doi.org/10.1016/j.bandc.2015.11.003 PMID: 26809759

72. Szymanski FD, García-Lázaro JA, Schnupp JWH. Current source density profiles of stimulus-specific adaptation in rat auditory cortex. J Neurophysiol. 2009; 102:1483–90. https://doi.org/10.1152/jn.00240.2009 PMID: 19571199

73. Nashida T, Yabe H, Sato Y, Hiruma T, Sutoh T, Shinozaki N, et al. Automatic auditory information processing in sleep. Sleep. 2000; 23:821–8. PMID: 11007449

74. Strauss M, Sitt JD, King J-R, Elbaz M, Azizi L, Buiatti M, et al. Disruption of hierarchical predictive coding during sleep. Proc Natl Acad Sci U S A. 2015; 112:E1353–62. https://doi.org/10.1073/pnas.1501026112 PMID: 25737555

75. Koelsch S, Heinke W, Sammler D, Olthoff D. Auditory processing during deep propofol sedation and recovery from unconsciousness. Clin Neurophysiol. 2006; 117:1746–59. https://doi.org/10.1016/j.clinph.2006.05.009 PMID: 16807099

76. Quaedflieg CW, Münte S, Kalso E, Sambeth A. Effects of remifentanil on processing of auditory stimuli: A combined MEG/EEG study. J Psychopharmacol. 2014; 28:39–48. https://doi.org/10.1177/0269881113512036 PMID: 24257810

77. Rodríguez RA, Bussière M, Froeschl M, Nathan HJ. Auditory-evoked potentials during coma: Do they improve our prediction of awakening in comatose patients? J Crit Care. 2014; 29:93–100. https://doi.org/10.1016/j.jcrc.2013.08.020 PMID: 24125771

78. Morlet D, Fischer C. MMN and novelty P3 in coma and other altered states of consciousness: A review. Brain Topogr. 2014; 27:467–79. https://doi.org/10.1007/s10548-013-0335-5 PMID: 24281786

79. Ayala YA, Pérez-González D, Duque D, Palmer AR, Malmierca MS. Extracellular Recording of Neuronal Activity Combined with Microiontophoretic Application of Neuroactive Substances in Awake Mice. J Vis Exp. 2016:e53914. https://doi.org/10.3791/53914 PMID: 27286308

80. Duque D, Malmierca MS. Stimulus-specific adaptation in the inferior colliculus of the mouse: anesthesia and spontaneous activity effects. Brain Struct Funct. 2015; 220:3385–98. https://doi.org/10.1007/s00429-014-0862-1 PMID: 25115620

81. Hara K, Harris RA. The Anesthetic Mechanism of Urethane: The Effects on Neurotransmitter-Gated Ion Channels. Anesth Analg. 2002; 94:313–8. https://doi.org/10.1097/00000539-200202000-00015 PMID: 11812690

82. Trautmann EM, Stavisky SD, Lahiri S, Ames KC, Kaufman MT, O'Shea DJ, et al. Accurate Estimation of Neural Population Dynamics without Spike Sorting. Neuron. 2019; 103: 292–308.e4. https://doi.org/10.1016/j.neuron.2019.05.003 PMID: 31171448

83. Lu K, Liu W, Zan P, David SV, Fritz JB, Shamma SA. Implicit memory for complex sounds in higher auditory cortex of the ferret. J Neurosci. 2018. https://doi.org/10.1523/JNEUROSCI.2118-18.2018 PMID: 30266740

84. Paxinos G, Watson C. The rat brain in stereotaxic coordinates. Elsevier; 2007.

85. Benjamini Y, Hochberg Y. Controlling the False Discovery Rate: A Practical and Powerful Approach to Multiple Testing. J R Stat Soc Ser B. 1995; 57:289–300. https://doi.org/10.1111/j.2517-6161.1995.tb02031.x

9 Acknowledgments

Agradecimientos

Gracias a Manolo por darme esta oportunidad, por apostar y confiar en mí. Agradezco su gran capacidad de trabajo parar tirar de todo, pero también dejarnos desarrollar independientemente. Gracias a David por confiar en mí, apoyarme y asegurarse de que todos los barcos lleguen a buen puerto con su mayor experiencia. Gracias a los dos por irme descubriendo parte de los entresijos del mundo de la ciencia

Estoy muy agradecida a todos los Canelitos por su gran sentido del compañerismo, haber hecho del laboratorio una pequeña familia y que estos años sean una experiencia para recordar. Infinitas gracias a Gloria por compartirlo todo para que pudiera ser muy pronto independiente en el lab y por el día a día con momentos de muchas risas y los desahogos de menos risas. Gracias a Guillermo por su entusiasmo y esfuerzo en aprender tanto y compartirlo tan generosamente, motivándome y ayudándome a mejorar en la ciencia y en la vida que hay más allá. Gracias a Catalina por su enorme capacidad de trabajo e infinita generosidad enseñando y colaborando siempre con buen humor y disposición. Gracias a Javier por haber tenido la habilidad de enseñarme mucho en muy poco tiempo y sentar las bases de gran parte de mi trabajo. Gracias a Antonio y a María por toda su dedicación como técnicos yendo más allá del simple trabajo. Gracias a Cristian por los buenos ratos, el apoyo y por enseñarme a tomarme las cosas con mejor filosofía. Gracias a Ana por las conversaciones, por hacer sencilla la física y su buena disposición siempre con todo. Gracias a Flora por trasmitirme parte de su sabiduría y animarme a que confíe en mi trabajo. Gracias a Camilo por las risas y por compartir toda su experiencia sobre el mundo de la ciencia. Gracias a Blanca por tantas buenas charlas y risas muy necesarias haciendo más agradable el día a día.

Agradezco a toda la gente del INCYL que con su trabajo y compañerismo hace que sea las cosas funcionen. Así como a toda la gente entregada en dignificar la carrera científica con su grandísimo esfuerzo como los compañeros de INNOVA y la FJI.

Big thanks to the LISTEN consortium for being such a great enriching environment and giving me endless opportunities for learning and inspiration. Thanks for making us feel welcome at every institution we visited and becoming scientific family. Thanks to the LISTEN students for sharing this experience as friends.

Thanks a lot to everyone who contributed to improve my research at any point with comments, explanations, revisions or technical support: Drs Ryszard Auksztulewicz, Edward L. Bartlett, Conrado A. Bosman, Yves Boubenec, Nell B. Cant, Lucia Melloni, Kirill V. Nourski, Gerard G. Borst, Aaron B. Wong and Mr. Ignacio Plaza. Specially, THANKS

to Catalina and Guillermo because big part of this work is the result of their generous collaboration.

Thanks to Lianne and Conrado where it all started introducing me to the electrophysiology world and all the great support since then.

I am infinitely grateful to all my friends here and abroad for being the best support always and all the unforgatable times, can´t wait to see you all again! Mención especial merecen las primas por conseguir que aunque todo cambie haya cosas que nunca cambien. Gracias a Alba por compartir todo y haber hecho un poco más fácil lo muy difícil en muchas ocasiones.

En especial quiero agradecer a mis padres el haber hecho posible que llegue hasta aquí con su gran sacrificio y apoyo para que eligiera siempre lo que me hiciera feliz. Gracias por haber sido un ejemplo enseñándome que rendirse nunca en una opción. A mi hermano le agradezco que me haya apoyado siempre que lo he necesitado y por demostrarme una infinita capacidad de superación. Gracias también al resto de mi familia por ser simplemente los mejores para compartir esta vida y estar siempre en lo importante.

Gracias a Alberto por haber sido el ancla de estos años, soportar gran parte de su peso y lo más importante, por haber crecido junto a mí para disfrutarlos al máximo.